Final Technical Report
Advanced Controls for the Multi-pod Centipod WEC device
DE-EE0006404
Dec 2013 - Oct 2015

15 Feb 2016

Principle Investigator:
Alex Fleming, CTO
afleming@ecomerittech.com
805-845-9100

Report Author:
Alan McCall, Mechanical Engineer
amccall@ecomerittech.com
805-845-0496

Dehlsen Associates, LLC
101 E. Victoria Street, Suite F, Santa Barbara, CA 93101

Working Partners:
Dr. Ted Brekken
Mike Starrett
Ratanak So
Oregon State University
brekken@eecs.oregonstate.edu
541-737-2995

Jarett Goldsmith
DNV GL - Energy
Jarett.Goldsmith@dnvgl.com
858-836-3370

Dr. Sandeep Gupta
Helios Engineering Inc.
sgupta@heliosengineeringinc.com
805-701-8506

U.S. Department of Energy Disclaimer

This report was prepared as an account of work partially sponsored by an agency of the United States Government. Neither the United States Government nor any agency thereof, nor any of their employees, makes any warranty, express or implied, or assumes any legal liability or responsibility for the accuracy, completeness, or usefulness of any information, apparatus, product, or process disclosed, or represents that its use would not infringe privately owned rights. Reference herein to any specific commercial product, process, or service by trade name, trademark, manufacturer, or otherwise does not necessarily constitute or imply its endorsement, recommendation, or favoring by the United States Government or any agency thereof. The views and opinions of authors expressed herein do not necessarily state or reflect those of the United States Government or any agency thereof.

Project Consortium Legal Notice/Disclaimer

NOTE:

For further information about Dehlsen Associates, LLC, call 805-845-7575 or e-mail Alex Fleming at afleming@ecomerittech.com.

This publication is a corporate document that should be cited in the literature in the following manner: " Advanced Controls for the Multi-pod Centipod WEC device". Dehlsen Associates, LLC, Santa Barbara, CA and U.S. Department of Energy, Washington, DC. 2016.

Table of Contents

1.0   Contractual Information

Federal Agency to which Report is submitted: DOE EERE – Wind & Water Power Program

Recipient: Dehlsen Associates, LLC - DUNS 830226317
Award Number: DE-EE0006404
Project Title: Advanced Controls for the Multi-pod Centipod WEC device
Project Period: Dec 1 2013 to Oct 31, 2015

Principle Investigator: Alex Fleming, VP of Engineering, afleming@ecomerittech.com; 101 E. Victoria Street, Suite F, Santa Barbara, CA 93101; 805-845-9100

Report Submitted by: Dave Arthurs, CFO, darthurs@ecomerittech.com; 101 E. Victoria Street, Suite F, Santa Barbara, CA 93101; 805-845-9101

Date of Report: Feb 15, 2016

Covering Period: Dec 1 2013 to Oct 31, 2015

Working Partners:
Ted Brekken
Oregon State University
brekken@eecs.oregonstate.edu
541-737-2995

Jarett Goldsmith
DNV GL - Energy
Jarett.Goldsmith@dnvgl.com
858-836-3370

Dr. Sandeep Gupta
Helios Engineering Inc.,
sgupta@heliosengineeringinc.com
805-701-8506

Cost-Sharing Partners: N/A

DOE Project Team: DOE HQ Program Manager – Jose Zayas
                DOE Field Contract Officer – Pamela Brodie
                DOE Field Grants Management Specialist – Yvette Peterson
                DOE Field Project Officer – Tim Ramsey
                DOE/CNJV Project Monitor – Michael Carella

Signature of Submitting Official: _____
(electronic signature is acceptable)

2.0　Executive Summary

Dehlsen Associates, LLC (DA) has developed a Wave Energy Converter (WEC), Centipod, which is a multiple point absorber, extracting wave energy primarily in the heave direction through a plurality of point absorber floats sharing a common stable reference structure. The objective of this project was to develop advanced control algorithms that will be used to reduce Levelized Cost of Energy (LCOE). This project investigated the use of Model Predictive Control (MPC) to improve the power capture of the WEC.

The MPC controller developed in this work is a state-space, "look ahead" controller approach using knowledge of past and current states to predict future states to take action with the PTO to maximize power capture while still respecting system constraints. In order to maximize power, which is the product of force and velocity, the controller must aim to create phase alignment between excitation force and velocity.

This project showed a 161% improvement in the Annual Energy Production (AEP) for the Centipod WEC when utilizing MPC, compared to a baseline, fixed passive damping control strategy.　This improvement in AEP was shown to provide a substantial benefit to the WEC's overall Cost of Energy, reducing LCOE by 50% from baseline. The results of this work proved great potential for the adoption of Model Predictive Controls in Wave Energy Converters.

3.0　Proposed Project Parameters

3.1　Project Objectives

Dehlsen Associates, LLC (DA) proposed to develop innovative advanced control algorithms to optimize power production and dynamic loads for the multi-pod Centipod Wave Energy Converter (WEC) utilizing a novel energy efficient PTO system. The scope and tasking for this project, as written in the original Statement of Project Objectives (SOPO) is described below.

3.2　Project Scope

Dehlsen Associates, LLC (DA) has developed a novel concept, Centipod, which has evolved from extensive research and several rounds of prototype testing to arrive at a design which shows significant improvements in the area of material usage. The objective of this project was to develop advanced control algorithms that will be used to further reduce Levelized Cost of Energy (LCOE), improve Power-to-Weight Ratio (PWR) for Centipod and achieve DOE Wind and Water Power Technologies Office's Water Program's goal of performance enhancement of Marine Hydrokinetic (MHK) devices.

This project investigated the use of Model Predictive Control (MPC) to improve the power capture and reduce design loads for the MHK device. Real time implementation of such algorithms was also to be evaluated. In addition, control algorithms were developed for the survival system or detuning for an extreme sea state with the pod feathering mechanism on Centipod.

3.3 Tasks Performed

Task 1.0   Develop reduced model representation for Centipod
Milestones: Validation of reduced order model.
Deliverables: Reduced order model, performance results for reference site.

Subtask 1.1.   Reduced model for single pod and Power Take Off (PTO)
Develop a reduced order model for single pod and PTO to create the plant model. ANSYS AQWA, or similar Software tool will be used to estimate hydrodynamic parameters in frequency domain. Results from this simple model will be compared against Dehlsen Associates previous work on pod optimization and geometry.

Subtask 1.2.   Reduced model for multi pod Centipod
Develop a reduced order model for Centipod with multiple pods, PTO and the backbone. Simulations will be performed assuming no interference of pods. Hydrodynamic models will then be developed to account for interference between pods and results compared with the former. The boundary conditions will be based on likely deployment test sites and target commercial sites.

Subtask 1.3.   Performance calculations and validation
Use the reduced order models and calculate performance at the site with basic controller and passive damping. These will be used as baseline results to compare against calculations resulting from task 3, carried out in parallel with this effort to perform validation of the reduced order model.

Task 2.0   Develop baseline global integration model in WEC performance and loading design software (WaveDyn or similar)
Milestones: Global integration model for Centipod.
Deliverables: Fully integrated model of Centipod.

Subtask 2.1.   Obtain hydrodynamic data for wetted geometry
Obtain hydrodynamic data for geometry using a wave analysis flow solver. The wetted geometry will be meshed in the MultiSurf surface modeling CAD package. Convergence studies will be performed using mesh refinement in MultiSurf. The flow solver data will be post-processed, to dimensionalize the flow solver data to derive the input hydrodynamic information for the global integration model.

Subtask 2.2.   Build system model of Centipod using   WEC performance and loading design software
Build a system model of the machine, including the backbone, pods, and PTO components. Hydrodynamics components will be attached to the backbone and pods, allowing the processed hydrodynamic properties to be incorporated. PTO will be defined that meets the target PTO characteristics. Parametric studies involving advanced controls to optimize PTO topologies will be explored. Mooring lines will be modeled as quasi-static. Stability and robustness tests on the model using a neutral control setting will be run.

Task 3.0   Baseline performance and operational loads calculations in WEC performance and loading design software

Milestones: Benchmark baseline performance and loads.

Deliverables: Performance results, Operational load calculation report.

Subtask 3.1.   Performance calculation

Develop comprehensive performance assessment data set for Centipod. Irregular wave simulations covering phase and spectral variability would be run using measured or standard shape spectral data. Power capture will be derived; in particular, a power matrix for the device (either using specific site data or a utilizing a generic spectral shape) will be derived.

Subtask 3.2.   Operational loads calculation

Simulate operational loads either using specific site data or a utilizing a generic spectral shape. PTO loading and system loads baseline will be established.

Subtask 3.3.   Baseline performance and loads report

Generate a performance and loads report that will serve as a baseline for comparison purposes. This report will not include extreme loads but only operational loads.

Task 4.0   Develop model predictive control framework

Milestones: Deliver Simulink model for MPC controller.

Deliverables: Simulink controller model, Simulation results with MPC.

Subtask 4.1.   Develop cost function and constraints

Develop a cost function that needs to be minimized or maximized using model predictive control based on performance and loads calculations available. Constraints that drive the system cost (e.g. generator force, heave velocity etc.) will be specified to add to the model. Perform Techno-economic model that optimizes between advanced controls, PTO, subsystems, reliability, efficiency, operations and maintenance for a 20 year design life.

Subtask 4.2.   Incorporate and validate wave prediction algorithm

Model wave predicting algorithms using adaptive least square or extended Kalman filter based methods will be investigated and the most appropriate method will be used. Accuracy will be traded against computational complexity. These algorithms will then be validated using the wave data available for regular and irregular waves.

Subtask 4.3.   Develop model predictive control in Simulink

Create model predictive control algorithm and simulate in Simulink. Based on results from earlier tasks, a simplified model (with no pod interaction) will be used if the results indicate that there is no substantial difference in controller response for the device with and without modeling interaction. Performance calculations will be performed either using site data or a utilizing a generic spectral shape and MPC tuned based on the cost function and results compared with baseline controller.

Task 5.0   MPC performance and operational loads calculation
Incorporate MPC into global integration model and simulate performance and operational loads calculations. Perform optimization studies with different cost functions.
Milestones: Complete analysis of MPC controller versus baseline
Deliverables: Fully integrated MPC controller in WEC performance and loading design software, Performance and operational loads results.

> **Subtask 5.1.   Incorporate MPC controller in WEC performance and loading design software**
> Incorporate MPC controller in WEC performance and loading design software. The WEC performance and loading design software will communicate with external controller using a Windows DLL. Simulink controller model will be re-programmed in C to create Windows DLL. After linking the controller DLL with WaveDyn, validation runs will be done to compare results against Simulink/AQWA model.
>
> **Subtask 5.2.   Performance and loads calculations with MPC controller**
> Simulate performance and operational loads for the same set of conditions either using specific site data or a utilizing a generic spectral shape. Results will be investigated to ensure that the specified constraints are met and performance and operational loads compared against baseline results. Simulations will be benchmarked to record the computational time required on a desktop computer and estimates for state of the art embedded processors.
>
> **Subtask 5.3.   Optimization of MPC algorithm**
> An optimization study will be performed using various cost functions and constraint for MPC. Additionally, a hardware unconstrained case will be explored. This will demonstrate the power of MPC framework and online optimization to account for various constraints as may be applicable for different kind of devices as well as the potential outside of existing technology. Two different scenarios will be looked at (1) Power maximization (2) Loads minimization.

Task 6.0   Extreme sea state load calculations in WEC performance and loading design software
Milestones: Development of Centipod "extreme condition response" controls
Deliverables: Extreme loads reduction report with advanced controls

> **Subtask 6.1.   Create extreme sea state condition matrix**
> Dehlsen Associates will create the extreme sea state conditions based on either site-specific data or based on DNV standard to calculate extreme loads on Centipod.
>
> **Subtask 6.2.   Perform Simulation under Extreme Conditions**
> Use the system integration model built in Task 1 to simulate the load cases under extreme sea state for pitching and non-pitching pods.
>
> **Subtask 6.3.   Optimization of extreme response controls with MPC**
> Investigate the use of MPC to optimize controls under extreme sea state conditions.

Task 7.0   Perform impact analysis

Use loads results of the simulation to update design and calculate new SPA metrics.

Milestones: Updated design of Centipod device.

Deliverables: Finite element analysis reports, weights and cost spreadsheets

> **Subtask 7.1.   Perform structural design iteration with updated loads**
>
> Perform finite element analysis in ANSYS/NASTRAN for the backbone structure, pods and heave plates with updated loads from performance modeling results. PTO design will be updated to reflect reduced requirements of force and heave velocity.
>
> **Subtask 7.2.   Updated PWR and Availability Metrics**
>
> Update complete analysis of the stated FOA metrics of PWR and Availability using performance calculations for MPC controller and device weight with updated loads. Compare the results to baseline controller.

Task 8.0   Design real-time implementation of MPC controller

Implement advanced convex optimization techniques to develop a real-time MPC controller.

Milestones: Controller benchmarking with and without convex optimization

Deliverables: Controller code in C or MATLAB with convex optimization, hardware requirements for MPC implementation

> **Subtask 8.1.   Implement convex optimization coding for MPC**
>
> Investigate the convex optimization techniques and decide on the best implementation strategy. Implement the chosen strategy in CVXGEN (convex optimization auto-coder from Stanford) or a similar tool to get a C-code or MATLAB mex function for Simulink analysis.
>
> **Subtask 8.2.   Benchmark speed-up with convex optimization**
>
> Simulate selected cases with the MPC controller with and without the convex optimization code to benchmark speed-up of online optimization and evaluate if the speed-up is sufficient for real-time implementation. Based on these results, hardware requirements (processor speed, cache, memory) will be defined for system integration into Centipod.

4.0   Project Organization

Dehlsen Associates took on this project with the support of working partners with expertise in both control system development and numerical modeling of Wave Energy Converters. Oregon State University and Helios Engineering were the leading working partners in the domain of control system development within this project, providing leadership and experience to the development of the model predictive framework. Meanwhile DNV GL led the numerical modeling effort through the application of their commercial WEC analysis tool, WaveDyn. The National Renewable Energy Laboratory and Sandia National Laboratories provided guidance with regard to Extreme Condition Modeling which formed the basis of the methodology utilized in this project.
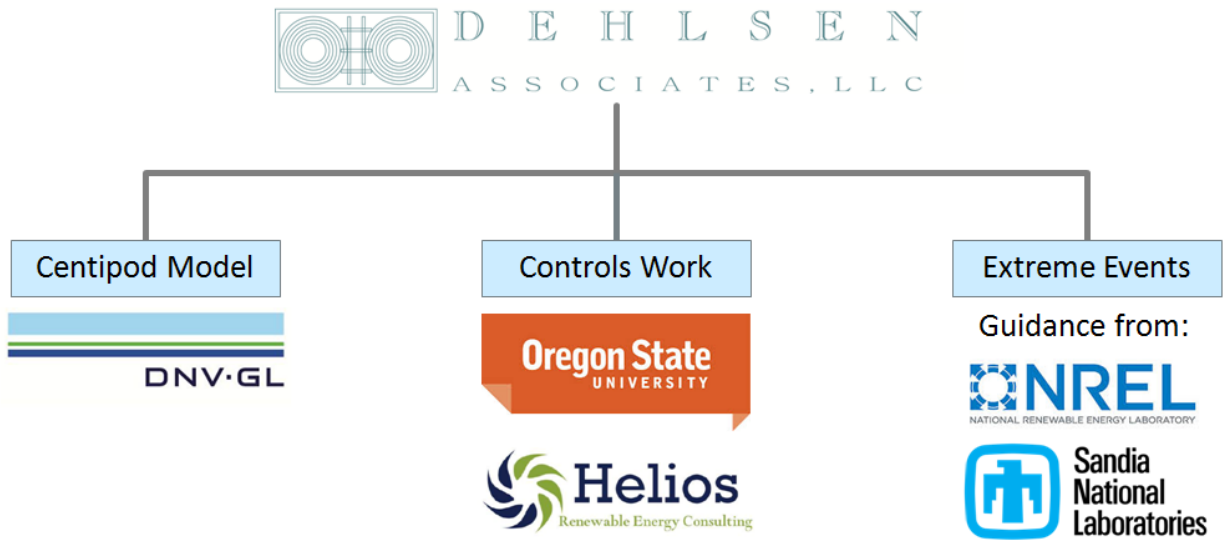
5.0 Project Task Activities

5.1 Task 1.0 - Develop reduced model representation for Centipod

The objective of Task 1 was to produce a reduced order model of Centipod, created in MATLAB, and verified against the more complex WaveDyn model. This reduced order model served two purposes. First, it was a fast and sufficiently accurate plant model to provide closed loop feedback during the development of the controller in MATLAB. Without the plant model, the controller would have had to be developed and run in C-code with WaveDyn providing closed loop feedback. This would have made both the development and simulation orders of magnitude slower.

In addition to representing the Centipod for closed loop feedback, the plant model is also an integral part of the fundamental operation of this specific estimation and control strategy. The plant model is used in the estimator (to estimate the excitation force acting on the body using only measured signals of position, velocity, and Fpto) and it is "model" portion of model predictive control (used to optimize the control action based on the expected plant response).The development of this model started with the general basis shown below:
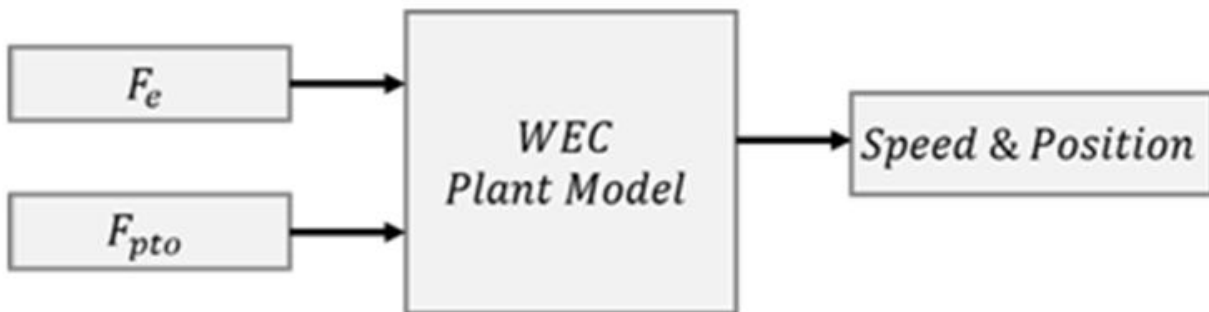
Figure 5.1.1: Basis of Centipod plant model.

The plant model is a state-space representation of the pod which is used to calculate and track position and velocity as well as several additional, unobservable states. This is a key component used by the MPC controller in that it is the model on top of which predictive control is executed. A simplified, frequency independent version of the plant model is given as:

$$\frac{d}{dt}\begin{bmatrix}\dot{z}\\z\end{bmatrix} = \underbrace{\begin{bmatrix}\frac{-B}{m+A} & \frac{-k}{m+A}\\1 & 0\end{bmatrix}}_{A}\begin{bmatrix}\dot{z}\\z\end{bmatrix} + \underbrace{\begin{bmatrix}\frac{1}{m+A}\\0\end{bmatrix}}_{Bu}\begin{bmatrix}F_{pto}\end{bmatrix} + \underbrace{\begin{bmatrix}\frac{1}{m+A}\\0\end{bmatrix}}_{Bv}\begin{bmatrix}F_e\end{bmatrix}$$

Where:

z	–	Pod/PTO position
$z\ dot$	–	Pod/PTO velocity
B	–	Hydrodynamic damping
A	–	Hydrodynamic added mass
m	–	Pod mass
k	–	Hydrodynamic stiffness
Fe	–	Hydrodynamic excitation force
$Fpto$	–	PTO force

The added mass and damping components (A and B) of the above formula are body geometry and mass derived outputs from a boundary element method (BEM) solver such as WAMIT. In reality, these values are also frequency dependent, meaning they differ depending on the wave frequency, which is variable throughout any real time series. A plot illustrating this frequency dependence is shown below:
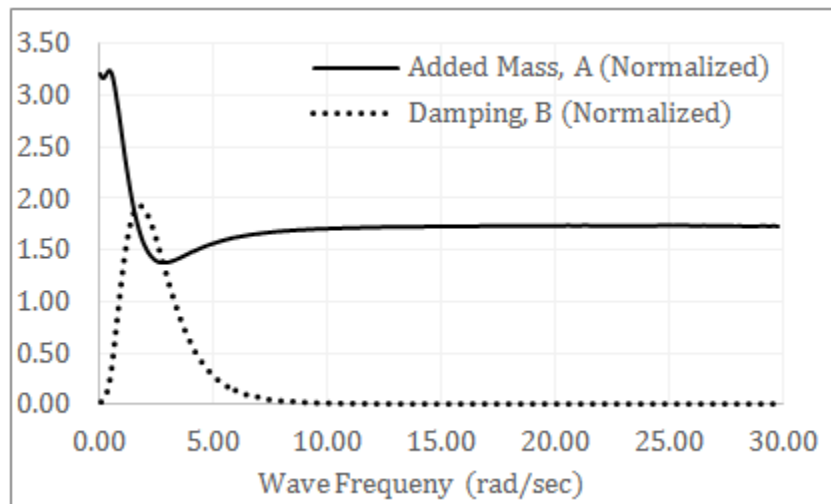
Figure 5.1.2: Normalized added mass and damping vs. wave frequency for an example WEC modelled in a BEM solver [1].

Since real sea conditions are not of uniform wave frequency, it was critical that the frequency dependent added mass and damping parameters be incorporated into the model rather than frequency independent values. This is well illustrated in the comparison of the two methods

against WaveDyn, a commercially available wave energy converter dynamics software package which has been experimentally validated, and thus serves as the source of truth in these figures.
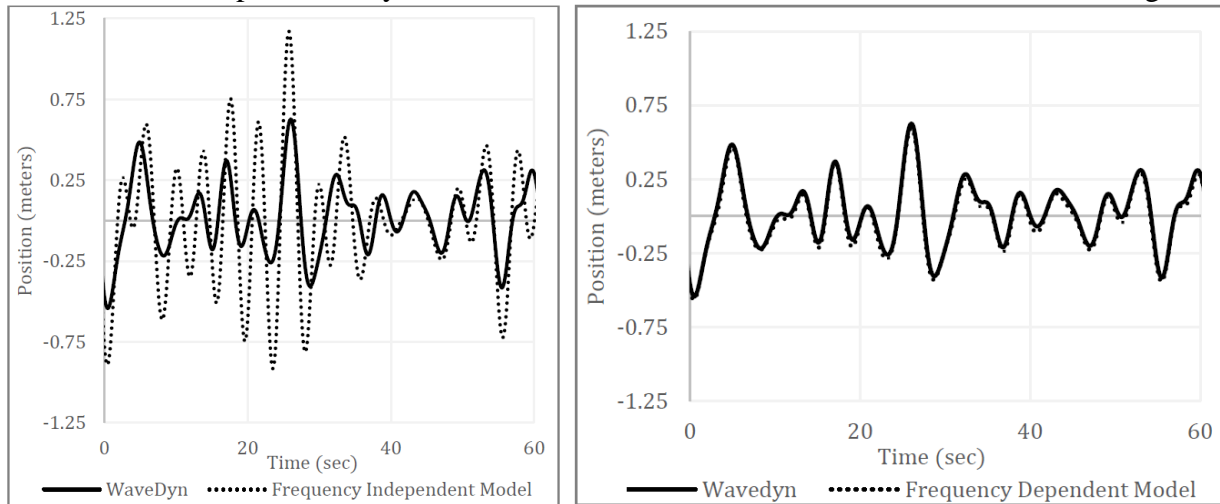
Figure 5.1.3: Comparison of Frequency Independent and Dependant models.

With the completion of a plant model for a single pod, the single pod plant model was extended to a multi-pod model which represented the complete Centipod WEC structure. The initial implementation of the full five pod system did not incorporate pod-to-pod interactions which would exist in a multiple pods placed in proximity to each other. This cross-coupling force is manifested through a body-to-body radiative force, *Fr*, and can be understood as waves created by the motion of one body acting as an external force on another body. To examine the importance of including this body-to-body interaction, the five pod model as augmented to include frequency dependent cross-coupling and the relative magnitudes of each force were compared. As is shown in Figure 5.1.5 for Pod 3, the external excitation force is significantly larger than all radiative forces, and the self-radiation force (Fr33) is furthermore much larger than cross-terms which are almost indiscernible along the x-axis.
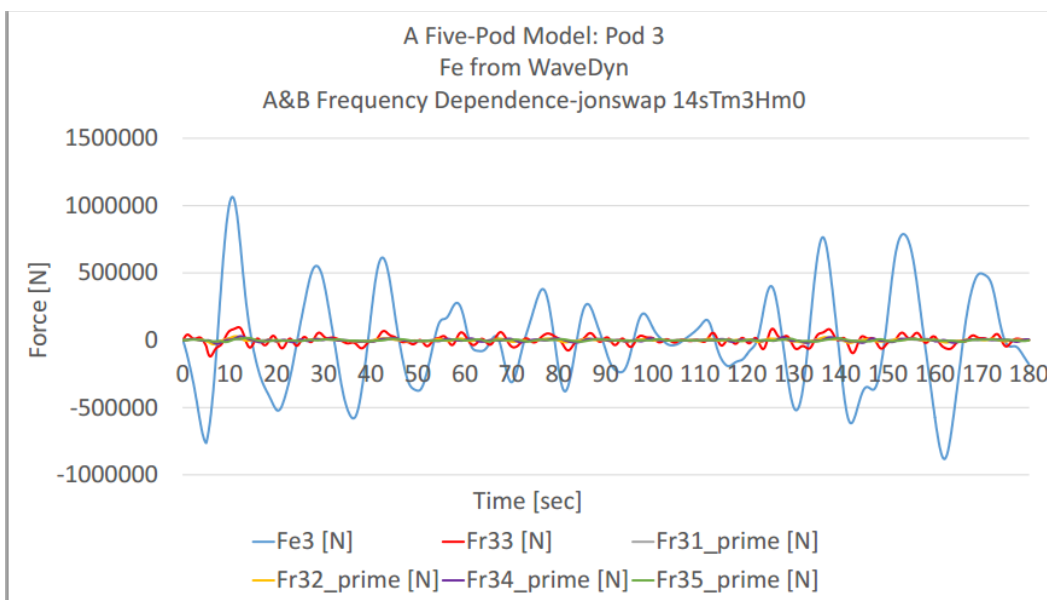
Figure 5.1.4: Excitation force of Pod 3 (blue) vs. all other pods radiation forces on Pod 3.

Given that the controller is being developed to run in real time, the team decided to omit the cross-coupling forces on the basis of their small relative magnitude. The five body plant model without cross-coupling was then validated against WaveDyn and confirmed to be accurate.

Further Detail on the mathematics behind this plant model can be found in the controller documentation in Appendix 1.

5.2 Task 2.0 - Develop baseline global integration model in WaveDyn

The numerical model of Centipod was created in DNV GL's WaveDyn software with the assistance of DNV GL. The construction of the numerical model was comprised of two parts: calculation of hydrodynamic data, and creation of the model itself within WaveDyn.

In order to obtain the hydrodynamic data for Centipod's geometry, a mesh of the WEC's wetted geometry was created from the existing CAD files. This mesh was then fed into WAMIT, a BEM hydrodynamics solver, alongside parametric data describing each of the 6 bodies of the WEC. WAMIT was then used to compute the hydrodynamic data, which would be fed into WaveDyn. The following sub-sections provide excerpts from DNV GL's detailed report on model creation which can be found in Appendices 2 and 3.

5.2.1 Hydrodynamics Data

The hydrodynamic coefficients and the wave exciting force associated with each body and the interactions between them were loaded into the 'Hydrodynamics' model from WAMIT. The hydrodynamics data were limited to first-order (linear) quantities. The model geometry used by the flow solver was defined using the Rhinoceros 3D modeling tool. This allows the definition of the geometry to be represented as splines for use with the high-order method option in WAMIT. An example of the mean wetted profile of the Centipod WEC is shown in Figure 5.2.1 and Figure 5.2.2. The mesh and frequency resolution were refined to allow the accurate representation of specific hydrodynamic quantities such as the radiation force.
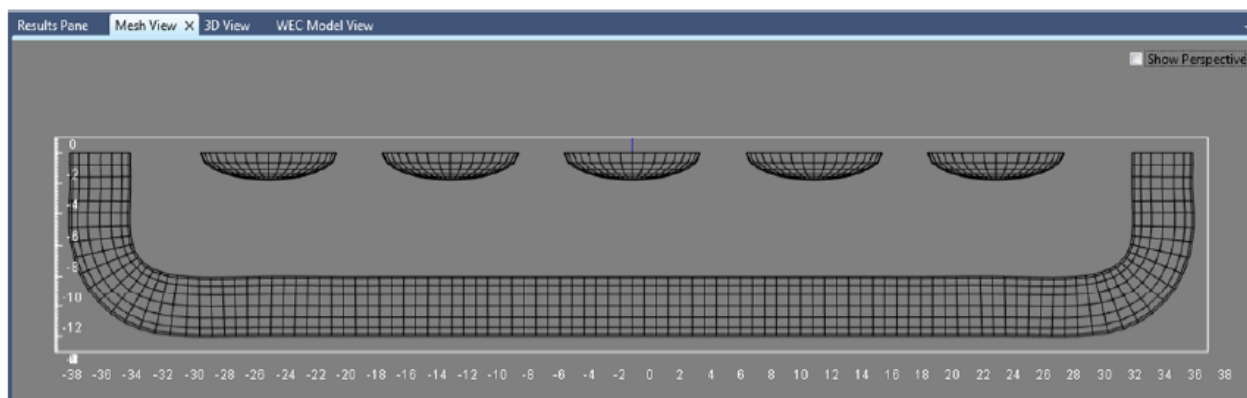
Figure 5.2.1: Profile showing the WAMIT mesh for a maximum panel size of 0.8m
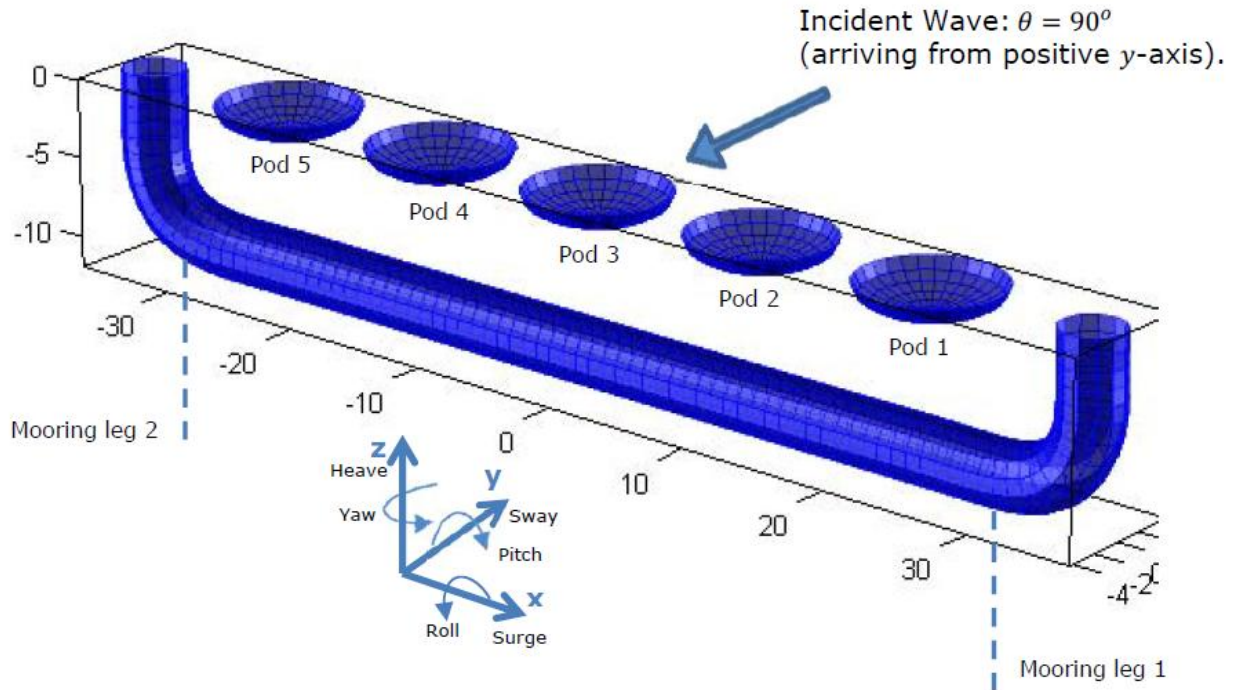
Figure 5.2.2: 3D view showing coordinate system of Centipod within WaveDyn.

The final set of hydrodynamic data was derived following a convergence exercise focusing on the mesh resolution. Convergence studies have investigated the frequency resolution, radiation damping decay at high and low frequencies and length of impulse response functions. The following describes the convergence study methodology DNV GL used focusing on the mesh resolution.

The mesh resolution of the pods was checked for convergence with special focus on the heave excitation force and radiation damping. The hydrodynamic data presented in this section for Pod 3 includes the influence of the 'backbone' and other pods in the vicinity. The focus for the excitation force convergence was on frequencies below 6rad/s, around 1s period, since for the sea-states investigated the energy beyond this frequency is negligible. The radiation damping was checked for convergence over a wider frequency range, providing a high level of confidence in values up to the frequencies where damping converged to zero (the complete set of data is integrated over all frequencies by the WaveDyn pre-processor). The WAMIT highorder method was used to discretize the wetted surface of the bodies and WAMIT was provided with a nominal 'Panel Size' characteristic length as a means of controlling the overall geometric resolution. For this investigation, the values used for the panel size parameter were 2m, 1m and 0.8m.

Figure 5.2.3 and Figure 5.2.5 show that the excitation amplitudes for the pods have converged for every mesh size up until around 2.5rad/s. For higher frequencies the 2m mesh appears to be of insufficient resolution. A mesh of 1m is sufficient for convergence up until around 6rad/s.

The radiation damping in heave also requires the panel size to be 1m before convergence is seen and it decays to zero within the frequency range considered, as shown in Figure 5.2.4. However

in sway (for translational motions in *y* – please see the axis orientations in Figure 5.2.2), the radiation damping (illustrated in Figure 5.2.6) only approaches zero for the highest frequencies studied. The non-complete decay to zero in the radiation damping is expected to have a very small effect on the final impulse response functions. Also a mesh size of 0.8m appears marginally superior in this case.
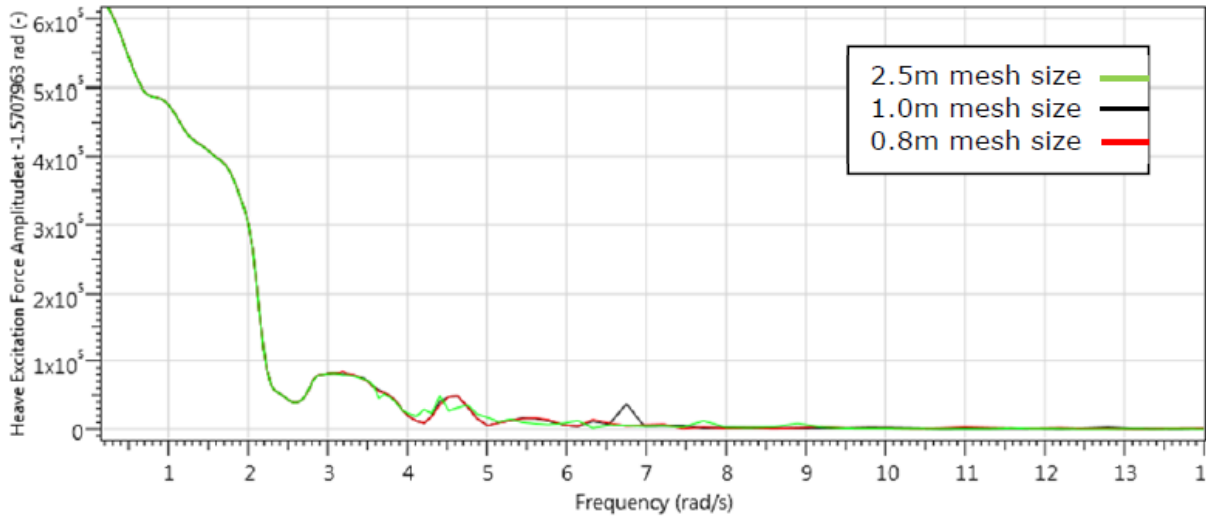
Figure 5.2.3: Heave excitation amplitude of Pod 3 for various mesh sizes with waves approaching from the positive global y axis.
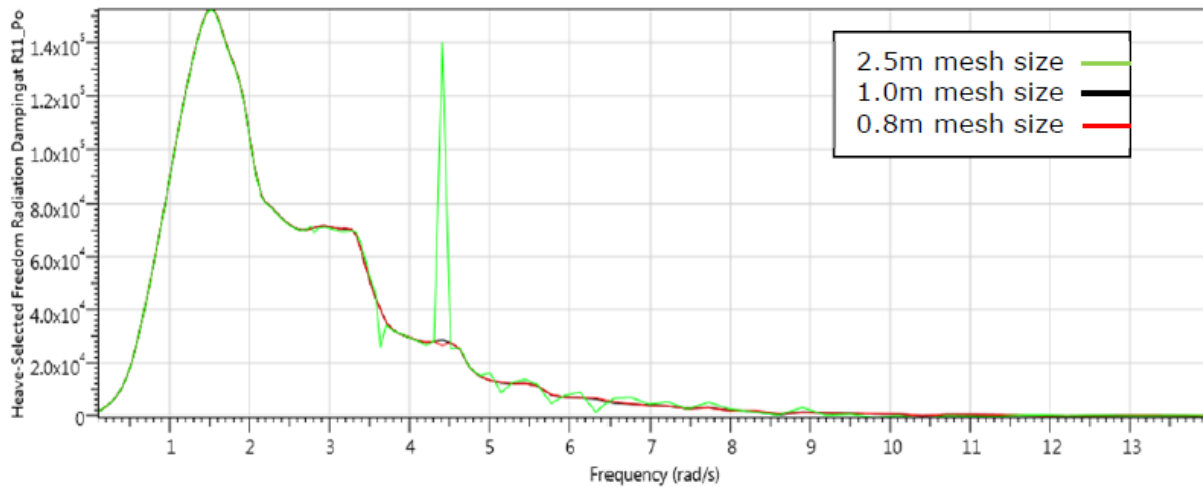
Figure 5.2.4: Heave radiation damping of Pod 3 for various mesh sizes.
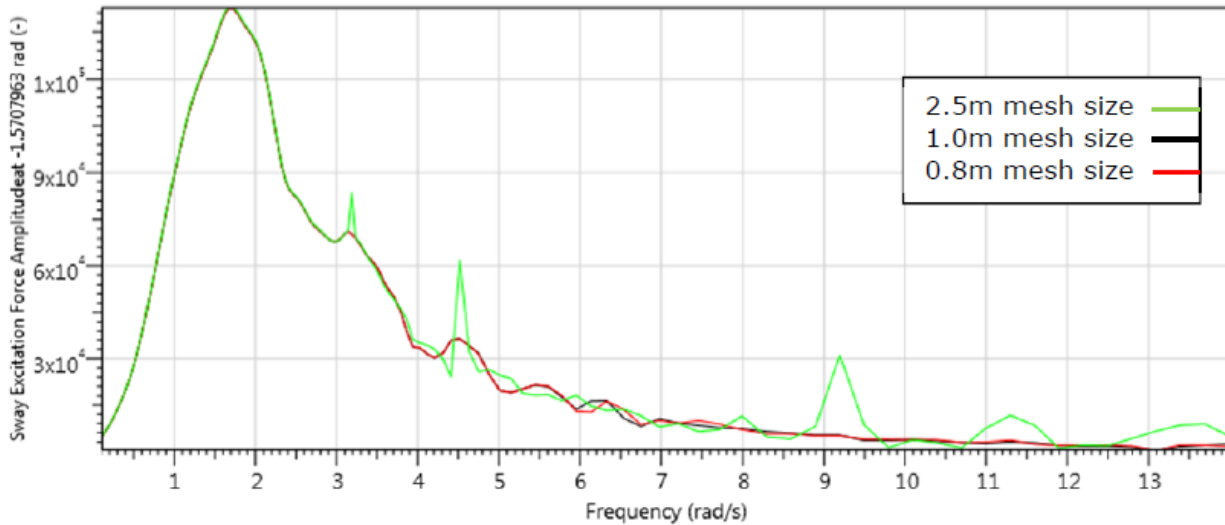
Figure 5.2.5: Sway excitation amplitude of Pod 3 for various mesh sizes with waves approaching from the positive global y axis.
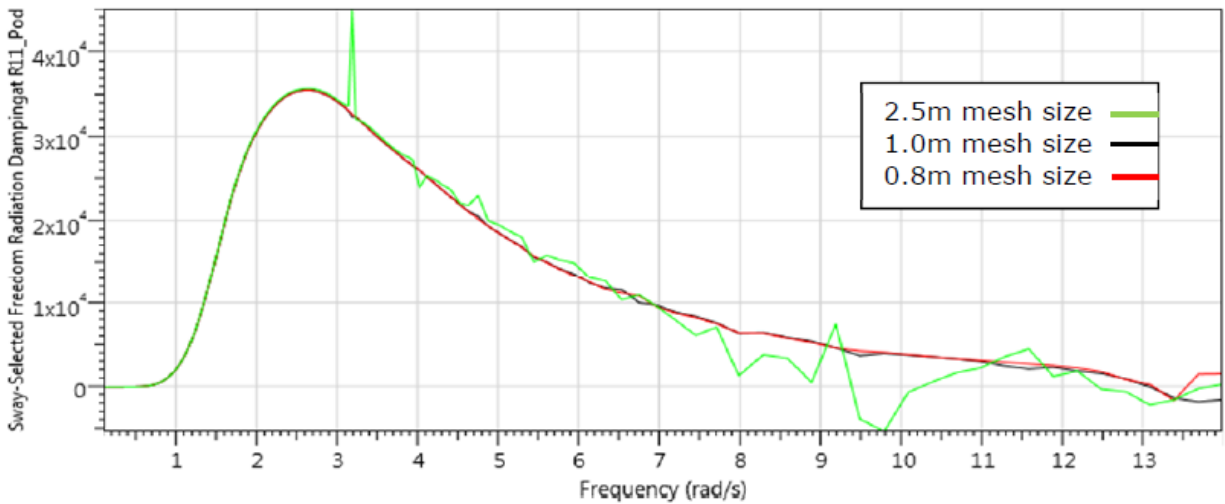
Figure 5.2.6: Sway radiation damping of Pod 3 for various mesh sizes.

5.2.2 WaveDyn Model

The WEC structural properties are represented in WaveDyn as rigid bodies with mass, moments of inertia and hydrodynamic properties. The component connectivity is defined using a series of nodes and massless rigid links which represent the physical offsets between individual parts of the WEC system. A block diagram representing the multi-body structure implemented in WaveDyn is provided in Figure 5.2.9.

A ground node, placed at the 'backbone' proximal node (0,0,60m), is connected via a floating free joint to the 'backbone' structure node, allowing it to float unrestrained in all 6 degrees-of freedom. The 'Pod Attachment' links provide the necessary horizontal offsets along the 'backbone' to the PTO units directly below each pod. A sliding joint PTO is used between the 'backbone' and each pod allowing single degree of freedom motion in the heave direction. A

rigid connection links each sliding joint to the center of mass of the corresponding pod. At the connection point between each pod's corresponding sliding PTO joint and the 'backbone' an additional hinge joint provides a further degree of freedom for rotational motion of the PTO and pod about the 'backbone' in the primary wave direction. This compliance is expected to reduce large moment arms which otherwise could have been experienced at the structural joint.

The masses and moments of inertia about the centers of gravity of the pods and 'backbone' have are summarized in Table 5.2.1 to Table 5.2.2 below. The center of mass positions have been provided relative to a reference location illustrated by the diagrams in Figure 5.2.8 and 5.2.9. It should be noted that in WaveDyn the z-axis is the default vertical axis, whereas the data used had a coordinate system where the y-axis is the vertical axis. Therefore, care was taken that the values for I_{yy} and I_{zz} were switched for both the pod and the 'backbone' when entering the inertia tensor matrix values into WaveDyn. The vertical offset for the 'backbone' center of mass should also be input as an offset along the z-axis in WaveDyn rather than the y-axis as shown in Table 5.2.3.

I_{xx}=9713714	0	0
0	I_{yy}=196981292	0
0	0	I_{zz}=205715877

*N.b. WaveDyn equivalent inertia tensor input for the structural 'Body: Backbone':
{9713714, 0, 0} {0, 205715877, 0} {0, 0, 196981292}
Table 5.2.1: Inertia tensor table for 'backbone' about center of mass including ballast (kgm2). Coordinate system illustrated in Figure 5.2.7.

I_{xx}=367958	0	0
0	I_{yy}=634402	0
0	0	I_{zz}=367958

*N.b. WaveDyn equivalent inertia tensor input for the structural 'Body: Pod [1-5]':
{367958, 0, 0} {0, 367958, 0} {0, 0, 634402}
Table 5.2.2: Inertia tensor table for pods about center of mass (kgm2). Coordinate system illustrated in Figure 5.2.8.

Component	Mass	Center of mass (coordinate system in Figure 4-2 and Figure 4-3)
Backbone	402000	(0, 0.95, 0)
Pods	78000	(0, 0, 0)

*N.b. WaveDyn equivalent center of mass input for the 'backbone': {0, 0, 0.95}
Table 5.2.3: Masses of device including ballast (kg) Component Mass Center of mass (coordinate system in Figure 5.2.7 and Figure 5.2.8)
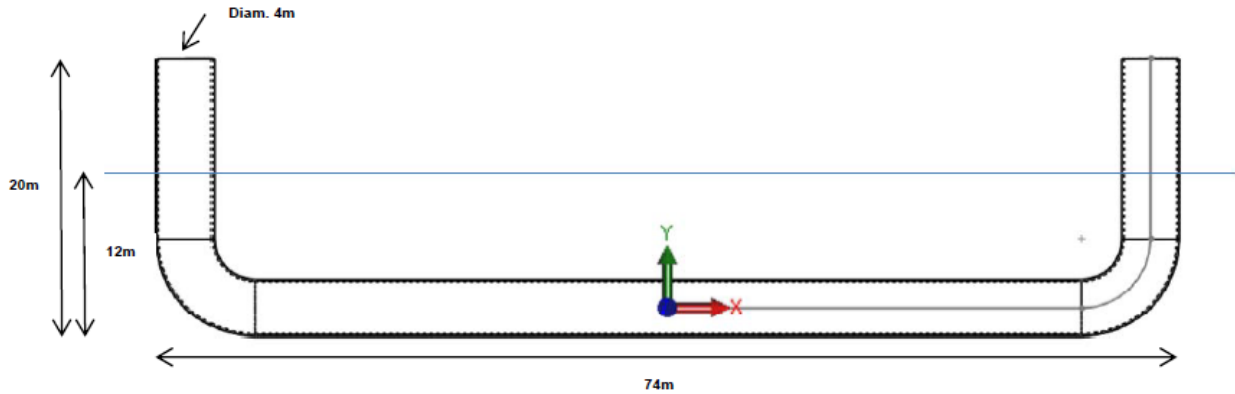
Figure 5.2.7: Reference coordinate system of 'backbone' center of gravity in Table 5.2.3.

(Note that WaveDyn uses a coordinate system where the z-axis is vertical)
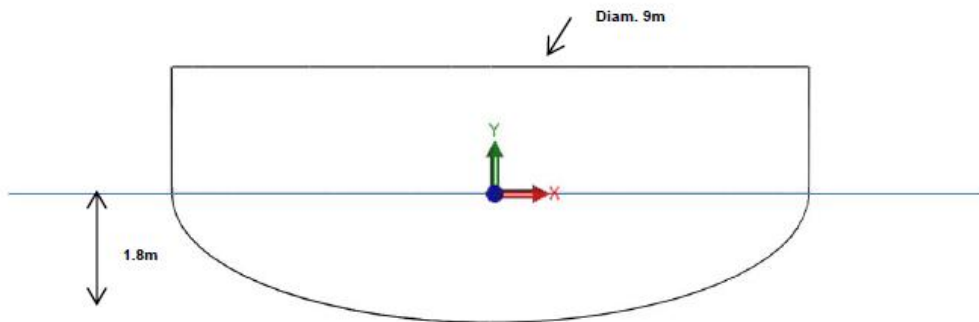
Figure 5.2.8: Reference coordinate system of pod center of gravity in Table 5.2.3. (Note that WaveDyn uses a coordinate system where the z-axis is vertical). The center of mass is located at the center of the body at the waterline. Not shown to scale with Figure 5.2.7.

The completed block diagram of Centipod modeled in WaveDyn can be seen below in Figure 5.2.9.
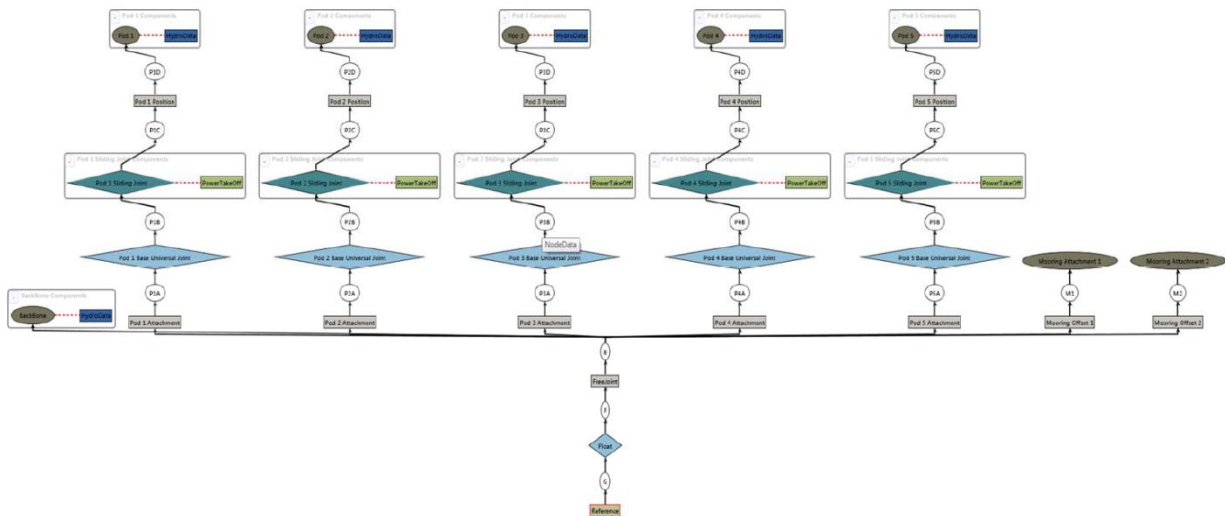
Figure 5.2.9: WaveDyn block diagram of Centipod.

5.3   Task 3.0 - Baseline performance and operational loads calculations

5.3.1 Performance Calculation:

5.3.1.1 Baseline Controller:

The baseline power take off (PTO) control scheme is fixed passive damping. This method applies a single damping value to the power take off system across all sea states. In order to optimize the damping value, the pod geometry and joint probability distribution (JPD) of the reference site both need to be considered. The optimal damping value is found using the formula below [3].

$$ B_m = B_{m\,opt} = \left(B_r{}^2 + \left(\omega(m_m + m_r) - \frac{(\rho_w g S_w)^2}{\omega} \right)^2 \right)^{1/2} $$

Where:

B_m –   PTO Damping Coefficient (Ns m^{-1})
B_r –   Added Damping Coefficient (or 'Radiation Resistance') (Ns m^{-1})
$B_{m\,opt}$ –   Optimum PTO damping rate for maximum energy absorption (Ns m^{-1})
m_m –   Physical mass (kg)
m_r –   Added mass (kg)
S_w –   Water plane area(m^2)
Ω –   Wave frequency (rad s^{-1})

This calculation was conducted using a wave frequency matching the most probable portion of the reference site JPD and the added mass from the WAMIT output data set at that wave period. The optimal PTO damping coefficient resulting from this work was 688 kNs m^{-1}.

5.3.1.2 Power Matrix Methodology:

Using the model created as part of Task 2, DNV GL was able to run the WaveDyn model of Centipod for a number of different sea states representative of the resource supplied by DA. The resource supplied was that from the April 2013 *Standardized Cost and Performance Reporting for Marine and Hydrokinetic Technologies* paper [4] which outlined the DOE's preferred resource for use in LCOE calculations.

The performance data was generated as specified, creating a time series of length 200 times the peak period from a Bretschneider Spectrum with a peak period interval of one second. Each of the 190 sea states were run for 200 times the peak period with a ramp-up period of 5s. The first 10 seconds of simulation where not included in the mean power calculation to omit unrealistic initial settling motions, however it was assumed to have a minimal impact on total mean power. The mean power over each bin's time series simulation was input into a mechanical power matrix and multiplied by the JPD, and other modifying factors to reach the final AEP estimation for the baseline.

5.3.1.3 AEP Calculation:

The AEP calculation method used the following procedure starting with the JPD and Mechanical Power Matrix:

		Peak Period, Tp [sec]																		
		1.7	2.7	3.7	4.7	5.7	6.7	7.7	8.7	9.7	10.7	11.7	12.7	13.7	14.7	15.7	16.7	17.7	18.7	19.7	20.7
Significant Wave Height, Hs [m]	0.25	0.00%	0.00%	0.00%	0.00%	0.00%	0.01%	0.00%	0.00%	0.00%	0.00%	0.00%	0.00%	0.00%	0.01%	0.00%	0.00%	0.00%	0.00%	0.00%	0.00%
	0.75	0.00%	0.00%	0.01%	0.15%	0.43%	1.07%	1.12%	1.30%	0.41%	0.63%	0.28%	0.20%	0.20%	0.34%	0.43%	0.48%	0.17%	0.00%	0.03%	0.00%
	1.25	0.00%	0.00%	0.02%	0.10%	0.98%	2.80%	2.38%	4.56%	1.85%	2.16%	1.12%	0.87%	0.66%	0.55%	0.37%	0.44%	0.24%	0.00%	0.05%	0.00%
	1.75	0.00%	0.00%	0.00%	0.03%	0.25%	2.47%	2.67%	3.64%	2.09%	3.53%	1.95%	1.36%	1.21%	0.95%	0.46%	0.51%	0.29%	0.00%	0.11%	0.00%
	2.25	0.00%	0.00%	0.00%	0.00%	0.04%	0.64%	2.32%	3.56%	1.65%	3.27%	2.45%	1.86%	1.51%	1.03%	0.56%	0.51%	0.31%	0.00%	0.12%	0.00%
	2.75	0.00%	0.00%	0.00%	0.00%	0.00%	0.19%	0.90%	2.73%	1.00%	2.16%	1.96%	1.51%	1.34%	0.85%	0.52%	0.49%	0.33%	0.00%	0.14%	0.00%
	3.25	0.00%	0.00%	0.00%	0.00%	0.00%	0.03%	0.18%	1.06%	0.69%	1.21%	1.29%	1.19%	1.05%	0.83%	0.49%	0.43%	0.19%	0.00%	0.07%	0.00%
	3.75	0.00%	0.00%	0.00%	0.00%	0.00%	0.00%	0.04%	0.29%	0.32%	0.53%	0.75%	0.68%	0.70%	0.60%	0.34%	0.27%	0.12%	0.00%	0.06%	0.00%
	4.25	0.00%	0.00%	0.00%	0.00%	0.00%	0.00%	0.00%	0.09%	0.10%	0.18%	0.28%	0.34%	0.41%	0.36%	0.22%	0.23%	0.09%	0.00%	0.03%	0.00%
	4.75	0.00%	0.00%	0.00%	0.00%	0.00%	0.00%	0.00%	0.00%	0.01%	0.03%	0.07%	0.08%	0.12%	0.18%	0.24%	0.15%	0.16%	0.00%	0.03%	0.00%
	5.25	0.00%	0.00%	0.00%	0.00%	0.00%	0.00%	0.00%	0.00%	0.01%	0.01%	0.03%	0.05%	0.09%	0.12%	0.09%	0.10%	0.05%	0.00%	0.02%	0.00%
	5.75	0.00%	0.00%	0.00%	0.00%	0.00%	0.00%	0.00%	0.00%	0.00%	0.00%	0.00%	0.01%	0.03%	0.05%	0.04%	0.05%	0.02%	0.00%	0.01%	0.00%
	6.25	0.00%	0.00%	0.00%	0.00%	0.00%	0.00%	0.00%	0.00%	0.00%	0.00%	0.00%	0.01%	0.01%	0.04%	0.02%	0.03%	0.02%	0.00%	0.00%	0.00%
	6.75	0.00%	0.00%	0.00%	0.00%	0.00%	0.00%	0.00%	0.00%	0.00%	0.00%	0.00%	0.00%	0.01%	0.01%	0.01%	0.01%	0.01%	0.00%	0.00%	0.00%
	7.25	0.00%	0.00%	0.00%	0.00%	0.00%	0.00%	0.00%	0.00%	0.00%	0.00%	0.00%	0.00%	0.00%	0.00%	0.01%	0.01%	0.00%	0.00%	0.00%	0.00%
	7.75	0.00%	0.00%	0.00%	0.00%	0.00%	0.00%	0.00%	0.00%	0.00%	0.00%	0.00%	0.00%	0.00%	0.00%	0.00%	0.00%	0.00%	0.00%	0.00%	0.00%
	8.25	0.00%	0.00%	0.00%	0.00%	0.00%	0.00%	0.00%	0.00%	0.00%	0.00%	0.00%	0.00%	0.00%	0.00%	0.00%	0.00%	0.00%	0.00%	0.00%	0.00%
	8.75	0.00%	0.00%	0.00%	0.00%	0.00%	0.00%	0.00%	0.00%	0.00%	0.00%	0.00%	0.00%	0.00%	0.00%	0.00%	0.00%	0.00%	0.00%	0.00%	0.00%

Figure 5.3.1: Northern California Joint Probability Distribution [4].

Wave State vs. Mechanical Power Extraction (kW)

Hm0 (m)	Tp (sec) 3.7	4.7	5.7	6.7	7.7	8.7	9.7	10.7	11.7	12.7	13.7	14.7	15.7	16.7	17.7	18.7	19.7	20.7
0.25				3.1	3.1			2.9	2.8	2.6	2.5	2.4	2.2		2			
0.75	12	18.6	22.6	24	24.1	24	23.7	23.5	22.4	21.6	20.6	19.4	18.3	17.3	16.4		14.7	
1.25	32.5	51.6	55.6	61.5	62	61.9	64.2	62.6	59.9	58	55.3	50.8	50	46.4	43.8		40.1	
1.75	63.9	102.6	113.6	117.1	120	106.2	118.7	116.5	123.8	108.2	102.6	95.3	87.7	88	82.4		72.1	
2.25		168.5	186.6	179.5	180.3	172	192.1	181.1	178.1	168.1	161.6	158.2	145.3	134.1	125.9		111.5	
2.75			253.9	238.6	239.9	240.2	257.3	255.8	261.4	240.4	212.6	203.1	196.7	189.3	179.4		162.3	
3.25			382.4	338.3	316.8	334.3	343.1	348.2	335.3	315.6	274	278.8	253.8	234.7	231.4		216.4	
3.75				461	389.3	432.5	421.9	421.3	433	401.7	349.5	331.6	330.1	306.5	288.2		260.8	
4.25				500.9	503.6	512.7	498.9	487.2	442.8	441.7	406	402.1	370.8	346.1			293.3	
4.75					588.5	600.2	610.8	587.4	541.9	522.1	489.9	425	416.1	393.1			369.5	

Figure 5.3.2: Baseline Mechanical Power Matrix.

The mechanical power matrix was then modified to account for a uniformly applied 85% efficiency, a rated power of 1500kW and a cut off sea state of 5m Hs and greater. Per AEP calculation guidance [4] a 10% array loss and 95% availability were then applied. A final AEP of 1170MWh/yr was reached for the baseline calculation.

5.3.2 Operational Loads:

5.3.2.1 Operational Loads Methodology:

The loads on the various WEC components are calculated (and output) within WaveDyn for all the elements in the structure. For the Centipod machine, the loads on the pods, mooring loads and loads on the PTO are considered the outputs of most interest. A statistical analysis of the loads has been performed (min, max, mean, standard deviation). The non-exceedance curves for the various sea states have also been calculated. The use of this type of output allows a good understanding of the various loads levels experienced by the WEC components. It also provides a useful way to compare the influence on the loads of changing the WEC configurations. The use of these cumulative probability curves can also be used at a later stage for loads extrapolation and fatigue analysis.

5.3.2.1 Operational Loads Results:

Loads were analyzed and post processed for a number of nodes on the Centipod device under baseline operational conditions. The most critical to the structural design, and the load directly influenced by controller choice, is the axial force at each Pod connection. The maximum axial force for each sea state at the central pod, Pod 3, is shown in the figure below.

		Tp [s]																
		3.7	4.7	5.7	6.7	7.7	8.7	9.7	10.7	11.7	12.7	13.7	14.7	15.7	16.7	17.7	18.7	19.7
	0.25				66	78			75	60	60	58	56	64		58		
	0.75	142	195	190	186	205	222	215	226	196	193	194	171	205	172	169		151
	1.25	191	383	350	349	383	339	282	383	280	276	300	254	277	312	280		270
	1.75	345	395	549	424	481	472	434	438	410	449	394	352	358	387	366		315
	2.25		679	768	655	600	693	595	591	590	460	509	624	516	447	459		390
	2.75			888	872	696	640	699	753	743	610	572	558	602	627	548		483
	3.25			1237	871	897	868	804	803	875	645	800	752	572	640	602		522
	3.75				986	932	913	960	816	834	769	859	782	704	701	762		603
Hs [m]	4.25					1195	1155	921	1082	888	883	954	705	796	829	844		705
	4.75						1185	1084	1111	1235	1145	1254	970	802	885	841		963

Figure 5.3.3: Maximum axial force [kN] for Pod 3 for all sea states investigated.

An identical methodology was utilized for the analysis of loads after implementation of MPC, this will be further described in Section 5.5.

5.4   Task 4.0 - Develop model predictive control framework

5.4.1 Controller overview:

The MPC controller developed in this work is a state-space, "look ahead" controller approach using knowledge of past and current states to predict future states to take action with the PTO to maximize power capture while still respecting system constraints. In order to maximize power, which is the productof force and velocity, the controller must aim to create phase alignment between excitation force and velocity.

A diagram of the developed controller is shown below in Figure 5.4.1.
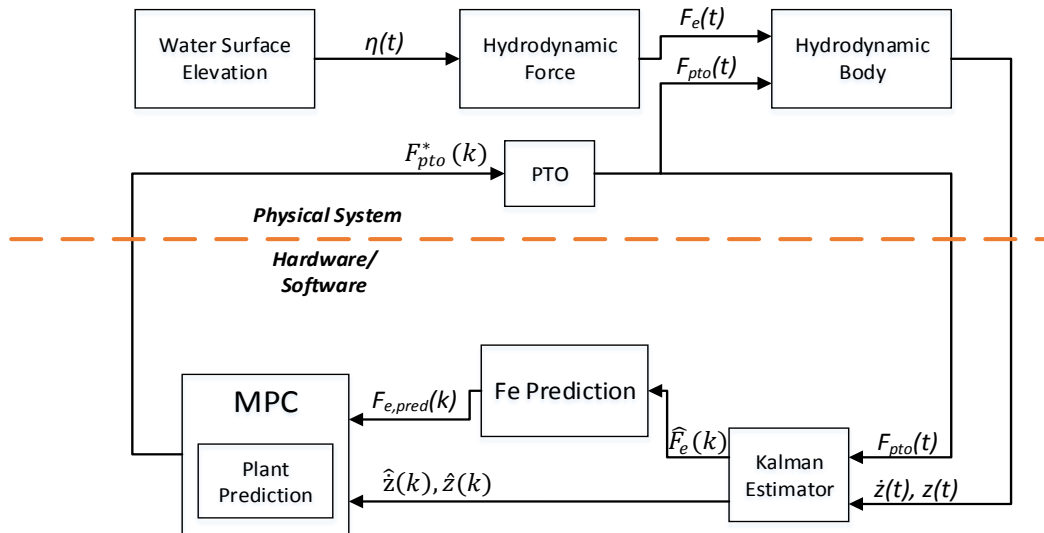
Figure 5.4.1: Controller block diagram

The controller has a single output, PTO force (Fpto), and three inputs: Fpto, Pod position (z), and velocity ($\dot{z}$). This controller requires no external or up-stream measurement of waves, it simply makes use of the aforementioned PTO force, position, and velocity time series, inputs which can be obtained easily without additional sensors. These inputs are fed into an estimator that outputs the hydrodynamic excitation force (Fe) imparted on the pod along with several internal states. A prediction block is utilized to take this excitation force history and predict future excitation force through the horizon for control. The controller uses the estimated current state and the prediction of future excitation forces to find an optimal Fpto which maximizes power as the product of force and velocity.

The blocks within the controller are described in detail in the following sub-sections.

5.4.2 Kalman Estimator:

The estimator uses the known commanded Fpto, alongside the measured inputs for position and velocity to estimate the excitation force time series history. All other signals, including all plant states (measureable or otherwise) as well as the excitation force acting on each body, are estimated through a linear Kalman filter.
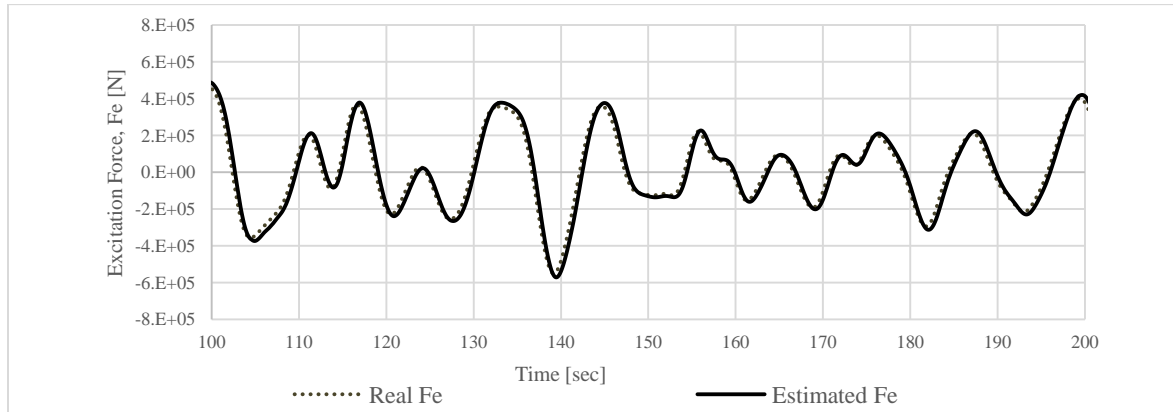
Figure 5.4.2: Estimate of excitation force, Fe, in a realistic sea state from Kalman filter using only measured velocity and position and the commanded PTO force [1].

In addition to that which is shown in the figure above, a strong correlation between the real and estimated excitation force was demonstrated across multiple sea states.

5.4.3 Fe Prediction:

Using previous and current estimated excitation force, an auto-regressive sliding window adaptive least-squares approach was used to model and predict future values. The output, future Fe prediction, is used as an input in the MPC block to inform Fpto selection. Where k is the current time and $k+H_p$ is the time horizon, the vector $F_e(k)...F_e(k+H_p)$ can be calculated for each of the N total bodies in the WEC system at every time k through N independent iterations of the following [2]:

$$F_e(k + 1|k) = \alpha_1 F_e(k) + \alpha_2 F_e(k - 1) + \cdots + \alpha_n F_e(k - n + 1) \tag{1}$$

$$F_e(k+2|k) = \alpha_1 F_e(k+1|k) + \alpha_2 F_e(k) + \cdots + \alpha_n F_e(k-n+2) \tag{2}$$

up to:

$$F_e(k+H_p|k) = \alpha_1 F_e(k+H_p-1|k) + \alpha_2 F_e(k+H_p-2|k) + \cdots$$
$$+ \alpha_n F_e(k+H_p-n|k) \tag{3}$$

$\alpha 1 \ldots \alpha n$ are calculated for each time in the observation horizon using a linear regression matrix [2]:

$$\begin{bmatrix} F_{e,k} \\ F_{e,k-1} \\ \vdots \\ F_{e,k-h} \end{bmatrix} = \begin{bmatrix} F_{e,k-1} & \cdots & F_{e,k-n} \\ F_{e,k-2} & \cdots & F_{e,k-1-n} \\ \vdots & \ddots & \vdots \\ F_{e,k-h-1} & \cdots & F_{e,k-h-n} \end{bmatrix} \begin{bmatrix} \alpha_1 \\ \vdots \\ \alpha_n \end{bmatrix} \tag{4}$$

The accuracy of Fe predicted in this way is only somewhat accurate and is more useful to consider as showing the overall expected trend of the excitation force over the prediction horizon.
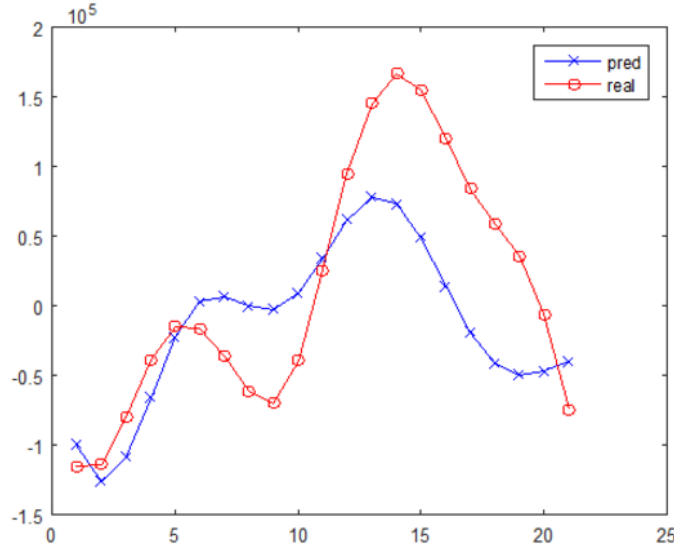
Figure 5.4.3: An example plot of real versus predicted Fe

Importantly, though, because MPC works on a wave-to-wave time scale to optimize power, the accuracy of this prediction strategy was determined to be sufficient by comparing power production using predicted values *vs.* known "test" future data. These results demonstrated less than 5% reduction in power production improvement when using predicted values from estimated excitation forces. In other, slower control schemes (*i.e.* slow active damping tuning) the prediction accuracy would likely be more important.

Various prediction horizons (Hp) were also investigated. Short prediction horizons would give an incomplete picture to the controller for optimizing power over the time horizon, while long time horizons would force the controller to optimize power using less accurate predictions of Fe far in the future. A balance between these two challenges was sought. Mean power was calculated on a number of time series from different sea states along with using the known future

excitation force. This work led to the conclusion that a 10 second prediction horizon would yield the best performance. One example time series result is shown below in Figure 5.4.4.

	Hp	Estimated v_arrow_k in hessian and constraint	Real v_arrow_k in hessian and constraint
Power from Matlab		4.73E+04	5.29E+04
Infeasibility	3	5	1
Over max		0	0
		8.87E+04	9.72E+04
	5	7	1
		15	13
		1.06E+05	1.19E+05
	8	11	1
		17	18
		1.07E+05	1.20E+05
	10	14	1
		17	18
		1.06E+05	1.17E+05
	15	14	1
		14	21

Figure 5.4.4: Example mean power with varying prediction horizons, estimated Fe vs. real Fe

5.4.4 MPC:

The cornerstone of the MPC controller developed in this work is an optimization function which maximizes power as the product of force and velocity. The general form of the quadratic optimization function which achieves this outcome can be written as [2]:

$$\min J(x) = \frac{1}{2} x^T H x + f^T x \qquad (5)$$

Subject to

$$Ax \leq B \qquad (6)$$

(5) can be re-written in terms specific to the MPC controller as shown below in (7)[2]:

$$J(k) = \frac{1}{2} \vec{y}(k)^T Q \vec{y}(k) + \frac{1}{2} \vec{u}(k)^T R \vec{u}(k) \qquad (7)$$

$\vec{y}(k)$ represents states from the WEC from the current time, k, to the horizon, $k + H_p$, as given by the predictive plant model. Importantly, $\vec{y}(k)$ includes terms for both force and velocity which the matrix Q selects to multiply as power. The vector $\vec{u}(k)$ represents the rate of change in the force of the PTO (*i.e.* $\dot{F}_{pto}$) and serves as the control input for optimization. The matrix R penalizes controller action to reduce large swings in force. The result is that the minimization of $J(k)$ yields the control action $\dot{F}_{pto}$ (given in the vector $\vec{u}(k)$) which each WEC should apply at each step through the horizon to maximize power. As is typical to MPC, only $\dot{F}_{pto}$ for the current time is applied, and the controller re-runs at the next time step to repeat this process [2].

5.4.5 Constraints:

The constraints utilized for this work are considered hard constraints. The solver must find a solution which is within the bounds of all the constraints or else the solution is infeasible. In the event that the solution is infeasible, the most recent solution to satisfy the constraints is used. In future work alternate constraint methodologies will be explored to improve performance of the controller and reduce infeasibilities.

Due to the desire to model the benefit of MPC without being restricted by PTO choice, loose constraints were applied to create what is effectively an unconstrained controller for most operational seas. The constraints are as follows:

Fpto max   =   1000kN
Max PTO Stroke   =   effectively unconstrained – See Figure 5.5.3
Max PTO Velocity   =   +-3m/s

Further detail on the mathematics behind the MPC formulation can be found in the controller documentation in Appendix 1, as well as [2] "Increasing Power Capture From Multibody Wave Energy Conversion Systems Using Model Predictive Control".

5.5   Task 5.0 - MPC performance and operational loads calculation

5.5.1 Performance Calculation:

5.5.1.1 Implementation of MPC:

In order to incorporate the MPC controller into WaveDyn, the controller had to be re-written in C before it was linked with WaveDyn. To better utilize the framework developed in MATLAB, Armadillo, a high quality C++ linear algebra library, was used. Armadillo is aimed towards a good balance between speed and ease of use and the syntax (API) is deliberately similar to MATLAB. It is an open source library that can be used for both R&D and production environments. The convex optimization problem is solved using C code generated using qpOASES. This model provided a quick and efficient way to use the MATLAB code developed for MPC implementation.

With the controller re-written in C, the process of coupling the controller with WaveDyn began. Using the controller produced in C, a DLL was created to be run alongside WaveDyn as an external controller. This controller DLL also uses a number of separate input files, which contain all the physical constraints such as maximum stroke, velocity and force of the PTO. Since these input files are external to the DLL, the constraints can easily be modified without the need to re-compile the DLL, leading to a much easier environment for troubleshooting.

The impact of the utilization of MPC with the WEC was then evaluated through the creation of a power matrix.

5.5.1.2 Power Matrix Methodology:

Using the model created as part of Task 2, coupled with the controller, DNV GL was able to run the WaveDyn model of Centipod for a number of different sea states representative of the same reference resource used in the baseline assessment. The resource supplied was that from the

April 2013 *Standardized Cost and Performance Reporting for Marine and Hydrokinetic Technologies* paper [4].

The performance data was generated as specified, creating a time series of length 200 times the peak period from a Bretschneider Spectrum for each sea state bin in the JPD. Each of the 190 sea states were run for 200 times the peak period. The short duration of simulation time prior to controller start-up was not included in the mean power calculation.

The mean power over each bin's time series simulation was input into a mechanical power matrix and multiplied by the JPD, and other modifying factors to reach the final AEP estimation for the baseline.

5.5.1.3 AEP Calculation:

The AEP calculation was calculated from the JPD and Mechanical Power Matrix:

Hs [m]	Peak Period, Tp [sec]																			
	1.7	2.7	3.7	4.7	5.7	6.7	7.7	8.7	9.7	10.7	11.7	12.7	13.7	14.7	15.7	16.7	17.7	18.7	19.7	20.7
0.25	0.00%	0.00%	0.00%	0.00%	0.00%	0.01%	0.00%	0.00%	0.00%	0.00%	0.00%	0.00%	0.00%	0.01%	0.00%	0.00%	0.00%	0.00%	0.00%	0.00%
0.75	0.00%	0.00%	0.01%	0.15%	0.43%	1.07%	1.12%	1.30%	0.41%	0.63%	0.28%	0.20%	0.20%	0.34%	0.43%	0.48%	0.17%	0.00%	0.03%	0.00%
1.25	0.00%	0.00%	0.02%	0.10%	0.98%	2.80%	2.38%	4.56%	1.85%	2.16%	1.12%	0.87%	0.66%	0.55%	0.37%	0.44%	0.24%	0.00%	0.05%	0.00%
1.75	0.00%	0.00%	0.00%	0.03%	0.25%	2.47%	2.67%	3.64%	2.09%	3.53%	1.95%	1.36%	1.21%	0.95%	0.46%	0.51%	0.29%	0.00%	0.11%	0.00%
2.25	0.00%	0.00%	0.00%	0.00%	0.04%	0.64%	2.32%	3.56%	1.65%	3.27%	2.45%	1.86%	1.51%	1.03%	0.56%	0.51%	0.31%	0.00%	0.12%	0.00%
2.75	0.00%	0.00%	0.00%	0.00%	0.00%	0.19%	0.90%	2.73%	1.00%	2.16%	1.96%	1.51%	1.34%	0.85%	0.52%	0.49%	0.33%	0.00%	0.14%	0.00%
3.25	0.00%	0.00%	0.00%	0.00%	0.00%	0.03%	0.18%	1.06%	0.69%	1.21%	1.29%	1.19%	1.05%	0.83%	0.49%	0.43%	0.19%	0.00%	0.07%	0.00%
3.75	0.00%	0.00%	0.00%	0.00%	0.00%	0.00%	0.04%	0.29%	0.32%	0.53%	0.75%	0.68%	0.70%	0.60%	0.34%	0.27%	0.12%	0.00%	0.06%	0.00%
4.25	0.00%	0.00%	0.00%	0.00%	0.00%	0.00%	0.00%	0.09%	0.10%	0.18%	0.28%	0.34%	0.41%	0.36%	0.22%	0.23%	0.09%	0.00%	0.03%	0.00%
4.75	0.00%	0.00%	0.00%	0.00%	0.00%	0.00%	0.00%	0.01%	0.03%	0.07%	0.08%	0.12%	0.18%	0.24%	0.15%	0.16%	0.07%	0.00%	0.03%	0.00%
5.25	0.00%	0.00%	0.00%	0.00%	0.00%	0.00%	0.00%	0.00%	0.01%	0.01%	0.03%	0.05%	0.09%	0.12%	0.09%	0.10%	0.05%	0.00%	0.02%	0.00%
5.75	0.00%	0.00%	0.00%	0.00%	0.00%	0.00%	0.00%	0.00%	0.00%	0.00%	0.00%	0.01%	0.03%	0.05%	0.04%	0.05%	0.02%	0.00%	0.01%	0.00%
6.25	0.00%	0.00%	0.00%	0.00%	0.00%	0.00%	0.00%	0.00%	0.00%	0.00%	0.00%	0.01%	0.01%	0.04%	0.02%	0.03%	0.02%	0.00%	0.00%	0.00%
6.75	0.00%	0.00%	0.00%	0.00%	0.00%	0.00%	0.00%	0.00%	0.00%	0.00%	0.00%	0.00%	0.01%	0.01%	0.01%	0.01%	0.01%	0.00%	0.00%	0.00%
7.25	0.00%	0.00%	0.00%	0.00%	0.00%	0.00%	0.00%	0.00%	0.00%	0.00%	0.00%	0.00%	0.00%	0.00%	0.01%	0.01%	0.00%	0.00%	0.00%	0.00%
7.75	0.00%	0.00%	0.00%	0.00%	0.00%	0.00%	0.00%	0.00%	0.00%	0.00%	0.00%	0.00%	0.00%	0.00%	0.00%	0.00%	0.00%	0.00%	0.00%	0.00%
8.25	0.00%	0.00%	0.00%	0.00%	0.00%	0.00%	0.00%	0.00%	0.00%	0.00%	0.00%	0.00%	0.00%	0.00%	0.00%	0.00%	0.00%	0.00%	0.00%	0.00%
8.75	0.00%	0.00%	0.00%	0.00%	0.00%	0.00%	0.00%	0.00%	0.00%	0.00%	0.00%	0.00%	0.00%	0.00%	0.00%	0.00%	0.00%	0.00%	0.00%	0.00%

Significant Wave Height, Hs [m]

Figure 5.5.1: Northern California Joint Probability Distribution [4].

Hs, [m]	Peak Period, Tp [s]Tp [s]																
	3.7	4.7	5.7	6.7	7.7	8.7	9.7	10.7	11.7	12.7	13.7	14.7	15.7	16.7	17.7	18.7	19.7
0.25				5.3	6.1			8.7	9.8	11.1	12.3	12.7	13.3		13.4		
0.75	17.4	28.5	39.1	47.6	54.4	61.6	69.6	76.7	85.6	96.1	104.0	99.3	99.7	106.0	115.0		102.0
1.25	48.0	78.6	108.0	133.0	151.0	170.0	190.0	208.0	209.0	246.0	228.0	229.0	229.0	212.0	185.0		178.0
1.75	94.1	153.0	212.0	258.0	291.0	314.0	321.0	320.0	317.0	366.0	339.0	367.0	264.0	348.0	293.0		325.0
2.25		253.0	345.0	418.0	465.0	470.0	474.0	468.0	485.0	482.0	470.0	481.0	430.0	438.0	465.0		480.0
2.75			508.0	589.0	656.0	656.0	613.0	601.0	614.0	661.0	573.0	617.0	587.0	574.0	520.0		528.0
3.25			672.0	799.0	843.0	864.0	840.0	740.0	764.0	684.0	760.0	692.0	649.0	671.0	672.0		697.0
3.75				1020.0	1070.0	1010.0	921.0	894.0	923.0	920.0	877.0	865.0	845.0	854.0	860.0		829.0
4.25					1290.0	1220.0	1030.0	1060.0	1090.0	1040.0	1120.0	1010.0	1020.0	931.0	882.0		974.0
4.75						1390.0	1270.0	1260.0	1200.0	1220.0	1180.0	1110.0	1200.0	1140.0	1080.0		1140.0

Figure 5.5.2: Mechanical Power Matrix with MPC.

The mechanical power matrix was then modified to account for a uniformly applied 85% efficiency, a rated power of 1500kW and a cut off sea state of 5m Hs and greater. Per AEP calculation guidance [4] a 10% array loss and 95% availability were then applied. These modifications were identical to those applied to the Baseline Mechanical Power Matrix.

A final AEP of 3054MWh/yr was reached for the MPC enabled WEC, a 161% improvement or 2.61 times larger than the baseline AEP.

With respect to the unconstrained nature of the PTO constraints used for this performance evaluation, it should be shown that the PTO stroke maintained realistic throughout the simulation.
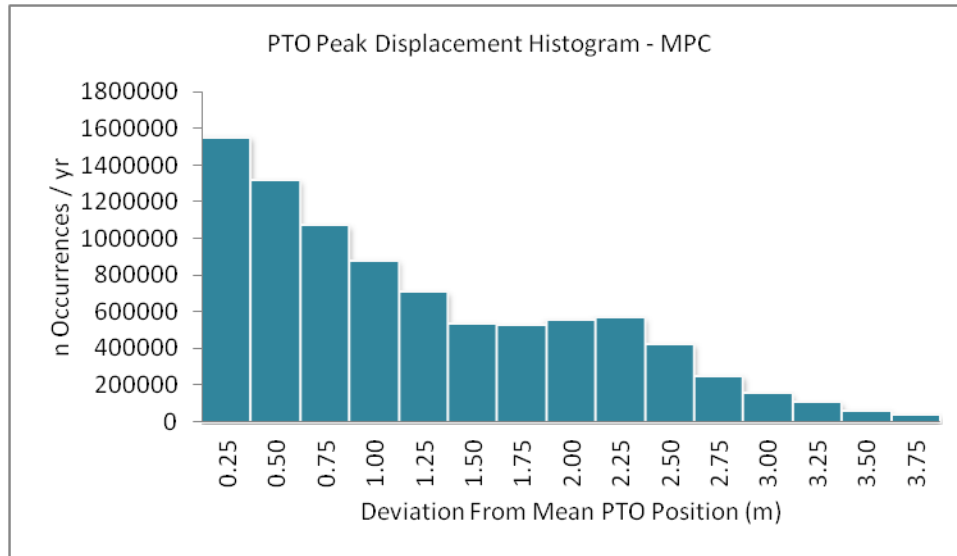
Figure 5.5.3: Peak PTO displacement histogram by occurrence annually.

The figure above demonstrates that, while unrestricted, the PTO stroke stayed within a reasonable bound. Furthermore, if a constraint were applied, the AEP would only be minimally affected.

5.5.2 Operational Loads:

5.5.2.1 Operational Loads Methodology:
Once again, for the comparative assessment of Centipod's loads with and without MPC, the loads on the various WEC components were calculated (and output) within WaveDyn for all the elements in the structure. For the Centipod machine, the loads on the pods, mooring loads and loads on the PTO are considered the outputs of most interest. A statistical analysis of the loads has been performed (min, max, mean, standard deviation). The non-exceedance curves for the various sea states have also been calculated. The use of this type of output allows a good understanding of the various loads levels experienced by the WEC components. It also provides a useful way to compare the influence on the loads of changing the WEC configurations. The use of these cumulative probability curves can also be used at a later stage for loads extrapolation and fatigue analysis.

5.5.2.2 Operational Loads Results:
Loads were analyzed and post processed for a number of nodes on the Centipod device under baseline operational conditions. The most critical to the structural design, and the load directly influenced by controller choice, is the axial force at each Pod connection. The maximum axial force for each sea state at the central pod, Pod 3, is shown in the figure below.

		Peak Period, Tp [s]															
		3.7	4.7	5.7	6.7	7.7	8.7	9.7	10.7	11.7	12.7	13.7	14.7	15.7	16.7	17.7	18.7	19.7
Hs [m]	0.25				230	280			401	399	487	662	570	668		775		
	0.75	246	358	440	447	551	600	859	972	1025	1026	1031	1034	1028	1036	1021		1019
	1.25	336	631	585	750	863	876	1080	1123	1065	1067	1069	1062	1051	1053	1050		1050
	1.75	515	712	817	952	1108	1100	1115	1098	1114	1091	1075	1072	1059	1081	1050		1053
	2.25		1005	976	1001	1160	1203	1137	1167	1131	1113	1103	1106	1078	1084	1074		1058
	2.75			1033	1186	1234	1215	1206	1164	1157	1133	1112	1123	1107	1099	1093		1082
	3.25			1115	1237	1337	1308	1234	1198	1186	1160	1129	1137	1103	1103	1090		1081
	3.75				1262	1258	1273	1306	1253	1221	1190	1162	1175	1137	1118	1109		1093
	4.25					1353	1375	1313	1277	1207	1218	1192	1161	1159	1168	1151		1126
	4.75				1367	1323	1326	1324	1298	1206	1170	1176	1156	1175				1129

Figure 5.5.4: Maximum axial force [kN] for Pod 3 for all sea states investigated.

When compared to the baseline table of maximum axial force, an increase in loads can be observed. Figure 5.5.5 shows the increase in maximum axial force, MPC relative to baseline.

Maximum Axial Force Increase (%)

		Tp (sec)																
		3.7	4.7	5.7	6.7	7.7	8.7	9.7	10.7	11.7	12.7	13.7	14.7	15.7	16.7	17.7	18.7	19.7
Hm0 (m)	0.25				248%	259%			435%	565%	712%	1041%	918%	944%		1236%		
	0.75	73%	84%	132%	140%	169%	170%	300%	330%	423%	432%	431%	505%	401%	502%	504%		575%
	1.25	76%	65%	67%	115%	125%	158%	283%	193%	280%	287%	256%	318%	279%	238%	275%		289%
	1.75	49%	80%	49%	125%	130%	133%	157%	151%	172%	143%	173%	205%	196%	179%	187%		234%
	2.25		48%	27%	53%	93%	74%	91%	97%	92%	142%	117%	77%	109%	143%	134%		171%
	2.75			16%	36%	77%	90%	73%	55%	56%	86%	94%	101%	84%	75%	99%		124%
	3.25			-10%	42%	49%	51%	53%	49%	36%	80%	41%	51%	93%	72%	81%		107%
	3.75				28%	35%	39%	36%	54%	46%	55%	35%	50%	62%	59%	46%		81%
	4.25					13%	19%	43%	18%	36%	38%	25%	65%	46%	41%	36%		60%
	4.75						15%	22%	19%	7%	13%	-4%	21%	47%	31%	40%		17%

Figure 5.5.5: Relative maximum axial force [kN] for Pod 3 for all sea states investigated.

The most significant load increases occur primarily in small significant wave height sea states. This is tied to the MPC enabled system's capability of better extracting energy from smaller sea states, thus larger forces are observed. Critically, the maximum forces in the higher energy sea states only show minor increases in MPC relative to baseline. This, coupled with the knowledge that most of the ultimate loads will occur in extreme sea state conditions, rather than operational loads, lead to the conclusion that the implementation of MPC will not have a significant impact on any ultimate load driven structural requirements.

Cyclic loading and fatigue driven design requirements, however, will be significantly impacted by the implementation of MPC. The following, Figure 5.5.6, shows the annual loading histogram with MPC and baseline.
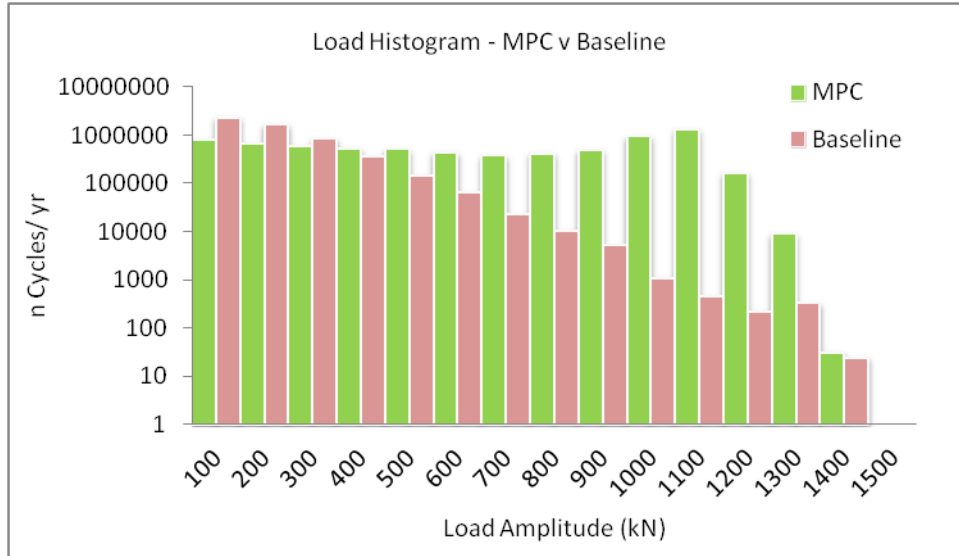
Figure 5.5.6: Load histogram by annual occurrences.

Figure 5.5.6 was produced by using the WAFO Toolbox for MATLAB [5] recording the peak force of each wave in each 200*Tp time series per sea state. All 190 sea states were multiplied by their occurrence probability in the JPD to reach an annual number of cycles for each load bin shown in the histogram. This loading histogram was then used in the System Impact analysis, which will be further discussed in Section 5.7, to help identify the impact of MPC on structural requirements of Centipod.

5.6   Task 6.0 - Extreme sea state load calculations

5.6.1 Methodology:

A proper investigation into Extreme Conditions Modelling (ECM) requires identification of load cases through analysis various sea states and modes of operation in a mid-fidelity tool such as WaveDyn or WECSim, followed by a thorough study of these load cases with a high-fidelity (CFD) tool. This project does not allow for the full scope of a complete ECM study. Thus only the identification of load cases and relative loading between modes of operation will be completed in a mid-fidelity tool (WaveDyn). It is especially of interest how extreme loads of a baseline (fixed damping control) Centipod WEC compare to the same WEC employing 'detuned' MPC control. The results of this study will be adequate for roughly quantifying the relative loading of these techniques, but will fall short of what is needed to complete a structural design of the Centipod WEC.

The procedure for this study is broken down into five stages:
1) Identify the candidate sea states
2) Determine the number of seeds required
3) Investigate various wave headings (using baseline)
4) Identify the load cases of interest

Identify the candidate sea states: The site considered for all work undergone in this project was the DOE LCOE reference site in Northern California. This site's 100 year wave contour was

published by Sandia National Labs in *Extreme Ocean Wave Conditions for Northern California Wave Energy Conversion Device* [6].
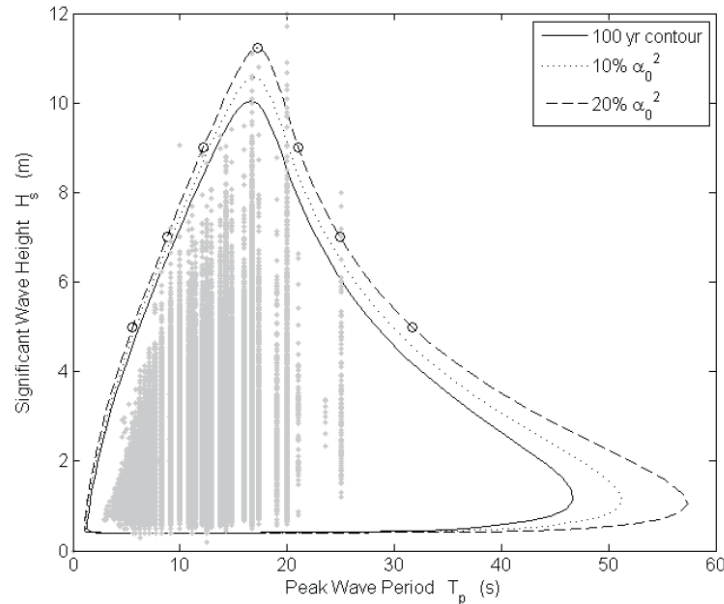
Significant wave height Hs (m)	5	7	9	11.22	9	7	5
Peak period Tp (s)	5.57	8.76	12.18	17.26	21.09	24.92	31.70

Figure 5.6.1: 100 yr. wave contour with candidate sea states [6].

Each of the sea states of interest along this contour was modelled with differing wave directions. The sea state and direction combinations yielding the highest loads were used for comparison with the MPC model variant.

Determine the number of seeds required: A convergence study was conducted to determine the number of seeds required for a good representation of each sea case. A seed is used to randomly generate a time series of wave elevation given significant wave height (Hs) and peak period (Tp). If the seed is the same, it will generate the same time series repeatedly, however each time series is created using a randomly generated seed and thus a random time series results. All the simulations used a time series duration of 200*Tp, thus the number of seeds required represents the number of randomly generated waves within a sea state required to converge upon a set of results.

A model was run through WaveDyn under a certain sea state (Hs, Tp, and direction) the results were then post-processed in MATLAB using the Wave Analysis for Fatigue and Oceanography (WAFO) toolbox [5] to identify each peak within the time series.
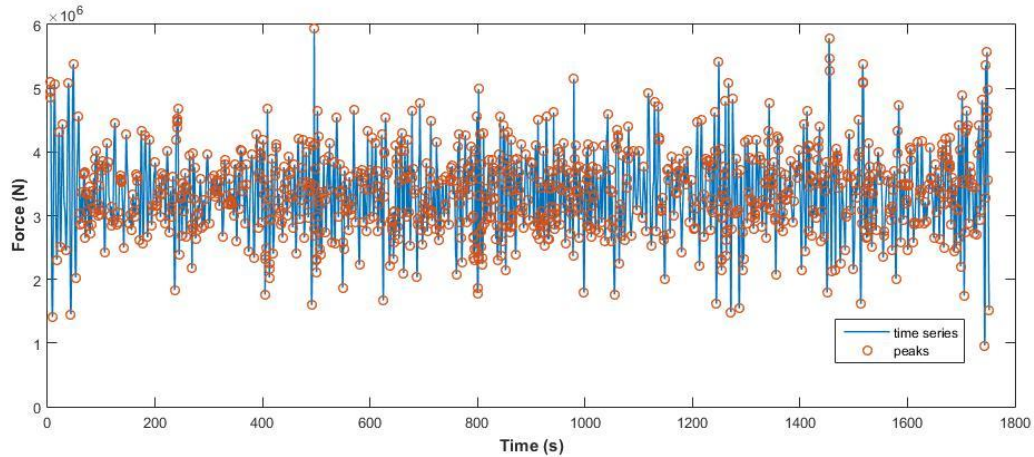
Figure 5.6.2: Peaks identified from time series.

The peaks were collected into a new vector within MATLAB. From the peaks vector, a non-exceedance plot was created to represent the probability of loads occurring for a given sea state.
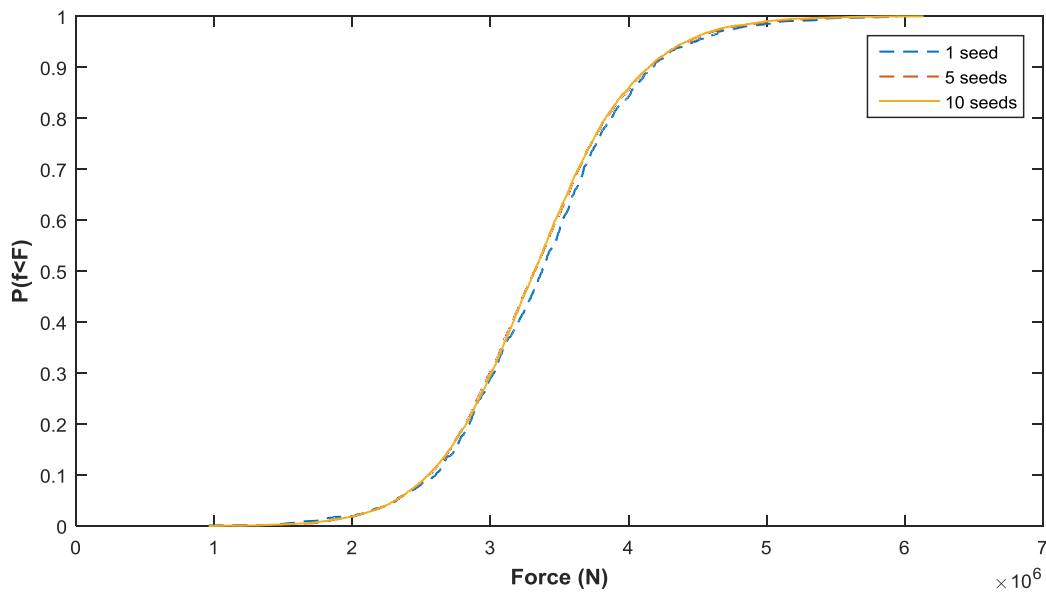
Figure 5.6.3: Non-exceedance plot of mooring tension for 1, 5, and 10 seeds.

From the results of this plot it can be seen that the load probability converges around 5 seeds, with any more seeds leading to a similar result.

Investigate various wave headings (using baseline): 0, 45, and 90 degree unidirectional waves were modelled at a given sea state. The coordinate system is shown along with the results of these three wave direction cases for some loads of interest.
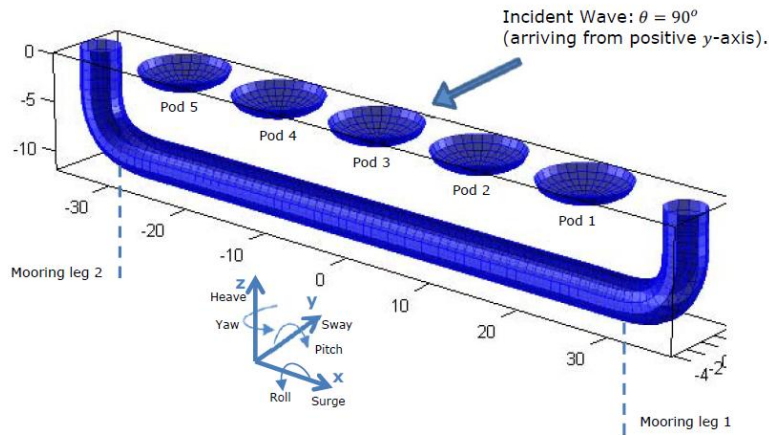
Figure 5.6.4: Coordinate system of Centipod.

The loads of interest in this investigation were:
1) Mooring line tension
2) PTO force in the heave direction (Pod 3 was used)
3) Pitch Moment at Pod Hinge connection (Pod 1 was used)

These loads are shown on the diagram below:
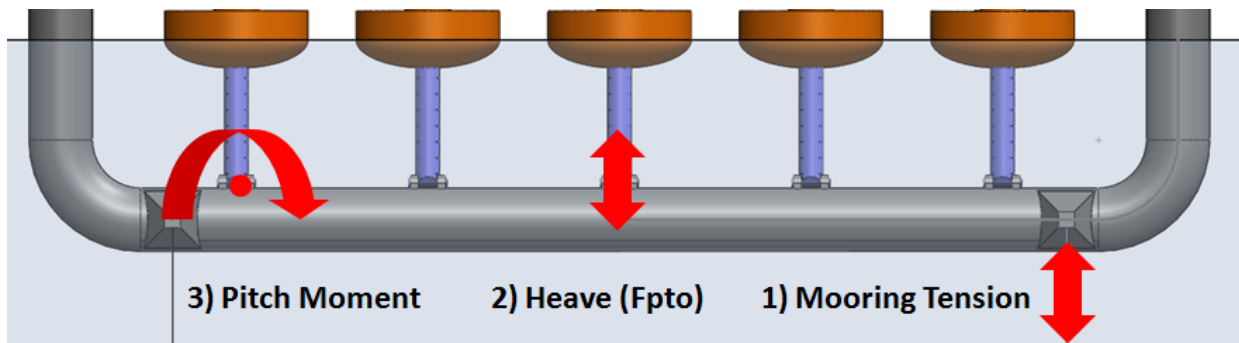
Figure 5.6.5: Visual representation of loads considered.
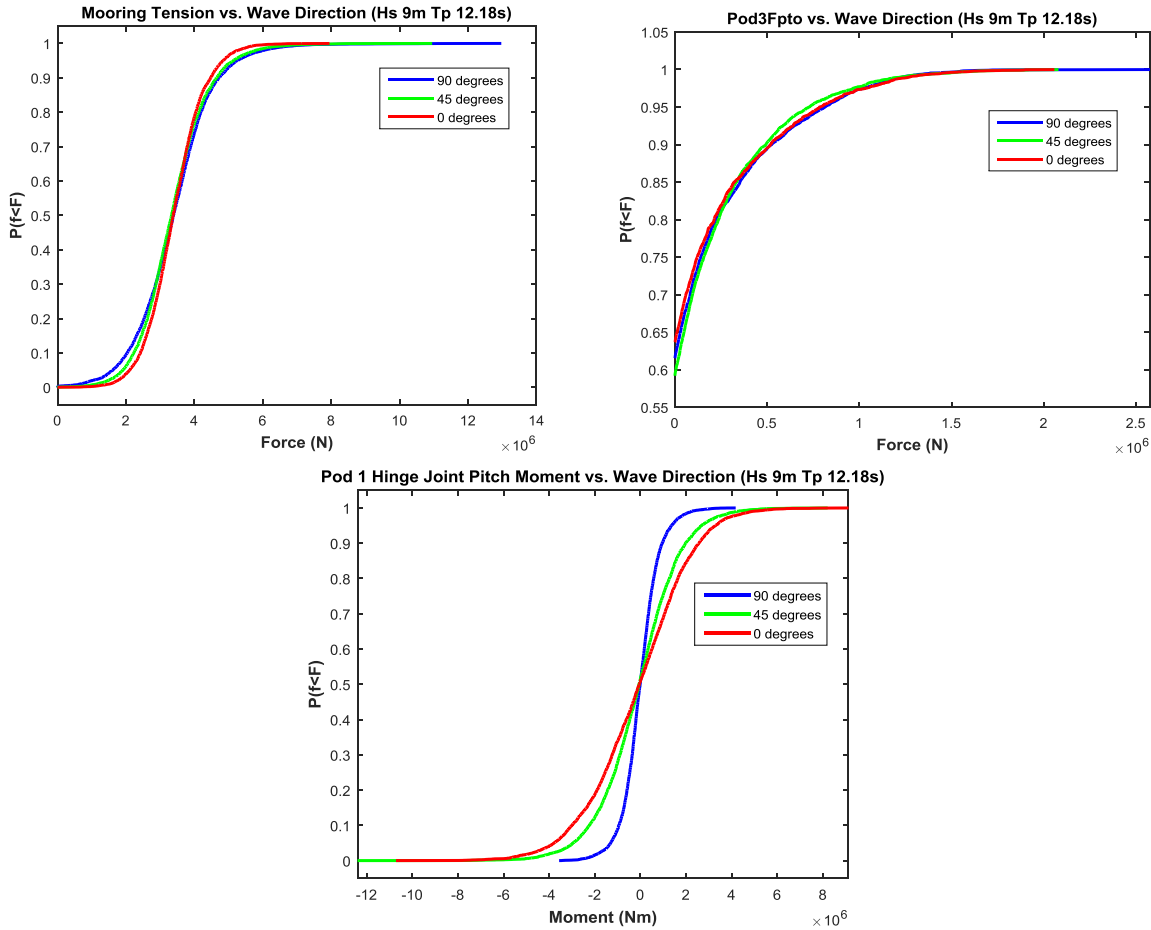
Figure 5.6.6: Non-exceedance plot of:
1) mooring tension for 90, 45 and 0 degree wave directions.
2) Fpto (in heave direction) for 90, 45 and 0 degree wave directions.
3) Pitch moment at Pod 1 hinge joint for 90, 45 and 0 degree wave directions.

Figures 5.6.6 -1 and 5.6.6 -2 show that a wave direction of 90 degrees (incident wave broadside to backbone) results in the highest loads. Meanwhile, Figure 5.6.6 -3 showed the largest moments on the hinge joint (Pod/Backbone connection) with a 0 degree wave direction. Consequently, the most interesting wave direction to investigate for purposes of extreme loading in the heave direction was the broadside, 90 degree, wave, while 0 degree waves were used to assess extreme loading in the case where pitch direction moments are the load of interest.

Identify the load cases of interest: Using a 90 degree wave direction for heave direction loads and a 0 degree wave direction for pitch moments, each candidate sea state on the shorter period side of the 100 year contour was run.

Significant wave height Hs (m)	5	7	9	11.22
Peak period Tp (s)	5.57	8.76	12.18	17.26

Table 5.6.1: Candidate sea states.

The following figures show the results of each sea state on the load cases of interest (Fpto Pod 3, Mooring line tension, Pitch moment at pod connection).
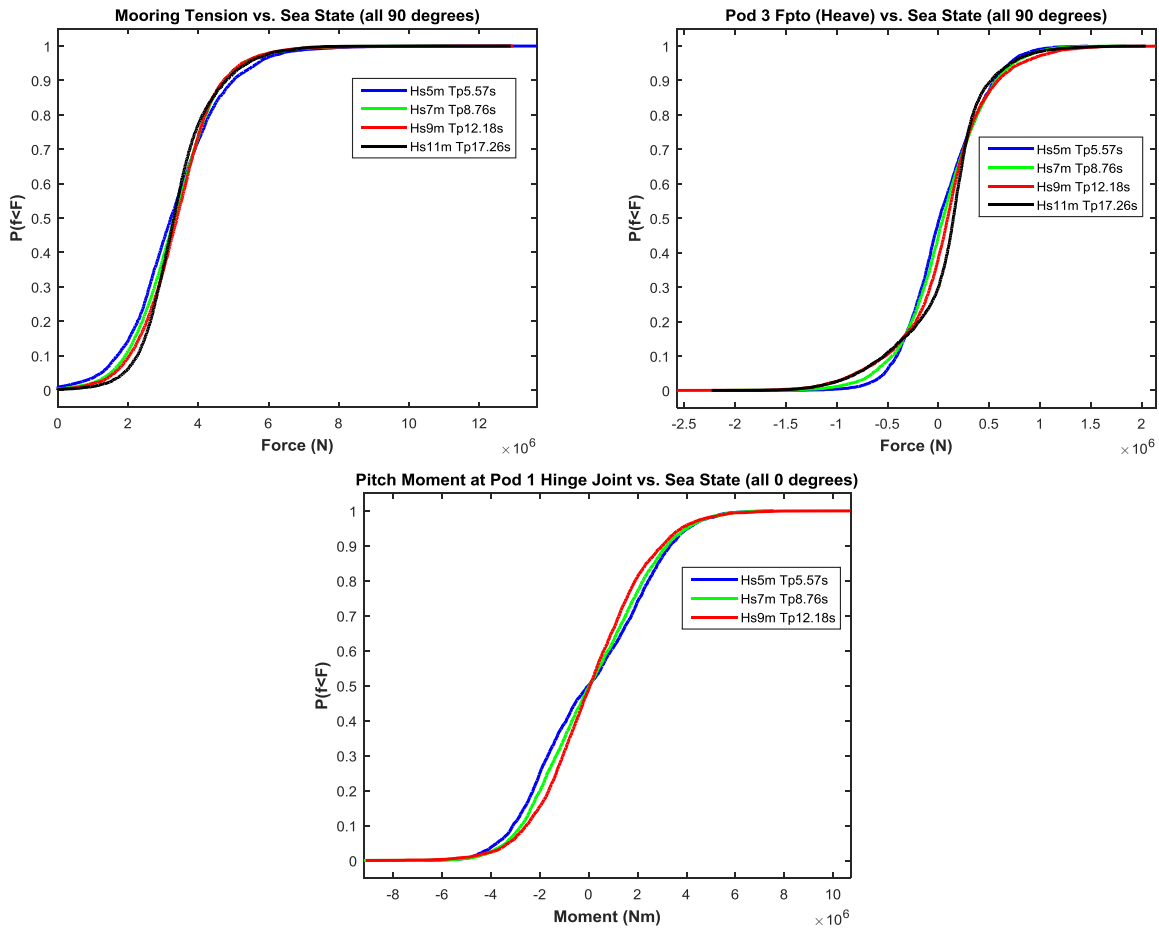
Figure 5.6.7: Non-exceedance plot of:
1) Mooring Tension for Pod 3 for candidate sea states.
2) Fpto for Pod 3 for candidate sea states.
3) Pitch moment at Pod 1 hinge joint for candidate sea

Figure 5.6.7 -1 above shows the non-exceedance of tension in a mooing line of Centipod, which has a pre-tension of approximately 3.3×10^6 N. The smallest, shortest period sea state, Hs5m, Tp5.57s shows the greatest likelihood of large deviations from the pre-tension as well as the largest individual tensions. This sea state will be of most interest when comparing the effects of MPC and load shedding to baseline.

Of the sea states depicted in Figure 5.6.7 -2, above, Hs9m, Tp12.18s is of most interest. This sea state exhibits both the highest probability of moderate to large loads as well as the largest individual loads.

The moments applied to the pod hinge joint in the pitch direction are shown in Figure 5.6.7 -3 above. The Hs5m, Tp5.57s sea results in a higher probability of moderate loads compared to the larger Hs9m, Tp12.18s sea state. However, the larger sea results in the largest overall moments, and is ultimately of more interest.

5.6.2: Baseline vs MPC

When MPC is applied and the cases of interest are re-run we see a significant reduction in loads. In the case of Fpto Heave force on Pod 3, MPC was run with two tunings, of controller action cost: the operational tune of R = 1e-3 and a "De-Tuned" variant which makes controller action cost one order of magnitude more, R = 1e-2. The results of these runs are shown below.
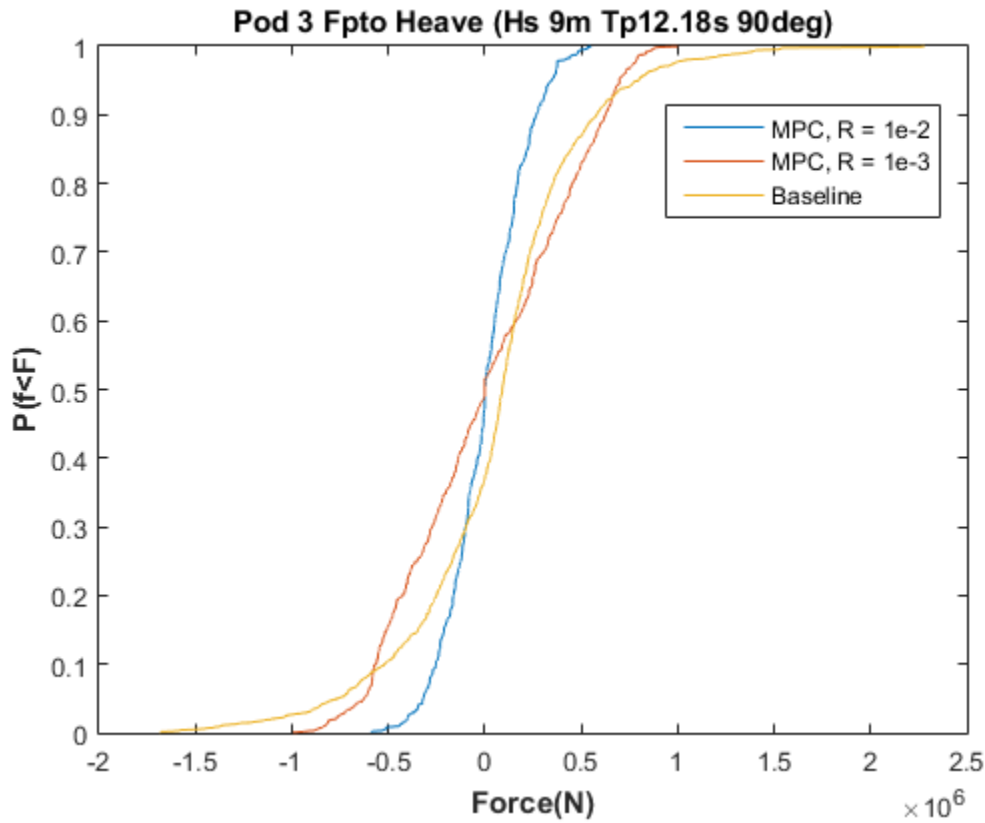
Figure 5.6.12: Pod 3 Fpto non-exceedance plots for baseline and with two tunings of MPC.

As can be seen in Figure 5.6.12, MPC drastically reduces loads. With the operational tune, ultimate loads are reduced approximately 50%, while they are reduced approximately 75% with the "De-Tuned" controller. This shows great promise for the method of controller "De-Tuning".

Of important note with all three methods shown, is the fact that PTO stroke end stops are not applied to this model. Thus, the Pods are free to heave without a position limit, a behavior that is not realistic. In all three cases above, the Pod heaves with amplitude much larger than would typically be allowed in a WEC. This underscores the importance of devoting a much more in-depth study to extreme condition response, which can fully model realistic considerations and utilize high fidelity tools such as CFD. Of particular interest in future work regarding controller use for extreme condition response will be constraint handling. A de-tuned controller may reduce loads on the WEC, but it is less capable of maintaining stroke constraints as well.

Comparisons were also made for the other two loads making up the baseline set.
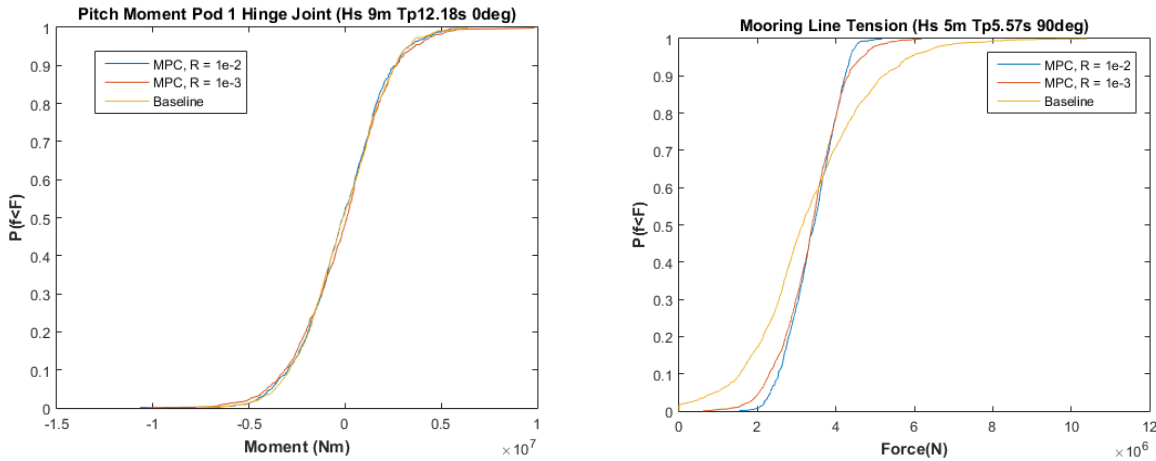
Figure 5.6.13: Non-exceedance plots of baseline and with two tunings of MPC for:
1) Pod 1 Hinge Moment
2) Mooring Line Tension

Figure 5.6.13 -1 shows that the implementation of MPC has little effect on the moments at the Pod's connection point to the backbone compared to the baseline. Meanwhile, in Figure 5.6.13 - 2, the impact on mooring tension is similar to that seen in Fpto.

In addition to reducing ultimate loads in the mooring lines, utilization of MPC, and further de-tuned MPC also reduces the chances of slack mooring line conditions. This is critical to reducing the probability of failure in the mooring lines since snap loads are unlikely.

5.7 Task 7.0 - Perform impact analysis

A 161% improvement in AEP was shown to be possible with the implementation of MPC, however, the impact of this performance improvement must be accounted for across the system in order to quantify the performance metrics, and ultimately the LCOE impact.

5.7.1 LCOE
LCOE is calculated with an FCR of 0.108 and the standardized formula of:

$$LCOE = \frac{ICC * FCR + O\&M}{AEP}$$

Where:

ICC – Installed Capital Cost ($)
FCR – Fixed Charge Rate
O&M – Operations & Maintenance ($/yr)
AEP – Annual Energy Production (MWh/yr)

In the above formula, ICC and O&M come from a modified version of the Aug 1, 2014 version of NREL's Cost Breakdown Structure (CBS) template [7]. Meanwhile, the AEP was calculated as described in Sections 5.3 and 5.5.

The CBS holds the cost breakdown of the WEC down to a component level within the machine itself as well as the costs allocated for the balance of system.

5.7.1.1 Cost of the Machine

The cost of the machine itself is largely stable between the baseline and resulting design iterations. With the implementation of the MPC controller, larger operational loads are applied to the structure. Evaluation was required from a structural standpoint to confirm the structural impact of this load increase.

As described in Section 5.5, the increased loads resulting from MPC do not increase the ultimate loads, but rather the magnitude of cyclic loading on the structure. Therefore, the structural impact of MPC is primarily a concern for fatigue analysis. Furthermore, the analysis should focus on the backbone since this serves as the common structure through which all PTO loads are transmitted to the moorings, and it comprises 51% of the WEC's structural mass, making its structural design particularly impactful on overall LCOE.
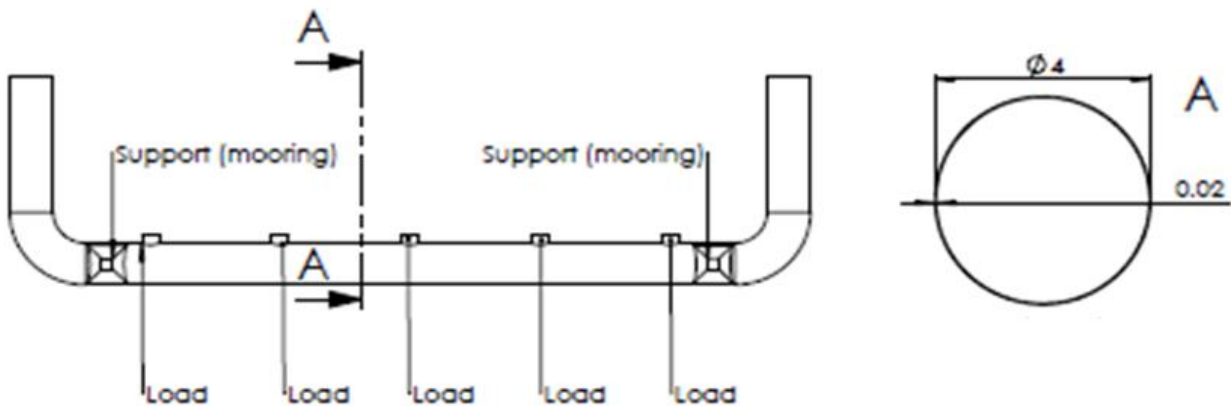
Fig 5.7.1: Backbone Structure

A cumulative damage approach was used to evaluate the loading on the backbone with and without MPC. A loading histogram was produced by recording the peak force of each wave in each 200*Tp time series per sea state. All 190 sea states were multiplied by their occurrence probability in the JPD to reach an annual number of cycles for each load bin.

The loads were then applied to as shown in Figure 5.7.1. Using the cross-sectional geometry parameters of the horizontal span of the backbone, stress was calculated for each load bin creating a histogram of stress magnitude cycles annually for baseline and MPC.
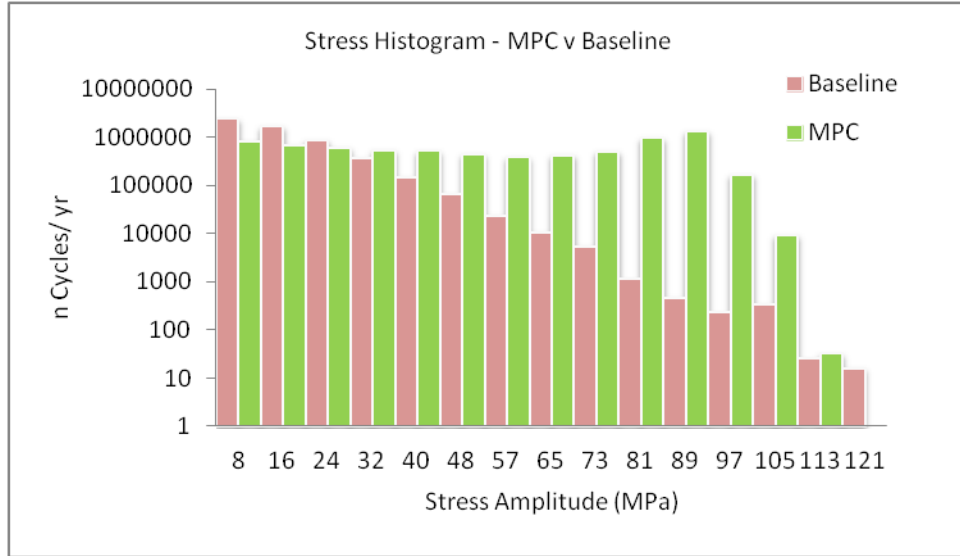
Fig 5.7.2: Stress histogram, MPC vs. Baseline.

Finally, cumulative damage theory was used to evaluate the life of the horizontal span under each of the two loading profiles. The Palmgen/Miner Rule (below) was applied.

$$\sum \frac{n_i}{N_{fi}} = \frac{n_1}{N_{fi}} + \frac{n_2}{N_{f2}} + \text{........} = 1$$

This method calculates the number of cycles allowable for each bucket of the stress histogram summing the buckets together to reach a combined value for life. The number of allowable cycles is a function of stress amplitude as defined by the particular Stess/Number of Cycles (SN) curve.

The SN curve for high strength steel with cathodic protection in seawater was used to evaluate the fatigue life of the base material of the backbone. This SN curve came from the DNV & Carbon Trust Guidelines on Design and Operation of Wave Energy Converters [9].
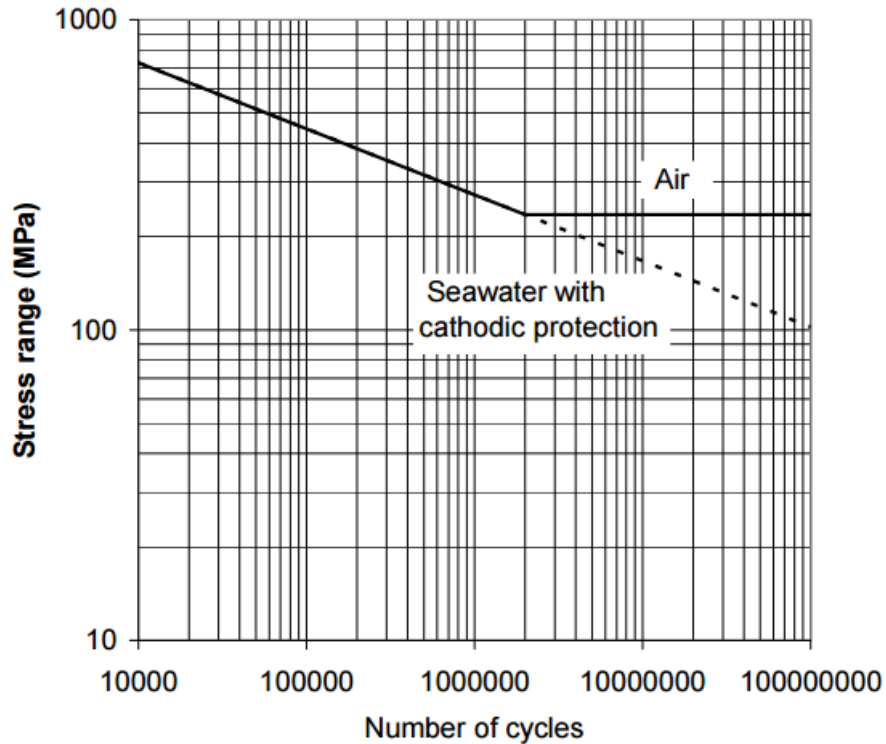
Fig 5.7.3: SN curve for high strength steel with cathodic protection in Seawater [9].

The resulting lifespan of the backbone base material for the MPC load set was 76 years, well beyond the 20 year design life. Fatigue will need to be continually re-assessed as the structural design matures and greater detail is specified as to potential stress concentrators such as joints and welds. While an important consideration due to the increase in stress amplitude over numerous cycles per year, fatigue was not ultimately a structural design driver in this specific analysis. Therefore, there was no resulting structural impact directly due to the operational loads increase.

The PTO cost was another aspect which needed to be assessed with respect to the WEC capital cost. The PTO required for MPC was scaled up to meet the increased mean and rated power. This project focused on the improvements possible with MPC without the constraints of any specific PTO system. As a result, the PTO has been generalized for this analysis. A cost per kW rated is applied to reach the PTO cost for this CBS. The methodology for this cost is identical to that of the Balance of System costs described in Section 5.7.1.2.

5.7.1.2 Balance of System

The following Balance of System Costs were assessed using industry data on a $/kW basis. The main source of data for this work was *The future potential of wave power in the United States* [8].
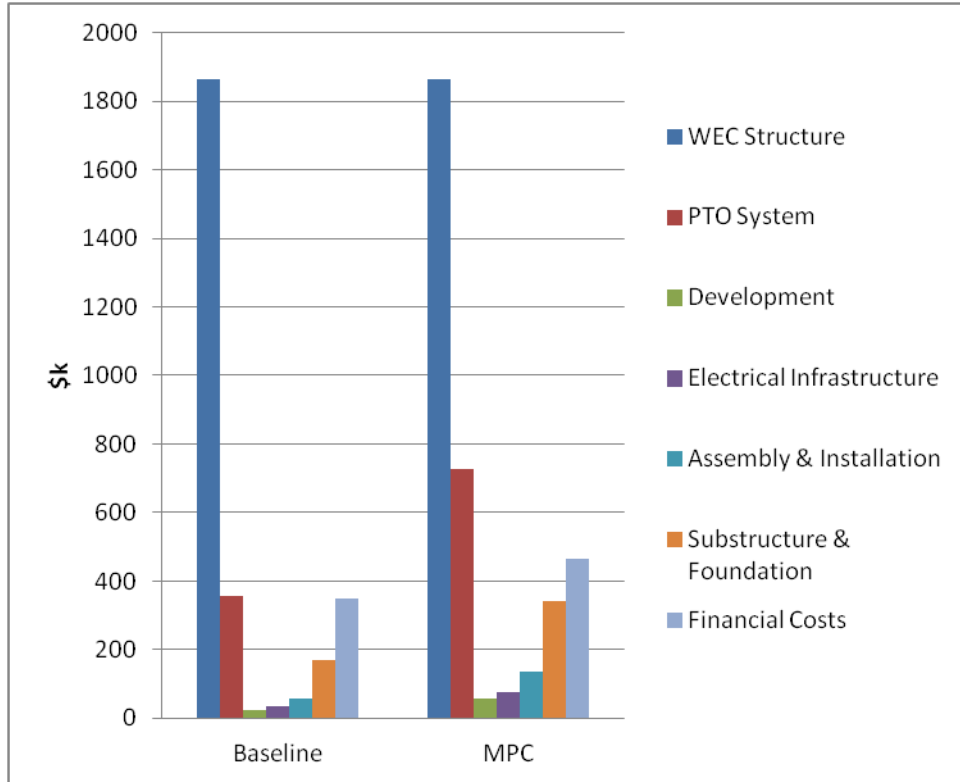
Fig 5.7.4: Balance of System Costs

Development - The development costs include all activities from project inception to financial close, where financial close is the date when project and financing agreements have been signed and all the required conditions have been met.

Electrical Infrastructure - All electrical infrastructure to collect power from generators and deliver to the grid.

Assembly and Installation - Captured within the *Assembly and Installation* category of the cost breakdown was the transport of the WEC and piles to site, installation of piles and the installation of the WEC on its moorings.

Substructure and Foundation - Captured within the *Substructure and Foundation* category of the cost breakdown was the capital expense of the piles and mooring lines themselves.

Financial Costs - Financial costs are comprised of insurance, finance, and contingency costs. These costs are functions of the other capital cost categories, thus an increase in any other capital cost will result in an increase in the financial cost.

5.7.2 AEP

AEP was calculated per the DOE's *Standardized Cost and Performance Reporting for Marine and Hydrokinetic Technologies (2014).* Each tab on the AEP calculation Excel document is labeled corresponding to the numbered reporting requirements (pg. 9-10). Of most importance in this work is the mechanical power matrix, which was produced according to specification (i.e.

200*Tp time series simulation of a Bretschneider spectrum for each bin of the resource JPD). It should be noted that the reference resource used in this project is the (Tp-Hs) JPD associated with the 2013 guidance document as this was the most recent at project start and was used throughout for consistency.

5.7.3 PWR

Power to weight ratio (PWR) was calculated on Centipod before and after the implementation of MPC. Mean power increased 161% while the structural mass of Centipod remained constant. The resulting PWR impact was then the calculated using the baseline mass and power, and the MPC mass and power yielding a 161% increase in PWR.

5.7.4 Summary of Metrics

A summary of the System Performance Advancement metrics is shown in Figure 5.7.5 below:

Metric	Baseline	Proposed Improvement	Value after project completion	Achieved Improvement
AEP (MWh/year)				
Whole Centipod (5 pods) - NorCal resource	1170	95%	3052	161%
LCOE ($/kW-h)				
260000MWh/yr array scale at DOE LCOE ref resource	0.375	35%	0.187	50%
PWR (W/kg)				
Mean power (W) structural mass (kg)	0.255	10%	0.665	161%

Fig 5.7.5: System Performance Advancement Metrics Table

The proposed system performance metrics in this project were exceeded by a large margin resulting in an AEP 2.6 larger than baseline, with LCOE cut in half.

5.8   Task 8.0 - Design real-time implementation of MPC controller

The aim of this task was to confirm that the controller created in this project could be run on an embedded micro-controller for practical implementation in a wave energy converter (WEC). Most of the experience with wave energy converters has been in laboratory setting with PC based control or field testing with limited controls capability. Embedded micro-controllers to implement model based controls in wave energy application will require high performance for closed loop control tasks, process control and signal processing, as well as extensive communication protocols. A large memory is required for storing all data safely and in the event of a power failure; critical data should be stored in non-volatile data memory.

Figure 5.8.1: Bachmann MC210 processor module

Embedded micro-controllers have traditionally been limited in CPU speed and memory to implement model predictive control. Limited power and cooling means limited computational resources for computationally intensive numerical optimization with hard real-time constraints that normally rely on the accuracy of floating-point arithmetic. Embedded controller CPU clock speeds range from 40 MHz to 600 MHz with limited memory. Recent advances in embedded controller have pushed the CPU

speeds to 1700 Mh. An example of this is the Bachmann MC210 module that uses Intel Atom processor with clock speed of up to 1.6GHz and a 1GB RAM.

The MPC implementation used a controller time step of 0.5 seconds. The embedded controller needs to be able to carry out the computation at each step faster than the controller time step to be functional for field implementation. Additional tasks such as data acquisition, communication and monitoring will also need to be performed in addition to controller calculation. The scope for the current project was limited to development of model predictive control in simulation and implementation on an embedded controller was not done. In order to evaluate the practicality of implementing this controller on an embedded micro-controller, an alternative method was devised. Real-time implementation of MPC controller was evaluated by simulating the controller on a desktop PC by artificially reducing CPU speed.

To control CPU speed, a tool called BES was used for limiting the CPU speed. BES is a tool that has been developed in the gaming community to limit the CPU usage of certain processes to improve the allocation of CPU to memory and CPU intensive games. BES was used to limit the percent of CPU being used by the MPC controller executable. It is slightly complicated and somewhat inaccurate to benchmark the task based on the clock speed of the CPU on a PC. A PC is performing multiple tasks including running Windows services and other background processes. Fortunately, Windows provides an estimate of the percent CPU usage per task. This was used to evaluate the actual CPU used by the executable and it is assumed that a dedicated processor on an embedded controller will spend 100% processing capacity on calculating the control action.

The simulations were run on a notebook using AMD A6-5350 – 2.9Ghz dual core with 1 GB cache. The MPC controller executable with a simple plant model was run for three different throttle speeds. In the baseline case, with no throttle, the executable used an average of 20% CPU and hence the baseline case can be estimated to be run a 580 Mhz processor. With increasing throttle, the percent CPU used by the executable was reduced increasing the processing time. As can be seen in Table 5.8.1 for a sea state with 8.7s time period and 1.25m significant wave height (Tp: 8s, Hs: 1.25m), the controller worked within the MPC controller time step of 0.5s for CPU speeds greater than 300Mhz. With a 600Mhz processor such as Bachmann MC205 series, the controller will have enough overhead to perform ancillary tasks in addition to solving the model predictive control problem even in high sea state cases where controller may take additional time to solve the optimization problem to avoid exceeding the constraints.

CPU Speed	CPU Time/ Controller step
580 MHz	0.13 s
435 Mhz	0.26 s
290 Mhz	0.52 s

Table 5.8.2: Controller step computational times by CPU speed.

Even though this benchmarking study was not done on an embedded processor, the exercise above demonstrates that the MPC implementation for wave energy converter is very likely feasible on modern embedded controllers. Dehlsen Associates and its partners are continuing to develop this technology and hope to demonstrate the benefits of MPC controller in tank test in the near future using actual hardware.

6.0   Accomplishments

This project proved the merit of MPC from both an AEP and LCOE standpoint, exceeding the performance advancement targets for all project metrics. The LCOE benefit in particular is impactful to the development of Centipod and other WECs, as it shows MPC could be a means of driving the LCOE of Wave Energy Converters down to a competitive level if such control schemes are implemented.

In addition to proving AEP and LCOE advances through this project, another important outcome is the confirmation that implementation of MPC is possible without any upstream sensors. Fe estimation and prediction using only the historical Fpto, velocity, and position time series was achieved in this work. This accomplishment will mean control systems such as this may be easily implemented with existing sensor packages.

7.0   Conclusions

The project showed a 161% improvement in the AEP for the Centipod WEC when utilizing MPC, compared to a baseline, fixed passive damping control strategy. This improvement in AEP was shown to provide a substantial benefit to the WEC's overall Cost of Energy. Furthermore, through the CPU benchmarking work, it has been demonstrated at high level that such a control scheme is implementable in the real world, and will yield substantial performance achievements when tested at scale in real environments.

Being that this work focused on the potential of MPC, and the PTO constraints were relaxed, a challenge facing implementation of the MPC strategy studied in the work is finding a balance between performance improvement and the limitation of constraints applied, such as maximum stroke and PTO force, from an LCOE perspective. Additionally, the development of a Power Take-off (PTO) system capable of providing the necessary reactive power for a reactive control scheme such as MPC will need to be undertaken. These challenges are mild relative to the potential for performance enhancement though the usage of an MPC control scheme, and thus MPC will be pursued into full scale hardware testing by Dehlsen Associates in the continued development of Centipod.

8.0   References

[1]   M. Starrett, R. So, T.K.A. Brekken, and A. McCall, "Development of a State Space Model for Wave Energy Conversion Systems," in IEEE Power and Energy Society , Denver, CO, 2015.

[2]   M. Starrett, R. So, T.K.A. Brekken, and A. McCall, "Increasing Power Capture From Multibody Wave Energy Conversion Systems Using Model Predictive Control," in Technologies for Sustainability (SusTech), 2015 IEEE Conference , Ogden, UT, 2015.

[3]   Livingston, M. and Plummer, A. R., "The Design, Simulation and Control of a Wave Energy Converter Power Take Off," In: 7th International Fluid Power Conference (IFK), Aachen, 2010.

[4]   LaBonte, Alison, et al. "Standardized cost and performance reporting for marine and hydrokinetic technologies." Proceedings of the 1st Marine Energy Technology Symposium (METS13), Washington, DC, USA. 2013.

[5]   Brodtkorb, Pär Andreas, et al. "WAFO-a Matlab toolbox for analysis of random waves and loads." The Tenth International Offshore and Polar Engineering Conference. International Society of Offshore and Polar Engineers, 2000.

[6]   Berg, Jonathan C. "Extreme Ocean Wave Conditions for Northern California Wave Energy Conversion Device" Sandia Natl. Lab. Doc. SAND 9304 (2011): 2011.

[7]   MHK LCOE Reporting Guidance Draft. OpenEI. NREL, 1 Aug. 2014. Web. 9 Dec. 2015. ‹ http://en.openei.org/community/document/mhk-lcoe-reporting-guidance-draft ›.

[8]   Previsic, Mirko, et al. "The future potential of wave power in the United States." US DOE EERE. August (2012).

[9]   DNV "Guidelines on Design and Operation of Wave Energy Converters." Carbon Trust. May (2005).

9.0 Appendices

9.1 Appendix 1 - MPC Controller technical documentation

MPC documentation

Copyright Ted Brekken, Micheal Starrett, and Ratanak So, 2016

Created: Feb 2014
Modified January 21, 2016

1 Overview
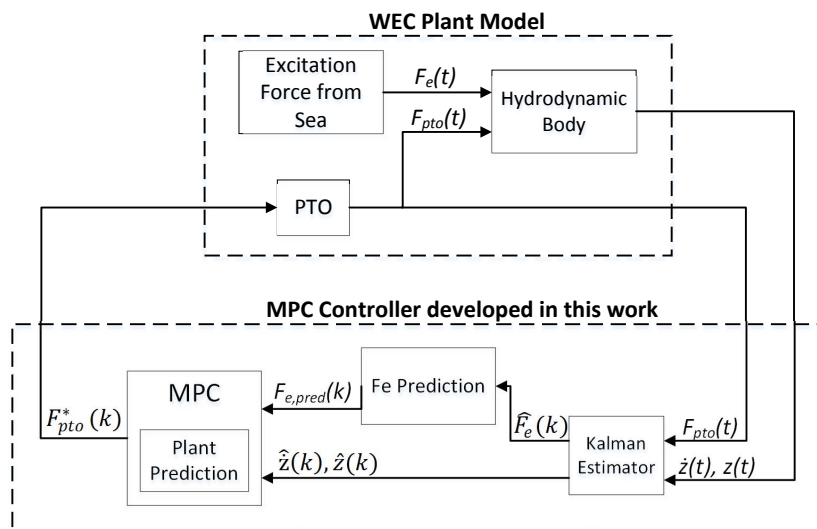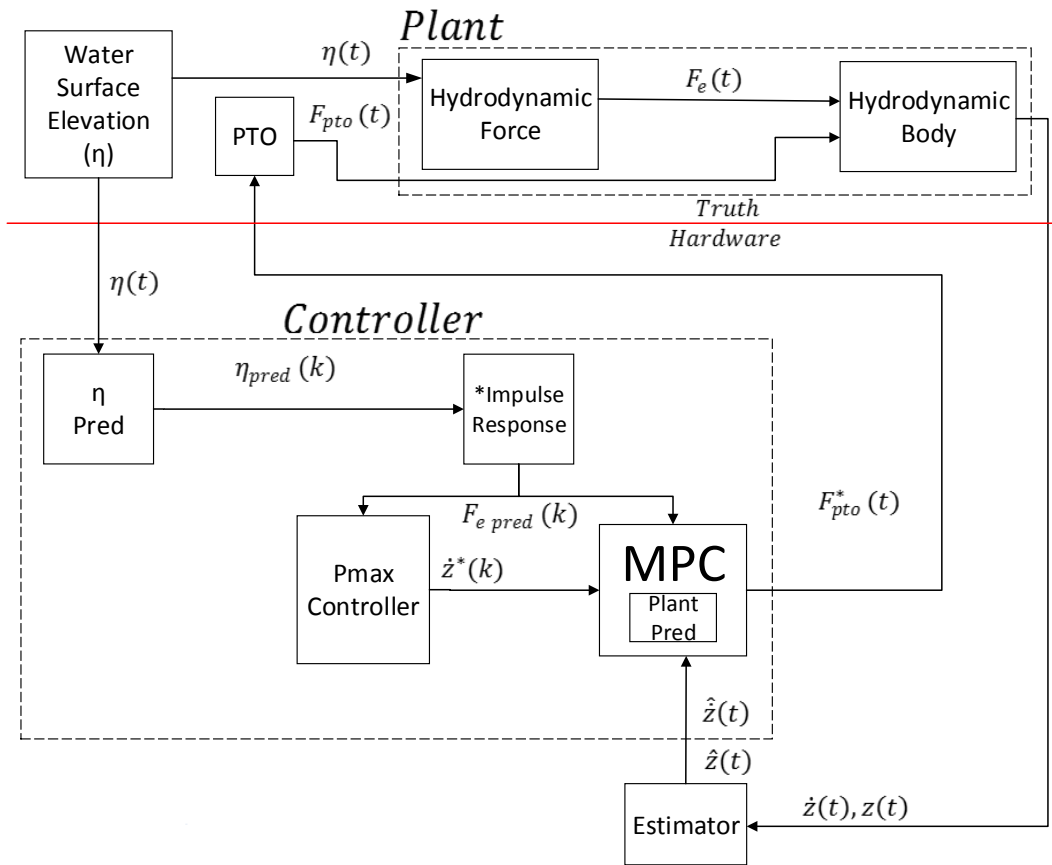
2   Hydrodynamic Force Model

- Description: Impulse response of water surface elevation to excitation force for a specific body geometry. Magnitude and phase of excitation force come from WAMIT. Typically non-causal (Falnes p. 142).

- Input: η (water surface elevation)

- States:

- Output: F_e (excitation force)

- Parameters: $f(t)$ (impulse response of excitation force)

$$f(t) = \frac{1}{2\pi} \int_{-\infty}^{\infty} \hat{F}_e e^{i\theta} e^{i\omega t} dt \tag{1}$$

$$F_e(t) = \int_{-\infty}^{t} f(t - \tau)\eta(\tau)d\tau \tag{2}$$

3   Hydrodynamic Body Model (Frequency Independent)

- Description: Frequency independent approximation of body speed and velocity. Used for initial development and augmented to include frequency dependence in final deliverable, as described in a subsequent section.

- Inputs: F_e (excitation force), F_{pto} (PTO force)

- States:

- Outputs: body position, body speed

- Parameters:

$$\frac{d}{dt}\begin{bmatrix} \dot{z} \\ z \end{bmatrix} = \underbrace{\begin{bmatrix} \frac{-B}{m+A} & \frac{-k}{m+A} \\ 1 & 0 \end{bmatrix}}_{A}\begin{bmatrix} \dot{z} \\ z \end{bmatrix} + \underbrace{\begin{bmatrix} \frac{1}{m+A} \\ 0 \end{bmatrix}}_{Bu}\begin{bmatrix} F_{pto} \end{bmatrix} + \underbrace{\begin{bmatrix} \frac{1}{m+A} \\ 0 \end{bmatrix}}_{Bv}\begin{bmatrix} F_e \end{bmatrix} \tag{3}$$

4   Fe Prediction Model

- Description: The disturbance F_e can be modeled with an auto regressive model which can be used to predict future values of F_e.

- Input: $\hat{F}_e$ (estimated excitation force)

- States:

- Output: $F_{e,pred}$ (predicted excitation force)

- Parameters:

3

$$F_e(k+1|k) = \alpha_1 F_e(k) + \alpha_2 F_e(k-1) + ... + \alpha_n F_e(k-n+1) \tag{4}$$

$$F_e(k+2|k) = \alpha_1 F_e(k+1|k) + \alpha_2 F_e(k) + ... + \alpha_n F_e(k-n+2) \tag{5}$$

and so on up to

$$F_e(k+Hp|k) = \alpha_1 F_e(k+Hp-1|k) + \alpha_2 F_e(k+Hp-2|k) + ... + \alpha_n F_e(k+Hp-n|k) \tag{6}$$

5 Maximum Power Controller (For Deterministic MPC)

- Description: A desired velocity trajectory as calculated through $V = H_{fv}{}^*F_e$, where the impulse response H_{fv} relates excitation force to body velocity. In the optimal case, the resulting velocity is in phase with F_e, leading to maximum P_{pto}. This approach was investigated initially however an unguided approach was determined to be more ideal and is used in the final deliverable.

- Inputs: $F_{e,pred}$ (predicted excitation force)

- States:

- Outputs: $\frac{d}{dt}z^*$ (desired body speed)

- Parameters:

$$\dot{z}^*(k) = \begin{bmatrix} \dot{z}^*(k+1) \\ \dot{z}^*(k+2) \\ \dot{z}^*(k+3) \\ \vdots \\ \dot{z}^*(k+H_p) \end{bmatrix} \tag{7}$$

6 Impulse Response For Desired Velocity (For Deterministic MPC)

- Description: Calculate an impulse response H_{fv} to be used by the Maximum Power Controller. H_{fv} can be found by first calculating the frequency dependent complex mechanical instrinsic impedence of the body. Then, define the impedence of the PTO as the complex conjugate of the plant to maximize power transfer (in the optimal case). PTO damping will act as the physical embodiment of this impedence. Finally, calculate H_{fv} (typically causal & noncausal).

- Input: Added mass and damping from WAMIT

- States:

- Output: H_{fv}

- Parameters:

First calculate mechanical intrinsic impedence:

$$F_e(s) + F_r(s) + F_b(s) + F_{pto}(s) = sV(s)m \tag{8}$$

$$F_e(s) + F_{pto}(s) = sV(s)\Big(A(s) + m\Big) + V(s)\Big(B(s) + \frac{K}{s}\Big) \tag{9}$$

$$Z_i(s) * V(s) = sV(s)\Big(A(s) + m\Big) + V(s)\Big(B(s) + \frac{K}{s}\Big) \tag{10}$$

$$Z_{i,plant}(s) = s\Big(A(s) + m\Big) + B(s) + \frac{K}{s} \tag{11}$$

Then calculate corresponding PTO impedence for control:

$$F_e(s) = (Z_{i,plant}(s) - Z_{pto}(s))V(s) \tag{12}$$

$$Z_{pto,optimal}(s) = conj(Z_{i,plant}(s)) \tag{13}$$

$$Z_{pto,suboptimal}(s) = abs(Z_{i,plant}(s)) \tag{14}$$

$$Z_{pto,fixed\ dampingl}(s) = abs(Z_{i,plant}(single\ freq.)) \tag{15}$$

Finally, calculate the transfer function $H_{fv}(s)$ which becomes the impulse response after taking the Inverse Fourier Transform.

$$H_{fv}(s) = \frac{1}{Z_{i,plant}(s) + Z_{pto}(s)} \tag{16}$$

As an important note, in the optimal case the PTO cancels the imaginary added mass $A(s)$ and spring m and equals the real damping $B(s)$. Therefore the PTO damping has a component proportional to speed, accaleration, and position per:

$$F_{pto,optimal}(s) = (-s(A(s) + m) + B(s) + \frac{-K}{s})\dot{z} \tag{17}$$

Given that $P = FV$ and, in the optimal case, $F_{pto,optimal}$ is complex, the power will be complex and will result in power being delivered as well as absorbed. In the suboptimal and fixed case, F_{pto} will be completely real and therefore power is only absorbed.

7 PTO Model

- Description: To provide F_{pto}.
- Input: F_{pto}^*
- States: F_{pto}
- Output: F_{pto}
- Parameters: τ

$$\tau \frac{d}{dt} F_{pto}(t) = -F_{pto}(t) + F_{pto}^*(t) \tag{18}$$

$$F_{pto}(s) = \frac{1}{s\tau + 1} F_{pto}^*(s) \tag{19}$$

8 Model Predictive Control (MPC)

- Description: Calculate a command F_{pto} which will maximize power production while respecting machine limits.
- Inputs:
  - Deterministic MPC: $F_{e,pred}$, $\dot{z}^*$ (desired body speed), constraints
  - Unguided MPC: $F_{e,pred}$, constraints
- States:
- Outputs: F_{pto}^*
- Parameters:

8.1 Plant Prediction Model

- Description: To predict future body speed and position.
- Inputs: Current state matrix (e.g. $\dot{z}$, z, *etc.*), current and future excitation force F_e
- States:
- Outputs: Future states at discrete time intervals
- Parameters:

$$\frac{d}{dt} \begin{bmatrix} \dot{z} \\ z \end{bmatrix} = \underbrace{\begin{bmatrix} \frac{-B}{m+A} & \frac{-k}{m+A} \\ 1 & 0 \end{bmatrix}}_{A} \begin{bmatrix} \dot{z} \\ z \end{bmatrix} + \underbrace{\begin{bmatrix} \frac{1}{m+A} \\ 0 \end{bmatrix}}_{Bu} \begin{bmatrix} F_{pto} \end{bmatrix} + \underbrace{\begin{bmatrix} \frac{1}{m+A} \\ 0 \end{bmatrix}}_{Bv} \begin{bmatrix} F_e \end{bmatrix} \tag{20}$$

This model (and the frequency dependent version of it) can be discretized into the form:

$$\mathbf{x}(k+1) = \mathbf{A}\mathbf{x}(k) + \mathbf{B}_u\mathbf{u}(k) + \mathbf{B}_v\mathbf{v}(k) \tag{21}$$

$$\begin{aligned}
\mathbf{x}(k+2) &= \mathbf{A}\mathbf{x}(k+1) + \mathbf{B}_u\mathbf{u}(k+1) + \mathbf{B}_v\mathbf{v}(k+1) \\
&= \mathbf{A}(\mathbf{A}\mathbf{x}(k) + \mathbf{B}_u\mathbf{u}(k) + \mathbf{B}_v\mathbf{v}(k)) + \mathbf{B}_u\mathbf{u}(k+1) + \mathbf{B}_v\mathbf{v}(k+1) \\
&= \mathbf{A}^2\mathbf{x}(k) + [\mathbf{A}\mathbf{B}_u\mathbf{u}(k) + \mathbf{B}_u\mathbf{u}(k+1)] + [\mathbf{A}\mathbf{B}_v\mathbf{v}(k) + \mathbf{B}_v\mathbf{v}(k+1)]
\end{aligned} \tag{22}$$

$$\begin{aligned}
\mathbf{x} &\in \Re^{n_x \times 1} \\
\mathbf{u} &\in \Re^{n_u \times 1} \\
\mathbf{v} &\in \Re^{n_v \times 1} \\
\mathbf{A} &\in \Re^{n_x \times n_x} \\
\mathbf{B}_u &\in \Re^{n_x \times n_u} \\
\mathbf{B}_v &\in \Re^{n_x \times n_v}
\end{aligned} \tag{23}$$

$$\mathbf{y}(k) = \mathbf{C}\mathbf{x}(k) + \mathbf{D}_u\mathbf{u}(k) + \mathbf{D}_v\mathbf{v}(k) \tag{24}$$

In the frequency independent version of the model, the states are the outputs, so C=I.

$$\begin{aligned}
\mathbf{y} &\in \Re^{n_y \times 1} \\
\mathbf{C} &\in \Re^{n_y \times n_x} \\
\mathbf{D}_u &\in \Re^{n_y \times n_u} \\
\mathbf{D}_v &\in \Re^{n_y \times n_v}
\end{aligned} \tag{25}$$

$$\begin{aligned}
\mathbf{y}(k+1) &= \mathbf{C}(\mathbf{A}\mathbf{x}(k) + \mathbf{B}_u\mathbf{u}(k) + \mathbf{B}_v\mathbf{v}(k)) + \mathbf{D}_u\mathbf{u}(k+1) + \mathbf{D}_v\mathbf{v}(k+1) \\
&= \mathbf{C}\mathbf{A}\mathbf{x}(k) \\
&\quad + \mathbf{C}\mathbf{B}_u\mathbf{u}(k) + \mathbf{D}_u\mathbf{u}(k+1) \\
&\quad + \mathbf{C}\mathbf{B}_v\mathbf{v}(k) + \mathbf{D}_v\mathbf{v}(k+1)
\end{aligned} \tag{26}$$

$$\begin{aligned}
\mathbf{y}(k+2) &= \mathbf{C}\mathbf{A}^2\mathbf{x}(k) \\
&\quad + \mathbf{C}\mathbf{A}\mathbf{B}_u\mathbf{u}(k) + \mathbf{C}\mathbf{B}_u\mathbf{u}(k+1) \\
&\quad + \mathbf{C}\mathbf{A}\mathbf{B}_v\mathbf{v}(k)) + \mathbf{C}\mathbf{B}_v\mathbf{v}(k+1) \\
&\quad + \mathbf{D}_u\mathbf{u}(k+2) + \mathbf{D}_v\mathbf{v}(k+2) \\
&= \mathbf{C}\mathbf{A}^2\mathbf{x}(k) \\
&\quad + \mathbf{C}\mathbf{A}\mathbf{B}_u\mathbf{u}(k) + \mathbf{C}\mathbf{B}_u\mathbf{u}(k+1) + \mathbf{D}_u\mathbf{u}(k+2) \\
&\quad + \mathbf{C}\mathbf{A}\mathbf{B}_v\mathbf{v}(k)) + \mathbf{C}\mathbf{B}_v\mathbf{v}(k+1) + \mathbf{D}_v\mathbf{v}(k+2)
\end{aligned} \tag{27}$$

The prediction horizon is H_p.

$$\underbrace{\begin{bmatrix} \mathbf{y}(k) \\ \mathbf{y}(k+1) \\ \mathbf{y}(k+2) \\ \mathbf{y}(k+3) \\ \vdots \\ \mathbf{y}(k+H_p) \end{bmatrix}}_{\vec{\mathbf{y}}(k)} = \underbrace{\begin{bmatrix} \mathbf{C} \\ \mathbf{CA} \\ \mathbf{CA}^2 \\ \mathbf{CA}^3 \\ \vdots \\ \mathbf{CA}^{H_p} \end{bmatrix}}_{\mathbf{S}_x} \mathbf{x}(k)$$

$$+ \underbrace{\begin{bmatrix} \mathbf{D}_u & 0 & 0 & 0 & \cdots & 0 \\ \mathbf{CB}_u & \mathbf{D}_u & 0 & 0 & \cdots & 0 \\ \mathbf{CAB}_u & \mathbf{CB}_u & \mathbf{D}_u & 0 & \cdots & 0 \\ \mathbf{CA}^2\mathbf{B}_u & \mathbf{CAB}_u & \mathbf{CB}_u & \mathbf{D}_u & \cdots & 0 \\ \vdots & \vdots & \vdots & \vdots & \ddots & \vdots \\ \mathbf{CA}^{H_p-1}\mathbf{B}_u & \mathbf{CA}^{H_p-2}\mathbf{B}_u & \cdots & \cdots & \mathbf{CB}_u & \mathbf{D}_u \end{bmatrix}}_{\mathbf{S}_u} \underbrace{\begin{bmatrix} \mathbf{u}(k) \\ \mathbf{u}(k+1) \\ \mathbf{u}(k+2) \\ \mathbf{u}(k+3) \\ \vdots \\ \mathbf{u}(k+H_p) \end{bmatrix}}_{\vec{\mathbf{u}}(k)} \quad (28)$$

$$+ \underbrace{\begin{bmatrix} \mathbf{D}_v & 0 & 0 & 0 & \cdots & 0 \\ \mathbf{CB}_v & \mathbf{D}_v & 0 & 0 & \cdots & 0 \\ \mathbf{CAB}_v & \mathbf{CB}_v & \mathbf{D}_v & 0 & \cdots & 0 \\ \mathbf{CA}^2\mathbf{B}_v & \mathbf{CAB}_v & \mathbf{CB}_u & \mathbf{D}_v & \cdots & 0 \\ \vdots & \vdots & \vdots & \vdots & \ddots & \vdots \\ \mathbf{CA}^{H_p-1}\mathbf{B}_v & \mathbf{CA}^{H_p-2}\mathbf{B}_v & \cdots & \cdots & \mathbf{CB}_v & \mathbf{D}_v \end{bmatrix}}_{\mathbf{S}_v} \underbrace{\begin{bmatrix} \mathbf{v}(k) \\ \mathbf{v}(k+1) \\ \mathbf{v}(k+2) \\ \mathbf{v}(k+3) \\ \vdots \\ \mathbf{v}(k+H_p) \end{bmatrix}}_{\vec{\mathbf{v}}(k)}$$

8.2 Deterministic MPC

Provide a quadratic solver with a pre-calculated velocity trajectory and ask it to find a vector F_{pto} to obtain that trajectory.

$$\vec{\mathbf{y}}(k) = \mathbf{S}_x\mathbf{x}(k) + \mathbf{S}_u\vec{\mathbf{u}}(k) + \mathbf{S}_v\vec{\mathbf{v}}(k) \quad (29)$$

$$\begin{aligned} \vec{\mathbf{y}} &\in \Re^{n_y \cdot (H_p+1) \times 1} \\ \vec{\mathbf{u}} &\in \Re^{n_u \cdot (H_p+1) \times 1} \\ \vec{\mathbf{v}} &\in \Re^{n_v \cdot (H_p+1) \times 1} \\ \mathbf{S}_x &\in \Re^{n_y \cdot (H_p+1) \times n_x} \\ \mathbf{S}_u &\in \Re^{n_y \cdot (H_p+1) \times n_u \cdot (H_p+1)} \\ \mathbf{S}_v &\in \Re^{n_y \cdot (H_p+1) \times n_v \cdot (H_p+1)} \end{aligned} \quad (30)$$

$$J(k) = (\vec{\mathbf{t}}(k) - \vec{\mathbf{y}}(k))^T \mathbf{Q}(\vec{\mathbf{t}}(k) - \vec{\mathbf{y}}(k)) + \vec{\mathbf{u}}(k)^T \mathbf{R}\vec{\mathbf{u}}(k) \quad (31)$$

$$\begin{aligned} \mathbf{Q} &\in \Re^{n_y \cdot (H_p+1) \times n_y \cdot (H_p+1)} \\ \mathbf{R} &\in \Re^{n_u \cdot (H_p+1) \times n_u \cdot (H_p+1)} \end{aligned} \quad (32)$$

$$\vec{e}(k) = \vec{t}(k) - (\vec{y}(k) - \mathbf{S}_u \vec{u}(k)) = \vec{t}(k) - (\mathbf{S}_x \mathbf{x}(k) + \mathbf{S}_v \vec{v}(k)) \tag{33}$$

Where $\vec{t}(k)$ is the commanded velocity from the Max Power Controller, and $\vec{y}(k) - \mathbf{S}_u \vec{u}(k)$ is the free evolution, i.e. an evaluation of outputs with no control action. Then,

$$J(k) = (\vec{e}(k) - \mathbf{S}_u \vec{u}(k))^T \mathbf{Q}(\vec{e}(k) - \mathbf{S}_u \vec{u}(k)) + \vec{u}(k)^T \mathbf{R} \vec{u}(k) \tag{34}$$

$$J(k) = \vec{e}(k)^T \mathbf{Q} \vec{e}(k) - \vec{e}(k)^T \mathbf{Q} \mathbf{S}_u \vec{u}(k) - \vec{u}(k)^T \mathbf{S}_u^T \mathbf{Q} \vec{e}(k) + \vec{u}(k)^T \mathbf{S}_u^T \mathbf{Q} \mathbf{S}_u \vec{u}(k) + \vec{u}(k)^T \mathbf{R} \vec{u}(k) \tag{35}$$

$$J(k) = \vec{e}(k)^T \mathbf{Q} \vec{e}(k) - 2\vec{e}(k)^T \mathbf{Q} \mathbf{S}_u \vec{u}(k) + \vec{u}(k)^T (\mathbf{S}_u^T \mathbf{Q} \mathbf{S}_u + \mathbf{R}) \vec{u}(k) \tag{36}$$

$$\begin{aligned} \hat{J}(k) &= \frac{1}{2} \vec{u}(k)^T (\mathbf{S}_u^T \mathbf{Q} \mathbf{S}_u + \mathbf{R}) \vec{u}(k) - \vec{e}(k)^T \mathbf{Q} \mathbf{S}_u \vec{u}(k) \\ &= \frac{1}{2} \vec{u}(k)^T (\mathbf{S}_u^T \mathbf{Q} \mathbf{S}_u + \mathbf{R}) \vec{u}(k) - (\mathbf{S}_u^T \mathbf{Q} \vec{e}(k))^T \vec{u}(k) \end{aligned} \tag{37}$$

Matlab's quadprog expresses the control variable $\vec{u}(k)$ as x and expects the form

$$\min J(x) = \frac{1}{2} x^T H x + f^T x \tag{38}$$

Subject to

$$Ax \leq b \tag{39}$$

$$A_{eq} x = b_{eq} \tag{40}$$

The equality constraint can be used to enforce input blocking.

$$\hat{J}(k) = \frac{1}{2} \vec{u}(k)^T (\mathbf{S}_u^T \mathbf{Q} \mathbf{S}_u + \mathbf{R}) \vec{u}(k) - (\mathbf{S}_u^T \mathbf{Q} \vec{e}(k)^T)^T \vec{u}(k) \tag{41}$$

Subject to

$$\begin{bmatrix} \mathbf{I} \\ -\mathbf{I} \\ \mathbf{S}_u \\ -\mathbf{S}_u \end{bmatrix} \begin{bmatrix} \vec{u}(k) \end{bmatrix} \leq \begin{bmatrix} \vec{u}_{upperbound} \\ -\vec{u}_{lowerbound} \\ \vec{y}_{upperbound} - \mathbf{S}_x \mathbf{x}(k) - \mathbf{S}_v \vec{v}(k) \\ -\vec{y}_{lowerbound} + \mathbf{S}_x \mathbf{x}(k) + \mathbf{S}_v \vec{v}(k) \end{bmatrix} \tag{42}$$

8.3 Unguided MPC

Provide no pre-calculated velocity trajectory. Instead, use the incremental model to move F_{pto} into the states and ask MPC to solve for the input $\dot{\mathbf{u}}$ (which is now the change in F_{pto}) which maximizes power as $P = FV$. The result will put velocity in phase with excitation force. Importantly, this problem is only convex when the hessian is formatted as below, *i.e.* $A'xA$. It cannot be $A'xB$, although the reason why is unclear.

$$\overrightarrow{\mathbf{y}}(k) = \mathbf{S}_x \mathbf{x}(k) + \mathbf{S}_u \overrightarrow{\mathbf{u}}(k) + \mathbf{S}_v \overrightarrow{\mathbf{v}}(k) \tag{43}$$

$$J(k) = \frac{1}{2}\overrightarrow{\mathbf{y}}(k)^T \mathbf{Q} \overrightarrow{\mathbf{y}}(k) + \frac{1}{2}\overrightarrow{\mathbf{u}}(k)^T \mathbf{R} \overrightarrow{\mathbf{u}}(k) \tag{44}$$

$$J(k) = \frac{1}{2}\big(\mathbf{S}_x \mathbf{x}(k) + \mathbf{S}_u \overrightarrow{\mathbf{u}}(k) + \mathbf{S}_v \overrightarrow{\mathbf{v}}(k)\big)^T \mathbf{Q}\big(\mathbf{S}_x \mathbf{x}(k) + \mathbf{S}_u \overrightarrow{\mathbf{u}}(k) + \mathbf{S}_v \overrightarrow{\mathbf{v}}(k)\big) + \frac{1}{2}\overrightarrow{\mathbf{u}}(k)^T \mathbf{R} \overrightarrow{\mathbf{u}}(k)\big) \tag{45}$$

$$\begin{aligned}
J(k) = \frac{1}{2}\Big[&\mathbf{x}(k)^T \mathbf{S_x}^T \mathbf{Q} \mathbf{S_x} \mathbf{x}(k) + \mathbf{x}(k)^T \mathbf{S}_x^T \mathbf{Q} \mathbf{S_u} \overrightarrow{\mathbf{u}}(k) + \mathbf{x}(k)^T \mathbf{S_x}^T \mathbf{Q} \mathbf{S_v} \overrightarrow{\mathbf{v}}(k) \\
&+ \overrightarrow{\mathbf{u}}(k)^T \mathbf{S_u}^T \mathbf{Q} \mathbf{S_x} \mathbf{x}(k) + \overrightarrow{\mathbf{u}}(k)^T \mathbf{S_u}^T \mathbf{Q} \mathbf{S_u} \overrightarrow{\mathbf{u}}(k) + \overrightarrow{\mathbf{u}}(k)^T \mathbf{S_u}^T \mathbf{Q} \mathbf{S_v} \overrightarrow{\mathbf{v}}(k) \\
&+ \overrightarrow{\mathbf{v}}(k)^T \mathbf{S_v}^T \mathbf{Q} \mathbf{S_x} \mathbf{x}(k) + \overrightarrow{\mathbf{v}}(k)^T \mathbf{S_v}^T \mathbf{Q} \mathbf{S_u} \overrightarrow{\mathbf{u}}(k) + \overrightarrow{\mathbf{v}}(k)^T \mathbf{S_v}^T \mathbf{Q} \mathbf{S_v} \overrightarrow{\mathbf{v}}(k) \Big] \\
&\hspace{8cm} + \frac{1}{2}\overrightarrow{\mathbf{u}}(k)^T \mathbf{R} \overrightarrow{\mathbf{u}}(k) \tag{46}
\end{aligned}$$

$$\begin{aligned}
J(k) = \frac{1}{2}\overrightarrow{\mathbf{u}}(k)^T \mathbf{S_u}^T \mathbf{Q} \mathbf{S_u} \overrightarrow{\mathbf{u}}(k) + \overrightarrow{\mathbf{u}}(k)^T \mathbf{S_u}^T \mathbf{Q}(\mathbf{S_x}\mathbf{x}(k) + \mathbf{S_v}\overrightarrow{\mathbf{v}}(k)) \\
+ \frac{1}{2}(\mathbf{S_x}\mathbf{x}(k) + \mathbf{S_v}\overrightarrow{\mathbf{v}}(k))^T \mathbf{Q}(\mathbf{S_x}\mathbf{x}(k) + \mathbf{S_v}\overrightarrow{\mathbf{v}}(k)) + \frac{1}{2}\overrightarrow{\mathbf{u}}(k)^T \mathbf{R} \overrightarrow{\mathbf{u}}(k) \tag{47}
\end{aligned}$$

Dropping the bias term with no dependence on $\overrightarrow{\mathbf{u}}(k)$:

$$J(k) = \frac{1}{2}\overrightarrow{\mathbf{u}}(k)^T \underbrace{(\mathbf{S_u}^T \mathbf{Q} \mathbf{S_u} + \mathbf{R})}_{\mathbf{H}} \overrightarrow{\mathbf{u}}(k) + \overrightarrow{\mathbf{u}}(k)^T \underbrace{\mathbf{S_u}^T \mathbf{Q}(\mathbf{S_x}\mathbf{x}(k) + \mathbf{S_v}\overrightarrow{\mathbf{v}}(k))}_{\mathbf{f}} \tag{48}$$

Where $\mathbf{Q}$ can be chosen to select speed times force terms. The matrix $\mathbf{R}$ can be chosen to penalize rate of change of force, and likely should be set to some value to avoid erratic behavior.

9 MPC Constraint Strategies

9.1 Hard Constraints

A constraint of the form given in (42) is considered a hard constraint. The convex optimization solver must find a solution which meets all constraints or the problem is considered infeasible; the

solver has no flexibility to find the best possible solution which does violate any constraint. If the problem is infeasible, the last known good PTO force can be applied (from a previous MPC solution), or the solver may be run again with a new relaxed constraint matrix, or some other manually programmed strategy may be employed.

9.2 Soft Constraints Through Slack Variables

A soft constraint has an initial value for all constraints which can be widened (i.e. softened) by the solver during runtime if neccesary to find a feasible solution. Soft constraints can be implemented by augmenting the objective to include new, high cost slack variables for the control input, the output states, or both. In the latter case, the unguided MPC formulation given in (44) is re-written as

$$J(k)_{soft} = \frac{1}{2}\overrightarrow{\mathbf{y}}(k)^T\mathbf{Q}\overrightarrow{\mathbf{y}}(k) + \frac{1}{2}\overrightarrow{\mathbf{u}}(k)^T\mathbf{R}\overrightarrow{\mathbf{u}}(k) + \frac{1}{2}\overrightarrow{\boldsymbol{\delta}_u}(k)^T\mathbf{W}_u\overrightarrow{\boldsymbol{\delta}_u}(k) + \frac{1}{2}\overrightarrow{\boldsymbol{\delta}_y}(k)^T\mathbf{W}_y\overrightarrow{\boldsymbol{\delta}_y}(k) \qquad (49)$$

Where the slack variable $\boldsymbol{\delta}_u$ represents the ability to soften the constraint on the control input $\overrightarrow{\mathbf{u}}(k)$, and the matrix $\mathbf{W}_u$ is chosen to place a high cost on doing so. The slack variable $\boldsymbol{\delta}_y$ is used and scaled likewise to soften constraints on $\overrightarrow{\mathbf{y}}(k)$.

Continuing to develop the expression now written in the form of (48) to illuminate how the slack variables are included in the minimizing vector returned from the solver,

$$J(k)_{soft} = \frac{1}{2}\underbrace{\begin{bmatrix}\overrightarrow{\mathbf{u}}(k) \\ \overrightarrow{\boldsymbol{\delta}_u} \\ \overrightarrow{\boldsymbol{\delta}_y}\end{bmatrix}^T}_{\overrightarrow{\mathbf{u}}_{soft}(k)^T}\underbrace{\begin{bmatrix}\mathbf{H} & 0 & 0 \\ 0 & \mathbf{W}_u & 0 \\ 0 & 0 & \mathbf{W}_y\end{bmatrix}}_{\mathbf{H}_{soft}}\begin{bmatrix}\overrightarrow{\mathbf{u}}(k) \\ \overrightarrow{\boldsymbol{\delta}_u} \\ \overrightarrow{\boldsymbol{\delta}_y}\end{bmatrix} + \begin{bmatrix}\overrightarrow{\mathbf{u}}(k) \\ \overrightarrow{\boldsymbol{\delta}_u} \\ \overrightarrow{\boldsymbol{\delta}_y}\end{bmatrix}^T\underbrace{\begin{bmatrix}\boldsymbol{f} \\ 0 \\ 0\end{bmatrix}}_{\boldsymbol{f}_{soft}} \qquad (50)$$

Subject to

$$\begin{bmatrix}\mathbf{I} & \text{-}\mathbf{I} & 0 \\ \text{-}\mathbf{I} & \text{-}\mathbf{I} & 0 \\ 0 & \text{-}\mathbf{I} & 0 \\ 0 & 0 & \text{-}\mathbf{I} \\ \mathbf{S}_u & 0 & \text{-}\mathbf{I} \\ -\mathbf{S}_u & 0 & \text{-}\mathbf{I}\end{bmatrix}\begin{bmatrix}\overrightarrow{\mathbf{u}}(k) \\ \overrightarrow{\boldsymbol{\delta}_u} \\ \overrightarrow{\boldsymbol{\delta}_y}\end{bmatrix} \leq \begin{bmatrix}\overrightarrow{\mathbf{u}}_{upperbound} \\ -\overrightarrow{\mathbf{u}}_{lowerbound} \\ 0 \\ 0 \\ \overrightarrow{\mathbf{y}}_{upperbound} - \mathbf{S}_x\mathbf{x}(k) - \mathbf{S}_v\overrightarrow{\mathbf{v}}(k) \\ -\overrightarrow{\mathbf{y}}_{lowerbound} + \mathbf{S}_x\mathbf{x}(k) + \mathbf{S}_v\overrightarrow{\mathbf{v}}(k)\end{bmatrix} \qquad (51)$$

Writing the constraints in this way ensures that the slack variables cannot make the problem more restrictive.

There are several approaches to implement $\boldsymbol{\delta}_u$ and $\boldsymbol{\delta}_y$ which change the size of the problem. For example, the vector $\boldsymbol{\delta}_u$ could be the same size as $\overrightarrow{\mathbf{u}}(k)$, or a single $\boldsymbol{\delta}_u$ (i.e. [1x1]) could be shared as the slack variable across all $\overrightarrow{\mathbf{u}}(k)$. In the latter case, the optimization problem is smaller but the value of $\boldsymbol{\delta}_u$ would be determined by the $\overrightarrow{\mathbf{u}}(k)$ which needed the largest slack term. The result of sharing this would be that the constraint on all $\overrightarrow{\mathbf{u}}(k)$ would be softened by the same slack amount, which may be more than is actually needed to make the problem feasible at some time steps. This could result in an unneccesary increase in values of $\overrightarrow{\mathbf{u}}(k)$ which exceed the initial constraint.

9.3 Costs in Objective

Rather than (or in addition to) using constraints, a cost for the control action and each state in $\overrightarrow{\mathbf{y}}(k)$ can be directly added to the objective by augmenting the vector $\mathbf{Q}$ in (48).

10 Incremental Plant Model for MPC

This model moves F_{pto} into the states and takes $\dot{\mathbf{u}}$ as the input variable for control. To perform the transformation, begin with continuous time model. The "c" subscript is for "continuous."

$$\frac{d}{dt}\mathbf{x}_c(t) = \mathbf{A}_c\mathbf{x}_c(t) + \mathbf{B}_{cu}\mathbf{u}(t) + \mathbf{B}_{cv}\mathbf{v}(t) \tag{52}$$

$$\mathbf{y}(t) = \mathbf{C}_c\mathbf{x}_c(t) + \mathbf{D}_{cu}\mathbf{u}(t) + \mathbf{D}_{cv}\mathbf{v}(t) \tag{53}$$

Move $\mathbf{u}(t)$ in to the states. The "a" subscript is for "augmented."

$$\frac{d}{dt}\underbrace{\begin{bmatrix}\mathbf{x}_c(t) \\ \mathbf{u}(t)\end{bmatrix}}_{\mathbf{x}_{ac}(t)} = \underbrace{\begin{bmatrix}\mathbf{A}_c & \mathbf{B}_{cu} \\ \mathbf{0} & \mathbf{0}\end{bmatrix}}_{\mathbf{A}_{ac}}\underbrace{\begin{bmatrix}\mathbf{x}_c(t) \\ \mathbf{u}(t)\end{bmatrix}}_{\mathbf{x}_{ac}(t)} + \underbrace{\begin{bmatrix}0 \\ \mathbf{I}\end{bmatrix}}_{\mathbf{B}_{acu}}\dot{\mathbf{u}}(t) + \underbrace{\begin{bmatrix}\mathbf{B}_{cv} \\ \mathbf{0}\end{bmatrix}}_{\mathbf{B}_{acv}}\mathbf{v}(t) \tag{54}$$

$$\mathbf{y}_a(t) = \underbrace{\begin{bmatrix}\mathbf{C}_c & \mathbf{D}_{cu} \\ \mathbf{0} & \mathbf{C}_{cu}\end{bmatrix}}_{\mathbf{C}_{ac}}\underbrace{\begin{bmatrix}\mathbf{x}_c(t) \\ \mathbf{u}(t)\end{bmatrix}}_{\mathbf{x}_{ac}(t)} + \underbrace{\begin{bmatrix}\mathbf{0}\end{bmatrix}}_{\mathbf{D}_{acu}}\dot{\mathbf{u}}(t) + \underbrace{\begin{bmatrix}\mathbf{D}_{cv} \\ \mathbf{0}\end{bmatrix}}_{\mathbf{D}_{acv}}\mathbf{v}(t) \tag{55}$$

Then perform continuous to discrete transform on

$$\mathbf{A}_{ac}, \begin{bmatrix}\mathbf{B}_{acu} & \mathbf{B}_{acv}\end{bmatrix}, \mathbf{C}_{ac}, \begin{bmatrix}\mathbf{D}_{acu} & \mathbf{D}_{acv}\end{bmatrix} \tag{56}$$

After the discretization, we will have

$$\mathbf{x}(k+1) = \mathbf{A}\mathbf{x}(k) + \mathbf{B}_u\mathbf{u}(k) + \mathbf{B}_v\mathbf{v}(k) \tag{57}$$

$$\mathbf{y}(k) = \mathbf{C}\mathbf{x}(k) + \mathbf{D}_u\mathbf{u}(k) + \mathbf{D}_v\mathbf{v}(k) \tag{58}$$

Where the discrete state $\mathbf{x}(k)$ is the concatenated continuous states and the previous continuous input. The discrete input $\mathbf{u}(k)$ is now the continuous $\dot{\mathbf{u}}$. (Assuming the continuous to discrete transform has preserved the state identities, as is the case with ZOH).

11 Model for Estimation

To estimate the unknown input F_e, move it into the states and add a term for white guassian process noise. This can serve as an estimation model for use with a Kalman filter, for example.

$$\frac{d}{dt}\begin{bmatrix} \dot{z} \\ z \\ F_e \end{bmatrix} = \underbrace{\begin{bmatrix} \frac{-B}{m+A} & \frac{-k}{m+A} & \frac{1}{m+A} \\ 1 & 0 & 0 \\ 0 & 0 & 0 \end{bmatrix}}_{A}\begin{bmatrix} \dot{z} \\ z \\ F_e \end{bmatrix} + \underbrace{\begin{bmatrix} \frac{1}{m+A} \\ 0 \\ 0 \end{bmatrix}}_{Bu}\begin{bmatrix} F_{pto} \end{bmatrix} + \underbrace{\begin{bmatrix} 0 \\ 0 \\ 1 \end{bmatrix}}_{Bw}\begin{bmatrix} w_{F_e} \end{bmatrix} \tag{59}$$

12 Frequency Dependent Radiation Force

The transform $C(\omega)$ relates heave speed to radiation force.

$$F_r(\omega) = -C(\omega)\dot{z}(\omega) \tag{60}$$

In the time domain, this is the convolution of the force/speed impulse response and speed.

$$F_r(t) = -c(t) * \dot{z}(t) \tag{61}$$

The impulse response $c(t)$ must be causal. That is $c(t) = 0$ for $t < 0$.

The transform $C(\omega)$ can be considered separated into a real and imaginary component, which corresponds to speed dependent and acceleration dependent terms, which can be considered a damping term and mass term, respectively.

$$C(\omega) = B(\omega) + i\omega A(\omega) \tag{62}$$

However, there is an issue taking $F^{-1}\{C(\omega)\} = c(t) = \frac{1}{2\pi}\int_{-\infty}^{\infty}(B(\omega) + i\omega A(\omega))e^{i\omega t}d\omega$ in that generally $A(\omega)$ does not tend to 0 as ω tends to infinity, thus the integral is not convergent.

This can be addressed by subtracting $A(\infty)$ from the integration, where $A(\infty)$ is approximated by the value for the added mass corresponding to the highest frequency evaluated by the BEM solver (such as WAMIT). Thus we define a new transform

$$C_\infty(\omega) = B(\omega) + i\omega(A(\omega) - A(\infty)) \tag{63}$$

$$F_r'(\omega) = -C_\infty(\omega)\dot{z}(\omega) \tag{64}$$

$$F_r(\omega) = F_r'(\omega) - i\omega A(\infty)\dot{z}(\omega) \tag{65}$$

$$F_r(\omega) = -C_\infty(\omega)\dot{z}(\omega) - i\omega A(\infty)\dot{z}(\omega) \tag{66}$$

13

The transfer function $\hat{C}_\infty(\omega)$ that approximates $C_\infty(\omega)$ is assumed to be of the form

$$\hat{C}_\infty(\omega) = \frac{i\omega c_{aa} + c_{ab}}{(i\omega)^2 c_{ba} + i\omega c_{bb} + c_{bc}} \tag{67}$$

For the simplest frequency independent model, for which $B(\omega)$ and $A(\omega)$ are approximated as $\hat{B}$ and $\hat{A}$,

$$c_{aa} = \hat{A} - A(\infty) \tag{68}$$
$$c_{ab} = \hat{B} \tag{69}$$
$$c_{ba} = 0 \tag{70}$$
$$c_{bb} = 0 \tag{71}$$
$$c_{bc} = 1 \tag{72}$$
$$\tag{73}$$

For frequency dependence, the following values were found as a good approximation. Details are appended as a published m-file.

$$c_{aa} = 252700 \tag{74}$$
$$c_{ab} = 0 \tag{75}$$
$$c_{ba} = 1 \tag{76}$$
$$c_{bb} = 3.8 \tag{77}$$
$$c_{bc} = 3.61 \tag{78}$$
$$\tag{79}$$

Assuming the form of (67) as an approximation of $C_\infty(\omega)$, we can take the inverse transform of (64) to get

$$\ddot{F}_r'(t) + \frac{c_{bb}}{c_{ba}}\dot{F}_r'(t) + \frac{c_{bc}}{c_{ba}}F_r'(t) = -\frac{c_{aa}}{c_{ba}}\ddot{z}(t) - \frac{c_{ab}}{c_{ba}}\dot{z}(t) \tag{80}$$

$$F_r(t) = F_r'(t) - A(\infty)\ddot{z}(t) \tag{81}$$

The equation of motion then becomes

$$F_e + F_r + F_b + F_{pto} = m\ddot{z} \tag{82}$$

$$F_r = F_r' - A(\infty)\ddot{z} \tag{83}$$

$$F_b = -k\,z \tag{84}$$

$$\ddot{F}_r' = -\frac{c_{bb}}{c_{ba}}\dot{F}_r' - \frac{c_{bc}}{c_{ba}}F_r' - \frac{c_{aa}}{c_{ba}}\ddot{z} - \frac{c_{ab}}{c_{ba}}\dot{z} \tag{85}$$

14

$$\ddot{z} = \frac{1}{m + A(\infty)}(F_e + F'_r + F_b + F_{pto}) \tag{86}$$

$$\frac{d}{dt}\begin{bmatrix} \dot{z} \\ z \\ \dot{F}'_r \\ F'_r \end{bmatrix} = \begin{bmatrix} 0 & \frac{-k}{m+A(\infty)} & 0 & \frac{1}{m+A(\infty)} \\ 1 & 0 & 0 & 0 \\ -\frac{c_{ab}}{c_{ba}} & -\frac{c_{aa}}{c_{ba}}\frac{-k}{m+A(\infty)} & -\frac{c_{bb}}{c_{ba}} & -\frac{c_{bc}}{c_{ba}} + -\frac{c_{aa}}{c_{ba}}\frac{1}{m+A(\infty)} \\ 0 & 0 & 1 & 0 \end{bmatrix}\begin{bmatrix} \dot{z} \\ z \\ \dot{F}'_r \\ F'_r \end{bmatrix}$$
$$+ \begin{bmatrix} \frac{1}{m+A(\infty)} \\ 0 \\ -\frac{c_{aa}}{c_{ba}}\frac{1}{m+A(\infty)} \\ 0 \end{bmatrix}\begin{bmatrix} F_{pto} \end{bmatrix} + \begin{bmatrix} \frac{1}{m+A(\infty)} \\ 0 \\ -\frac{c_{aa}}{c_{ba}}\frac{1}{m+A(\infty)} \\ 0 \end{bmatrix}\begin{bmatrix} F_e \end{bmatrix} \tag{87}$$

Alternatively, decrementing the derivative order of F'_r by one to avoid the algebraic dependence of F'_r on $\ddot{z}$

$$\dot{F}'_r = -\frac{c_{bb}}{c_{ba}}F'_r - \frac{c_{bc}}{c_{ba}}\int_{-\infty}^{t} F'_r \, dt - \frac{c_{aa}}{c_{ba}}\dot{z} - \frac{c_{ab}}{c_{ba}}z \tag{88}$$

$$\frac{d}{dt}\begin{bmatrix} \dot{z} \\ z \\ F'_r \\ \int_{-\infty}^{t} F'_r \, d\tau \end{bmatrix} = \begin{bmatrix} 0 & \frac{-k}{m+A(\infty)} & \frac{1}{m+A(\infty)} & 0 \\ 1 & 0 & 0 & 0 \\ -\frac{c_{aa}}{c_{ba}} & -\frac{c_{ab}}{c_{ba}} & -\frac{c_{bb}}{c_{ba}} & -\frac{c_{bc}}{c_{ba}} \\ 0 & 0 & 1 & 0 \end{bmatrix}\begin{bmatrix} \dot{z} \\ z \\ F'_r \\ \int_{-\infty}^{t} F'_r \, d\tau \end{bmatrix}$$
$$+ \begin{bmatrix} \frac{1}{m+A(\infty)} \\ 0 \\ 0 \\ 0 \end{bmatrix}\begin{bmatrix} F_{pto} \end{bmatrix} + \begin{bmatrix} \frac{1}{m+A(\infty)} \\ 0 \\ 0 \\ 0 \end{bmatrix}\begin{bmatrix} F_e \end{bmatrix} \tag{89}$$

13 A Multipod Model

Description: The interaction between bodies is a WEC system is manifested as a cross-coupled radiation force. F_{r12} is the radiation force on body 1 due to motion of body 2.

$$F_{e1} + F_{r11}(\ddot{z}_1, \dot{z}_1) + F_{r12}(\ddot{z}_2, \dot{z}_2) + F_{b1}(z_1) + F_{PTO1} = m_1\ddot{z}_1 \tag{90}$$

$$F_{e2} + F_{r22}(\ddot{z}_2, \dot{z}_2) + F_{r21}(\ddot{z}_1, \dot{z}_1) + F_{b2}(z_2) + F_{PTO2} = m_2\ddot{z}_2 \tag{91}$$

13.1   Frequency Independent Radiation Force

Description: A multipod model developed with a frequency indpendent cross-body radiation force. This is not the form used in the final deliverable.

$$F_{r12} = -(A_{12}\ddot{z}_2 + B_{12}\dot{z}_2) \tag{92}$$

$$F_{r21} = -(A_{21}\ddot{z}_1 + B_{21}\dot{z}_1) \tag{93}$$

State-Space Form for Frequency Independence:

$$\frac{d}{dt}\begin{bmatrix} \dot{z}_1 \\ z_1 \end{bmatrix} = \underbrace{\begin{bmatrix} \frac{-B_{11}}{m+A_{11}} & \frac{-k}{m+A_{11}} \\ 1 & 0 \end{bmatrix}}_{\mathbf{A}_1}\begin{bmatrix} \dot{z}_1 \\ z_1 \end{bmatrix} + \underbrace{\begin{bmatrix} \frac{-A_{12}}{m+A_{11}} & \frac{-B_{12}}{m+A_{11}} \\ 0 & 0 \end{bmatrix}}_{\mathbf{A}_{12}}\begin{bmatrix} \ddot{z}_2 \\ \dot{z}_2 \end{bmatrix} + \underbrace{\begin{bmatrix} \frac{1}{m+A_{11}} \\ 0 \end{bmatrix}}_{\mathbf{B}_{u1}}\begin{bmatrix} F_{PTO1} \end{bmatrix} + \underbrace{\begin{bmatrix} \frac{1}{m+A_{11}} \\ 0 \end{bmatrix}}_{\mathbf{B}_{v1}}\begin{bmatrix} F_{e1} \end{bmatrix}$$

$$\tag{94}$$

$$\frac{d}{dt}\begin{bmatrix} \dot{z}_2 \\ z_2 \end{bmatrix} = \underbrace{\begin{bmatrix} \frac{-B_{22}}{m+A_{22}} & \frac{-k}{m+A_{22}} \\ 1 & 0 \end{bmatrix}}_{\mathbf{A}_2}\begin{bmatrix} \dot{z}_2 \\ z_2 \end{bmatrix} + \underbrace{\begin{bmatrix} \frac{-A_{21}}{m+A_{22}} & \frac{-B_{21}}{m+A_{22}} \\ 0 & 0 \end{bmatrix}}_{\mathbf{A}_{21}}\begin{bmatrix} \ddot{z}_1 \\ \dot{z}_1 \end{bmatrix} + \underbrace{\begin{bmatrix} \frac{1}{m+A_{22}} \\ 0 \end{bmatrix}}_{\mathbf{B}_{u2}}\begin{bmatrix} F_{PTO2} \end{bmatrix} + \underbrace{\begin{bmatrix} \frac{1}{m+A_{22}} \\ 0 \end{bmatrix}}_{\mathbf{B}_{v2}}\begin{bmatrix} F_{e2} \end{bmatrix}$$

$$\tag{95}$$

Let,

$$\mathbf{z}_1 = \begin{bmatrix} \dot{z}_1 \\ z_1 \end{bmatrix}$$

$$\mathbf{z}_2 = \begin{bmatrix} \dot{z}_2 \\ z_2 \end{bmatrix}$$

$$\dot{\mathbf{z}}_1 = \frac{d}{dt}\begin{bmatrix} \dot{z}_1 \\ z_1 \end{bmatrix}$$

$$\dot{\mathbf{z}}_2 = \frac{d}{dt}\begin{bmatrix} \dot{z}_2 \\ z_2 \end{bmatrix}$$

$$\dot{\mathbf{z}}_1 = \mathbf{A}_1\mathbf{z}_1 + \mathbf{A}_{12}\dot{\mathbf{z}}_2 + \mathbf{B}_{u1}F_{PTO1} + \mathbf{B}_{v1}F_{e1} \tag{96}$$

$$\dot{\mathbf{z}}_2 = \mathbf{A}_2\mathbf{z}_2 + \mathbf{A}_{21}\dot{\mathbf{z}}_1 + \mathbf{B}_{u2}F_{PTO2} + \mathbf{B}_{v2}F_{e2} \tag{97}$$

$$\dot{\mathbf{z}}_1 - \mathbf{A}_{12}\dot{\mathbf{z}}_2 = \mathbf{A}_1\mathbf{z}_1 + \mathbf{B}_{u1}F_{PTO1} + \mathbf{B}_{v1}F_{e1} \tag{98}$$

$$\dot{\mathbf{z}}_2 - \mathbf{A}_{21}\dot{\mathbf{z}}_1 = \mathbf{A}_2\mathbf{z}_2 + \mathbf{B}_{u2}F_{PTO2} + \mathbf{B}_{v2}F_{e2} \tag{99}$$

$$
\underbrace{\begin{bmatrix} \mathbf{I} & -\mathbf{A}_{12} \\ -\mathbf{A}_{21} & \mathbf{I} \end{bmatrix}}_{\mathbf{E}} \underbrace{\begin{bmatrix} \dot{\mathbf{z}}_1 \\ \dot{\mathbf{z}}_2 \end{bmatrix}}_{\dot{\mathbf{z}}} = \underbrace{\begin{bmatrix} \mathbf{A}_1 & 0 \\ 0 & \mathbf{A}_2 \end{bmatrix}}_{\mathbf{A}} \underbrace{\begin{bmatrix} \mathbf{z}_1 \\ \mathbf{z}_2 \end{bmatrix}}_{\mathbf{z}} + \underbrace{\begin{bmatrix} \mathbf{B}_{u1} & 0 \\ 0 & \mathbf{B}_{u2} \end{bmatrix}}_{\mathbf{B}_u} \underbrace{\begin{bmatrix} F_{PTO1} \\ F_{PTO2} \end{bmatrix}}_{F_{pto}} + \underbrace{\begin{bmatrix} \mathbf{B}_{v1} & 0 \\ 0 & \mathbf{B}_{v2} \end{bmatrix}}_{\mathbf{B}_v} \underbrace{\begin{bmatrix} F_{e1} \\ F_{e2} \end{bmatrix}}_{F_e} \tag{100}
$$

$$
\dot{\mathbf{z}} = \mathbf{E}^{-1}(\mathbf{A}\mathbf{z} + \mathbf{B}_u F_{pto} + \mathbf{B}_v F_e) \tag{101}
$$

13.2 Frequency Dependent Radiation Force

The self terms for frequency dependent radiantion force (*e.g.* $F_{r,11}$) are all as previously defined for a single body. The frequency dependent cross-coupling terms in a multibody system can be developed in a similiar process as before. This is the form used in the final deliverable.

$$
F_{r,11}(\omega) = -C_{11}(\omega)\dot{z}_1(\omega) \tag{102}
$$

$$
F_{r,12}(\omega) = -C_{12}(\omega)\dot{z}_2(\omega) \tag{103}
$$

$$
C_{\infty,11}(\omega) = B_{11}(\omega) + i\omega(A_{11}(\omega) - A_{11}(\infty)) \tag{104}
$$

$$
C_{\infty,12}(\omega) = B_{12}(\omega) + i\omega(A_{12}(\omega) - A_{12}(\infty)) \tag{105}
$$

$$
F'_{r,11}(\omega) = -C_{\infty,11}(\omega)\dot{z}_1(\omega) \tag{106}
$$

$$
F'_{r,12}(\omega) = -C_{\infty,12}(\omega)\dot{z}_2(\omega) \tag{107}
$$

The transfer function $\hat{C}_{\infty,12}(\omega)$ that approximates $C_{\infty,12}(\omega)$ is assumed to be of the form

$$
\hat{C}_{\infty,12}(\omega) = \frac{i\omega c_{aa,12} + c_{ab,12}}{(i\omega)^2 c_{ba,12} + i\omega c_{bb,12} + c_{bc,12}} \tag{108}
$$

For the simplest frequency independent model, for which $B_{12}(\omega)$ and $A_{12}(\omega)$ are approximated as $\hat{B}_{12}$ and $\hat{A}_{12}$,

$$
c_{aa,12} = \hat{A}_{12} - A_{12}(\infty) \tag{109}
$$

$$
c_{ab,12} = \hat{B}_{12} \tag{110}
$$

$$
\tag{111}
$$

$$\ddot{F}'_{r,12} = -\frac{c_{bb,12}}{c_{ba,12}} \dot{F}'_{r,12} - \frac{c_{bc,12}}{c_{ba,12}} F'_{r,12} - \frac{c_{aa,12}}{c_{ba,12}} \ddot{z}_2 - \frac{c_{ab,12}}{c_{ba,12}} \dot{z}_2 \tag{112}$$

The equation of motion then becomes

$$F_{e,1} + F_{r,11} + F_{r,12} + F_{b,1} + F_{pto,1} = m\ddot{z}_1 \tag{113}$$

$$F_{r,11} = F'_{r,11} - A_{11}(\infty)\ddot{z} \tag{114}$$

$$F_{r,12} = F'_{r,12} - A_{12}(\infty)\ddot{z} \tag{115}$$

$$F_{b,1} = -k\,z_1 \tag{116}$$

$$F_{e1} + (F'_{r,11} - A_{11}(\infty)\ddot{z}_1) + (F'_{r,12} - A_{12}(\infty)\ddot{z}_2) - k\,z_1 + F_{pto1} = m\ddot{z}_1 \tag{117}$$

Unlike the self added mass, the added mass of the cross term $A(\omega)$ does tend to 0 as ω tends towards infinity. Therefore, $A_{12}(\infty) = 0$ and can be dropped.

$$F_{e,1} + F'_{r,11} + F'_{r,12} - k\,z_1 + F_{pto,1} = (m + A_{11}(\infty))\ddot{z}_1 \tag{118}$$

$$\ddot{z}_1 = \frac{1}{(m + A_{11}(\infty))}(-k\,z_1 + F'_{r,11} + F'_{r,12} + F_{pto,1} + F_{e,1}) \tag{119}$$

$$\ddot{z}_2 = \frac{1}{(m + A_{22}(\infty))}(-k\,z_2 + F'_{r,22} + F'_{r,21} + F_{pto,2} + F_{e,2}) \tag{120}$$

Therefore,

$$\ddot{F}'_{r12} = -\frac{c_{bb,12}}{c_{ba,12}} \dot{F}'_{r12} - \frac{c_{bc,12}}{c_{ba,12}} F'_{r12} - \frac{c_{aa,12}}{c_{ba,12}} \ddot{z}_2 - \frac{c_{ab,12}}{c_{ba,12}} \dot{z}_2 \tag{121}$$

$$\ddot{F}'_{r21} = -\frac{c_{bb,21}}{c_{ba,21}} \dot{F}'_{r21} - \frac{c_{bc,21}}{c_{ba,21}} F'_{r21} - \frac{c_{aa,21}}{c_{ba,21}} \ddot{z}_1 - \frac{c_{ab,21}}{c_{ba,21}} \dot{z}_1 \tag{122}$$

And by decrementing the derivative order by one to directly eliminate the depence on acceleration,

$$\dot{F}'_{r12} = -\frac{c_{12,bb}}{c_{12,ba}} F'_{r12} - \frac{c_{12,bc}}{c_{12,ba}} \int_{-\infty}^{t} F'_{r12}\, dt - \frac{c_{12,aa}}{c_{12,ba}} \dot{z}_2 - \frac{c_{12,ab}}{c_{12,ba}} z_2 \tag{123}$$

$$\dot{F}'_{r21} = -\frac{c_{21,bb}}{c_{21,ba}} F'_{r21} - \frac{c_{21,bc}}{c_{21,ba}} \int_{-\infty}^{t} F'_{r21}\, dt - \frac{c_{21,aa}}{c_{21,ba}} \dot{z}_1 - \frac{c_{21,ab}}{c_{21,ba}} z_1 \tag{124}$$

13.3 State Space Model for Multibody Frequency Dependent Radiation Force with Incremental Input

18

$$
\frac{d}{dt}
\begin{bmatrix}
\dot{z}_1 \\
z_1 \\
F'_{r,11} \\
\int_{-\infty}^{t} F'_{r,11}\,d\tau \\
F_{pto,1} \\
\dot{z}_2 \\
z_2 \\
F'_{r22} \\
\int_{-\infty}^{t} F'_{r22}\,d\tau \\
F_{pto,1} \\
F'_{r12} \\
\int_{-\infty}^{t} F'_{r12}\,d\tau \\
F'_{r21} \\
\int_{-\infty}^{t} F'_{r21}\,d\tau
\end{bmatrix}
$$

$$
=
\begin{bmatrix}
0 & \frac{-k}{m+A_{11}(\infty)} & \frac{1}{m+A_{11}(\infty)} & 0 & \frac{1}{m+A_{11}(\infty)} & 0 & 0 & 0 & 0 & 0 & \frac{1}{m+A_{11}(\infty)} & 0 & 0 & 0 \\
1 & 0 & 0 & 0 & 0 & 0 & 0 & 0 & 0 & 0 & 0 & 0 & 0 & 0 \\
-\frac{c_{aa}}{c_{ba}} & -\frac{c_{ab}}{c_{ba}} & -\frac{c_{bb}}{c_{ba}} & -\frac{c_{bc}}{c_{ba}} & 0 & 0 & 0 & 0 & 0 & 0 & 0 & 0 & 0 & 0 \\
0 & 0 & 1 & 0 & 0 & 0 & 0 & 0 & 0 & 0 & 0 & 0 & 0 & 0 \\
0 & 0 & 0 & 0 & 0 & 0 & \frac{-k}{m+A_{22}(\infty)} & \frac{1}{m+A_{22}(\infty)} & 0 & \frac{1}{m+A_{22}(\infty)} & 0 & 0 & \frac{1}{m+A_{22}(\infty)} & 0 \\
0 & 0 & 0 & 0 & 0 & 1 & 0 & 0 & 0 & 0 & 0 & 0 & 0 & 0 \\
0 & 0 & 0 & 0 & 0 & -\frac{c_{aa}}{c_{ba}} & -\frac{c_{ab}}{c_{ba}} & -\frac{c_{bb}}{c_{ba}} & -\frac{c_{bc}}{c_{ba}} & 0 & 0 & 0 & 0 & 0 \\
0 & 0 & 0 & 0 & 0 & 0 & 0 & 1 & 0 & 0 & 0 & 0 & 0 & 0 \\
0 & 0 & 0 & 0 & 0 & -\frac{c_{aa,12}}{c_{ba,12}} & -\frac{c_{ab,12}}{c_{ba,12}} & 0 & 0 & 0 & -\frac{c_{bb,12}}{c_{ba,12}} & -\frac{c_{bc,12}}{c_{ba,12}} & 0 & 0 \\
0 & 0 & 0 & 0 & 0 & 0 & 0 & 0 & 0 & 0 & 1 & 0 & 0 & 0 \\
-\frac{c_{aa,21}}{c_{ba,21}} & -\frac{c_{ab,21}}{c_{ba,21}} & 0 & 0 & 0 & 0 & 0 & 0 & 0 & 0 & 0 & 0 & -\frac{c_{bb,21}}{c_{ba,21}} & -\frac{c_{bc,21}}{c_{ba,21}} \\
0 & 0 & 0 & 0 & 0 & 0 & 0 & 0 & 0 & 0 & 0 & 0 & 1 & 0
\end{bmatrix}
\begin{bmatrix}
\dot{z}_1 \\
z_1 \\
F'_{r,11} \\
\int_{-\infty}^{t} F'_{r,11}\,d\tau \\
F_{pto,1} \\
\dot{z}_2 \\
z_2 \\
F'_{r22} \\
\int_{-\infty}^{t} F'_{r22}\,d\tau \\
F_{pto,1} \\
F'_{r12} \\
\int_{-\infty}^{t} F'_{r12}\,d\tau \\
F'_{r21} \\
\int_{-\infty}^{t} F'_{r21}\,d\tau
\end{bmatrix}
$$

$$
+
\begin{bmatrix}
0 & 0 \\
0 & 0 \\
0 & 0 \\
0 & 0 \\
1 & 0 \\
0 & 0 \\
0 & 0 \\
0 & 0 \\
0 & 0 \\
0 & 1 \\
0 & 0 \\
0 & 0 \\
0 & 0 \\
0 & 0
\end{bmatrix}
\begin{bmatrix} \dot{F}_{pto,1} \\ \dot{F}_{pto,2} \end{bmatrix}
+
\begin{bmatrix}
\frac{1}{m+A_{11}(\infty)} & 0 \\
0 & 0 \\
0 & 0 \\
0 & 0 \\
0 & 0 \\
0 & \frac{1}{m+A_{22}(\infty)} \\
0 & 0 \\
0 & 0 \\
0 & 0 \\
0 & 0 \\
0 & 0 \\
0 & 0 \\
0 & 0 \\
0 & 0
\end{bmatrix}
\begin{bmatrix} F_{e,1} \\ F_{e,2} \end{bmatrix}
\quad (125)
$$

14   Appendix

Contents

```
%%%%%%%%%%%%%%%%%%%%%%%%%%%%%%%%%%%%%%%%%%%%%%%%%%%%%%%%%%%%%%%%%
% Created by: Mike Starrett, Dr. Ted Brekken, Ratanak So(Oregon State University)
% Created on: May 15, 2014
%
% Purpose: Develop transfer function for radiation force based on added
% mass (A) and damping (B) from WAMIT. Fr is the only place where these
% terms are used, so this would remove constants A&B from the model.
%
%%%%%%%%%%%%%%%%%%%%%%%%%%%%%%%%%%%%%%%%%%%%%%%%%%%%%%%%%%%%%%%%%
```

Prepare the workspace

```
clc, clear variables global mex, format compact %close all
```

Load added mass, radiation damping, and period vectors

```
load('A_B_w_for_tf-9_21_in_chain_2_AWAY-UPDATED_GEOMETRY WITH BACKBONE-sent_from_alan_6_29');
    % See contents of folder for options -- file names too long!
m = abtf_data.m;    % Added Mass
R = abtf_data.R;    % Radiation Damping
w = abtf_data.w;    % Frequency [Rad/sec]
```

Make two sided

```
m = [fliplr(m') 0 m'];
R = [fliplr(R') 0 R'];
w = [-fliplr(w') 0 w'];

% %% Plot initial data set
% % Using find(w>0,1) to only plot RHS (positive frequencies)
% figure
% subplot(211)
% semilogx(w(find(w>0,1):end),m(find(w>0,1):end))
% legend('added mass');
% ylabel('kg');
% xlabel('rad/s');
% subplot(212)
% semilogx(w(find(w>0,1):end),R(find(w>0,1):end))
```

```
% legend('radiation damping');
% ylabel('N/(m/s)');
% xlabel('rad/s');
```

Make transfer functions

Z = radiation impedence (speed to force) — it's the impulse response of Fr to be multiplied by velocity to give Fr, where
Fr(s) = -(sA(s)+B)*V(s) so if Fr=Z*V, Z = (B + jw*A) = (R*jw*A) = (R+i*w*m) per Falnes convention

```
Z = R + 1i*w.*m;

% Subtract added mass at infinity to address non-convergence of inverse
% transform of Z to z (p.139 - 140 of Falnes)
K = R + 1*i*w.*(m-m(end));
%K = R + 1*i*w.*m; % Really don't need to subtract of m(end) in
%cross-coupled formulation as cross-coupled added mass does tend towards
%zero as omega goes to infinity
```

Calculate Impulse responses

```
c = 0;
t = [-30:0.1:30];        % Across all W that we used (omega from -29.8 to + 29.8)
for ti = t
        c = c+1;
        k(c) = 1/(2*pi)*trapz(w,K.*exp(1i*w*ti));

        % Experimental: Calculate z anyway
        % The result is non-causal, but perhaps valid for frequencies below
        % w(end)

        z(c) = 1/(2*pi)*trapz(w,Z.*exp(1*i*w*ti));
end
k = real(k);     % Remove residual imaginary components
z = real(z);     % Remove residual imaginary components
%
% figure;
% plot(t,k)
% legend('k: speed to force (without d/dt (speed)*m(inf)')
```

Initial system to make a TF for

```
Ksys = frd(K(find(w>0,1):end),w(find(w>0,1):end));

% Frequency dependent aproximation
s = tf('s');
```

New Coeff dialed in on 9-4-15 using model w/ BB.

```
K_dep = 5e05*s/(12.7*s^2 + 12*s + 13.7)   % CROSS coeff for TWO AWAY (9 21)
```

```
figure
%bode(Ksys,K_ind,K_dep,logspace(-1,2,50));
bode(Ksys,K_dep,logspace(-1,1,50));
legend('K','K dep')
```

K_dep =

```
        500000 s
  ---------------------
  12.7 s^2 + 12 s + 13.7
```

Continuous-time transfer function.

Bode Diagram
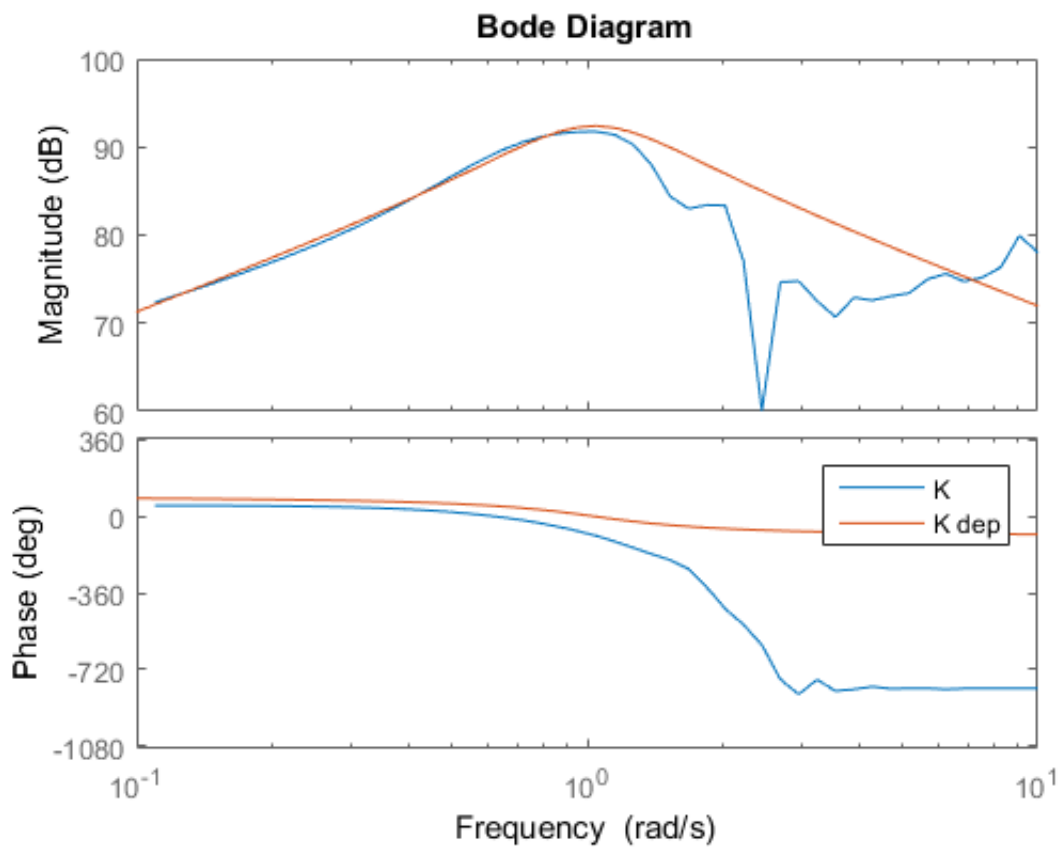
9.2   Appendix 2 - Baseline performance and loads report

TENSION LEG WAVEDYN MODEL - PERFORMANCE & OPERATIONAL LOADS

Centipod CPX3

Dehlsen Associates LLC

Document No.: 702480-USSD-R-02-A
Date: 2/6/2015

IMPORTANT NOTICE AND DISCLAIMER

1. This document is intended for the sole use of the Customer as detailed on the front page of this document to whom the document is addressed and who has entered into a written agreement with the DNV GL entity issuing this document ("DNV GL"). To the extent permitted by law, neither DNV GL nor any group company (the "Group") assumes any responsibility whether in contract, tort including without limitation negligence, or otherwise howsoever, to third parties (being persons other than the Customer), and no company in the Group other than DNV GL shall be liable for any loss or damage whatsoever suffered by virtue of any act, omission or default (whether arising by negligence or otherwise) by DNV GL, the Group or any of its or their servants, subcontractors or agents. This document must be read in its entirety and is subject to any assumptions and qualifications expressed therein as well as in any other relevant communications in connection with it. This document may contain detailed technical data which is intended for use only by persons possessing requisite expertise in its subject matter.

2. This document is protected by copyright and may only be reproduced and circulated in accordance with the Document Classification and associated conditions stipulated or referred to in this document and/or in DNV GL's written agreement with the Customer. No part of this document may be disclosed in any public offering memorandum, prospectus or stock exchange listing, circular or announcement without the express and prior written consent of DNV GL. A Document Classification permitting the Customer to redistribute this document shall not thereby imply that DNV GL has any liability to any recipient other than the Customer.

3. This document has been produced from information relating to dates and periods referred to in this document. This document does not imply that any information is not subject to change. Except and to the extent that checking or verification of information or data is expressly agreed within the written scope of its services, DNV GL shall not be responsible in any way in connection with erroneous information or data provided to it by the Customer or any third party, or for the effects of any such erroneous information or data whether or not contained or referred to in this document.

4. Any energy forecasts estimates or predictions are subject to factors not all of which are within the scope of the probability and uncertainties contained or referred to in this document and nothing in this document guarantees any particular wind speed or energy output.

KEY TO DOCUMENT CLASSIFICATION

Strictly Confidential	:	For disclosure only to named individuals within the Customer's organisation.
Private and Confidential	:	For disclosure only to individuals directly concerned with the subject matter of the document within the Customer's organisation.
Commercial in Confidence	:	Not to be disclosed outside the Customer's organisation.
DNV GL only	:	Not to be disclosed to non-DNV GL staff
Customer's Discretion	:	Distribution for information only at the discretion of the Customer (subject to the above Important Notice and Disclaimer and the terms of DNV GL's written agreement with the Customer).
Published	:	Available for information only to the general public (subject to the above Important Notice and Disclaimer).

Project name:	Tension Leg WaveDyn Model – Performance & Operational Loads	DNV GL - Energy Renewables Advisory
Report title:	Centipod CPX3	9665 Chesapeake Drive
Customer:	Dehlsen Associates LLC	Suite 435
		San Diego, CA 92123
Contact person:	A. Fleming	Tel: +1 858 836 3370
Date of issue:	11 Feb 2015	Enterprise No.: 94-3402236
Project No.:	702480	
Document No.:	702480-USSD-R-02, Rev. A	

Task and objective:

Creation of a WaveDyn model of the tension-leg Centipod CPX3 concept WEC.

Preliminary performance data are presented for idealized conditions and PTO characteristics.

Baseline operational loads are presented.

Prepared by: Verified by: Approved by:

_____   _____   _____
Jarett Goldsmith   Robert Harries   Ed Mackay
Engineer   Engineer   Head of Wave & Tidal
Wave & Tidal   Loads

_____
Armando Alexandre
Engineer
Wave & Tidal

Issue	Date	Reason for Issue	Prepared by	Verified by	Approved by
A	11-Feb-2015	First issue– electronic copy only	J. Goldsmith A. Alexandre	R. Harries	E. Mackay

Table of contents

Appendices

1   INTRODUCTION

DNV GL is a leading provider of independent wind, wave and tidal turbine engineering services. The Wave and Tidal group within DNV GL has been established to offer a range of consultancy services to marine energy device and project developers, investors, contractors, financiers and other stakeholders.

DNV GL has been contracted by Dehlsen Associates LLC (DA) to conduct numerical modelling activities related to the development of the Centipod CPX3 wave energy converter (WEC). Time domain simulations have been carried out in WaveDyn [1], DNV GL's WEC numerical modelling software, for a floating tension leg model of the Centipod WEC. This report (Issue A) presents results from 190 simulations which evaluate the performance of the WEC model under the sea states that have non-zero rates of occurrence according to the wave scatter plot selected by DA. This builds off the work done and reported in 702480-USSD-R-01-A for an initial Centipod model with a fixed 'backbone' where power performance was assessed and a second moorings study to compare moorings options power performance to that fixed case. The WaveDyn models and an overview presentation from the moorings study were provided to DA and helped inform DA's decision to pursue a tension leg moorings system for Centipod.

The report is organized into 9 main sections. In Section 2, WaveDyn, the time-domain multi-body simulation package used in this work, is briefly introduced. There is a description of the device in Section 3 followed by a complete description of the Centipod CPX3 WEC model used in the WaveDyn simulations in Section 4. An overview of the simulation setup is provided in Section 5, whilst the main power performance results are presented in Section 6. The operational loads are described in Section 7. A brief section describing some alternative models is given in Section 8. Finally, the key findings and conclusions regarding this work and specific recommendations related to future work are summarized in Section 9.

Any enquiries regarding this report should be addressed to:

Jarett Goldsmith

Email: Jarett.Goldsmith@dnvgl.com

Tel.: +1 (858) 836-3370, x132

2 WAVEDYN OVERVIEW

WaveDyn is a multi-body, time-domain, simulation tool developed specifically for evaluating WEC performance. The software allows a user to construct a numerical representation of a WEC by connecting structural, hydrodynamic, power take-off (PTO) and moorings components using a flexible user interface. Control actions may be implemented through the PTO components, and simulations may be run with regular or irregular input sea states, for multiple wave directions or directionally spread waves.

In the WaveDyn release used for the present Centipod WEC modelling (version 1.2), the hydrodynamics module is restricted to a linear formulation based on a boundary element method (BEM), potential flow solver. Diffraction, radiation and hydrostatic effects are included in the model, however viscous effects are assumed negligible for power performance calculations, with the machine response being largely dominated by reactive, rather than resistive, hydrodynamic forces. It is important to evaluate WaveDyn simulation results with an appreciation for the magnitude of the body motions in the system. Large body motions as a result of low PTO damping, or the excitation of resonant modes can result in high levels of reported output power where, in reality, nonlinearity in the hydrodynamic loading or the presence of viscous effects may act to suppress such motions. The WaveDyn BEM-based model is particularly suited for situations where body motions are of a similar order of magnitude to the water particle kinematics (the case for many WECs operating in moderate, performance related sea-states) and for realistic, irregular wave simulations which are less likely to exhibit pronounced resonance effects than those that may occur in regular waves.

WaveDyn allows PTO properties to be applied to any joint in the system, where energy converted from the relative motion between adjacent bodies may be used to drive the WEC powertrain. For the initial set of performance calculations presented here, an idealized, passive linear damping control strategy has been used; PTO settings in terms of damping coefficients are specified at the beginning of a simulation and remain fixed throughout. This represents a simple, conservative approximation ahead of the inclusion of a more realistic PTO and controller model.

For this floating model the WEC 'backbone' is modeled with two vertical tendons attaching to each end of structure connecting it to the seabed with the tethers in tension. The tendons are considered in WaveDyn as a spring with an associated stiffness calculated based on the line properties. This is a quasi-static representation of the mooring forces where the applied mooring load is looked up as a function of the attachment point displacement relative to the anchor points. Therefore, mooring line inertial dynamics and line viscous drag effects are neglected.

A linearized model of the hydrostatic force has been assumed in this report. However the Centipod WEC device modeling may benefit from instantaneous hydrostatics being included as nonlinearities may arise if the water plane area changes significantly in larger waves. These effects could be included with the creation of an additional mesh incorporating panels above the mean free surface, allowing the instantaneous pressure over the wetted area to be computed at each timestep.

A description of the concept and the relevant input parameters for the Centipod CPX3 WaveDyn model are provided in following sections.

3 DESCRIPTION OF THE CENTIPOD CPX3 WEC

The Centipod WEC is designed to convert energy from the motion of five floats or "pods" found in a chain attached to a single structural backbone. The relative motion between the pods and 'backbone' are used to drive hydraulic PTO systems, with advanced control of the PTO being envisioned as a means of increasing efficiency. A preliminary moorings study found that if a catenary spread mooring system was incorporated for station-keeping purposes, it would be difficult to obtain adequate relative motion for acceptable power performance with the given geometry without the addition of heave plates suspended below the 'backbone' or other significant changes to design's physical characteristics and layout. It was also seen that, while using the current geometry, good relative motion could be obtained (similar to the initial fixed 'backbone' analysis presented in DNV GL report 702480-USSD-R-01-A) if a tension leg mooring system was incorporated. As such, a tension leg system has been added to the model analyzed in this report.

An early concept assembly drawing of the device is shown in Figure 3-1, although the dimensions and geometry have since been updated by DA to include additional 'backbone' buoyancy as required for the tension leg system and symmetrical pods. Therefore, the current system does not appear exactly as shown in the figure. The 'backbone' now consists of a 4 meter diameter tubular structure with a length of 74 meters and a total height of 20 meters, 8 meters of which is freeboard and 12 meters of which is the draft below the design still water line. The pods now have a circular profile when looking down from above with a diameter of 9 meters and the pod's draft below the still water level is 1.8 meters. There are no longer any lines connecting the pods to each other. The pods connect to the 'backbone' via the PTO unit (represented in the numerical models as a sliding joint) which is joined on the bottom end to the 'backbone' via a hinge joint allowing rotational motion about an axis parallel to the 'backbone' centerline. The updated geometry is reflected in the model as shown in Section 4 and Figures 4-1 to 4-4.

Figure 3-1: The Centipod WEC [3][1]

---
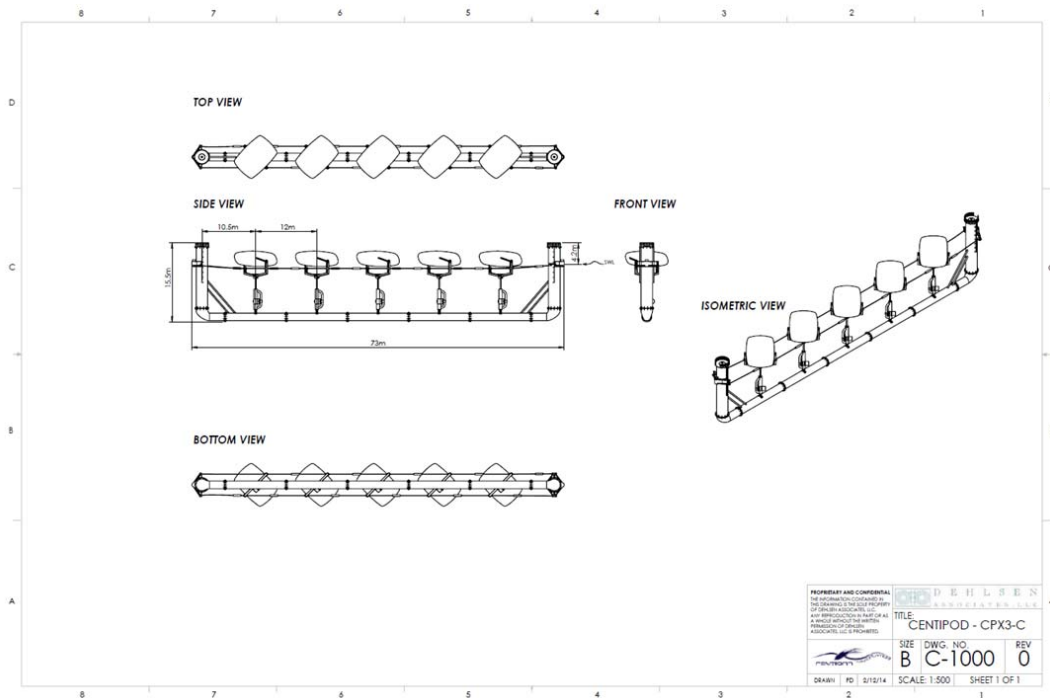
[1] The design has been significantly updated since this early Centipod CPX3 concept assembly drawing was generated.

4 CENTIPOD CPX3 WEC MODEL CONFIGURATION

4.1 Model Summary

WaveDyn simulation models are constructed on a multi-body basis, as a collection of linked components with specific physical properties. These components include wave-activated rigid bodies, joints at which PTO forces may be applied and mooring lines that may be assigned an anchor point and attached to the WEC structure.

The WaveDyn model of the Centipod CPX3 WEC is described below.

Several modules of WaveDyn interact to solve the multi-body dynamics of the Centipod CPX3 WEC model; these include:
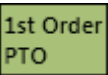
- Sea state;

- Structural Dynamics;

- Hydrodynamics;

- PTO response;

- Control (not incorporated into the current baseline model);

- Moorings

Each module incorporates a library of component models that may be used to build up a mathematical representation of the WEC. Figure 4-1 shows a complete block diagram of the components used to model the Centipod CPX3 device. An overview of the component types is provided in Table 4-1. More detail on each of the specific aspects of the model is given in the following sections.

Figure 4-1: WaveDyn WEC model schematic
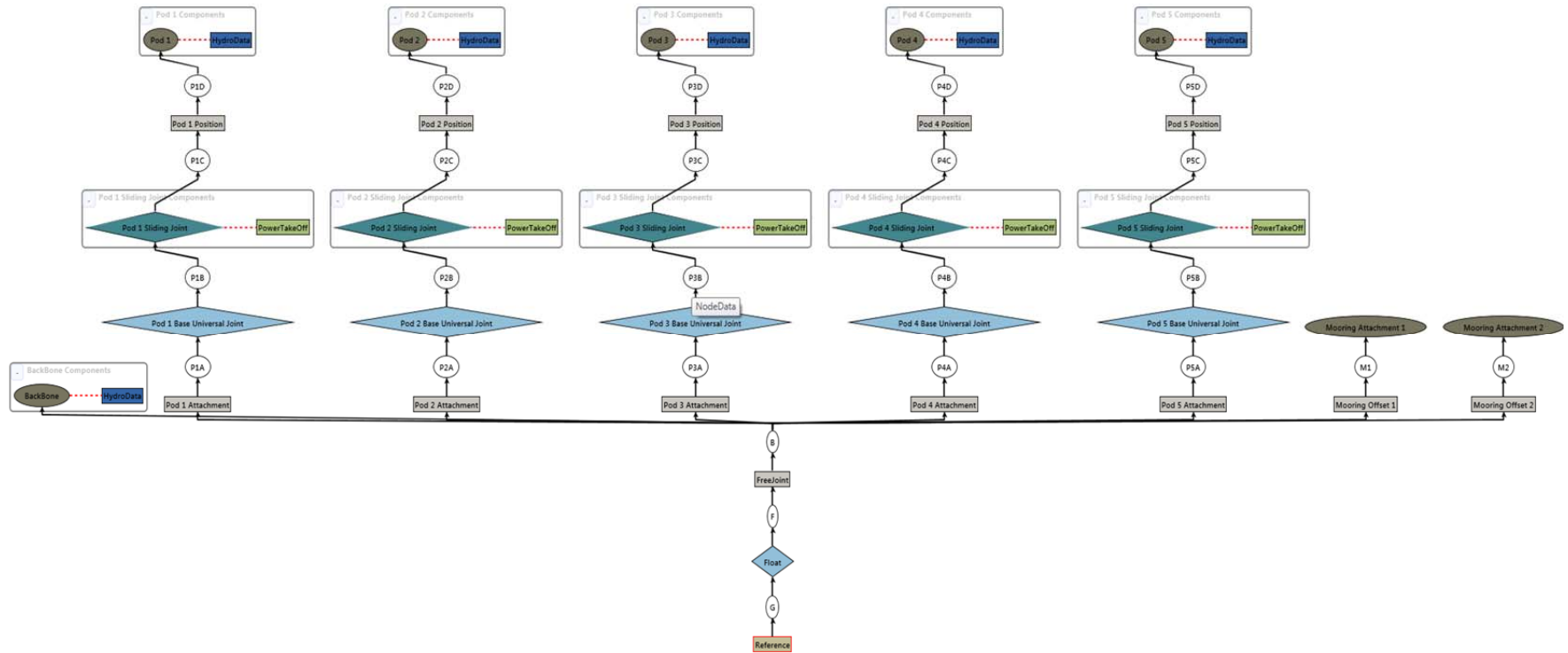
Table 4-1: WaveDyn multi-body components used in the Centipod model

Symbol	Type	Description
Ground	**Ground**	Special 'Ground' component. The starting point in global space from which the structural connectivity may be defined. All WaveDyn models must have a body with a Ground structural component.
Rigid Link	**Rigid Link**	A physical, completely rigid, but massless connection. Connects two nodes in any location in space. The nodes at either end of the rigid link may be specified with a rotational as well as translational offset.
Sliding Joint	**Sliding Joint**	A single degree of freedom translational joint. The translation axis can be defined in any direction. The proximal and distal nodes are coincident only in their initial position, but have a fixed relative orientation. The sliding joint freedom may be assigned structural stiffness or damping values that resist deflection from the initial position but do not contribute to the power take-off. A power take-off component may be assigned to the same body.
Rigid Body	**Rigid Body**	A point mass which experiences linear and nonlinear inertial and weight forces. A Rigid Body component may be accompanied by hydrodynamic and hydrostatic properties so that it is affected by the wave field (the body is said to be 'wave activated'). A Rigid Body is connected to a single node, its proximal node, only and has no distal node (as any distal node would simply sit exactly on top of the proximal node).
Floating	**Floating**	A free joint with 6 unrestrained degrees-of-freedom. The structure built onwards from the distal node will have no physical connection to the structure at the proximal node.
BEM Hydro	**Hydrodynamics**	Linear hydrodynamics component. The WaveDyn hydrodynamics module will apply wave excitation, radiation and hydrostatic loads to the body.
1st Order PTO	**1st Order PTO**	First order power take-off system. A linear damping, stiffness and pre-load may be specified and an appropriate PTO force is applied to the associated structural joint based on the joint freedom kinematics.

4.2 Structural Model

4.2.1 Pod and 'backbone' geometry

The WEC structural properties are represented in WaveDyn as rigid bodies with mass, moments of inertia and hydrodynamic properties. The component connectivity is defined using a series of nodes and massless rigid links which represent the physical offsets between individual parts of the WEC system. A block diagram representing the multi-body structure implemented in WaveDyn is provided in Figure 4-1.

In the present model, a ground node, placed at the 'backbone' proximal node (0,0,60m), is connected via a floating free joint to the 'backbone' structure node, allowing it to float unrestrained in all 6 degrees-of-freedom. The 'Pod Attachment' links provide the necessary horizontal offsets along the 'backbone' to the PTO units directly below each pod. A sliding joint PTO is used between the 'backbone' and each pod allowing single degree of freedom motion in the heave direction. A rigid connection links each sliding joint to the center of mass of the corresponding pod. At the connection point between each pod's corresponding sliding PTO joint and the 'backbone' an additional hinge joint provides a further degree of freedom for rotational motion of the PTO and pod about the 'backbone' in the primary wave direction. This compliance is expected to reduce large moment arms which otherwise could have been experienced at the structural joint.

The masses and moments of inertia about the centers of gravity of the pods and 'backbone' have been provided by DA and are summarized in Table 4-2 to Table 4-4 below. The center of mass positions have been provided relative to a reference location illustrated by the diagrams provided in Figure 4-2 and Figure 4-3. It should be noted that in WaveDyn the z-axis is the default vertical axis, whereas DA have supplied data using a coordinate system where the y-axis is the vertical axis. Therefore, care should be taken that the values for I_{yy} and I_{zz} are switched for both the pod and the 'backbone' when entering the inertia tensor matrix values into WaveDyn. The vertical offset for the 'backbone' center of mass should also be input as an offset along the z-axis in WaveDyn rather than the y-axis as shown in Table 4-4.**Table 4-2: Inertia tensor table for 'backbone' about center of mass including ballast (kgm^2). Coordinate system illustrated in Figure 4-2.**

I_{xx}=9713714	0	0
0	I_{yy}=196981292	0
0	0	I_{zz}=205715877

*N.b. WaveDyn equivalent inertia tensor input for the structural 'Body: Backbone':
{9713714, 0, 0} {0, 205715877, 0} {0, 0, 196981292}

Table 4-3: Inertia tensor table for pods about center of mass (kgm^2). Coordinate system illustrated in Figure 4-3.

I_{xx}=367958	0	0
0	I_{yy}=634402	0
0	0	I_{zz}=367958

*N.b. WaveDyn equivalent inertia tensor input for the structural 'Body: Pod [1-5]':
{367958, 0, 0} {0, 367958, 0} {0, 0, 634402}

Table 4-4: Masses of device including ballast (kg)

Component	Mass	Center of mass (coordinate system in Figure 4-2 and Figure 4-3)
Backbone	402000	(0, 0.95, 0)
Pods	78000	(0, 0, 0)

*N.b. WaveDyn equivalent center of mass input for the 'backbone':

{0, 0, 0.95}

Figure 4-2: Reference coordinate system used by DA of 'backbone' center of gravity in Table 4-4. (Note that WaveDyn uses a coordinate system where the z-axis is vertical)
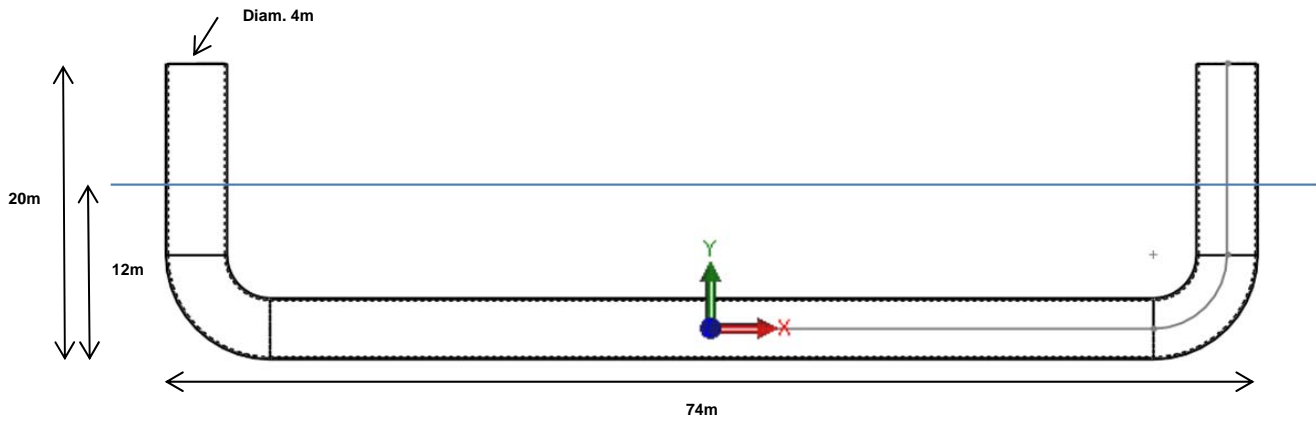
Figure 4-3: Reference coordinate system used by DA of pod center of gravity in Table 4-4. (Note that WaveDyn uses a coordinate system where the z-axis is vertical). The center of mass is located at the center of the body at the waterline. Not shown to scale with Figure 4-2.
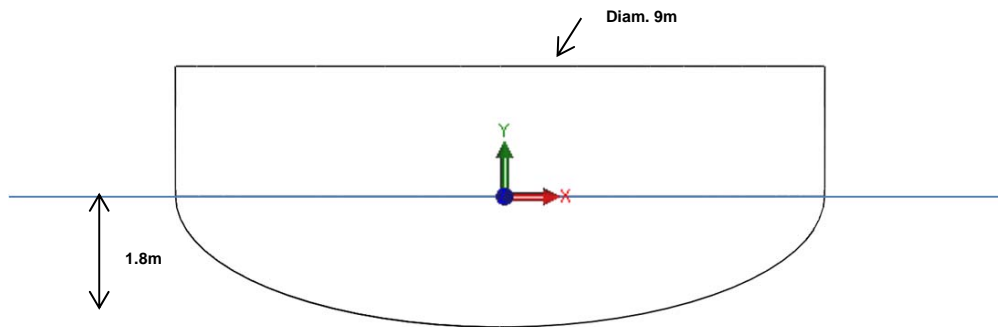
4.2.2 WEC geometry and WaveDyn coordinate systems

The Centipod model in this study comprises 5 pods and a 'backbone'. The pods are 12m apart and are located 10m above the longitudinal axis of the 'backbone'. Figure 4-4 displays the position of the pods, the orientation of the global coordinate system and the direction of the incident wave.

Figure 4-4: Centipod model, WaveDyn coordinate system and wave direction (distances in m).
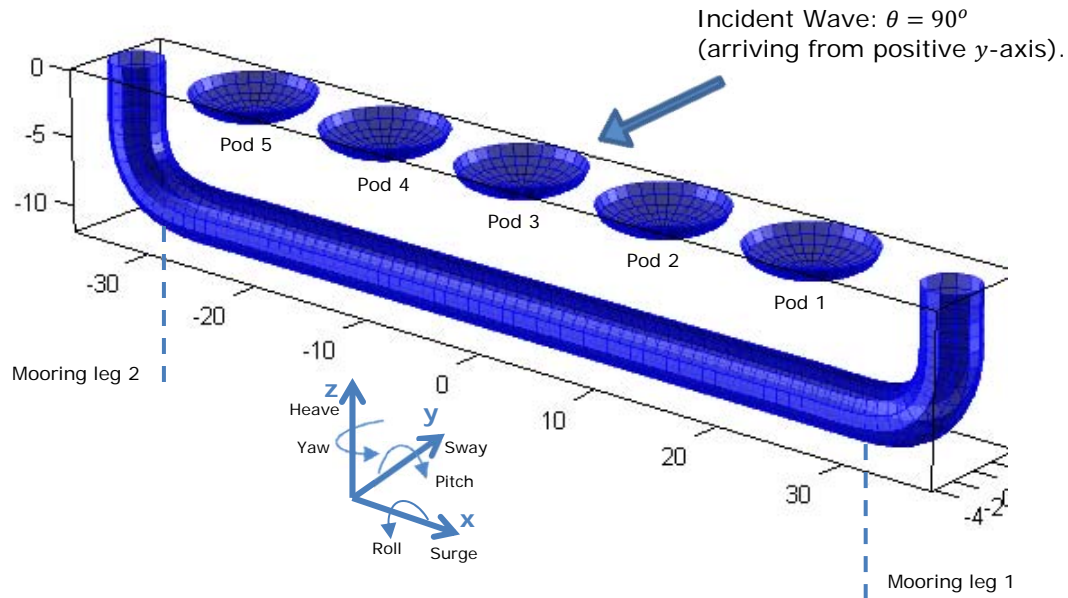
4.3 Hydrodynamics Model

4.3.1 Flow solver model

The hydrodynamic coefficients and the wave exciting force associated with each body and the interactions between them were loaded into the 'Hydrodynamics' model from WAMIT. The hydrodynamics data were limited to first-order (linear) quantities. The model geometry used by the flow solver was defined using the Rhinoceros 3D modelling tool. This allows the definition of the geometry to be represented as splines for use with the high-order method option in WAMIT. An example of the mean wetted profile of the Centipod WEC is shown in Figure 4-5 and Figure 4-6. The mesh and frequency resolution were refined to allow the accurate representation of specific hydrodynamic quantities such as the radiation force.

Figure 4-5: Profile showing the WAMIT mesh for a maximum panel size of 0.8m
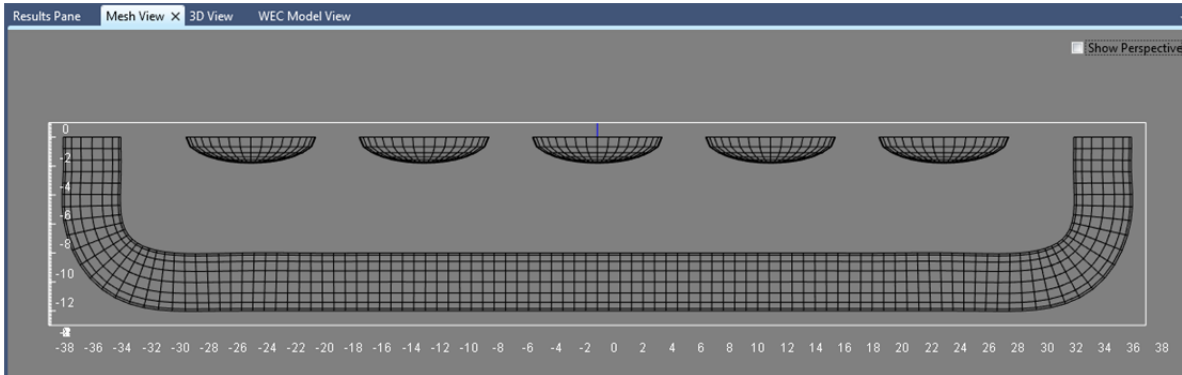
Figure 4-6: 3D view showing WAMIT mesh for maximum panel size of 0.8m
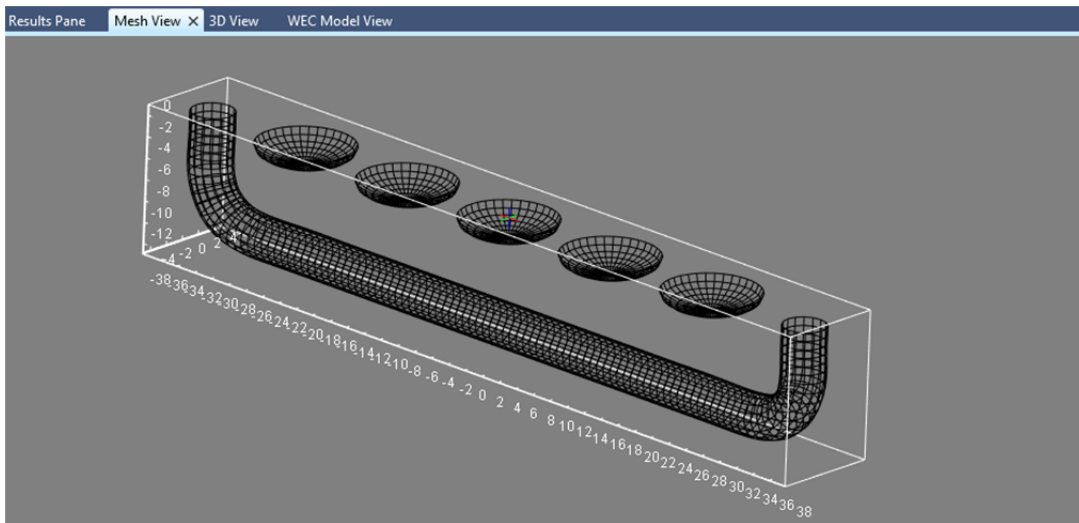
4.3.2 Hydrodynamic properties convergence tests

The final set of hydrodynamic data was derived following a convergence exercise focusing on the mesh resolution. Previous convergence studies [4] had investigated the frequency resolution (stated in 10APPENDIX B), radiation damping decay at high and low frequencies and length of impulse response functions. It was assumed that these results were still applicable given the similarities of the structure so focus was given to the mesh resolution.

4.3.2.1 Pod convergence

The mesh resolution of the pods was checked for convergence with special focus on the heave excitation force and radiation damping. The hydrodynamic data presented in this section for Pod 3 includes the influence of the 'backbone' and other pods in the vicinity. The focus for the excitation force convergence was on frequencies below 6rad/s, around 1s period, since for the sea-states investigated the energy beyond this frequency is negligible. The radiation damping was checked for convergence over a wider frequency range, providing a high level of confidence in values up to the frequencies where damping converged to zero (the

complete set of data is integrated over all frequencies by the WaveDyn pre-processor). The WAMIT high-order method was used to discretize the wetted surface of the bodies and WAMIT was provided with a nominal 'Panel Size' characteristic length as a means of controlling the overall geometric resolution. For this investigation, the values used for the panel size parameter were 2m, 1m and 0.8m.

Figure 4-7 and Figure 4-9 show that the excitation amplitudes for the pods have converged for every mesh size up until around 2.5rad/s. For higher frequencies the 2m mesh appears to be of insufficient resolution. A mesh of 1m is sufficient for convergence up until around 6rad/s.

The radiation damping in heave also requires the panel size to be 1m before convergence is seen and it decays to zero within the frequency range considered, as shown in Figure 4-8. However in sway (for translational motions in y – please see the axis orientations in Figure 4-4), the radiation damping (illustrated in Figure 4-10) only approaches zero for the highest frequencies studied. The non-complete decay to zero in the radiation damping is expected to have a very small effect on the final impulse response functions. Also a mesh size of 0.8m appears marginally superior in this case.

Figure 4-7: Heave excitation amplitude of Pod 3 for various mesh sizes with waves approaching from the positive global y axis
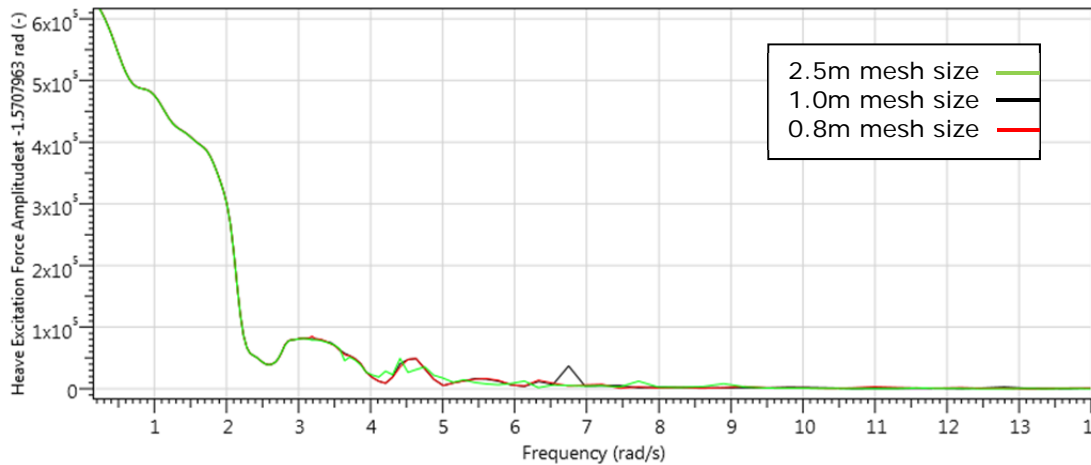
Figure 4-8: Heave radiation damping of Pod 3 for various mesh sizes
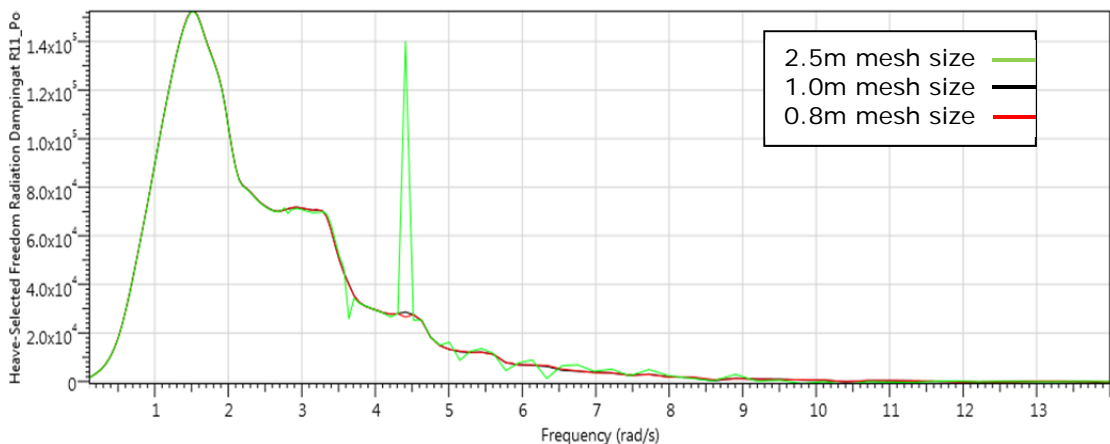
Figure 4-9: Sway excitation amplitude of Pod 3 for various mesh sizes with waves approaching from the positive global y axis
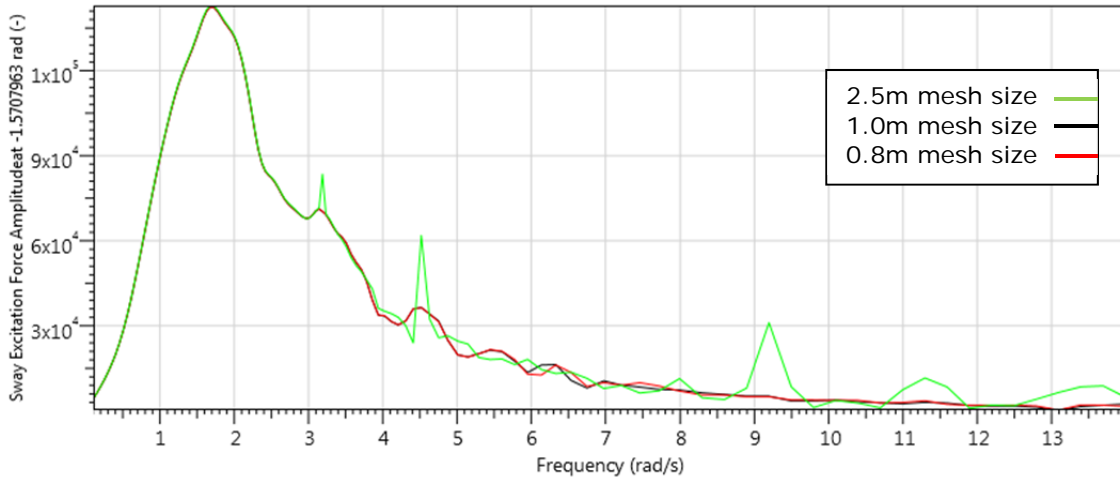
Figure 4-10: Sway radiation damping of Pod 3 for various mesh sizes
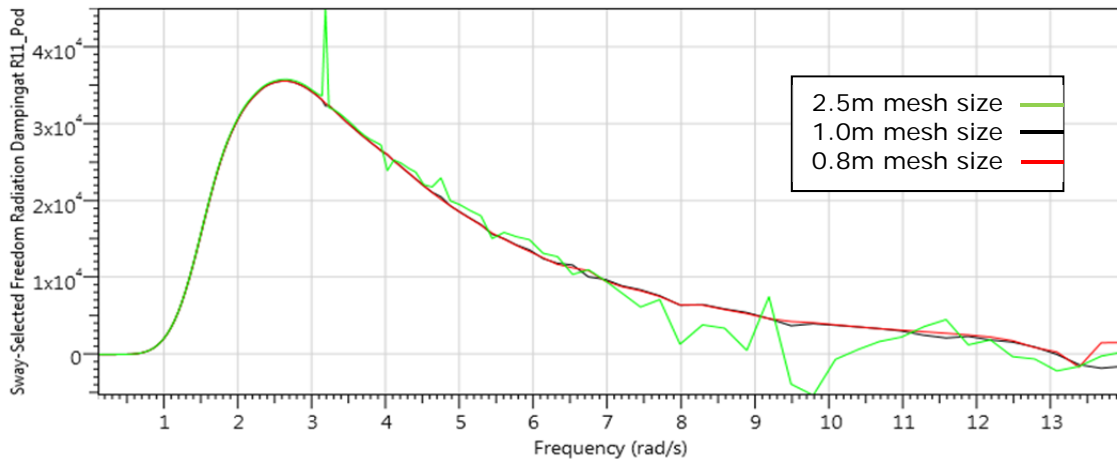
4.3.2.2 Backbone convergence

Figure 4-11 to Figure 4-14 show the convergence of the 'backbone' hydrodynamics with increasing mesh resolution. The data includes the effect of the pods being in the vicinity of the backbone. The first and third plots (Figure 4-11 and Figure 4-13) show that the excitation force of the 'backbone' is little affected by the mesh resolution, and given the large size of the back bone this could be expected. Figure 4-14 has the radiation damping plot for sway (motion in y axis) and shows that a resolution of 1m is sufficient to capture the hydrodynamic behavior of the backbone. As a mesh resolution of 1m was sufficient for the hydrodynamic properties to converge, that was the mesh size utilized to calculate the hydrodynamic properties for the model in WAMIT to be used in all WaveDyn simulations. The frequency resolution and range appear sufficient from the assumptions of previous work.

Figure 4-11: Heave excitation amplitude of 'backbone' for various mesh sizes with waves approaching from the positive global x axis
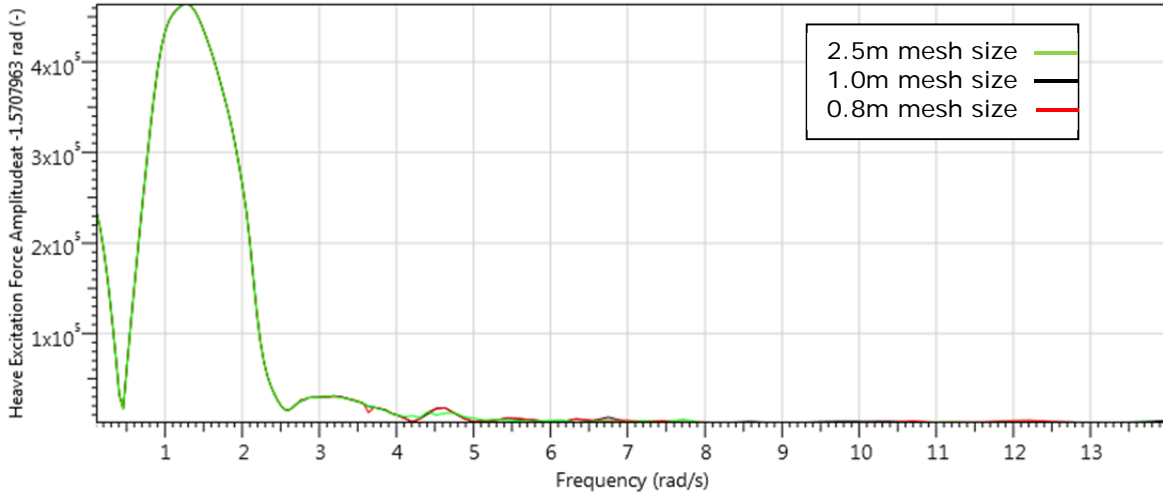
Figure 4-12: Heave radiation damping of 'backbone' for various mesh sizes
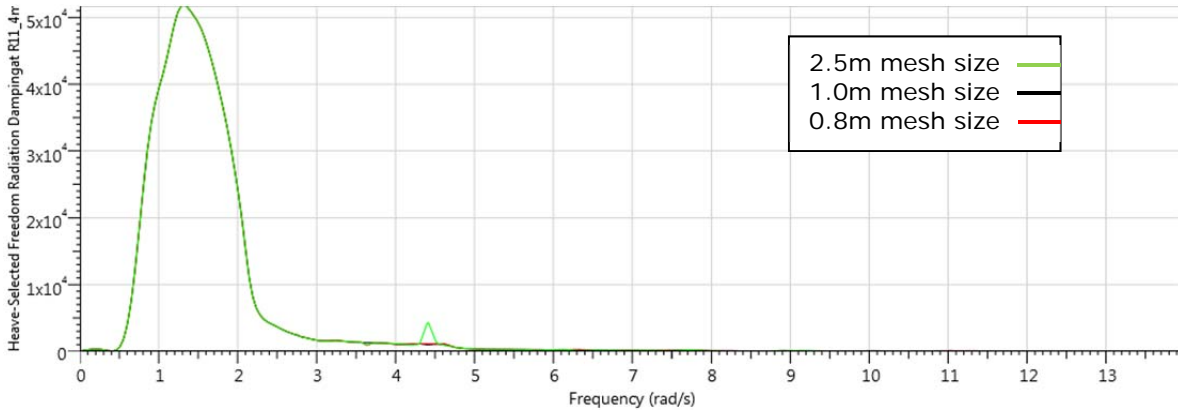
Figure 4-13: Sway excitation amplitude of 'backbone' for various mesh sizes with waves approaching from the positive global y axis
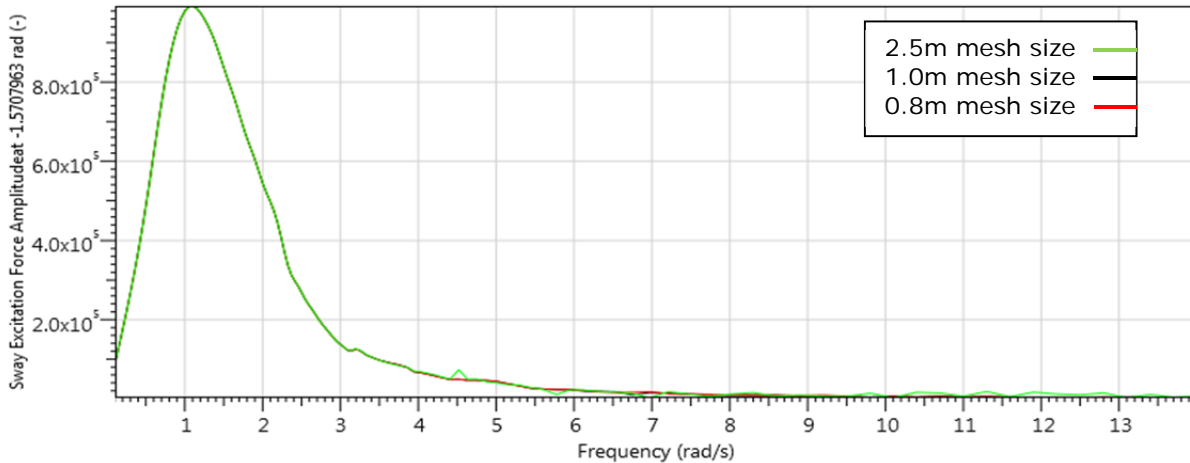
Figure 4-14: Sway radiation damping of 'backbone' for various mesh sizes
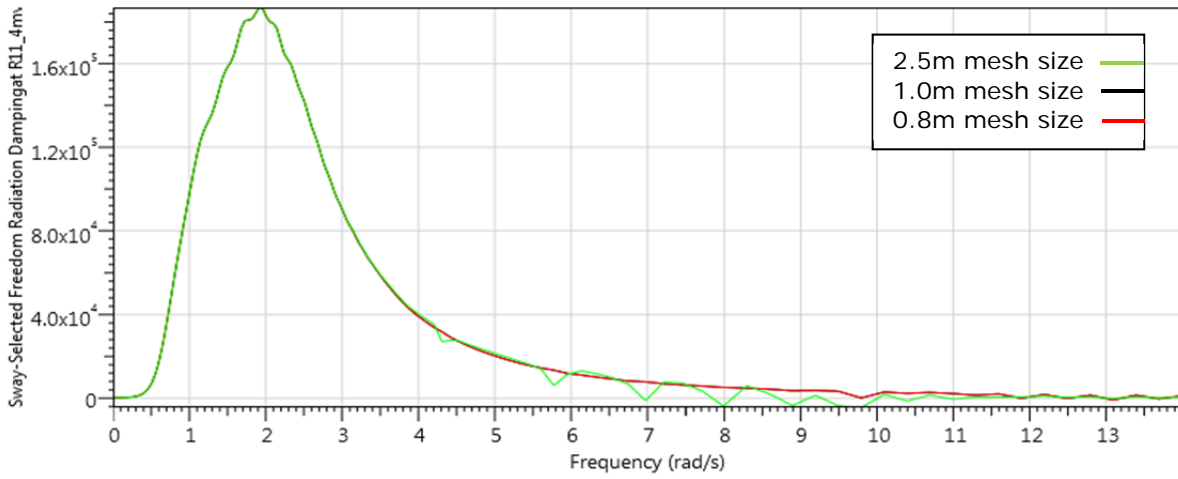
4.3.3 Hydrodynamics components in WaveDyn

The pre-processed hydrodynamics data has been imported into the WaveDyn model and is represented by the hydrodynamics components attached to the Backbone, Pod 1, Pod 2, Pod 3, Pod 4 and Pod 5 bodies. WaveDyn uses the hydrodynamic data to evaluate the incident, diffraction, radiation and hydrostatic forces on the bodies each time step.

4.4 Mooring System

For this study a tension leg mooring system has been considered and the 'backbone' has been freed to 'float' in space in all 6 degrees of freedom.

For an initial system design, galvanized spiral strand steel cable was selected for the tendon lines. These cables provide high strength, good torque balance, excellent fatigue performance and they can be sheathed resulting in design lifetimes of 20+ years. Examples from two different manufactures, Redaelli and Bridon, are shown in Figure 4-15 and Figure 4-16 below.

Figure 4-15:   Spiral strand steel cable – Redaelli [http://www.redaelli.com/en/products/ropes/spiral-ropes/]
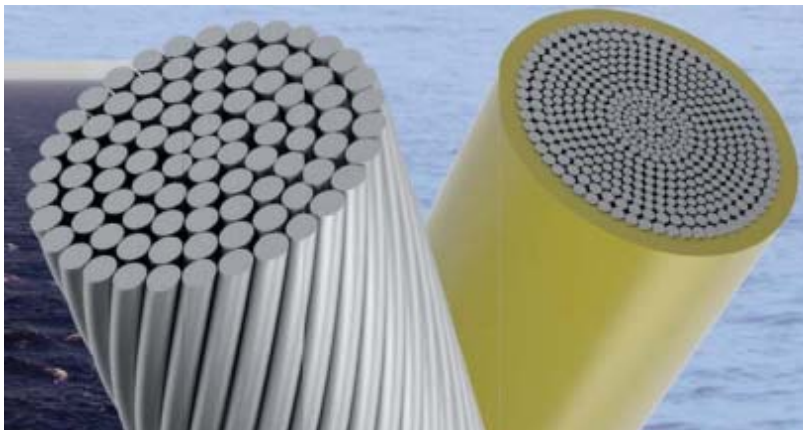
Figure 4-16: Spiral strand steel cable – Bridon [http://www.bridon.com/uk/oil-and-gas-ropes/floating-production-mooring-systems/floating-production-mooring-system-ropes/sheathed-spiral-strand-spr2plus/**]**
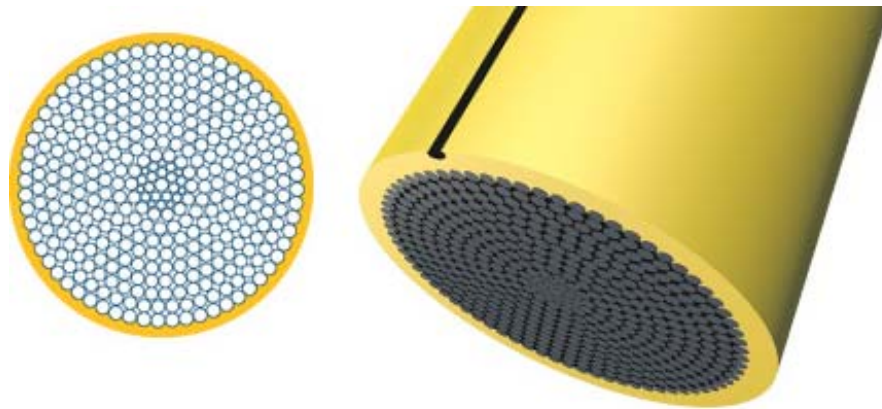
The mooring pre-tension is the difference between the water displacement provided by the 'backbone' at the design draught and the dry weight of the platform structure, and was given by DA as 903.96 tonnes.[2] The pretension in each of the two tension legs (one connecting to each end of the 'backbone') is half of the total pretension or 451.98 tonnes. Two cables in each leg are assumed in order to provide redundancy in case of a single-line failure. As an initial estimate for line sizing, complete submersion of the 'backbone' under extreme conditions would result in an additional static buoyancy force of 206.2 tonnes adding to leg tension (or 103.1 tonnes per leg). Therefore it was decided that, as a starting point, each line should initially be sized to withstand a minimum breaking force of approximately 555 tonnes (~5,445 kN) in static conditions. This corresponds to a line of at least 72mm core diameter (see table for Raedelli cable in Figure 4-17).

Maximum dynamic tensions experienced should be checked during future extreme conditions analysis and mooring line selection should be revisited to ensure adequate tendon sizing, but this static estimate formed an initial basis for determining the first line stiffness to be implemented in the WaveDyn model. Future adjustments to line size (and the resulting stiffness inputs) can be made based on the maximum dynamic tensions observed to ensure lines are adequately sized. It is noted, that lines of this type can be manufactured up to 150mm diameters with minimum breaking forces roughly 5x as large (see table for Bridon cable in Figure 4-18).

---

[2] DA determined that the pod buoyancy should not be considered to contribute to overall buoyancy for the purposes of these initial calculations. The pods are not meant to provide any design buoyancy or support the backbone, although they can be considered to provide some reserve buoyancy.

Figure 4-17 Spiral ropes properties

[http://www.redaelli.com/fileadmin/documents/Leaflet_flyer/Offshore/PML_Anchoring_and_mooring.pdf]

Spiral ropes XF (X-Force)

Core diameter (Nom.)		Metallic cross section	Mass						MBF			Sheathing radial thickness(*)	Axial stiffness @ 20% load
			Unsheathed in air		Unsheathed in water		Sheathed in air						
mm	inches	mm²	kg/m	lb/ft	kg/m	lb/ft	kg/m	lb/ft	kN	Mtons	Shtons	mm	MN
40		930	8.16	5.47	6.94	4.65	8.70	5.85	1685	172	189	4	153
41	1 5/8	977	8.69	5.82	7.39	4.95	9.30	6.25	1770	180	199	4	161
42		1025	9.00	6.03	7.65	5.13	9.70	6.52	1857	189	209	5	169
44		1125	9.87	6.62	8.39	5.63	10.6	7.12	2039	208	229	5	186
44.5	1 3/4	1151	10.1	6.75	8.59	5.74	10.9	7.32	2085	213	234	5	190
46		1230	10.8	7.23	9.18	6.15	11.6	7.79	2228	227	250	5	203
48	1 7/8	1339	11.8	7.87	10.0	6.69	12.6	8.47	2426	247	273	5	221
50		1453	12.8	8.54	10.9	7.26	13.8	9.27	2632	268	296	6	240
	2	1500	13.2	8.82	11.2	7.50	14.3	9.61	2717	277	305	6	247
52		1572	13.8	9.24	11.7	7.85	14.9	10.0	2847	290	320	6	259
54	2 1/8	1695	14.9	10.0	12.7	8.47	16.0	10.8	3071	313	345	6	280
56		1823	16.0	10.7	13.6	9.10	17.1	11.5	3302	337	371	6	301
58	2 1/4	1955	17.2	11.5	14.6	9.78	18.4	12.4	3542	361	398	6	323
60	2 3/8	2092	18.6	12.4	15.8	10.5	20.0	13.4	3791	386	426	7	345
62		2234	19.6	13.1	16.7	11.1	21.1	14.2	4048	413	455	7	369
64	2 1/2	2381	20.9	14.0	17.8	11.9	22.4	15.1	4313	440	485	7	393
66		2532	22.2	14.9	18.9	12.7	22.5	15.1	4587	468	515	7	418
	2 5/8	2583	22.7	15.2	19.3	12.9	24.5	16.5	4680	477	526	8	426
68		2687	23.6	15.8	20.1	13.4	25.4	17.1	4869	496	547	8	443
70	2 3/4	2848	25.0	16.7	21.3	14.2	26.9	18.1	5344	545	600	8	470
72		3013	26.4	17.7	22.4	15.0	28.3	19.0	5692	580	640	8	497
73	2 7/8	3097	27.2	18.2	23.1	15.5	29.2	19.6	5892	601	662	8	511
74		3183	27.9	18.7	23.7	15.9	29.9	20.1	6051	617	680	8	525
76		3357	29.5	19.7	25.1	16.7	31.8	21.4	6382	651	717	9	554
	3	3375	29.6	19.8	25.2	16.8	31.9	21.4	6416	654	721	9	557
77		3446	30.2	20.3	25.7	17.3	32.5	21.8	6581	671	740	9	562
80	3 1/8	3720	32.6	21.9	27.7	18.6	35.0	23.5	7168	731	805	9	606
82	3 1/4	3908	34.8	23.3	29.6	19.8	37.3	25.1	7635	778	858	9	637
84		4101	36.0	24.1	30.6	20.5	38.8	26.1	7867	802	884	10	668
86	3 3/8	4299	37.7	25.3	32.0	21.5	40.6	27.3	8095	825	910	10	701
88		4501	39.5	26.5	33.6	22.5	42.4	28.5	8402	856	944	10	734
90	3 1/2	4708	41.3	27.7	35.1	23.5	44.3	29.8	8706	887	978	10	767
92	3 5/8	4919	43.2	29.0	36.7	24.7	46.6	31.3	9183	936	1032	11	802
94		5135	45.1	30.2	38.3	25.7	48.6	32.7	9675	986	1087	11	837
95	3 3/4	5245	46.3	31.0	39.4	26.4	49.8	33.5	9973	1017	1121	11	855
96		5356	47.0	31.5	40.0	26.8	50.5	33.9	10331	1053	1161	11	873
98	3 7/8	5582	49.4	33.1	42.0	28.1	53.0	35.6	10847	1106	1219	11	910
100		5812	51.0	34.2	43.4	29.1	55.0	37.0	11201	1142	1259	12	947
102	4	6047	53.1	35.6	45.1	30.3	57.2	38.4	11558	1178	1299	12	986
104		6286	55.2	37.0	46.9	31.5	59.4	39.9	12006	1224	1349	12	1025
105	4 1/8	6408	56.2	37.7	47.8	32.0	60.4	40.6	12238	1247	1375	12	1044
106		6530	57.3	38.4	48.7	32.6	61.5	41.3	12360	1260	1389	12	1064
108	4 1/4	6773	59.5	39.9	50.6	33.9	63.8	42.9	12814	1306	1440	12	1104
109		6905	60.6	40.6	51.5	34.5	65.3	43.9	13022	1327	1463	13	1126
110		7032	61.7	41.3	52.4	35.1	66.5	44.7	13225	1348	1486	13	1146
112	4 3/8	7291	64.0	42.9	54.4	36.5	68.8	46.2	13675	1394	1537	13	1188
114	4 1/2	7553	66.6	44.6	56.6	37.9	71.5	48.0	14468	1475	1626	13	1231
115		7686	67.4	45.2	57.3	38.4	72.4	48.7	14548	1483	1635	13	1253
117	4 5/8	7956	70.4	47.2	59.8	40.1	75.9	51.0	15177	1547	1705	14	1297
119		8230	72.2	48.4	61.4	41.1	77.7	52.2	15577	1588	1750	14	1342

Figure 4-18   Spiral strand line properties

[http://www.bridon.com/x/downloads/oilandgas/Oil%20and%20Gas%20brochure.pdf]

Spiral Strand

Strand diameter		Approximate mass						Minimum breaking force (Fmin)						Sheathing radial thickness	Axial stiffness @20% load	Metallic cross section
		Unsheathed in air		Sheathed in air		Submerged		SPR2plus			Xtreme					
mm	in	kg/m	lb/ft	kg/m	lb/ft	kg/m	lb/ft	kN	Tonnes	Tons (2000lbs)	kN	Tonnes	Tons (2000lbs)	mm	MN	mm²
65	2½	21.0	14.1	22.7	15.2	17.6	11.8	4072	415	458	4553	464	511	6	416	2519
68	2⅝	22.6	15.2	24.4	16.4	18.9	12.7	4445	453	499	4869	496	547	6	441	2674
70	2¾	24.8	16.7	26.7	17.9	20.9	14.0	4700	479	528	5344	545	600	8	484	2935
73	2⅞	27.3	18.3	29.3	19.7	23.0	15.5	5120	522	575	5892	601	662	8	537	3252
76	3	29.7	20.0	31.8	21.4	25.2	16.9	5647	576	635	6416	654	721	8	584	3541
79	3⅛	32.7	22.0	34.9	23.4	27.7	18.6	6090	621	684	7059	720	793	8	620	3878
82	3¼	35.4	23.8	37.7	25.3	29.9	20.1	6550	668	736	7635	778	858	8	671	4194
86	3⅜	37.3	25.1	38.9	26.1	31.3	21.0	7190	733	808	8095	825	909	8	712	4451
90	3½	40.1	27.0	43.1	29.0	33.6	22.6	7938	809	892	8706	887	978	10	766	4787
92.5	3⅝	42.9	28.8	46.1	31.0	36.0	24.2	8394	856	943	9267	945	1041	10	813	5080
95.5	3¾	45.9	30.8	49.2	33.1	38.6	25.9	8930	911	1004	9917	1011	1114	10	870	5436
98	3⅞	50.4	33.9	54.0	36.3	42.7	28.7	9457	964	1063	10847	1106	1218	10	954	5963
102	4	53.7	36.1	57.6	38.7	45.3	30.4	10266	1047	1154	11558	1178	1298	11	1017	6354
105.5	4⅛	55.6	37.4	59.4	39.9	46.6	31.3	10867	1108	1221	12071	1230	1356	11	1056	6597
108	4¼	59.0	39.6	62.9	42.3	49.6	33.3	11427	1165	1284	12814	1306	1439	11	1120	7003
111.5	4⅜	63.1	42.4	67.2	45.1	53.1	35.7	12129	1237	1363	13675	1394	1536	11	1197	7480
114	4½	66.8	44.9	71.1	47.8	56.3	37.8	12775	1303	1436	14468	1475	1625	11	1266	7914
118	4⅝	70.3	47.2	74.6	50.1	59.1	39.7	13594	1386	1528	15177	1547	1705	11	1313	8309
121.5	4¾	74.1	49.8	78.5	52.7	62.2	41.8	14362	1465	1614	16008	1632	1798	11	1385	8764
124	4⅞	77.7	52.2	82.2	55.2	65.3	43.9	15073	1537	1694	16760	1708	1883	11	1452	9193
127	5	81.7	54.9	86.3	58.0	68.7	46.2	15722	1603	1767	17631	1797	1981	11	1528	9670
131	5⅛	84.6	56.8	89.3	60.0	70.8	47.6	16775	1711	1885	18300	1865	2056	11	1552	10010
133	5¼	88.8	59.7	93.6	62.9	74.6	50.1	17171	1751	1930	19204	1958	2157	11	1628	10505
137.5	5⅜	94.7	63.6	99.6	66.9	79.5	53.4	18272	1863	2053	20542	2094	2308	11	1736	11198
141	5½	99.1	66.6	104	69.9	83.1	55.8	19180	1956	2155	21509	2193	2416	11	1817	11725
144	5⅝	103	69.5	108	72.6	86.3	58.0	19867	2026	2233	22259	2269	2500	11	1884	12154
146.5	5¾	108	72.5	113	76.1	90.7	60.9	20469	2087	2300	23257	2371	2613	11	1969	12700
147.5	5⅞	113	76.0	119	79.6	95.5	64.2	20900	2131	2349	24259	2473	2725	11	2058	13275
153	6	118	79.0	123	82.9	99.1	66.6	22070	2251	2480	25302	2579	2842	11	2146	13846

The initial relaxed line length, L, is calculated from the design water depth (70m) and draught (12m) to be 58m. Under tension, after a small initial or permanent constructional extension, steel cables extend in a manner which complies approximately with Hooke's Law. As obtained from the tables in Figure 4-17 and Figure 4-18, the axial stiffness, EA, for 72mm-diameter line is approximately 500 MN.

The stiffness, K for each line can be calculated by dividing the axial stiffness by the length, L:

$$K_{line} = EA/L = 500 \text{ MN} / 58 \text{ m} = 8.62E6 \text{ N/m}$$

$$K_{leg} = K_{line2} + K_{line2} = 1.73E7 \text{ N/m}$$

As each leg represents 2 lines in parallel, a single mooring attachment point and combined stiffness was used as the input to the WaveDyn model. A WaveDyn screenshot showing the mooring line data inputs is shown in Figure 4-19.

Figure 4-19 Mooring line data inputs
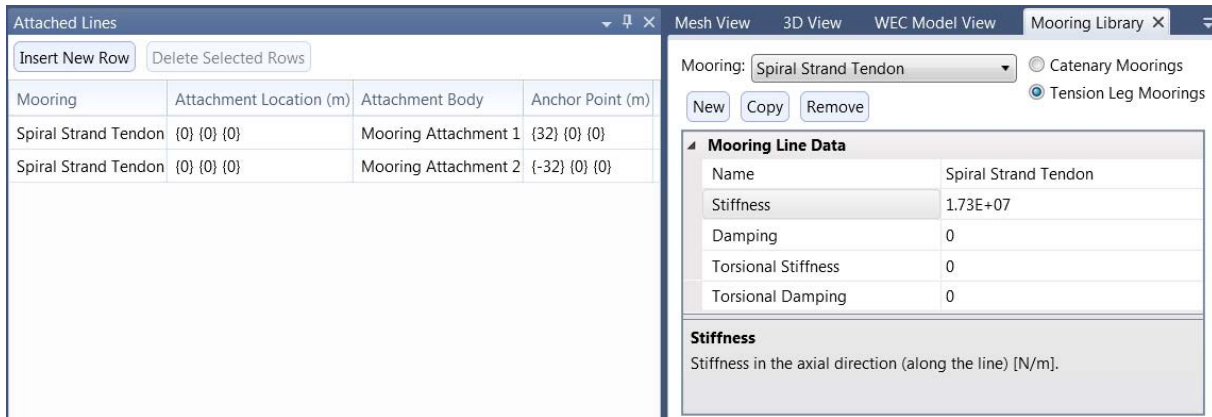
It's noted that the hydrostatic stiffness is roughly $2.5E5$ N/m and so the stiffness of the unconstrained system is many orders of magnitude lower than the line stiffness. The mooring lines used do need to be sufficiently stiff to avoid mooring natural heave periods where incoming wave spectrums have energy (e.g. less than 1s). That is, it is necessary to detune the system's heave period from the predominant wave frequency. Generally, steel wire provides sufficient stiffness to accomplish this in shallow and intermediate depths.

4.5 Power Take-Off (PTO) Model

WaveDyn contains a range of potential PTO models. The simplest of these is a first-order model which uses a fixed value of damping throughout the simulation. DA have provided a single damping value to be applied in all sea states [5]. It is understood that the value has been calculated by DA as the optimum for a single pod at a wave period of 8.7s and that it is an updated value from that used for a fixed 'backbone' in accordance with the updated geometries for the model utilized here.

Table 4-5: PTO parameters

	Damping (kNs/m)	Stiffness (kN/m)
Pod 1 sliding joint	688	0
Pod 2 sliding joint	688	0
Pod 3 sliding joint	688	0
Pod 4 sliding joint	688	0
Pod 5 sliding joint	688	0

5 OVERVIEW OF SIMULATION SETUP

5.1 Assessment of Extrapolation Method

The power in the waves increases with the square of the wave height. For a machine that demonstrates a linear response, it is possible to predict the absorbed power at one wave period and height, and extrapolate the absorbed power for the other heights (and the same period) from this result. A study has been conducted to confirm if this is applicable to the current Centipod WEC model, which incorporates a floating, tension tethered 'backbone' as was the case for a more constrained fixed 'backbone' case analyzed in an earlier effort (see 702480-USSD-R-01-A). The mechanically absorbed power at three significant wave heights and three peak periods has been computed assuming a Bretschneider spectrum for each sea state. Each sea state was run for 200 times the peak period with a ramp-up period[3] of 5s. The first 10 seconds of simulation where not included in the mean power calculation to omit unrealistic initial settling motions, however it was assumed to have a minimal impact on total mean power.

The simulated values for each wave height can be compared to corresponding values obtained by extrapolating the results from the simulations in Hs=1.75m. The results of the comparisons are shown in Table 5-2. Significant differences between the extrapolated and simulated values were observed. Therefore it was considered unacceptable to follow an extrapolation approach. All the 190 sea states with any occurrence in the scatter diagram shown in Table 5-5 were simulated.

Table 5-1: Simulated mean power capture for a variety of wave heights and periods.

Significant wave height	Peak period		
	8.7s	11.7s	15.7s
0.75m	24.0kW	22.4kW	18.3kW
1.75m	106.2kW	123.8kW	87.7kW
2.25m	172.0kW	178.1kW	145.3kW
4.75m	588.5kW	587.4kW	425.0kW

---

[3] The ramp-up period is the period over which the simulation gradually increases the wave amplitudes until fully developed conditions are reached, resulting in a reduction of the transient regime.

Table 5-2: Ratio of mean power extrapolated from the results for Hs=1.75m to the values from WaveDyn simulations presented in Table 5-1.

Significant wave height	Peak period		
	8.7s	11.7s	15.7s
0.75m	81.3%	101.4%	88.0%
1.75m	100.0%	100.0%	100.0%
2.25m	102.0%	114.9%	99.8%
4.75m	132.9%	155.3%	152.0%

5.2 Seed Uncertainty

Analysis earlier in the project (see 702480-USSD-R-01) showed that for the length of simulations in the various sea states (200 * Tp seconds) there was very little variation in the average power results from using different random seeds to generate the SEA files. This knowledge, in combination with the number of simulations required to fully populate the new power matrix, led to a single random seed being used to generate each sea state's SEA file for use in the WaveDyn simulations.

However, it should be noted that when running loads analysis, the minimum and maximum loads registered may vary between simulations using different random seeds. Therefore, the use of various seeds would be necessary to have the full characterization of the loads. In order to reduce the number of calculations carried out for this baseline effort, a statistical approach to the load calculations will be applied as described in Section 6. The load time-series for each component will be subject to a peak analysis and a probability of non-exceedance is attributed to each of the peaks.

5.3 Power Matrix Simulations

The WaveDyn time domain simulations of the Centipod CPX3 WEC provide an estimate of the total mean absorbed power for the machine as well as the power absorption associated with each individual PTO unit. A range of other variables, including wave induced forces, float motions and PTO forces are also generated and will be supplied to DA as part of the WaveDyn output files. Guidance found in "Standardized cost and Performance Reporting for Marine and Hydrokinetic Technologies" [6] was followed as a guide during the setup of these simulations.

A unidirectional Bretschneider spectrum was used to represent the sea states for each bin with an occurrence value greater than zero in the wave scatter plot provided in [4] and shown in Table 5-5. The use of a standard spectral shape characterized by a peak period is based on performance reporting guidance published by the Department of Energy (DOE) [6], as requested by the client. It is noted that the spectral shape resulting from site measurements may vary significantly from the standard Bretschneider spectrum shape. The length of the simulations has to be sufficient to capture the energy seen for the particular sea state with a length equal to the peak period multiplied by 200, as advised in the guidance note [6]. The

repetition period of the input sea state and the WaveDyn simulation have the same length. The ramp-up period (5s) remained unchanged for all simulations and the post-processed data consisted of the full time series starting at the 10s mark until the end of the simulation. Waves were assumed to come from a single idealized direction perpendicular to the 'backbone' centerline. The sensitivity of the device to directional spreading effects and to spectral shape may additionally be considered in the future.

Wave scatter probability data provided by DA [7], summarized in Table 5-5, was combined with the generated power matrix to predict the annual energy capture of the device assuming 100% availability. During this analysis no mechanical or electrical losses are assumed and so the values presented are idealized.

It should be noted, that although simulations were run for Hs up to 8.75m in a couple of instances, assumptions for linear theory are less valid for large wave heights, and therefore the results from simulations in large and steep waves are likely to be less representative of the true behavior of the system. Since the number of occurrences at these larger sea states are small, there is not much impact on overall power performance and annual energy yield as shown in Table 6-2. For this reason, it may be considered a good strategy to have the WEC in a non-operational or 'survival mode' during these conditions. Any considerations of loads calculated during these states, should be made with caution.

Table 5-3: Summary of the environmental conditions simulated

Minimum Tp	3.7s
Maximum Tp	19.7s
Tp step	1s
Hs	1.75m – 8.75m (depending on occurrence)
Hs step	0.5m
Number of seeds per sea state	1
Water depth	70m

Table 5-4: Summary of the simulation parameters used in WaveDyn

WaveDyn version		1.2.0.9
Integrator		Variable time step; min 0.0001s, max. 1s
Excitation forces		Linear
Hydrostatic forces		Linear
Radiation force impulse response function	Cut-off time	60s
	Resolution	0.1s
	Min. time step	0.1s
Drag coefficient		0
PTO damping		Linear 688kNs/m
Simulation length		200 T_p s
Output time step		0.1s
Ramp-up time		5s

Table 5-5: Wave scatter table for an incident sea states (%).

Hs \ Tp	1.7	2.7	3.7	4.7	5.7	6.7	7.7	8.7	9.7	10.7	11.7	12.7	13.7	14.7	15.7	16.7	17.7	18.7	19.7	20.7
0.25	0.00%	0.00%	0.00%	0.00%	0.00%	0.01%	0.00%	0.00%	0.00%	0.00%	0.00%	0.00%	0.00%	0.01%	0.00%	0.00%	0.00%	0.00%	0.00%	0.00%
0.75	0.00%	0.00%	0.01%	0.15%	0.43%	1.07%	1.12%	1.30%	0.41%	0.63%	0.28%	0.20%	0.20%	0.34%	0.43%	0.48%	0.17%	0.00%	0.03%	0.00%
1.25	0.00%	0.00%	0.02%	0.10%	0.98%	2.80%	2.38%	4.56%	1.85%	2.16%	1.12%	0.87%	0.66%	0.55%	0.37%	0.44%	0.24%	0.00%	0.05%	0.00%
1.75	0.00%	0.00%	0.00%	0.03%	0.25%	2.47%	2.67%	3.64%	2.09%	3.53%	1.95%	1.36%	1.21%	0.95%	0.46%	0.51%	0.29%	0.00%	0.11%	0.00%
2.25	0.00%	0.00%	0.00%	0.00%	0.04%	0.64%	2.32%	3.56%	1.65%	3.27%	2.45%	1.86%	1.51%	1.03%	0.56%	0.51%	0.31%	0.00%	0.12%	0.00%
2.75	0.00%	0.00%	0.00%	0.00%	0.00%	0.19%	0.90%	2.73%	1.00%	2.16%	1.96%	1.51%	1.34%	0.85%	0.52%	0.49%	0.33%	0.00%	0.14%	0.00%
3.25	0.00%	0.00%	0.00%	0.00%	0.00%	0.03%	0.18%	1.06%	0.69%	1.21%	1.29%	1.19%	1.05%	0.83%	0.49%	0.43%	0.19%	0.00%	0.07%	0.00%
3.75	0.00%	0.00%	0.00%	0.00%	0.00%	0.00%	0.04%	0.29%	0.32%	0.53%	0.75%	0.68%	0.70%	0.60%	0.34%	0.27%	0.12%	0.00%	0.06%	0.00%
4.25	0.00%	0.00%	0.00%	0.00%	0.00%	0.00%	0.00%	0.09%	0.10%	0.18%	0.28%	0.34%	0.41%	0.36%	0.22%	0.23%	0.09%	0.00%	0.03%	0.00%
4.75	0.00%	0.00%	0.00%	0.00%	0.00%	0.00%	0.00%	0.01%	0.03%	0.07%	0.08%	0.12%	0.18%	0.24%	0.15%	0.16%	0.07%	0.00%	0.03%	0.00%
5.25	0.00%	0.00%	0.00%	0.00%	0.00%	0.00%	0.00%	0.00%	0.01%	0.01%	0.03%	0.05%	0.09%	0.12%	0.09%	0.10%	0.05%	0.00%	0.02%	0.00%
5.75	0.00%	0.00%	0.00%	0.00%	0.00%	0.00%	0.00%	0.00%	0.00%	0.00%	0.00%	0.01%	0.03%	0.05%	0.04%	0.05%	0.02%	0.00%	0.01%	0.00%
6.25	0.00%	0.00%	0.00%	0.00%	0.00%	0.00%	0.00%	0.00%	0.00%	0.00%	0.00%	0.01%	0.01%	0.04%	0.02%	0.03%	0.02%	0.00%	0.00%	0.00%
6.75	0.00%	0.00%	0.00%	0.00%	0.00%	0.00%	0.00%	0.00%	0.00%	0.00%	0.00%	0.00%	0.01%	0.01%	0.01%	0.01%	0.01%	0.00%	0.00%	0.00%
7.25	0.00%	0.00%	0.00%	0.00%	0.00%	0.00%	0.00%	0.00%	0.00%	0.00%	0.00%	0.00%	0.00%	0.00%	0.01%	0.01%	0.00%	0.00%	0.00%	0.00%
7.75	0.00%	0.00%	0.00%	0.00%	0.00%	0.00%	0.00%	0.00%	0.00%	0.00%	0.00%	0.00%	0.00%	0.00%	0.00%	0.00%	0.00%	0.00%	0.00%	0.00%
8.25	0.00%	0.00%	0.00%	0.00%	0.00%	0.00%	0.00%	0.00%	0.00%	0.00%	0.00%	0.00%	0.00%	0.00%	0.00%	0.00%	0.00%	0.00%	0.00%	0.00%
8.75	0.00%	0.00%	0.00%	0.00%	0.00%	0.00%	0.00%	0.00%	0.00%	0.00%	0.00%	0.00%	0.00%	0.00%	0.00%	0.00%	0.00%	0.00%	0.00%	0.00%
9.25	0.00%	0.00%	0.00%	0.00%	0.00%	0.00%	0.00%	0.00%	0.00%	0.00%	0.00%	0.00%	0.00%	0.00%	0.00%	0.00%	0.00%	0.00%	0.00%	0.00%
9.75	0.00%	0.00%	0.00%	0.00%	0.00%	0.00%	0.00%	0.00%	0.00%	0.00%	0.00%	0.00%	0.00%	0.00%	0.00%	0.00%	0.00%	0.00%	0.00%	0.00%
10.3	0.00%	0.00%	0.00%	0.00%	0.00%	0.00%	0.00%	0.00%	0.00%	0.00%	0.00%	0.00%	0.00%	0.00%	0.00%	0.00%	0.00%	0.00%	0.00%	0.00%
10.8	0.00%	0.00%	0.00%	0.00%	0.00%	0.00%	0.00%	0.00%	0.00%	0.00%	0.00%	0.00%	0.00%	0.00%	0.00%	0.00%	0.00%	0.00%	0.00%	0.00%
11.3	0.00%	0.00%	0.00%	0.00%	0.00%	0.00%	0.00%	0.00%	0.00%	0.00%	0.00%	0.00%	0.00%	0.00%	0.00%	0.00%	0.00%	0.00%	0.00%	0.00%
11.8	0.00%	0.00%	0.00%	0.00%	0.00%	0.00%	0.00%	0.00%	0.00%	0.00%	0.00%	0.00%	0.00%	0.00%	0.00%	0.00%	0.00%	0.00%	0.00%	0.00%
12.3	0.00%	0.00%	0.00%	0.00%	0.00%	0.00%	0.00%	0.00%	0.00%	0.00%	0.00%	0.00%	0.00%	0.00%	0.00%	0.00%	0.00%	0.00%	0.00%	0.00%

Peak Period, Tp [sec] (column headers) — Significant Wave Height, Hs [m] (row headers)

6 POWER PERFORMANCE

6.1 Power matrix and nominal energy yield

The results of the simulations described in Section 5.3 are represented by the power matrix displayed in Table 6-1. A number of entries have been greyed out due to no occurrence in the wave scatter plot. A significant wave height up to 8.75m is shown for a couple of scatter table entries, however it should be noted that the assumptions associated with linear wave theory are less valid for large wave heights – with the general tendency to over predict motions and therefore power absorption. The power matrix has been combined with the scatter diagram presented in Table 5-5 to obtain an annual energy yield matrix and a nominal annual energy yield value shown in Table 6-2. This matrix provides a sense of which sea states are contributing the most energy production with the current design and assumptions.

The relative capture width (RCW) has also been evaluated for each sea state bin. This is the ratio between the averaged power absorbed by the WEC, $\overline{P_{abs}}$ and the available power in an equivalent width of incident wave front, $\overline{P_w}$ and may be viewed as a measure of WEC efficiency:

$$RCW = \frac{\overline{P_{abs}}}{\overline{P_w}} \tag{1}$$

$$\overline{P_w} = \frac{\rho g^2 H_s{}^2 T_e}{64\pi} l \tag{2}$$

where l is a characteristic width of the WEC (74m has been used in this case as the frontal width exposed to the on-coming waves), and $T_e = 0.8572 T_p$ for the Bretschneider spectrum.

Greatest relative capture width is achieved for periods of approximately 5-6s, although a greater proportion of the total wave energy presented in the scatter table is at higher periods and DNV GL understands that the PTO damping has been tuned for waves with a 8.7s period [3]. This suggests that there is significant room for power performance improvements, although this may require a larger structure if performance is to be improved at longer wavelengths.

Table 6-1: Full power matrix (kW). Incident wave direction perpendicular to the 'backbone'

Hs, [m]	Tp [s]																
	3.7	4.7	5.7	6.7	7.7	8.7	9.7	10.7	11.7	12.7	13.7	14.7	15.7	16.7	17.7	18.7	19.7
0.25				3.1	3.1			2.9	2.8	2.6	2.5	2.4	2.2		2.0		
0.75	12.0	18.6	22.6	24.0	24.1	24.0	23.7	23.5	22.4	21.6	20.6	19.4	18.3	17.3	16.4		14.7
1.25	32.5	51.6	55.6	61.5	62.0	61.9	64.2	62.6	59.9	58.0	55.3	50.8	50.0	46.4	43.8		40.1
1.75	63.9	102.6	113.6	117.1	120.0	106.2	118.7	116.5	123.8	108.2	102.6	95.3	87.7	88.0	82.4		72.1
2.25		168.5	186.6	179.5	180.3	172.0	192.1	181.1	178.1	168.1	161.6	158.2	145.3	134.1	125.9		111.5
2.75			253.9	238.6	239.9	240.2	257.3	255.8	261.4	240.4	212.6	203.1	196.7	189.3	179.4		162.3
3.25			382.4	338.3	316.8	334.3	343.1	348.2	335.3	315.6	274.0	278.8	253.8	234.7	231.4		216.4
3.75				461.0	389.3	432.5	421.9	421.3	433.0	401.7	349.5	331.6	330.1	306.5	288.2		260.8
4.25					500.9	503.6	512.7	498.9	487.2	442.8	441.7	406.0	402.1	370.8	346.1		293.3
4.75					588.5	600.2	610.8	587.4	541.9	522.1	489.9	425.0	416.1	393.1			369.5
5.25					755.8	768.4	700.9	699.5	678.5	641.4	597.8	567.7	542.9	521.5	463.0		419.8
5.75							796.1	779.8	829.1	710.9	647.0	649.4	597.1	555.0	538.4		488.2
6.25									831.0	822.6	713.6	699.5	620.3	597.6	580.8		555.4
6.75									902.7	939.0	807.8	754.9	648.8	660.1	627.1		581.7
7.25									1002.1	992.9	892.3	840.8	783.6	723.8	671.4		644.9
7.75												889.4	806.9	747.1	753.1		
8.25													855.1		742.0		
8.75												1027.2			793.4		

Table 6-2: Annual energy yield matrix (MWh) and total annual energy yield of single device assuming, linear hydrodynamics, no mechanical/electrical losses/constraints and 100% availability.

		Energy Matrix per year (MWh)															
		Peak Period, Tp [s]															
		3.7	4.7	5.7	6.7	7.7	8.7	9.7	10.7	11.7	12.7	13.7	14.7	15.7	16.7	17.7	18.7	19.7
Significant Wave Height, Hs [m]	0.25				0.002	0.000			0.000	0.000	0.001	0.000	0.001	0.000		0.000		
	0.75	0.012	0.237	0.848	2.245	2.371	2.736	0.847	1.301	0.544	0.388	0.362	0.574	0.697	0.729	0.240		0.036
	1.25	0.054	0.471	4.782	15.117	12.932	24.744	10.397	11.880	5.887	4.448	3.176	2.430	1.601	1.792	0.934		0.164
	1.75	0.018	0.296	2.442	25.318	28.067	33.923	21.764	36.042	21.143	12.910	10.867	7.974	3.510	3.940	2.109		0.698
	2.25		0.031	0.712	10.141	36.733	53.660	27.802	51.982	38.175	27.379	21.372	14.341	7.086	5.966	3.422		1.152
	2.75			0.047	3.975	18.934	57.522	22.606	48.401	44.960	31.749	24.892	15.141	8.897	8.122	5.243		2.024
	3.25			0.036	0.850	5.130	30.927	20.756	37.010	37.885	33.045	25.323	20.266	10.984	8.781	3.790		1.370
	3.75				0.086	1.449	11.070	11.741	19.488	28.371	23.816	21.404	17.530	9.893	7.132	3.058		1.359
	4.25					0.047	3.890	4.533	7.801	11.971	13.023	15.951	12.810	7.897	7.592	2.802		0.737
	4.75						0.712	1.676	3.525	3.882	5.649	8.407	10.122	5.419	6.003	2.488		0.963
	5.25					0.141	0.143	0.457	0.716	1.516	2.806	4.562	5.918	4.497	4.514	2.068		0.664
	5.75							0.148	0.290	0.231	0.728	1.807	3.022	2.334	2.273	1.102		0.318
	6.25									0.232	0.383	0.863	2.214	1.039	1.446	0.919		0.155
	6.75									0.168	0.262	0.451	0.843	0.302	0.860	0.409		0.108
	7.25									0.093	0.092	0.083	0.235	0.365	0.404	0.125		0.060
	7.75												0.083	0.150	0.209	0.140		
	8.25													0.159		0.069		
	8.75												0.191			0.074		

Total Annual energy yield

1502 MWh

Table 6-3: Relative capture width of device

Table 6-3: Relative capture width of device

RCW

Significant Wave Height, Hs [m] (rows) vs. Peak Period, Tp [sec] (columns)

Hs \ Tp	1.7	2.7	3.7	4.7	5.7	6.7	7.7	8.7	9.7	10.7	11.7	12.7	13.7	14.7	15.7	16.7	17.7	18.7	19.7
0.25						0.238	0.207			0.139	0.123	0.105	0.094	0.084	0.072		0.058		
0.75			0.185	0.226	0.226	0.205	0.179	0.158	0.140	0.125	0.109	0.097	0.086	0.075	0.067	0.059	0.053		0.043
1.25			0.181	0.226	0.200	0.189	0.166	0.146	0.136	0.120	0.105	0.094	0.083	0.071	0.065	0.057	0.051		0.042
1.75			0.181	0.229	0.209	0.183	0.163	0.128	0.128	0.114	0.111	0.089	0.079	0.068	0.059	0.055	0.049		0.038
2.25				0.227	0.208	0.170	0.149	0.125	0.126	0.107	0.097	0.084	0.075	0.068	0.059	0.051	0.045		0.036
2.75					0.189	0.151	0.132	0.117	0.113	0.102	0.095	0.080	0.066	0.059	0.053	0.048	0.043		0.035
3.25					0.204	0.154	0.125	0.117	0.108	0.099	0.087	0.076	0.061	0.058	0.049	0.043	0.040		0.033
3.75						0.157	0.115	0.114	0.099	0.090	0.085	0.072	0.058	0.052	0.048	0.042	0.037		0.030
4.25							0.116	0.103	0.094	0.083	0.074	0.062	0.057	0.049	0.046	0.039	0.035		0.026
4.75								0.096	0.088	0.081	0.071	0.061	0.054	0.047	0.039	0.035	0.032		0.027
5.25						0.114	0.103	0.084	0.076	0.068	0.059	0.051	0.045	0.040	0.036	0.030			0.025
5.75								0.080	0.071	0.069	0.054	0.046	0.043	0.037	0.032	0.030			0.024
6.25										0.058	0.053	0.043	0.039	0.032	0.029	0.027			0.023
6.75										0.054	0.052	0.042	0.036	0.029	0.028	0.025			0.021
7.25										0.052	0.048	0.040	0.035	0.030	0.026	0.023			0.020
7.75														0.032	0.027	0.024	0.023		
8.25															0.026		0.020		
8.75														0.029			0.019		

6.2 Key assumptions and caveats

The power matrix, relative capture width and annual energy yield data presented may be considered a baseline set of performance data for the initial 2-leg WaveDyn model of the concept floating TLP Centipod WEC. The WEC is modelled at an early stage of development, operating in idealized conditions and the following assumptions and caveats apply:

- The power values have been obtained using a PTO and control model manifested as a perfect linear damper. A single damping value has been applied across all sea states and this is not expected to result in optimal performance. No consideration of the true characteristics, efficiency and operating limitations of the PTO, controller or any other of the WEC subsystems has been incorporated in the model at this stage but should be seen as necessary development in the future.

- The performance data was derived using a linear hydrodynamic model without viscous damping. The validity of this model may be expected to be reduced in larger sea-states. The model would ideally be verified against a higher order formulation and validated against tank test results as part of future work.

- The sensitivity of the WEC model to spectral shape, mean wave direction and directional spreading has not been considered. Such effects would ideally be incorporated in full a site specific power matrix for a prototype machine.

- A nominal energy yield has been derived based on 100% availability under a single mode of operation without provision for faults or maintenance. This scenario is highly idealized and, whilst the yield value obtained may be used to inform the WEC development process, it should not be used directly in a cost of energy model.

7 OPERATIONAL LOADS

7.1 Methodology

The loads on the various WEC components are calculated (and output) within WaveDyn for all the elements in the structure. For the Centipod machine, the loads on the pods, mooring loads and loads on the PTO are considered the outputs of most interest. A statistical analysis of the loads has been performed (min, max, mean, standard deviation). The non-exceedance curves for the various sea states have also been calculated. The use of this type of output allows a good understanding of the various loads levels experienced by the WEC components. It also provides a useful way to compare the influence on the loads of changing the WEC configurations. The use of these cumulative probability curves can also be used at a later stage for loads extrapolation and fatigue analysis.

The scheme below illustrates the main steps used in this load analysis.

7.2 WaveDyn outputs

WaveDyn outputs structural loads for all the proximal nodes in the model. These forces and moments are the resultant forces and moments acting on a particular element. By default, WaveDyn outputs these structural forces at the location of the proximal node and the output coordinate system is orientated with the global axis defined in WaveDyn. The global WaveDyn model is located at sea bed, with the z-axis pointing up-wards Figure 7-1 (left). The global coordinate system is kept constant throughout all the simulation.

For most structural analysis, the loads given in a body fixed coordinate system are most useful. The body fixed coordinate system is defined at the element proximal node with the z-axis pointing upwards (central axis of the pod for example). The orientation of body $x-$ and $y-$ axis is equal to the global coordinates at

the beginning of the simulation. With the displacement of the body the coordinate system it is rotated such that the main axis follows the body main axis, see Figure 7-1 (right). The rotation of the body is defined at the body proximal node with the global coordinate system. The rotation angles A, B and C are measured around the global coordinate axis x_g, y_g and z_g . An example of this for angle A is given in Figure 7-1 (right). These angles are part of the WaveDyn displacements output.

Figure 7-1: Global coordinate system and body coordinate system (rotation around x-axis)
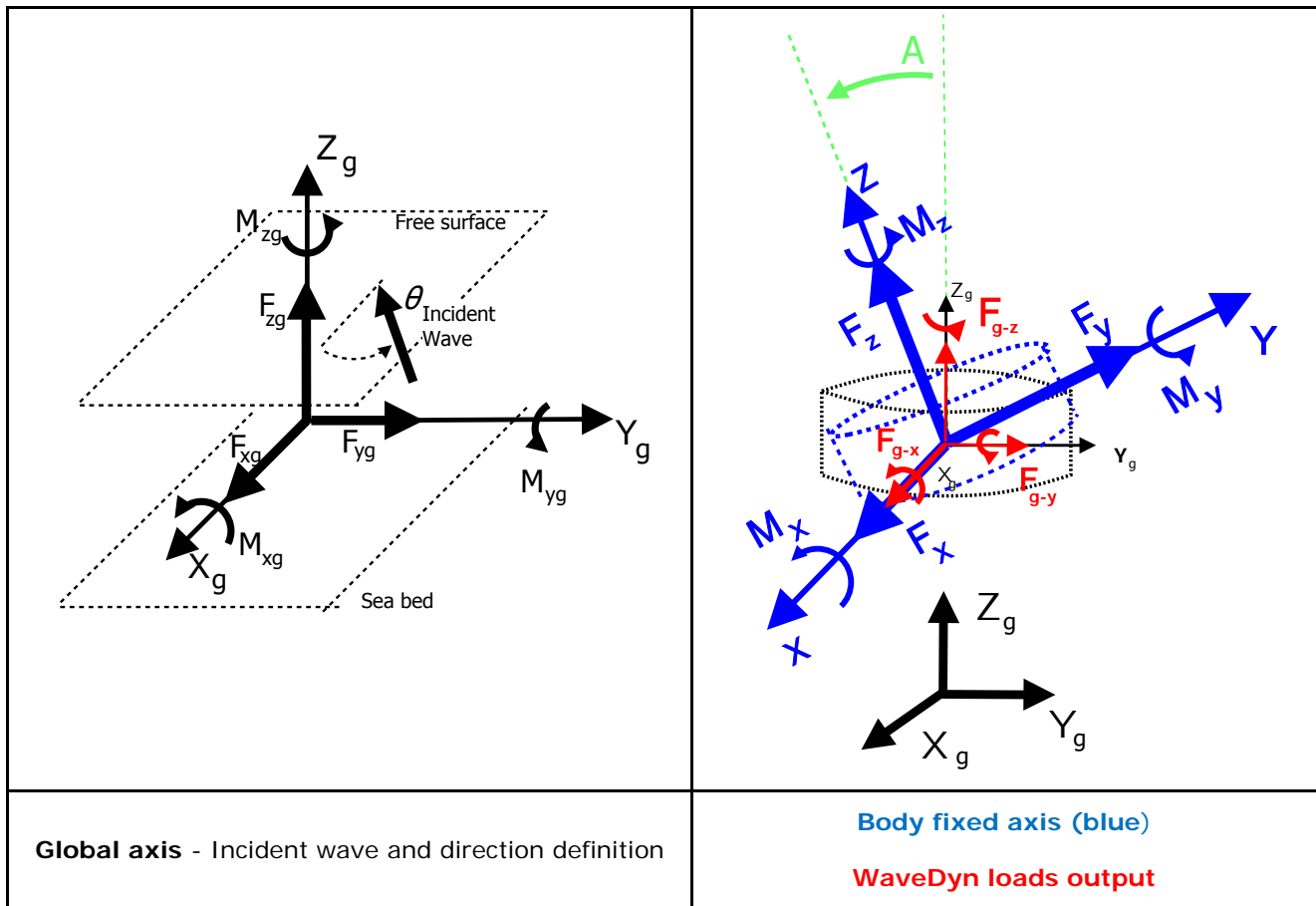
| Global axis - Incident wave and direction definition | Body fixed axis (blue)
 WaveDyn loads output |

The rotation of the loads to body-fixed coordinates is made using a passive rotation matrix. The rotations are made about the coordinate system located at each body's proximal node orientated using the Global coordinates. The rotation around the Z axis is made first, followed by the Y-axis and finally the X-axis. Considering the WaveDyn output force, F_g (red vectors in Figure 7-1), the output forces in a body fixed coordinate system $\boldsymbol{F}$ are found using:

$$\begin{bmatrix} \boldsymbol{F_x} \\ \boldsymbol{F_y} \\ \boldsymbol{F_z} \end{bmatrix} = \begin{bmatrix} \cos C \cos B & \sin C \cos B & -\sin B \\ -\sin C \cos A + \cos C \sin B \sin A & \cos C \cos A + \sin C \sin B \sin A & \cos B \sin A \\ \sin C \sin A + \cos C \sin B \cos A & -\cos C \sin A + \sin C \sin B \cos A & \cos A \cos B \end{bmatrix} \begin{bmatrix} F_{gx} \\ F_{gy} \\ F_{gz} \end{bmatrix}. \tag{3}$$

7.2.1 Reported loads

The Centipod WEC WaveDyn model was initially illustrated in Figure 4-1. For the structural analysis, a few nodes were selected to carry out the loads post-processing described above. The nodes used in the post-processing and a brief description of the loads involved are described in Table 7-1.

Table 7-1: Post-processed loads locations.

Body	Description of the Loads
Pod 1 Pod 2 Pod 3 Pod 4 Pod 5	Forces in body fixed coordinate system located at the centre of mass of the pods structures. The output loads at these locations include: - Hydrodynamic loads on the pods - Gravity loads - Inertia loads
Pod attachment, 3	Forces acting on the Pod 3 hinge (in body fixed coordinate system) located at the attachment location on the back bone.
Mooring lines 1,2	The tension on the mooring lines (F_{Line}) can be calculated as the magnitude of the resultant force of these 3 F_{moor} components: $$F_{Line} = \sqrt{F_{moor\,gx}^2 + F_{moor\,gy}^2 + F_{moor\,gz}^2}$$

For the pods the axial force is defined as being the F_z force on the body fixed coordinate system. The shear force is defined as the magnitude of the resultant of the x and y components.

$$F_{axial} = \boldsymbol{F_z} \tag{4}$$

$$F_{shear} = F_{xy} = \sqrt{\boldsymbol{F_x^2 + F_y^2}} \tag{5}$$

$$M_{bending} = M_{xy} = \sqrt{\boldsymbol{M_x^2 + M_y^2}} \tag{6}$$

7.3 Global results

The variation of several parameters with the sea state can be of importance in order to understand machine behaviour trends. Below the variation of some elements of the model with the sea states is presented, specifically:

- Maximum and minimum *PTO* displacement of the central pod (Pod 3) in Table 7-2 and Table 7-3.

- Maximum and minimum axial forces registered for Pod 3 in Table 7-4 and Table 7-5.

- Resultant shear force and bending moment acting on Pod 3 in Table 7-6 and Table 7-7.

- Resultant bending moment acting on Pod 3 connection with the 'backbone' in Table 7-8.

- Mooring line tension for line 1 (attachment point x=32m) and 2 (attachment point x=-32m) in Table 7-9 and Table 7-10.

- Maximum 'backbone' yaw motion in Table 7-11.

The PTO displacement for Pod 3 is seen to be highly dependent on Hs and to a lesser extent on Tp. A maximum PTO displacement of 12.7m is observed for an Hs=7.3m and Tp=19.7m. In future models a system to reduce the displacement of the PTO is advised for use in larger sea states. There is a slight mismatch between the initial displaced water mass and the mass of the pods (~1.2%). This causes the float initial position to be adjusted by approx. 2cm. The 'backbone' is highly buoyant and the pre-tension of the mooring lines results on a new position 25cm above the initial position. This leads to the PTO displaying negative displacement for the lowest sea states. The adjustment to the new steady state position is achieved in the initial 10sec of the analysis which are not used in the post-processing, so the influence of this adjustment in the results throughout this report are expected to be negligible.

It should be mentioned as a reminder once again that the applicability of the linear wave theory behind WaveDyn's hydrodynamic load calculation is limited for large sea states. The results for these sea states should be used with caution and subject to validation using experimental data. Linear theory tends to result in an overprediction of motions in larger sea states.

The loading on the mooring lines is very similar for both lines in most of the sea states. The maximum mooring line loads observed are approximately 10MN for the sea state with Tp=18.7s and Hs=8.75m. Only for Hs > 6.75m are the differences between maxima on the different lines larger than 5%. The differences in the two lines' maximum tension values is caused by the motions on the platform that lead to asymmetries in the system, and consequently on the loading.

This asymmetric behaviour of the WEC can be also observed in the yaw motion of the 'backbone'. The yaw motions are larger for the more energetic sea states (Hs > 3.25m). The cause for this asymmetry may be the small numerical instabilities resulting from the hydrodynamic data. These instabilities lead to small yaw displacements and consequent misalignment of the WEC with the unidirectional incident waves, increasing the asymmetric behaviour due to the excitation forces and possibly leading to some motions in the cross-wave degrees of freedom. The radiation damping is the only form of damping modeled in the system (excluding the PTO), and for low frequencies this is very small and unable to damp out the amplitude of these initial yaw displacements. If valid drag coefficients were to be determined in the future, the introduction of some viscous drag is likely to significantly reduce this yaw motion. An initial sensitivity study to other mooring arrangements and the viscous damping is described in Section 8.

Again it should be noted that these maximum results were obtained for a relatively short simulation lengths (200xTp). This is acceptable for power absorption estimations as specified by [5]. However, when considering extreme values analysis a larger simulation time is necessary. For more comprehensive structural analysis, it is recommended to increase the length of simulation. This can be achieved by increasing the number of seeds for each sea state.

Table 7-2:   Maximum PTO displacement [m] for Pod 3 (center pod).

Hs, m \ Tp, s	3.7	4.7	5.7	6.7	7.7	8.7	9.7	10.7	11.7	12.7	13.7	14.7	15.7	16.7	17.7	18.7	19.7
0.3				-0.1	-0.1		0.0	0.0	0.0	0.0	0.0	0.0	0.0		0.0		0.0
0.8	-0.1	0.1	0.2	0.2	0.1	0.3	0.3	0.3	0.3	0.4	0.3	0.3	0.3	0.3	0.3		0.5
1.3	0.0	0.3	0.5	0.8	0.7	0.7	0.6	0.7	0.6	0.7	0.7	0.6	0.7	0.8	0.8		0.8
1.8	0.2	1.1	1.3	1.2	1.2	1.4	0.9	1.0	1.1	1.1	1.2	1.2	1.1	1.1	1.0	1.4	1.3
2.3		1.9	2.1	2.0	1.8	2.0	1.4	1.6	1.5	1.5	1.6	1.7	1.5	1.7	2.0		2.0
2.8			2.4	2.9	2.4	2.0	2.3	2.6	1.9	2.0	2.4	2.5	2.5	2.2	2.2		3.1
3.3			2.9	3.4	2.5	3.1	2.4	2.3	2.5	2.7	3.3	2.6	3.1	2.9	2.6		3.6
3.8				4.0	3.1	2.9	3.0	2.4	2.5	2.8	2.8	3.2	2.9	3.2	3.3		4.5
4.3					3.6	3.2	3.5	3.1	3.2	3.3	3.5	3.4	4.0	3.8	3.9		4.5
4.8						3.9	4.6	3.9	4.0	3.3	3.7	3.7	4.3	5.0	4.2		9.3
5.3					4.2	4.1	4.2	4.6	5.3	4.3	4.0	3.8	6.2	4.8	4.0		6.8
5.8							5.8	5.2	4.9	4.4	5.1	5.3	5.0	4.7	5.0		8.1
6.3									5.3	4.5	5.8	6.6	6.2	5.9	5.6		8.8
6.8									6.7	5.2	5.5	5.4	5.8	8.4	6.5		9.9
7.3									6.1	9.6	6.5	6.4	8.1	7.0	7.4		12.7
7.8												7.4	6.4	7.5	8.8		
8.3													8.0		12.0		
8.8												8.7			8.1		

Table 7-3: Minimum PTO displacement [m] for Pod 3 (center pod).

Hs [m]	3.7	4.7	5.7	6.7	7.7	8.7	9.7	10.7	11.7	12.7	13.7	14.7	15.7	16.7	17.7	18.7	19.7
0.25				-0.3	-0.3			-0.3	-0.3	-0.3	-0.4	-0.4	-0.3		-0.4		
0.75	-0.3	-0.3	-0.4	-0.4	-0.5	-0.6	-0.5	-0.7	-0.6	-0.6	-0.7	-0.7	-0.7	-0.7	-0.7		-0.7
1.25	-0.3	-0.4	-0.5	-0.6	-0.7	-0.7	-0.7	-0.9	-0.9	-1.1	-0.9	-0.9	-0.9	-1.0	-0.9		-1.0
1.75	-0.4	-0.5	-0.5	-0.6	-0.7	-1.0	-0.9	-0.9	-0.9	-1.1	-1.1	-1.1	-1.1	-1.3	-1.0		-1.0
2.25		-0.5	-0.7	-0.9	-1.0	-1.1	-1.2	-1.2	-1.3	-1.2	-1.2	-1.9	-1.3	-1.3	-1.3		-1.5
2.75			-0.8	-0.8	-1.1	-1.4	-1.1	-1.4	-1.6	-1.4	-1.6	-1.3	-1.4	-1.5	-1.5		-1.6
3.25			-1.2	-1.2	-1.3	-1.1	-1.3	-1.4	-1.7	-1.6	-1.5	-2.0	-1.7	-1.7	-1.6		-2.1
3.75				-0.8	-1.1	-1.4	-1.6	-1.6	-1.7	-1.7	-1.7	-1.6	-1.7	-2.0	-2.3		-2.2
4.25					-1.5	-1.3	-1.7	-1.9	-1.5	-2.2	-2.1	-1.9	-2.8	-1.8	-2.4		-1.9
4.75						-1.5	-1.8	-1.8	-2.6	-2.0	-2.6	-2.6	-2.1	-2.8	-2.1		-2.4
5.25					-1.9	-1.6	-2.1	-2.3	-2.0	-2.2	-2.4	-2.3	-2.8	-2.5	-2.7		-2.1
5.75							-2.1	-1.9	-2.5	-2.2	-2.3	-2.2	-2.8	-3.1	-2.7		-2.4
6.25									-2.3	-2.8	-2.7	-2.8	-2.2	-2.8	-3.2		-2.3
6.75									-3.2	-2.2	-3.1	-2.6	-3.5	-3.0	-2.1		-3.1
7.25									-3.4	-2.8	-2.4	-3.7	-2.8	-2.6	-2.8		-3.4
7.75												-3.0	-2.8	-2.4	-4.0		
8.25													-2.3		-2.3		
8.75												-2.8			-2.6		

Hs [m]	Tp [s]																
	3.7	4.7	5.7	6.7	7.7	8.7	9.7	10.7	11.7	12.7	13.7	14.7	15.7	16.7	17.7	18.7	19.7
0.25				66	78			75	60	60	58	56	64		58		
0.75	142	195	190	186	205	222	215	226	196	193	194	171	205	172	169		151
1.25	191	383	350	349	383	339	282	383	280	276	300	254	277	312	280		270
1.75	345	395	549	424	481	472	434	438	410	449	394	352	358	387	366		315
2.25		679	768	655	600	693	595	591	590	460	509	624	516	447	459		390
2.75			888	872	696	640	699	753	743	610	572	558	602	627	548		483
3.25			1237	871	897	868	804	803	875	645	800	752	572	640	602		522
3.75				986	932	913	960	816	834	769	859	782	704	701	762		603
4.25					1195	1155	921	1082	888	883	954	705	796	829	844		705
4.75						1185	1084	1111	1235	1145	1254	970	802	885	841		963
5.25					1602	1466	1299	1598	1179	1171	1041	1132	1106	868	1017		993
5.75							1247	1500	1283	1166	1039	1310	1145	1121	1342		944
6.25									1411	1462	1447	1124	1064	1327	1116		1058
6.75									1569	1495	1785	1407	1164	1253	1264		1266
7.25									1526	1714	1569	1211	1376	1517	1137		1408
7.75												1785	1509	1584	1731		
8.25													1431		1392		
8.75												1675			1460		

Table 7-5: Minimum axial force [kN] for Pod 3 for all sea states investigated.

	Tp [s]																
Hs [m]	3.7	4.7	5.7	6.7	7.7	8.7	9.7	10.7	11.7	12.7	13.7	14.7	15.7	16.7	17.7	18.7	19.7
0.25				-70	-69			-74	-61	-56	-58	-61	-60		-59		
0.75	-140	-169	-202	-181	-209	-243	-239	-175	-165	-194	-212	-155	-167	-177	-158		-179
1.25	-208	-373	-311	-327	-369	-361	-333	-346	-305	-345	-305	-284	-289	-344	-260		-283
1.75	-353	-467	-629	-446	-500	-430	-501	-371	-414	-442	-577	-441	-380	-426	-385		-368
2.25		-698	-773	-647	-570	-554	-606	-568	-541	-524	-519	-612	-529	-581	-581		-550
2.75			-799	-838	-723	-638	-543	-657	-703	-751	-642	-749	-702	-649	-616		-717
3.25			-861	-749	-841	-841	-727	-657	-758	-798	-1053	-909	-877	-847	-776		-850
3.75				-897	-963	-899	-885	-770	-1026	-957	-763	-846	-806	-895	-760		-834
4.25					-1142	-997	-864	-987	-988	-1028	-1137	-1021	-958	-792	-970		-821
4.75						-1029	-908	-1080	-1083	-1082	-1001	-1106	-970	-1108	-975		-1058
5.25					-1097	-1289	-1260	-1141	-1228	-1173	-1299	-1042	-1110	-1158	-1012		-1084
5.75							-1077	-1348	-1316	-1223	-1218	-1304	-1259	-1228	-1046		-1132
6.25									-1366	-1459	-1205	-1321	-1299	-1228	-1267		-1359
6.75									-1498	-1411	-1290	-1313	-1308	-1488	-1194		-1232
7.25									-1434	-1808	-1361	-1584	-1792	-1589	-1377		-1715
7.75												-1594	-1340	-1432	-1545		
8.25													-1364		-1678		
8.75												-1879			-1795		

Table 7-6: Maximum F_{xy} force [kN] for Pod 3 for all sea states investigated.

Hs [m]	Tp [s] 3.7	4.7	5.7	6.7	7.7	8.7	9.7	10.7	11.7	12.7	13.7	14.7	15.7	16.7	17.7	18.7	19.7
0.25				6	7			13	15	14	12	10	11		11		
0.75	15	55	74	75	59	63	56	43	47	40	43	39	34	36	36		64
1.25	23	131	126	138	129	116	101	90	78	83	79	78	79	95	89		99
1.75	69	183	200	176	173	155	108	123	112	112	162	129	112	123	130		148
2.25		270	273	248	222	239	165	179	179	180	159	195	170	205	185		217
2.75			276	299	232	216	193	208	170	211	186	242	228	192	193		259
3.25			372	351	270	294	230	226	207	282	338	241	284	228	224		305
3.75				352	298	279	309	261	243	317	278	281	270	288	265		326
4.25					452	354	285	283	319	337	338	314	278	288	293		277
4.75						436	405	345	327	327	322	380	304	358	322		412
5.25					459	455	362	372	403	440	403	374	366	309	349		415
5.75							419	466	397	363	413	471	324	446	371		420
6.25									519	573	389	464	409	390	405		466
6.75									456	508	482	430	413	461	428		514
7.25									436	670	449	492	472	560	497		626
7.75												547	494	492	520		
8.25													476		620		
8.75												672			493		

Table 7-7: Maximum bending M_{xy} [kN.m] for Pod 3 for all sea states investigated.

Hs [m]	Tp [s] 3.7	4.7	5.7	6.7	7.7	8.7	9.7	10.7	11.7	12.7	13.7	14.7	15.7	16.7	17.7	18.7	19.7
0.25				118	117			198	167	172	149	128	135		126		
0.75	295	590	752	804	625	607	545	517	516	486	439	418	400	409	386		610
1.25	503	1221	1135	1402	1286	1328	1132	964	986	981	735	815	643	850	880		931
1.75	755	1608	2010	1586	1718	1597	1285	1236	1147	1127	1187	1210	1068	1280	1158		1404
2.25		1972	2295	1872	1958	1789	1496	1640	1593	1664	1454	1771	1492	1751	1713		1792
2.75			2171	2435	2467	1976	2008	1766	1751	1643	2092	2237	2007	1829	1834		2630
3.25			2619	2851	2599	2298	2244	2153	2279	2395	2497	2188	2244	2343	2570		2505
3.75				2881	2443	2706	2506	2345	2359	2255	2341	2735	2566	2249	2404		2490
4.25					3005	2615	2584	2673	2576	2376	2906	2839	2828	2485	2552		2707
4.75						3111	2704	2849	3232	2676	2594	3057	2914	3300	2973		3294
5.25					3381	3106	3075	2909	3146	2812	3010	3052	3069	3232	2940		3192
5.75							3300	3193	2854	3116	2993	3223	3041	3171	3069		3503
6.25									3161	3252	3147	3470	3220	3179	3863		3471
6.75									3224	3106	3456	3363	3452	3536	3674		3618
7.25									3395	3539	3784	3513	3417	3761	3413		3523
7.75												3640	3783	4002	3783		
8.25													3636		3811		
8.75												3836			3789		

Table 7-8: Maximum bending M_{xy} [kN.m] for base of Pod 3 for all sea states investigated.

Hs, m \ Tp, s	3.7	4.7	5.7	6.7	7.7	8.7	9.7	10.7	11.7	12.7	13.7	14.7	15.7	16.7	17.7	18.7	19.7
0.3				0	0		0	0	0	0	0	0	0		0		
0.8	7	5	2	1	0	0	0	0	0	0	0	0	0	0	0		0
1.3	10	7	4	1	1	1	2	1	0	0	0	0	0	0	0		0
1.8	14	12	6	2	2	14	7	1	1	1	0	0	0	0	0		0
2.3		11	10	4	21	1	14	1	4	1	1	2	0	0	1		0
2.8			10	2	284	1	39	829	124	1	1	0	0	0	1		0
3.3			14	11	52	12	16	151	438	177	4	17	2	1	1		1
3.8				1469	3	526	1431	1303	477	638	1	1	464	3	18		1
4.3					7	541	1286	1302	300	183	25	336	570	261	6		1
4.8						95	2096	788	2395	615	1103	436	24	196	2		4
5.3					1289	1683	1521	3049	1289	1034	1726	792	1180	962	4		5
5.8							2376	1659	2614	3665	1395	1848	1409	1311	1095		125
6.3									1255	2352	1967	1515	1209	1047	967		9
6.8									2994	2838	2267	1462	740	1428	1425		739
7.3									3256	2890	4101	2343	2305	1273	2090		139
7.8												1409	3042	1739	1441		
8.3													3432		661		
8.8												2454			1273		

Table 7-9 Maximum tension [MN] for mooring line 1.

Hs [m]	\ Tp [s] 3.7	4.7	5.7	6.7	7.7	8.7	9.7	10.7	11.7	12.7	13.7	14.7	15.7	16.7	17.7	18.7	19.7
0.25				3.58	3.58			3.59	3.57	3.55	3.56	3.57	3.57		3.57		
0.75	3.75	3.84	3.94	3.92	3.89	3.93	3.94	3.83	3.80	3.89	3.92	3.79	3.82	3.84	3.80		3.83
1.25	3.94	4.46	4.32	4.51	4.29	4.21	4.24	4.21	4.14	4.27	4.12	4.08	4.12	4.18	4.04		4.09
1.75	4.27	4.74	4.71	4.74	4.75	4.70	4.74	4.28	4.34	4.44	4.69	4.38	4.33	4.44	4.31		4.24
2.25		6.10	5.52	5.48	4.77	5.43	5.61	4.73	4.67	4.70	4.65	4.86	4.60	4.63	4.54		4.52
2.75			6.46	6.52	5.82	5.65	5.28	4.82	4.90	5.12	4.86	4.99	4.84	4.86	4.73		4.99
3.25			6.98	7.31	6.09	6.07	5.46	5.18	5.10	5.28	5.73	5.36	5.06	5.27	4.99		5.34
3.75				6.43	6.50	7.77	6.39	5.47	6.06	5.42	5.14	5.25	5.27	5.39	5.23		5.44
4.25					7.69	6.07	6.80	5.63	5.93	5.71	6.19	5.64	5.53	5.25	5.52		5.16
4.75					7.17	6.26	6.95	5.73	5.83	6.10	5.54	5.83	6.20	5.49			6.03
5.25				7.76	8.60	7.25	6.88	5.91	6.19	6.52	5.84	6.12	5.59	5.89			6.44
5.75							7.56	8.42	7.13	6.45	6.07	6.52	6.27	5.94	5.84		6.46
6.25									7.07	6.69	6.76	6.60	6.14	6.11	6.31		7.00
6.75									6.78	7.01	7.42	6.39	6.29	6.92	6.19		7.06
7.25									6.87	7.29	7.18	6.78	7.70	6.92	6.16		7.99
7.75												7.02	7.17	6.97	10.25		
8.25													7.16		7.23		
8.75												7.15			7.71		

Table 7-10 Maximum tension [MN] for mooring line 2.

Hs [m] \ Tp [s]	3.7	4.7	5.7	6.7	7.7	8.7	9.7	10.7	11.7	12.7	13.7	14.7	15.7	16.7	17.7	18.7	19.7
0.25				3.58	3.58		3.59	3.57	3.55	3.56	3.57	3.57	3.57		3.57		
0.75	3.75	3.84	3.94	3.92	3.89	3.93	3.94	3.83	3.80	3.89	3.92	3.79	3.82	3.84	3.80		3.83
1.25	3.94	4.46	4.32	4.51	4.29	4.21	4.24	4.21	4.14	4.27	4.12	4.07	4.12	4.18	4.04		4.09
1.75	4.27	4.74	4.71	4.74	4.75	4.70	4.74	4.28	4.34	4.44	4.69	4.38	4.33	4.44	4.31		4.24
2.25		6.10	5.52	5.48	4.77	5.43	5.62	4.73	4.67	4.70	4.65	4.86	4.60	4.63	4.54		4.52
2.75			6.46	6.52	5.80	5.65	5.28	4.82	4.90	5.12	4.86	4.99	4.84	4.86	4.73		4.99
3.25			6.98	7.31	6.09	6.07	5.46	5.18	5.10	5.28	5.72	5.37	5.06	5.27	4.99		5.34
3.75				6.80	6.50	7.77	6.94	5.47	6.09	5.42	5.14	5.25	5.28	5.39	5.23		5.44
4.25					7.69	5.99	6.80	5.60	5.93	5.71	6.19	5.66	5.53	5.23	5.52		5.16
4.75						7.18	6.05	7.03	5.99	5.83	5.87	5.54	5.83	6.20	5.49		6.03
5.25					7.75	8.60	7.75	6.82	6.03	6.19	6.53	5.84	6.23	5.64	5.89		6.44
5.75							7.56	8.42	6.70	6.44	6.05	6.35	6.27	5.94	5.84		6.46
6.25									7.40	6.36	6.44	6.47	6.14	6.20	6.20		7.00
6.75									7.28	6.76	6.28	6.38	6.29	6.88	6.34		7.06
7.25									7.58	6.61	7.69	7.43	7.70	6.69	6.34		8.00
7.75												7.22	7.08	7.07	9.36		
8.25													7.16		7.22		
8.75												7.07			7.72		

Table 7-11: Maximum 'backbone' yaw displacement [degrees].

Hs [m]	Tp [s]																
	3.7	4.7	5.7	6.7	7.7	8.7	9.7	10.7	11.7	12.7	13.7	14.7	15.7	16.7	17.7	18.7	19.7
0.25				0.0	0.0			0.0	0.0	0.0	0.0	0.0	0.0		0.0		
0.75	0.0	0.0	0.0	0.0	0.0	0.0	0.0	0.0	0.0	0.0	0.0	0.0	0.0	0.0	0.0		0.0
1.25	0.0	0.0	0.0	0.0	0.0	0.0	0.0	0.0	0.0	0.0	0.0	0.0	0.0	0.0	0.0		0.0
1.75	0.0	0.0	0.0	0.0	0.0	0.1	0.1	0.0	0.0	0.0	0.0	0.0	0.0	0.0	0.0		0.0
2.25		0.0	0.0	0.0	0.1	0.0	0.1	0.0	0.0	0.0	0.0	0.1	0.0	0.0	0.0		0.0
2.75			0.0	0.0	0.6	0.0	0.8	19.7	0.8	0.0	0.0	0.0	0.0	0.0	0.0		0.0
3.25			0.0	0.1	0.3	0.0	0.2	1.4	11.6	1.7	0.0	0.2	0.0	0.0	0.0		0.0
3.75				12.4	0.0	2.3	22.2	17.8	2.9	8.7	0.0	0.0	1.5	0.1	0.1		0.0
4.25					0.0	6.7	15.5	6.3	3.5	0.5	0.2	1.5	4.2	1.8	0.1		0.0
4.75						0.5	22.0	8.6	19.3	4.8	7.8	5.6	0.3	3.8	0.0		0.0
5.25					5.9	6.2	9.9	15.9	19.5	15.5	14.1	8.8	13.8	12.3	0.0		0.0
5.75							21.7	18.8	19.5	14.9	17.1	14.1	10.4	12.1	10.8		0.8
6.25									15.2	17.5	10.3	18.9	7.2	9.0	13.9		0.1
6.75									19.8	23.0	14.1	18.0	9.1	16.1	10.4		6.2
7.25									23.9	21.0	20.9	14.3	12.4	10.7	11.6		0.8
7.75												13.5	15.3	15.1	10.4		
8.25													16.2		8.4		
8.75												17.2			14.9		

7.4 Non-exceedance probability

7.4.1   Methodology

The maximum loads observed in a WEC are dependent on the length of the simulation of the sea state. To have a representative case for maximum loads a large time-series would be necessary.

A ranking technique is used to generate the cumulative probability for each relevant load. The ranking technique involves finding the relative peaks for a given signal (Figure 7-2) and then placing them based on their magnitude (ascending order).

Figure 7-2:   Heave force peaks for Hs=3.75m and Tp=8.7s
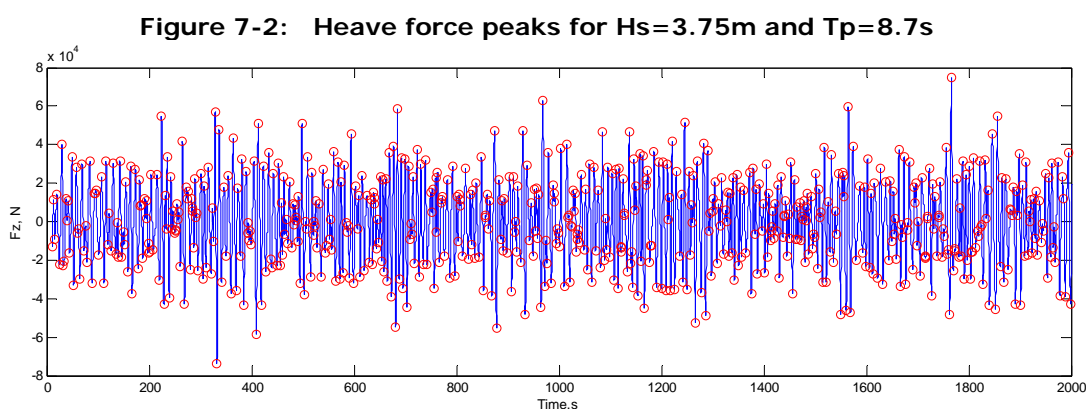
The non-exceedance probably for each of the loads can be found by

$$p(F < F_n) = \frac{n}{N + 1}.$$ **(7)**

Where n is the ranking of a given relative peak f_n and N the total number of peaks for a given time series.

7.4.2   Results

The figures below illustrate the probability of non-exceedance for the axial and shear loads on the center Pod 3. For illustrative proposes, in this report results for three different sea states are used: Hs=3.75m with Tp=8.7s and Tp=12.7s, and the larger sea state Hs=4.75m and Tp=8.7s. The probability of non-exceedance was also calculated for the remaining sea states. A database *.mat* file is to be provided to Ecomerit for all the bodies described in Table 7-1 containing the complete results presented in this section.

Figure 7-3 shows the increase of the maximum axial loads on the pod are function of the sea state - not only the extreme loads, but also the distribution of the relative peaks over the time series considered. The maximum values registered for the axial forces is approx. 900kN for the sea state Hs=3.75m and Tp=8.7s. The wave period seems to have impact on the distribution of the relative peak loads. The larger Tp values result in larger maximum loads. For example, 95% of the maximum forces found for the case where Hs=3.75m and Tp=8.7s are lower than 121kN whereas for Hs=3.75 and Tp=14.7s, this value is 123.2kN. For the larger sea state (Hs=4.75m and Tp=8.7s) 95% of the loads are lower than 193.5kN.   A similar approach can be followed for the other tail of the curve where negative forces are found.

As expected, the torsion moment (around the axial axis of the pod) is 2 orders of magnitude smaller than the bending moment. A variation of the yaw moment with the sea states is clearly observed. This moment was expected to be small due to the symmetry of the model and the circular geometry of the pods. However, small motions of the platform can lead to asymmetric loading on the center float as mentioned above.

Figure 7-3: **Non-exceedance probability forces (top row : Axial F_z, Shear F_{xy}) and Moments (bottom row : Torsion M_z, Bending M_{xy}) on Pod 3 for 3 sea states**
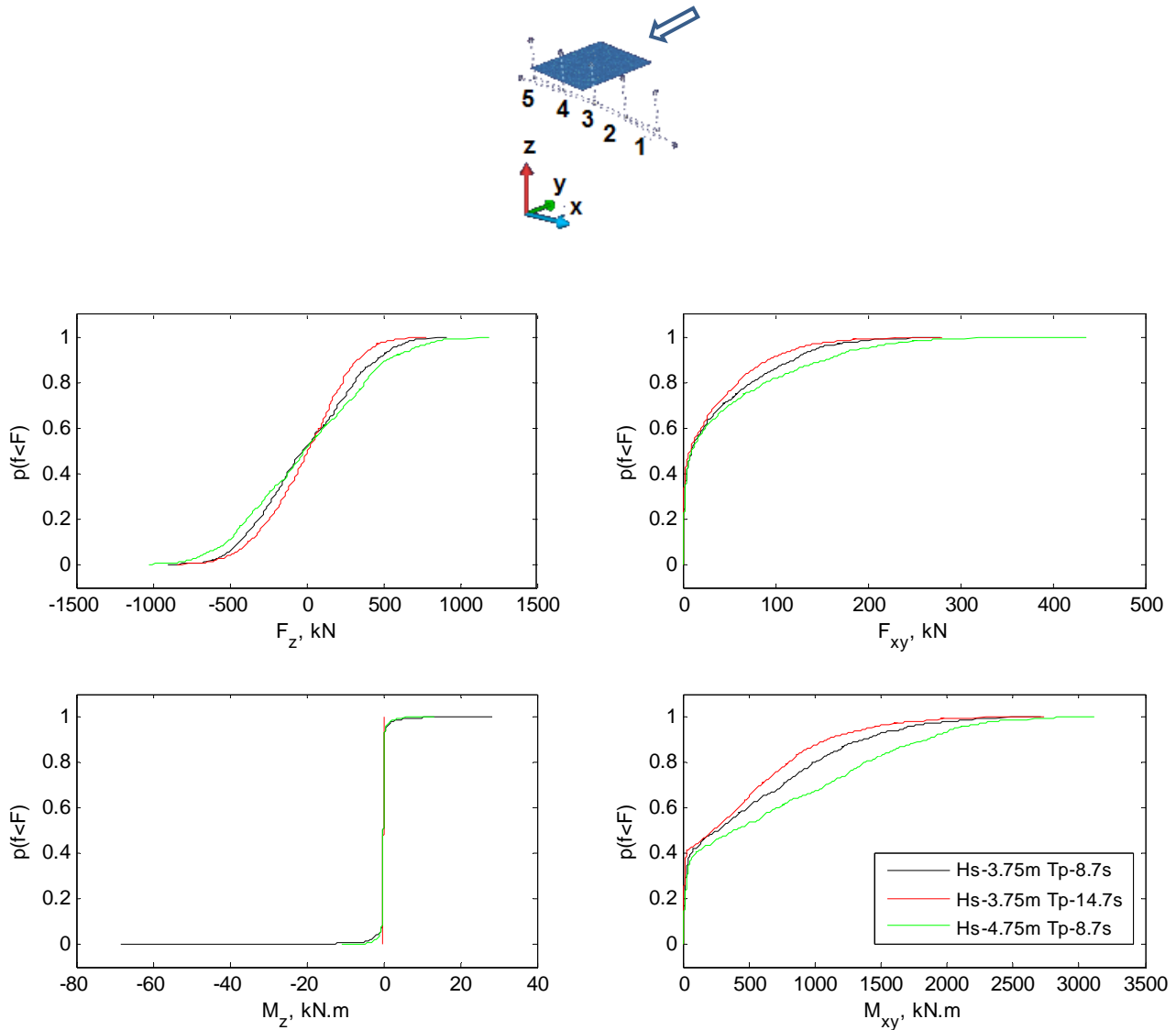
The mooring line tension distributions are illustrated in Figure 7-4 for 3 selected sea states. Both lines present a similar load distribution. The variation of the mooring line tension with the sea states appears similar as for the pod forces described on the paragraph above.

Figure 7-4: Non-exceedance probability for the tension on the mooring line 1 (left) and for mooring line 2 (right).
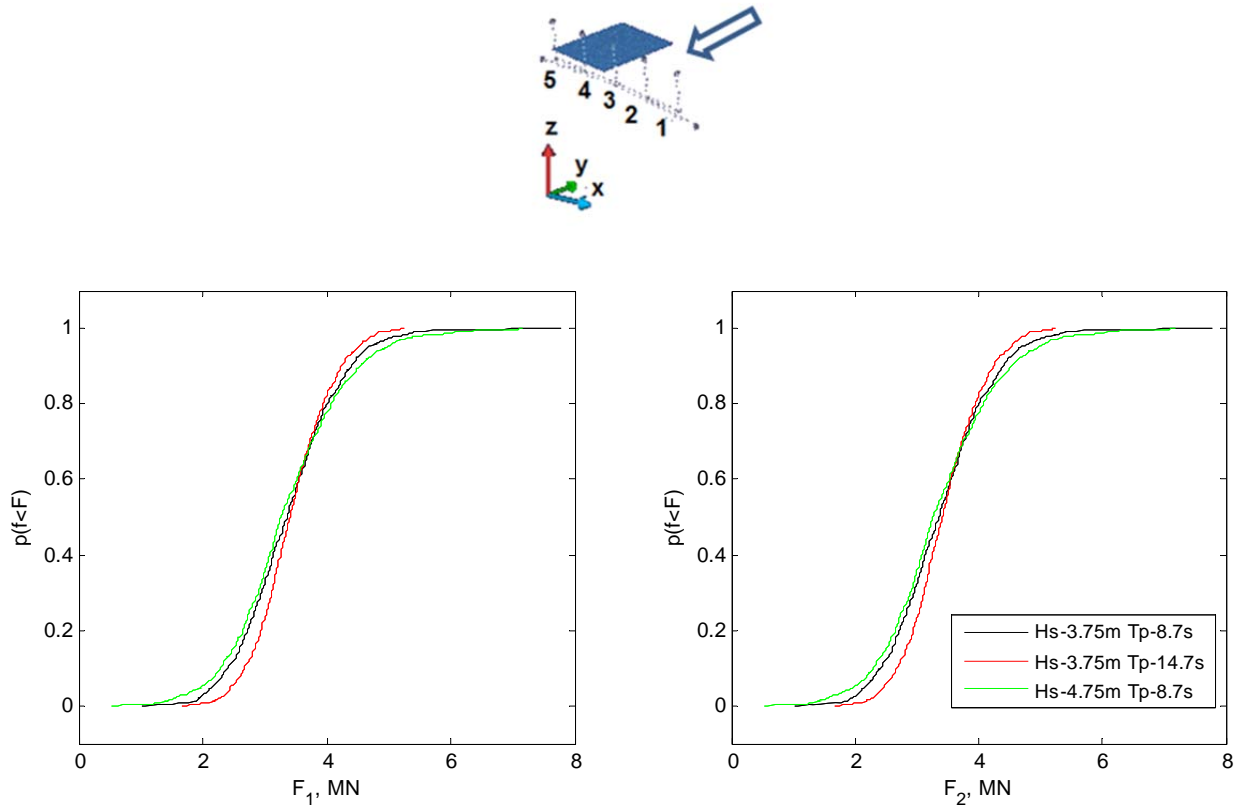
8 INITIAL ANALYSIS OF KINEMATICS

In order to explore some the potential impacts of possible model formulations that may want to be explored in more detail in future analysis, some initial sensitivity analysis was run and is discussed in this section. This was carried out for one of the most common sea states with mid-range significant wave height: Hs=3.75m and Tp=8.7s.

8.1 Addition of Viscous Damping

As was discussed in Section 7.3, the radiation damping is the only damping modeled in the system (excluding the PTO). If valid drag coefficients were determined in the future, the introduction of some viscous drag on structural elements in the model could lead to further damping in the resulting motions. To explore this, a model was built where Morison viscous drag terms were added to the 'backbone' structure in the model. The Morison loading was added by the inclusion of 3 cylindrical elements representing each of the vertical columns and the horizontal 'backbone' column with the appropriate characteristic cross-sectional areas for each cylinder. The drag coefficient was set equal to 1 for this initial sensitivity test.

As can be observed in Figure 8-1, the initial run with no viscous drag applied resulted in some 'backbone' motions in the cross-wave direction (surge) and corresponding yaw motions (potentially from some small numerical instabilities), when viscous drag is applied the extra damping is enough to quickly damp out such motion. There is an impact on power performance (~4%): the case with no viscous drag terms, the mean power absorbed over the simulation is 432kW while when viscous drag is applied the mean total PTO Output power is 413kW.

Figure 8-1: Time series of 'backbone' yaw motion (degrees) with (red line) and without (black line) viscous drag terms applied to the 'backbone' structure
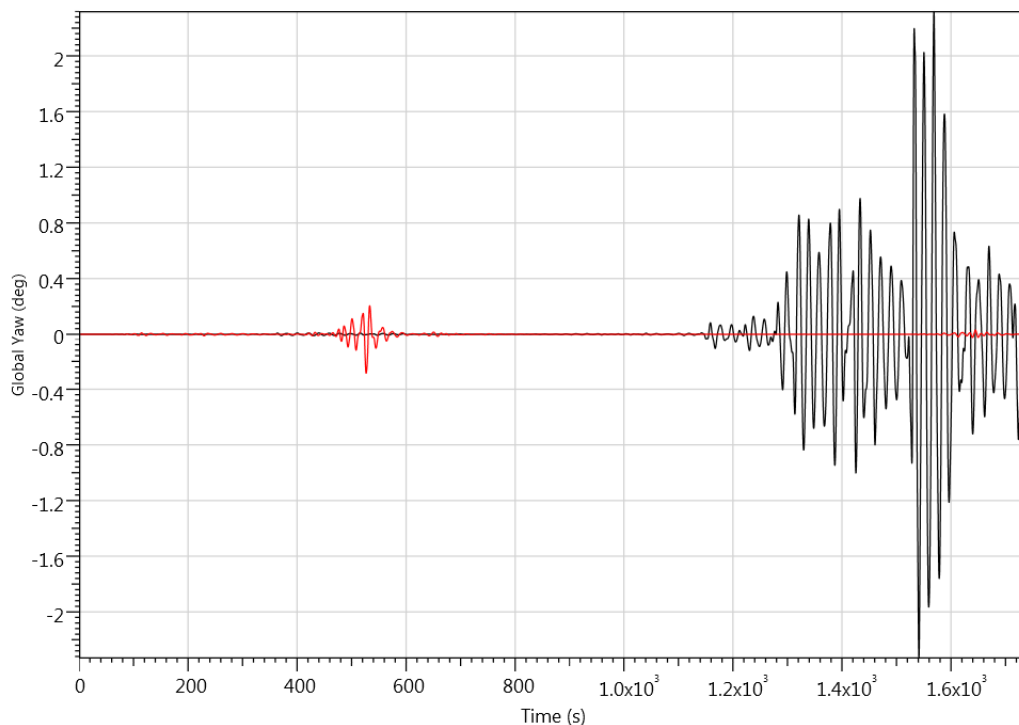
For viscous drag terms to be reliably applied in future iterations of the model, more diligence is required. The drag coefficient values would preferably be determined in conjunction with experimental data. In reality they would be a function of sea state and model dimensions, and the tabulated values are given as a function of the Keulegan-Carpenter and Reynolds numbers. The number of Morison cylindrical elements to be applied should also be investigated as body rotations and water kinematics lead to different Morison forces. Such an extensive exercise could be considered premature at this stage of the design, but would likely warrant further consideration after other more significant changes are implemented – namely, a more accurate PTO and control. Sensitivity of the model to drag terms across a range of seas states could also be explored.

8.2 Multidirectional Waves

In more real cases, waves will not be unidirectional and more directionally spread seas will occur. In order to demonstrate the impact this will have an initial sensitivity run was done where the SEA files were generated with a directional distribution as defined by Ewans [8].

As can be observed in the time series shown in Figure 8-2, the more realistic directionally spread seas (red line) immediately result in translational surge motions (across the primary wave direction) and corresponding rotational yaw motions of the 'backbone' to a greater extent than those caused by any small numerical instabilities in the unidirectional model (black line) for this intermediate height sea state. However, similar to what was demonstrated in Section 8.1 above, adding in viscous drag can reduce some of the kinematics in these directions (green line).

Figure 8-2: Time series of 'backbone' yaw motions in a unidirectional sea with no viscous drag (black), and directionally spread sea with no viscous drag (red) and directionally spread sea with viscous drag applied to backbone (green)
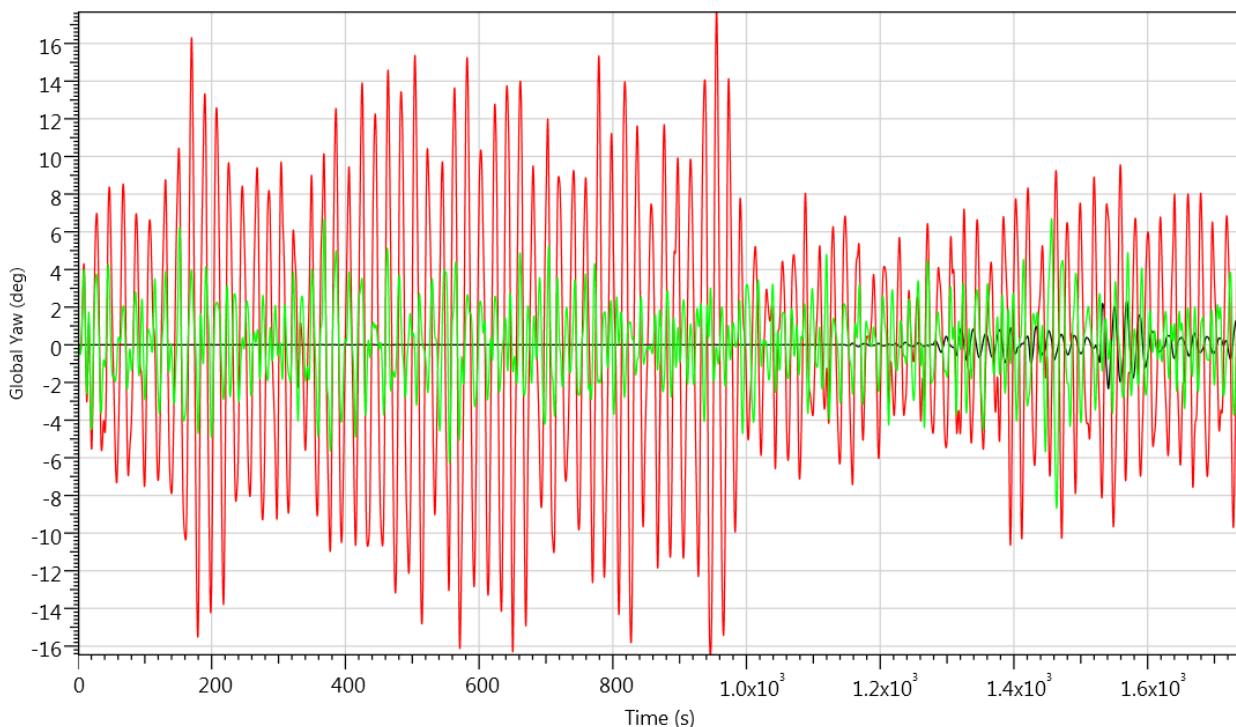
8.3 Alternative Mooring Arrangement

Finally, a short test was run to gain an initial sense of how separating the four mooring lines apart from each other a certain offset away from the 'backbone' to form four tendon legs, could potentially impact the device kinematics, as opposed to their current setup where the two lines at each end are placed right next to each other at the 'backbone' centerline, effectively forming just two tendon legs. To implement such a scheme in reality, more structure would need to be added to the 'backbone' to extend out from each end and provide the anchor attachment points offset in the wave direction from the backbone. This was not modeled or considered, but rather the mooring attachment points were set by assuming non-hydrodynamically relevant, massless elements were able to extend from near the ends of the 'backbone' at the centerline (at the same x-coordinates where the two lines on each end are assumed to currently both be attached) out 7m along both the positive and negative y-axis for the new mooring line connections. This type of set up would represent a more conventional tension leg platform arrangement where multiple tendon legs are radially spread about a platform axis.

As can be observed in Figure 8-3 and Figure 8-4, it does appear that such an arrangement leads to a much less kinetic and more stable 'backbone' structure. In particular such an arrangement nearly eliminates what are otherwise quite significant rotational roll motions of the 'backbone' in the primary wave direction (about the y-axis/backbone centerline). A more stable 'backbone' structure may be of interest for various reasons (e.g. access, O&M, and loads reductions) and DA may wish to explore such an arrangement in more depth in the future.

Figure 8-3: Time series of 'backbone' yaw in degrees for baseline (black) and with 4-leg TLP mooring arrangement (red)
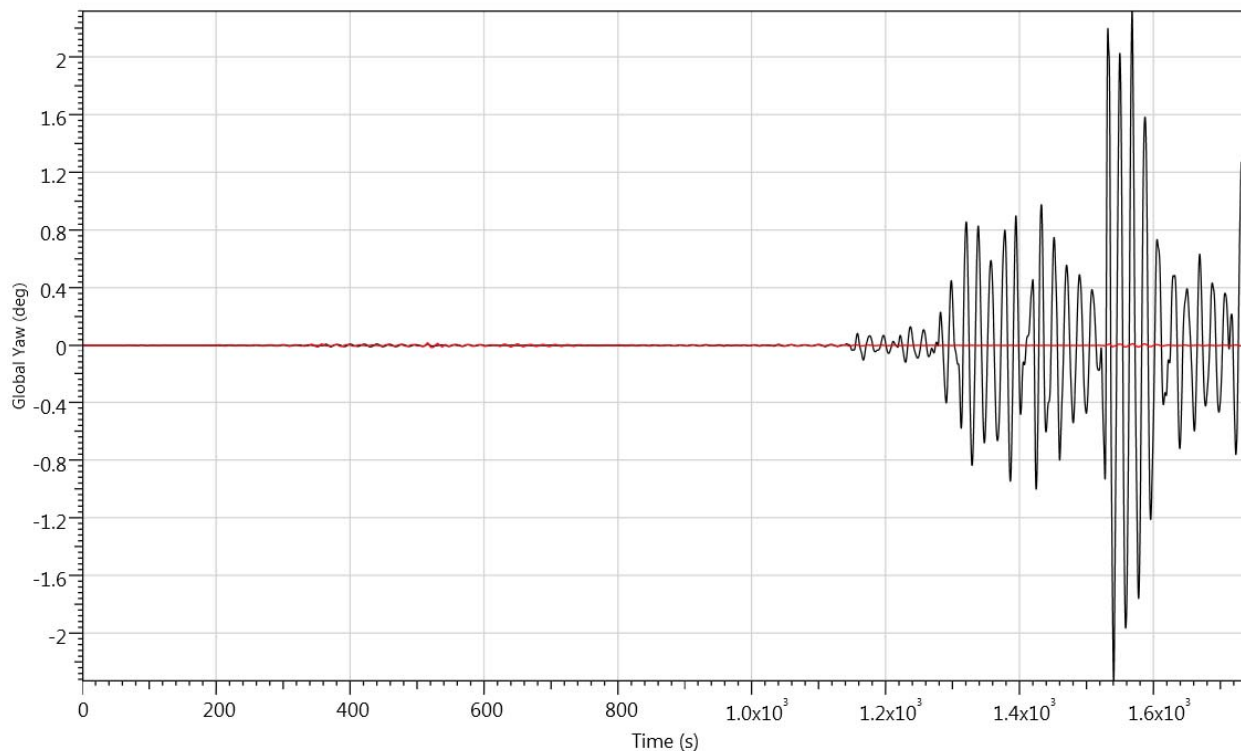
Figure 8-4: Global roll about y-axis for backbone for baseline (black) and with 4 tension leg mooring arrangement (red)
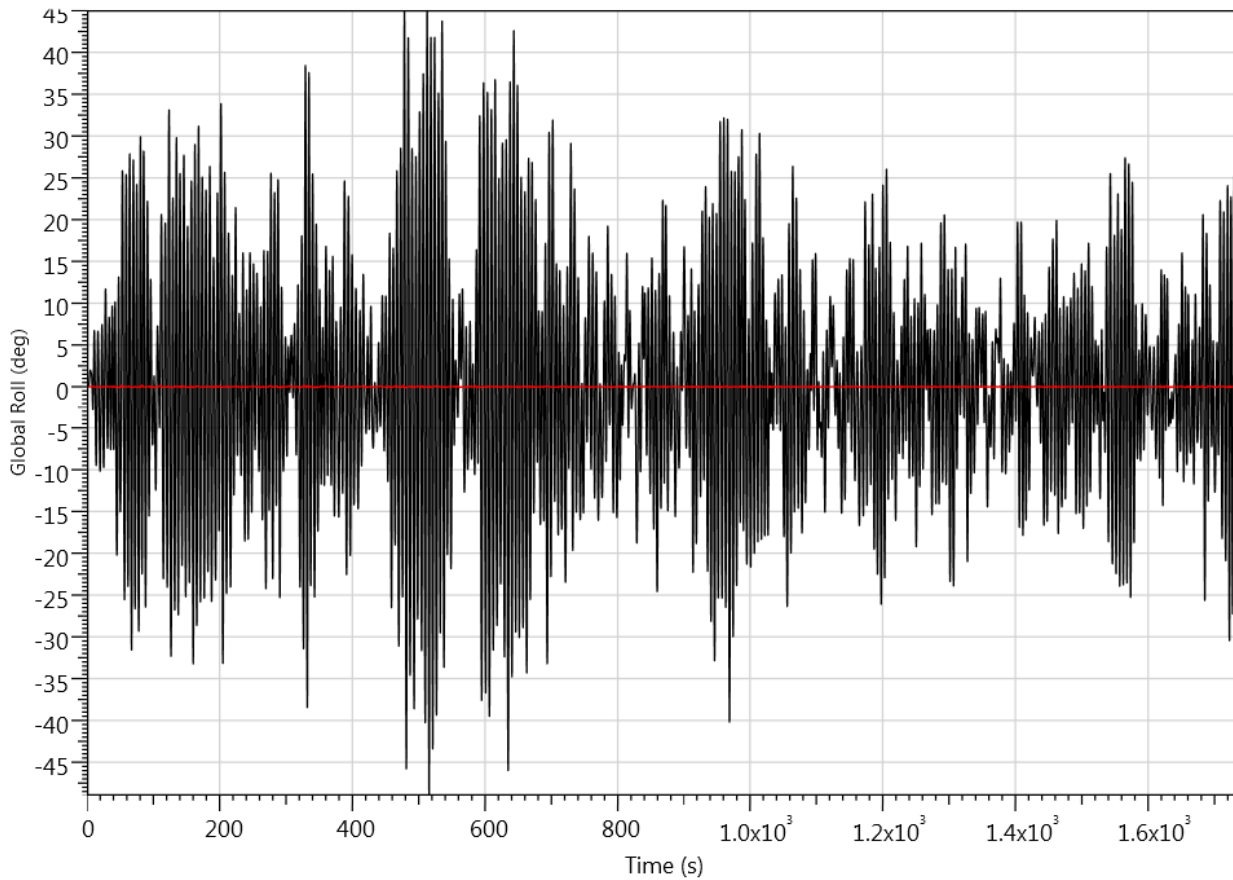
There is a reduction (~10.6%) on mean power absorbed from 432.5kW to 386.8kW which, based on some early analysis the moorings selection phase of the project, is likely due to the limitations the new 4-leg moorings arrangement places on 'backbone' roll as described. However, it's probably worth investigating in more detail if exchanging some diminished power production and added structural/mooring cost to eliminate roll, may prove a more practical design than one where rotational 'backbone' motions in the primary wave direction reach double-digit values in degrees during operational sea states. It is noted that application of viscous drag does appear to reduce the maximum values observed; however, as might be expected, roll motions are nevertheless quite pronounced in the two-leg mooring arrangement.

9 CONCLUSIONS

9.1 Summary of Key Findings

DNV GL have carried out an assessment of the Centipod CPX3 WEC using WaveDyn and derived a power matrix detailing the device performance in a variety of sea states, assuming linear waves and linear hydrodynamic forces.

The maximum capture width of the device is 0.238. This was estimated for a sea state with Hs=0.25m and Tp=6.7s. Due to the low Hs this corresponds to a low mean power absorbed (3kW). The maximum mean power extracted was approximately 1MW for Hs=7.5m and Tp=11.7s. Using the scatter table provided by DA the total annual energy yield is 1.5GWh. This power matrix can serve as an initial baseline for the current floating, tension-leg moored design for comparison with future models and design iterations - for example, models that incorporate more advanced representations of the PTO and control systems.

The minimum and maximum loads for various locations and components are presented in scatter tables for all the sea states considered. Besides these tables, curves showing probability of non-exceedance are also presented, providing a good means for comparing the loading of different WEC configurations in the future.

When looking at maximum loads on the center Pod 3, the axial load ranged from 1.785MN (Hs=6.8m and Tp=11.7s) to -1.8MN (Hs=7.3m and Tp=12.3s). The maximum shear force was 6.70kN and bending moment 4MNm (Hs=7.8m and Tp=16.7s).

The maximum mooring line tension was estimated to be 10.2MN. This was obtained for the sea state Hs=7.3m and Tp=17.7m.

9.2 Potential Next Steps

Future work could involve:

- Work related to the PTO control function as a means to increase the energy capture of the device may be pursued, and this may be dependent on the creation of a more complex and realistic PTO hardware formulation as an extension to the initial WaveDyn model.

- The inclusion of end-stops on the machine may also be considered to stop the PTO extension. This is likely to be a design driver, so its inclusion in the early stages of design is advised.

- The use of a partially nonlinear hydrostatics and/or hydrodynamics formulation so that the impact of the instantaneous wetted surface of the bodies in the overall WEC response may be evaluated.

- Inclusion of viscous drag effects on the 'backbone'. It is advised that this point and the preceding point on nonlinear hydrostatics/hydrodynamics are carried out together with an experimental validation exercise - particularly for the larger sea states where linear wave theory may not be applicable.

- Initial structural assessment of the WEC components - particularly, the connection between the PTO and the floats. A more detailed structural model for the loads on the pods using the hydrodynamic distributed loads can also be performed.

- The inclusion and analysis of any other potential design changes to the overall WEC arrangement (e.g. a 4-leg TLP option alluded to in Section 8.3).

- Iterate by reviewing and updating the mooring line sizing and characteristics (e.g. stiffness) based on the new set of dynamic mooring loads.

10 REFERENCES

[1]   WaveDyn 1.1 User Manual , DNV GL, 2014
[2]   Dehlsen Associates LLC, "Advanced controls for the Multi-pod Centipod WEC device", DE-FOA-0000848
[3]   Dehlsen Associates LLC, Dropbox, downloaded 04/03/2014
[4]   DNV GL, "Centipod CPX3", 702480-USSD-R-01-A, 06/06/2014
[5]   McCall A., Dehlsen Associates LLC, email: "RE: reminder", sent on 11/21/2014
[6]   LaBonte A., "Standardized cost and Performance Reporting for Marine and Hydrokinetic Technologies", Proceedings of the 1st Marine Energy Technology Symposium, April 2013
[7]   McCall, A., Dehlsen Associates LLC, email: "Sea state and methodology for WaveDyn power matrix", sent on 01/05/2014
[8]   K. Ewans, "Observation of the Directional Spectrum of Fectch Limited Waves," *J. Phys. Oceanography,* pp. 495-512, 1998.

APPENDIX A   NOMENCLATURE

APPENDIX A.1   Acronyms

BCS	Body-fixed coordinate system
CoM	Center of mass
DOF	Degree-of-freedom
PTO	Power take-off
WEC	Wave energy converter

APPENDIX A.2   Definitions and equations

A	Wave amplitude (regular waves)
f	Wave frequency (regular waves)
g	Modulus of the acceleration due to gravity
H_s	Significant Wave height
l	Characteristic length
ρ	Water density
EA	Axial stiffness properties of mooring line
L	Initial relaxed length of mooring line
K_{line}	Applied stiffness for each mooring line
$S(f)$	Variance density spectrum
T	Wave period (regular waves)
T_e	Energy Period
T_p	Peak Period
$\bar{E}_{abs}$	Annual averaged absorbed energy by the WEC
$\bar{P}_w$	Incident wave power
$\bar{P}_{abs}$	Average mechanically absorbed power
N	Total number of relative peaks in a sample
n	Ranking position
F_{xy}	Shear force
M_{xy}	Bending moment
p	Probability

SUBSCRIPTS

g	Global coordinate system
moor	Mooring lines force

APPENDIX B   CUSTOM FREQUENCY RESOLUTION

Table 10-1: Custom frequency resolution values used

Frequency (rad/s)					
0.00000	1.09811	2.09874	3.01710	4.40966	8.30000
0.10472	1.14707	2.14461	3.05823	4.51810	8.60000
0.15472	1.19593	2.19029	3.09910	4.63196	8.90000
0.20472	1.24468	2.23578	3.14201	4.75152	9.20000
0.2547	1.29332	2.28107	3.18707	4.87705	9.50000
0.30467	1.34184	2.32615	3.23438	5.00887	9.80000
0.35462	1.39024	2.37103	3.28406	5.14727	10.1000
0.40455	1.43852	2.41569	3.33623	5.29259	10.4000
0.45444	1.48666	2.46015	3.39100	5.44518	10.7000
0.5043	1.53467	2.50438	3.44851	5.6054	11.0000
0.55412	1.58254	2.54839	3.50889	5.77363	11.3000
0.6039	1.63027	2.59219	3.57229	5.95027	11.6000
0.65362	1.67785	2.63575	3.63887	6.13574	11.9000
0.70329	1.72528	2.67908	3.70877	6.33049	12.2000
0.7529	1.77255	2.72218	3.78217	6.53497	12.5000
0.80245	1.81966	2.76504	3.85924	6.74968	12.8000
0.85193	1.86661	2.80767	3.94016	6.97512	13.1000
0.90133	1.91339	2.85005	4.02512	7.21184	13.4000
0.95066	1.96000	2.89219	4.11434	7.46039	13.7000
0.99990	2.00642	2.93408	4.20802	7.72137	
1.04905	2.05267	2.97571	4.30638	7.99540	

APPENDIX C   DATA DESCRIPTION

This section describes the data that DNV GL will provide Ecomerit as result of the post-processing.

A Matlab data structure for each load output location is presented with :

- Statistical properties of the load signal in all the relevant degrees of freedom.
    - o   Min, Max, Mean, Standard deviation, RMS values
    - o   2 vectors with the probability of non-exceedance curve :
        - ▪   VAR.coord : values of the load , f
        - ▪   VAR.prob : Probability of non-exceedance.

ABOUT DNV GL

Driven by our purpose of safeguarding life, property and the environment, DNV GL enables organizations to advance the safety and sustainability of their business. We provide classification and technical assurance along with software and independent expert advisory services to the maritime, oil and gas, and energy industries. We also provide certification services to customers across a wide range of industries. Operating in more than 100 countries, our 16,000 professionals are dedicated to helping our customers make the world safer, smarter and greener.

9.3 Appendix 3 - MPC performance and loads report

CENTIPOD WAVEDYN MODEL WITH MPC –
PERFORMANCE & OPERATIONAL LOADS

Centipod CPX3

Dehlsen Associates LLC

Document No.: 702480-USSD-R-03-A
Date: 4 September 2015

IMPORTANT NOTICE AND DISCLAIMER

1. This document is intended for the sole use of the Customer as detailed on the front page of this document to whom the document is addressed and who has entered into a written agreement with the DNV GL entity issuing this document ("DNV GL"). To the extent permitted by law, neither DNV GL nor any group company (the "Group") assumes any responsibility whether in contract, tort including without limitation negligence, or otherwise howsoever, to third parties (being persons other than the Customer), and no company in the Group other than DNV GL shall be liable for any loss or damage whatsoever suffered by virtue of any act, omission or default (whether arising by negligence or otherwise) by DNV GL, the Group or any of its or their servants, subcontractors or agents. This document must be read in its entirety and is subject to any assumptions and qualifications expressed therein as well as in any other relevant communications in connection with it. This document may contain detailed technical data which is intended for use only by persons possessing requisite expertise in its subject matter.

2. This document is protected by copyright and may only be reproduced and circulated in accordance with the Document Classification and associated conditions stipulated or referred to in this document and/or in DNV GL's written agreement with the Customer. No part of this document may be disclosed in any public offering memorandum, prospectus or stock exchange listing, circular or announcement without the express and prior written consent of DNV GL. A Document Classification permitting the Customer to redistribute this document shall not thereby imply that DNV GL has any liability to any recipient other than the Customer.

3. This document has been produced from information relating to dates and periods referred to in this document. This document does not imply that any information is not subject to change. Except and to the extent that checking or verification of information or data is expressly agreed within the written scope of its services, DNV GL shall not be responsible in any way in connection with erroneous information or data provided to it by the Customer or any third party, or for the effects of any such erroneous information or data whether or not contained or referred to in this document.

4. Any energy forecasts estimates or predictions are subject to factors not all of which are within the scope of the probability and uncertainties contained or referred to in this document and nothing in this document guarantees any particular wind speed or energy output.

KEY TO DOCUMENT CLASSIFICATION

Strictly Confidential	:	For disclosure only to named individuals within the Customer's organisation.
Private and Confidential	:	For disclosure only to individuals directly concerned with the subject matter of the document within the Customer's organisation.
Commercial in Confidence	:	Not to be disclosed outside the Customer's organisation.
DNV GL only	:	Not to be disclosed to non-DNV GL staff
Customer's Discretion	:	Distribution for information only at the discretion of the Customer (subject to the above Important Notice and Disclaimer and the terms of DNV GL's written agreement with the Customer).
Published	:	Available for information only to the general public (subject to the above Important Notice and Disclaimer).

Project name:	Centipod WaveDyn Model with MPC – Performance & Operational Loads	DNV GL - Energy
		Renewables Advisory
Report title:	Centipod CPX3	9665 Chesapeake Drive
Customer:	Dehlsen Associates LLC	Suite 435
	101 East Victoria, Suite F	San Diego, CA 92123
	Santa Barbara, CA 93105	Tel: +1 858 836 3370
Contact person:	A. Fleming	Enterprise No.: 94-3402236
Date of issue:	04 Sep 2015	
Project No.:	702480	
Document No.:	702480-USSD-R-03, Rev. A	

Task and objective:

Simulations of a WaveDyn model of the tension-leg Centipod CPX3 concept WEC with MPC.

Preliminary performance data are presented for idealized conditions and PTO characteristics.

Baseline operational loads are presented.

Prepared by:	Verified by:	Approved by:
Jarett Goldsmith	Armando Alexandre	Ed Mackay
Engineer	Engineer	Head of Wave & Tidal
Wave & Tidal	Wave & Tidal	

☐ Strictly Confidential

☐ Private and Confidential

☒ Commercial in Confidence

☐ DNV GL only

☐ Customer's Discretion

☐ Published

Keywords:

WaveDyn

Centipod

Idealized Power Matrix

Operational loading

Issue	Date	Reason for Issue	Prepared by	Verified by	Approved by
A	04-Sep-2015	First issue– electronic copy only	J. Goldsmith	A. Alexandre	E. Mackay

Table of contents

Appendices

1 INTRODUCTION

DNV GL is a leading provider of independent wind, wave and tidal turbine engineering services. The Wave and Tidal group within DNV GL has been established to offer a range of consultancy services to marine energy device and project developers, investors, contractors, financiers and other stakeholders.

DNV GL has been contracted by Dehlsen Associates LLC (DA) to conduct numerical modelling activities related to the development of the Centipod CPX3 wave energy converter (WEC). Time domain simulations have been carried out in WaveDyn [1], DNV GL's WEC numerical modelling software, for a floating tension leg model of the Centipod WEC incorporating model predictive control (MPC). This report (Issue A) presents results from 136 simulations which evaluate the performance of the WEC model under the sea states up to significant wave height, Hs = 5m that have non-zero rates of occurrence according to the wave scatter plot selected by DA. This builds off the work done and reported in 702480-USSD-R-02-A for a baseline Centipod model, where a fixed damping value[1] was applied to represent a simple, passive approach to power take-off (PTO) design/control. Since issuance of baseline report, DA have worked with their partners to develop a bespoke MPC controller and integrate it into an updated WaveDyn model of the Centipod CPX3 machine. DA then passed the model and controller dynamic link library (DLL) [2] to DNV GL to conduct the simulations and post-processing reported on here. It is expected that DA will be able to use this report to assist them in comparing the impact of MPC on performance and operational loads in comparison to the baseline where no active PTO control was included.

The report is organized into 8 main sections. In Section 2, WaveDyn, the time-domain multi-body simulation package used in this work, is briefly introduced. There is a description of the device in Section 0 followed by a brief description of the Centipod CPX3 WEC model used in the WaveDyn simulations in Section 4. An overview of the simulation setup is provided in Section 5, whilst the main power performance results are presented in Section 6. The operational loads are described in Section 7. Finally, the key findings and conclusions regarding this work and specific recommendations related to future work are summarized in Section 8.

Any enquiries regarding this report should be addressed to:

Jarett Goldsmith

Email: Jarett.Goldsmith@dnvgl.com

Tel.: +1 (858) 836-3370, x132

---

[1] PTO damping value optimized for the most commonly occurring Tp for sea states in the reference scatter plot: Tp = 8.7s

2 WAVEDYN OVERVIEW

WaveDyn is a multi-body, time-domain, simulation tool developed specifically for evaluating WEC performance. The software allows a user to construct a numerical representation of a WEC by connecting structural, hydrodynamic, power take-off (PTO) and moorings components using a flexible user interface. Control actions may be implemented through the PTO components, and simulations may be run with regular or irregular input sea states, for multiple wave directions or directionally spread waves.

In the WaveDyn release used for the present Centipod WEC modelling, the hydrodynamics module is restricted to a linear formulation based on a boundary element method (BEM), potential flow solver. Diffraction, radiation and hydrostatic effects are included in the model, however viscous effects are assumed negligible for power performance calculations, with the machine response being largely dominated by reactive, rather than resistive, hydrodynamic forces. It is important to evaluate WaveDyn simulation results with an appreciation for the magnitude of the body motions in the system. Large body motions as a result of low PTO damping, or the excitation of resonant modes can result in high levels of reported output power where, in reality, nonlinearity in the hydrodynamic loading or the presence of viscous effects may act to suppress such motions. The WaveDyn BEM-based model is particularly suited for situations where body motions are of a similar order of magnitude to the water particle kinematics (the case for many WECs operating in moderate, performance related sea-states) and for realistic, irregular wave simulations which are less likely to exhibit pronounced resonance effects than those that may occur in regular waves.

WaveDyn allows PTO properties to be applied to any joint in the system, where energy converted from the relative motion between adjacent bodies may be used to drive the WEC powertrain. For the set of performance calculations presented here, a model predictive control (MPC) strategy has been used; PTO settings are specified by an external controller DLL developed by DA and project partners.

For this floating model the WEC 'backbone' is modeled with four vertical tendons attaching to each end of structure connecting it to the seabed with the tethers in tension. The tendons are considered in WaveDyn as a spring and damper with an associated stiffness calculated based on the line properties and damping coefficient selected by DA. This is a quasi-static representation of the mooring forces where the applied mooring load is looked up as a function of the attachment point displacement relative to the anchor points. Therefore, mooring line inertial dynamics are neglected.

A linearized model of the hydrostatic force has been assumed in this report. However the Centipod WEC device modeling may benefit from instantaneous hydrostatics being included as nonlinearities may arise if the water plane area changes significantly in larger waves. These effects could be included with the creation of an additional mesh incorporating panels above the mean free surface, allowing the instantaneous pressure over the wetted area to be computed at each timestep.

3 DESCRIPTION OF THE CENTIPOD CPX3 WEC

The Centipod WEC is designed to convert energy from the motion of five floats or "pods" found in a chain attached to a single structural backbone. The relative motion between the pods and 'backbone' are used to drive linear PTO systems, with advanced control (i.e. MPC) of the PTO being envisioned as a means of increasing efficiency. A preliminary moorings study found that if a catenary spread mooring system was incorporated for station-keeping purposes, it would be difficult to obtain adequate relative motion for acceptable power performance with the given geometry without the addition of heave plates suspended below the 'backbone' or other significant changes to design's physical characteristics and layout. It was also seen that, while using the current geometry, significant relative motion could be obtained (similar to the initial fixed 'backbone' analysis presented in DNV GL report 702480-USSD-R-01-A [6]) if a tension leg mooring system was incorporated. As such, a tension leg system has been added to the model analyzed in this report.

An early concept assembly drawing of the device is shown in Figure 3-1, although the dimensions and geometry have since been updated by DA to include additional 'backbone' buoyancy as required for the tension leg system and symmetrical pods. Therefore, the current system does not appear exactly as shown in the figure. The 'backbone' now consists of a 4 meter diameter tubular structure with a length of 74 meters and a total height of 20 meters, 8 meters of which is freeboard and 12 meters of which is the draft below the design still water line. The pods now have a circular profile when looking down from above with a diameter of 9 meters and the pod's draft below the still water level is 1.8 meters. There are no longer any lines connecting the pods to each other. The pods connect to the 'backbone' via the PTO unit (represented in the numerical models as a sliding joint) which is joined on the bottom end to the 'backbone.'

Figure 3-1: The Centipod WEC[5][2]

---
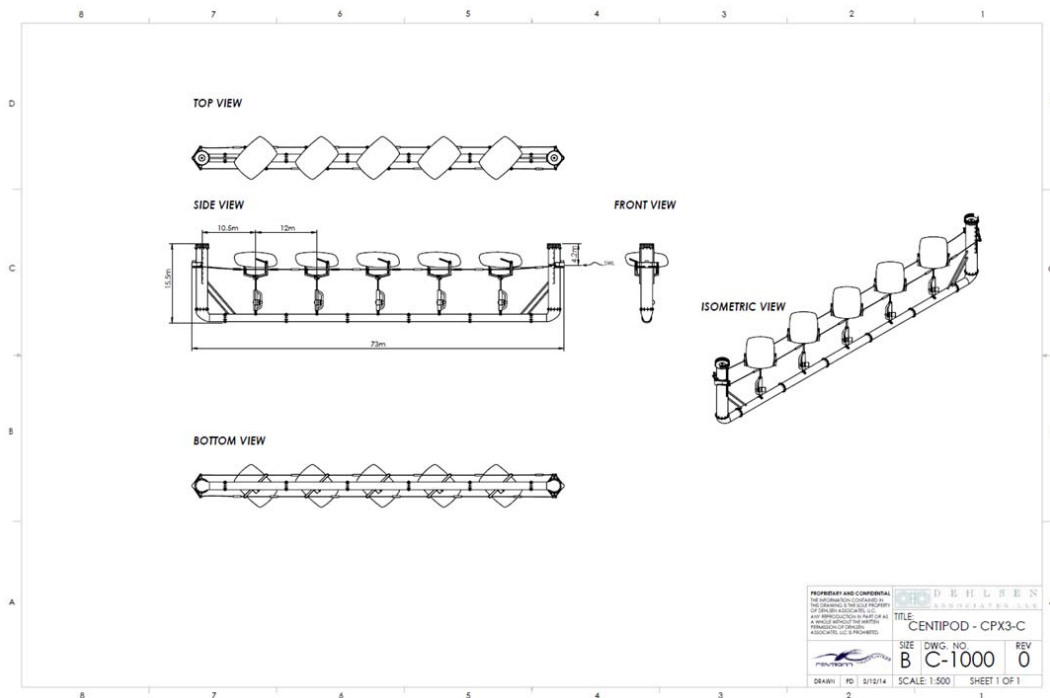
[2] The design has been significantly updated since this early Centipod CPX3 concept assembly drawing was generated.

4 CENTIPOD CPX3 WEC MODEL CONFIGURATION

WaveDyn simulation models are constructed on a multi-body basis, as a collection of linked components with specific physical properties. These components include wave-activated rigid bodies, joints at which PTO forces may be applied and mooring lines that may be assigned an anchor point and attached to the WEC structure.

Several modules of WaveDyn interact to solve the multi-body dynamics of the Centipod CPX3 WEC model; these include:

- Sea state;

- Structural Dynamics;

- Hydrodynamics;

- PTO response;

- Control; and,

- Moorings.

Each module incorporates a library of component models that may be used to build up a mathematical representation of the WEC.

The WaveDyn model of the Centipod CPX3 WEC used for the simulations discussed herein was developed by DA and provided for DNV GL once DA deemed it was ready. DNV GL understand that the model was based on the baseline WaveDyn model developed and described by DNV GL in Report 702480-USSD-R-02-A, but slightly adapted by DA and its partners to allow for the inclusion of MPC. The main modifications were [3]:

- Offset on some of the bodies and joints such that after the initial extension of the mooring lines the bodies are at correct position.

- 4 tension legs are now used and a small damping coefficient was also selected by DA to apply to each line (with a Ns/m value input at 10% of magnitude of the stiffness [N/m]).

- The hinge connecting the floats arm with the backbone was eliminated.

- Damping (1E4 Ns/m and 1E4 Nms/rad) was added to all backbone DoF except heave.

DNV GL did not review the updated model provided by DA in any detail, and therefore the results presented in this report assumed DA's provision of a functional model that incorporates MPC as designed.

5 OVERVIEW OF SIMULATION SETUP

5.1 Seed Uncertainty

Analysis earlier in the project (see 702480-USSD-R-01 [6]) showed that for similar length simulations in the various sea states analyzed here (200 * Tp seconds + an initial 100s excluded from post-processing) there was very little variation in the average power results from using different random seeds to generate the SEA files. This knowledge, in combination with the number of simulations required to fully populate the new power matrix, led to a single random seed being used to generate each sea state's SEA file for use in the WaveDyn simulations.

However, it should be noted that when running loads analysis, the minimum and maximum loads registered may vary between simulations using different random seeds. Therefore, the use of various seeds would be necessary to have the full characterization of the loads. In order to reduce the number of calculations carried out for this baseline effort, a statistical approach to the load calculations will be applied as described in Section 7. The load time-series for each component will be subject to a peak analysis and a probability of non-exceedance is attributed to each of the peaks.

5.2 Power Matrix Simulations

The WaveDyn time domain simulations of the Centipod CPX3 WEC with MPC provide an estimate of the total mean absorbed power for the machine as well as the power absorption associated with each individual PTO unit. A range of other variables, including wave induced forces, float motions and PTO forces are also generated and will be supplied to DA as part of the WaveDyn output files. Guidance found in "Standardized cost and Performance Reporting for Marine and Hydrokinetic Technologies" [8] was followed as a guide during the setup of these simulations.

A unidirectional Bretschneider spectrum was used to represent the sea states for each bin with an occurrence value greater than zero in the wave scatter plot provided in [9] and shown in Table 5-3. The use of a standard spectral shape characterized by a peak period is based on performance reporting guidance published by the Department of Energy (DOE) [8], as requested by the client. It is noted that the spectral shape resulting from site measurements may vary significantly from the standard Bretschneider spectrum shape. The length of the simulations has to be sufficient to capture the energy seen for the particular sea state with a length equal to the peak period multiplied by 200, as advised in the guidance note [8]. The repeat period of the input sea state and the WaveDyn simulation have the same length. The ramp-up period (5s) remained unchanged for all simulations; however, an additional 100s was added to the total simulation time (200Tp+100s) to further ensure steady state conditions and the post-processed data consisted of the full time series omitting this initial 100s. Waves were assumed to come from a single idealized direction perpendicular to the 'backbone' centerline. The sensitivity of the device to, wave direction relative to the backbone, directional spreading effects and to spectral shape may additionally be considered in the future.

Wave scatter probability data provided by DA [9], summarized in Table 5-3, was combined with the generated power matrix to predict the annual energy capture of the device assuming 100% availability. During this analysis no mechanical or electrical losses are assumed and so the values presented are idealized.

It should be noted, that although simulations were run for Hs up to 4.75m, assumptions for linear theory are less valid for large wave heights, and therefore the results from simulations in large and steep waves are

likely to be less representative of the true behavior of the system. Since the number of occurrences at the largest sea states are smaller, DA expects the WEC to be in a non-operational or 'survival mode' during these conditions and simulations above Hs = 5m, as specified by DA, were omitted. Any considerations of loads calculated during larger states using the WaveDyn model, should be made with caution.

Table 5-1: Summary of the environmental conditions simulated

Minimum Tp	3.7s
Maximum Tp	19.7s
Tp step	1s
Hs	0.25m – 4.75m (depending on occurrence)
Hs step	0.5m
Number of seeds per sea state	1
Repeat time of simulated waves	200 T_p
Water depth	70m

Table 5-2: Summary of the simulation parameters used in WaveDyn

WaveDyn version		1.2.0.9
Integrator		Variable time step; min 0.0001s, max. 1s
Excitation forces		Linear
Hydrostatic forces		Linear
Radiation force impulse response function	Cut-off time	60s
	Resolution	0.1s
	Min. time step	0.1s
Drag coefficient		0
PTO damping		MPC Controller DLL
Simulation length		200 T_p +100 s
Output time step		0.1s
Ramp-up time		5s

Table 5-3: Wave scatter table for incident sea states (%).

		Peak Period, Tp [sec]

Significant Wave Height, Hs [m]		1.7	2.7	3.7	4.7	5.7	6.7	7.7	8.7	9.7	10.7	11.7	12.7	13.7	14.7	15.7	16.7	17.7	18.7	19.7	20.7
	0.25	0.00%	0.00%	0.00%	0.00%	0.00%	0.01%	0.00%	0.00%	0.00%	0.00%	0.00%	0.00%	0.00%	0.01%	0.00%	0.00%	0.00%	0.00%	0.00%	0.00%
	0.75	0.00%	0.00%	0.01%	0.15%	0.43%	1.07%	1.12%	1.30%	0.41%	0.63%	0.28%	0.20%	0.20%	0.34%	0.43%	0.48%	0.17%	0.00%	0.03%	0.00%
	1.25	0.00%	0.00%	0.02%	0.10%	0.98%	2.80%	2.38%	4.56%	1.85%	2.16%	1.12%	0.87%	0.66%	0.55%	0.37%	0.44%	0.24%	0.00%	0.05%	0.00%
	1.75	0.00%	0.00%	0.00%	0.03%	0.25%	2.47%	2.67%	3.64%	2.09%	3.53%	1.95%	1.36%	1.21%	0.95%	0.46%	0.51%	0.29%	0.00%	0.11%	0.00%
	2.25	0.00%	0.00%	0.00%	0.00%	0.04%	0.64%	2.32%	3.56%	1.65%	3.27%	2.45%	1.86%	1.51%	1.03%	0.56%	0.51%	0.31%	0.00%	0.12%	0.00%
	2.75	0.00%	0.00%	0.00%	0.00%	0.00%	0.19%	0.90%	2.73%	1.00%	2.16%	1.96%	1.51%	1.34%	0.85%	0.52%	0.49%	0.33%	0.00%	0.14%	0.00%
	3.25	0.00%	0.00%	0.00%	0.00%	0.00%	0.03%	0.18%	1.06%	0.69%	1.21%	1.29%	1.19%	1.05%	0.83%	0.49%	0.43%	0.19%	0.00%	0.07%	0.00%
	3.75	0.00%	0.00%	0.00%	0.00%	0.00%	0.00%	0.04%	0.29%	0.32%	0.53%	0.75%	0.68%	0.70%	0.60%	0.34%	0.27%	0.12%	0.00%	0.06%	0.00%
	4.25	0.00%	0.00%	0.00%	0.00%	0.00%	0.00%	0.00%	0.09%	0.10%	0.18%	0.28%	0.34%	0.41%	0.36%	0.22%	0.23%	0.09%	0.00%	0.03%	0.00%
	4.75	0.00%	0.00%	0.00%	0.00%	0.00%	0.00%	0.00%	0.01%	0.03%	0.07%	0.08%	0.12%	0.18%	0.24%	0.15%	0.16%	0.07%	0.00%	0.03%	0.00%
	5.25	0.00%	0.00%	0.00%	0.00%	0.00%	0.00%	0.00%	0.00%	0.01%	0.01%	0.03%	0.05%	0.09%	0.12%	0.09%	0.10%	0.05%	0.00%	0.02%	0.00%
	5.75	0.00%	0.00%	0.00%	0.00%	0.00%	0.00%	0.00%	0.00%	0.00%	0.00%	0.00%	0.01%	0.03%	0.05%	0.04%	0.05%	0.02%	0.00%	0.01%	0.00%
	6.25	0.00%	0.00%	0.00%	0.00%	0.00%	0.00%	0.00%	0.00%	0.00%	0.00%	0.00%	0.01%	0.01%	0.04%	0.02%	0.03%	0.02%	0.00%	0.00%	0.00%
	6.75	0.00%	0.00%	0.00%	0.00%	0.00%	0.00%	0.00%	0.00%	0.00%	0.00%	0.00%	0.01%	0.01%	0.01%	0.01%	0.01%	0.01%	0.00%	0.00%	0.00%
	7.25	0.00%	0.00%	0.00%	0.00%	0.00%	0.00%	0.00%	0.00%	0.00%	0.00%	0.00%	0.00%	0.00%	0.00%	0.01%	0.01%	0.00%	0.00%	0.00%	0.00%
	7.75	0.00%	0.00%	0.00%	0.00%	0.00%	0.00%	0.00%	0.00%	0.00%	0.00%	0.00%	0.00%	0.00%	0.00%	0.00%	0.00%	0.00%	0.00%	0.00%	0.00%
	8.25	0.00%	0.00%	0.00%	0.00%	0.00%	0.00%	0.00%	0.00%	0.00%	0.00%	0.00%	0.00%	0.00%	0.00%	0.00%	0.00%	0.00%	0.00%	0.00%	0.00%
	8.75	0.00%	0.00%	0.00%	0.00%	0.00%	0.00%	0.00%	0.00%	0.00%	0.00%	0.00%	0.00%	0.00%	0.00%	0.00%	0.00%	0.00%	0.00%	0.00%	0.00%
	9.25	0.00%	0.00%	0.00%	0.00%	0.00%	0.00%	0.00%	0.00%	0.00%	0.00%	0.00%	0.00%	0.00%	0.00%	0.00%	0.00%	0.00%	0.00%	0.00%	0.00%
	9.75	0.00%	0.00%	0.00%	0.00%	0.00%	0.00%	0.00%	0.00%	0.00%	0.00%	0.00%	0.00%	0.00%	0.00%	0.00%	0.00%	0.00%	0.00%	0.00%	0.00%
	10.3	0.00%	0.00%	0.00%	0.00%	0.00%	0.00%	0.00%	0.00%	0.00%	0.00%	0.00%	0.00%	0.00%	0.00%	0.00%	0.00%	0.00%	0.00%	0.00%	0.00%
	10.8	0.00%	0.00%	0.00%	0.00%	0.00%	0.00%	0.00%	0.00%	0.00%	0.00%	0.00%	0.00%	0.00%	0.00%	0.00%	0.00%	0.00%	0.00%	0.00%	0.00%
	11.3	0.00%	0.00%	0.00%	0.00%	0.00%	0.00%	0.00%	0.00%	0.00%	0.00%	0.00%	0.00%	0.00%	0.00%	0.00%	0.00%	0.00%	0.00%	0.00%	0.00%
	11.8	0.00%	0.00%	0.00%	0.00%	0.00%	0.00%	0.00%	0.00%	0.00%	0.00%	0.00%	0.00%	0.00%	0.00%	0.00%	0.00%	0.00%	0.00%	0.00%	0.00%
	12.3	0.00%	0.00%	0.00%	0.00%	0.00%	0.00%	0.00%	0.00%	0.00%	0.00%	0.00%	0.00%	0.00%	0.00%	0.00%	0.00%	0.00%	0.00%	0.00%	0.00%

6 POWER PERFORMANCE

6.1 Power matrix and nominal energy yield

All simulations and figure shown in this report are subject to the assumptions and caveats presented in Section 6.2. The results of the simulations described in Section 5.2 are represented by the power matrix displayed in Table 6-1. A number of entries have been greyed out due to no occurrence in the wave scatter plot. A significant wave height up to 4.75m is shown. The power matrix has been combined with the scatter diagram presented in Table 5-3 to obtain an annual energy yield matrix and a nominal annual energy yield value shown in Table 6-2. This matrix provides a sense of which sea states are contributing the most energy production with the current design and assumptions. Total annual energy yield for the current Centipod model with MPC is calculated to be approximately 3782 MWh.

The relative capture width (RCW) has also been evaluated for each sea state bin. This is the ratio between the mean power absorbed by the WEC, $\overline{P_{abs}}$ and the mean available power in an equivalent width of incident wave front, $\overline{P_w}$ and may be viewed as a measure of WEC efficiency:

$$RCW = \frac{\overline{P_{abs}}}{\overline{P_w}} \tag{1}$$

$$\overline{P_w} = \frac{\rho g^2 H_s^2 T_e}{64\pi} l \tag{2}$$

where l is a characteristic width of the WEC (74m has been used in this case as the frontal width exposed to the on-coming waves), and $T_e = 0.8572 T_p$ for the Bretschneider spectrum.

The greatest relative capture widths are achieved for smaller sea states (~Hs < 2m) and lower periods of approximately 6-10s. Investigations into why this is may help DA to find ways to further understand and improve system performance.

Table 6-1: Full power matrix (kW) with MPC. Incident wave direction perpendicular to the 'backbone'

		Peak Period, Tp [s]Tp [s]																
		3.7	**4.7**	**5.7**	**6.7**	**7.7**	**8.7**	**9.7**	**10.7**	**11.7**	**12.7**	**13.7**	**14.7**	**15.7**	**16.7**	**17.7**	**18.7**	**19.7**
	0.25				5.3	6.1			8.7	9.8	11.1	12.3	12.7	13.3		13.4		
	0.75	17.4	28.5	39.1	47.6	54.4	61.6	69.6	76.7	85.6	96.1	104.0	99.3	99.7	106.0	115.0		102.0
	1.25	48.0	78.6	108.0	133.0	151.0	170.0	190.0	208.0	209.0	246.0	228.0	229.0	229.0	212.0	185.0		178.0
	1.75	94.1	153.0	212.0	258.0	291.0	314.0	321.0	320.0	317.0	366.0	339.0	367.0	264.0	348.0	293.0		325.0
Hs, [m]	**2.25**		253.0	345.0	418.0	465.0	470.0	474.0	468.0	485.0	482.0	470.0	481.0	430.0	438.0	465.0		480.0
	2.75			508.0	589.0	656.0	656.0	613.0	601.0	614.0	661.0	573.0	617.0	587.0	574.0	520.0		528.0
	3.25			672.0	799.0	843.0	864.0	840.0	740.0	764.0	684.0	760.0	692.0	649.0	671.0	672.0		697.0
	3.75				1020.0	1070.0	1010.0	921.0	894.0	923.0	920.0	877.0	865.0	845.0	854.0	860.0		829.0
	4.25					1290.0	1220.0	1030.0	1060.0	1090.0	1040.0	1120.0	1010.0	1020.0	931.0	882.0		974.0
	4.75						1390.0	1270.0	1260.0	1200.0	1220.0	1180.0	1110.0	1200.0	1140.0	1080.0		1140.0

Table 6-2: Annual energy yield matrix (MWh) and total annual energy yield of single device with MPC assuming, linear hydrodynamics, no mechanical/electrical losses/constraints or reactive power limits and 100% availability.

		Peak Period, Tp [s]																
		3.7	**4.7**	**5.7**	**6.7**	**7.7**	**8.7**	**9.7**	**10.7**	**11.7**	**12.7**	**13.7**	**14.7**	**15.7**	**16.7**	**17.7**	**18.7**	**19.7**
	0.25				0.0	0.0			0.0	0.0	0.0	0.0	0.0	0.0		0.0		
	0.75	0.0	0.4	1.5	4.4	5.4	7.0	2.5	4.2	2.1	1.7	1.8	2.9	3.8	4.5	1.7		0.2
	1.25	0.1	0.7	9.3	32.7	31.5	68.0	30.8	39.5	20.5	18.9	13.1	11.0	7.3	8.2	3.9		0.7
	1.75	0.0	0.4	4.6	55.8	68.1	100.3	58.9	99.0	54.1	43.7	35.9	30.7	10.6	15.6	7.5		3.1
Hs [m]	**2.25**		0.0	1.3	23.6	94.7	146.6	68.6	134.3	104.0	78.5	62.2	43.6	21.0	19.5	12.6		5.0
	2.75			0.1	9.8	51.8	157.1	53.9	113.7	105.6	87.3	67.1	46.0	26.6	24.6	15.2		6.6
	3.25			0.1	2.0	13.7	79.9	50.8	78.7	86.3	71.6	70.2	50.3	28.1	25.1	11.0		4.4
	3.75				0.2	4.0	25.9	25.6	41.4	60.5	54.5	53.7	45.7	25.3	19.9	9.1		4.3
	4.25				0.1		9.4	9.1	16.6	26.8	30.6	40.4	31.9	20.0	19.1	7.1		2.4
	4.75						1.7	3.5	7.3	7.9	12.7	19.0	22.9	15.3	16.4	6.8		3.0

Total annual energy yield
3782 MWh

Table 6-3: Relative capture width (RCW) of device

		Peak Period, Tp [s]																
		3.7	4.7	5.7	6.7	7.7	8.7	9.7	10.7	11.7	12.7	13.7	14.7	15.7	16.7	17.7	18.7	19.7
Hs [m]	0.25				0.405	0.406			0.417	0.428	0.447	0.460	0.443	0.436		0.390		
	0.75	0.268	0.347	0.392	0.405	0.404	0.404	0.410	0.409	0.418	0.432	0.433	0.386	0.363	0.362	0.371		0.296
	1.25	0.267	0.344	0.389	0.408	0.403	0.402	0.403	0.400	0.367	0.398	0.342	0.320	0.300	0.261	0.215		0.186
	1.75	0.267	0.341	0.390	0.404	0.396	0.379	0.347	0.314	0.284	0.302	0.259	0.262	0.176	0.219	0.174	0.181	0.173
	2.25		0.342	0.384	0.396	0.383	0.343	0.310	0.277	0.263	0.241	0.218	0.208	0.174	0.166	0.167		0.155
	2.75			0.378	0.373	0.362	0.320	0.268	0.239	0.223	0.221	0.178	0.178	0.159	0.146	0.125		0.114
	3.25			0.358	0.363	0.333	0.302	0.263	0.210	0.199	0.164	0.169	0.143	0.126	0.122	0.115		0.108
	3.75				0.348	0.317	0.265	0.217	0.191	0.180	0.165	0.146	0.134	0.123	0.117	0.111		0.096
	4.25					0.298	0.249	0.189	0.176	0.166	0.146	0.145	0.122	0.116	0.099	0.089		0.088
	4.75						0.227	0.186	0.168	0.146	0.137	0.123	0.107	0.109	0.097	0.087		0.082

6.2 Key assumptions and caveats

The power matrix, relative capture width and annual energy yield data presented may be considered an updated set of performance data for the 4-leg WaveDyn model of the concept floating TLP Centipod WEC with MPC. The WEC is modelled at an early stage of development, operating in idealized conditions and the following assumptions and caveats apply:

- The power values have been obtained using a PTO and control model provided by DA representative of an idealized MPC controller capable of incorporating reactive power. No consideration of the true characteristics, efficiency and operating limitations of the PTO, controller or any other of the WEC subsystems has been incorporated in the model at this stage but should be seen as necessary development in the future.

- The performance data was derived using a linear hydrodynamic model without viscous damping. The validity of this model may be expected to be reduced in larger sea-states. The model would ideally be verified against a higher order formulation and validated against tank test results as part of future work.

- The sensitivity of the WEC model to spectral shape, mean wave direction and directional spreading has not been considered. Such effects would ideally be incorporated in full a site specific power matrix for a prototype machine.

- A nominal energy yield has been derived based on 100% availability under a single mode of operation without provision for faults or maintenance. This scenario is highly idealized and, whilst the yield value obtained may be used to inform the WEC development process, it should not be used directly in a cost of energy model.

7 OPERATIONAL LOADS

7.1 Methodology

The loads on the various WEC components are calculated (and output) within WaveDyn for all the elements in the structure. For the Centipod machine, the loads on the pods, mooring loads and loads on the PTO are considered the outputs of most interest. A statistical analysis of the loads has been performed (min, max, mean, standard deviation). The non-exceedance curves for the various sea states have also been calculated. The use of this type of output allows a good understanding of the various loads levels experienced by the WEC components. It also provides a useful way to compare the influence on the loads of changing the WEC configurations. The use of these cumulative probability curves can also be used at a later stage for load extrapolation and fatigue analysis.

The scheme below illustrates the main steps used in this load analysis.

Figure 7-1   Post processing tasks

7.2 WaveDyn outputs

WaveDyn outputs structural loads for all the proximal nodes in the model. These forces and moments are the resultant forces and moments acting on a particular element. By default, WaveDyn outputs these structural forces at the location of the proximal node and the output coordinate system is orientated with the global axis defined in WaveDyn. The global WaveDyn model is located at sea bed, with the z-axis pointing up-wards Figure 7-2 (left). The global coordinate system is kept constant throughout all the simulation.

For most structural analysis, the loads given in a body fixed coordinate system are most useful. The body fixed coordinate system is defined at the element proximal node with the z-axis pointing upwards (central axis of the pod for example). The orientation of body $x-$ and $y-$ axis is equal to the global coordinates at the beginning of the simulation. With the displacement of the body coordinate system it is rotated such that the main axis follows the body main axis, see Figure 7-2 (right). The rotation of the body is defined at the body proximal node with the global coordinate system. The rotation angles A, B and C are measured around the global coordinate axis x_g, y_g and z_g . An example of this for angle A is given in Figure 7-2 (right). These angles are part of the WaveDyn displacements output.

Figure 7-2:   Global coordinate system and body coordinate system (rotation around x-axis)
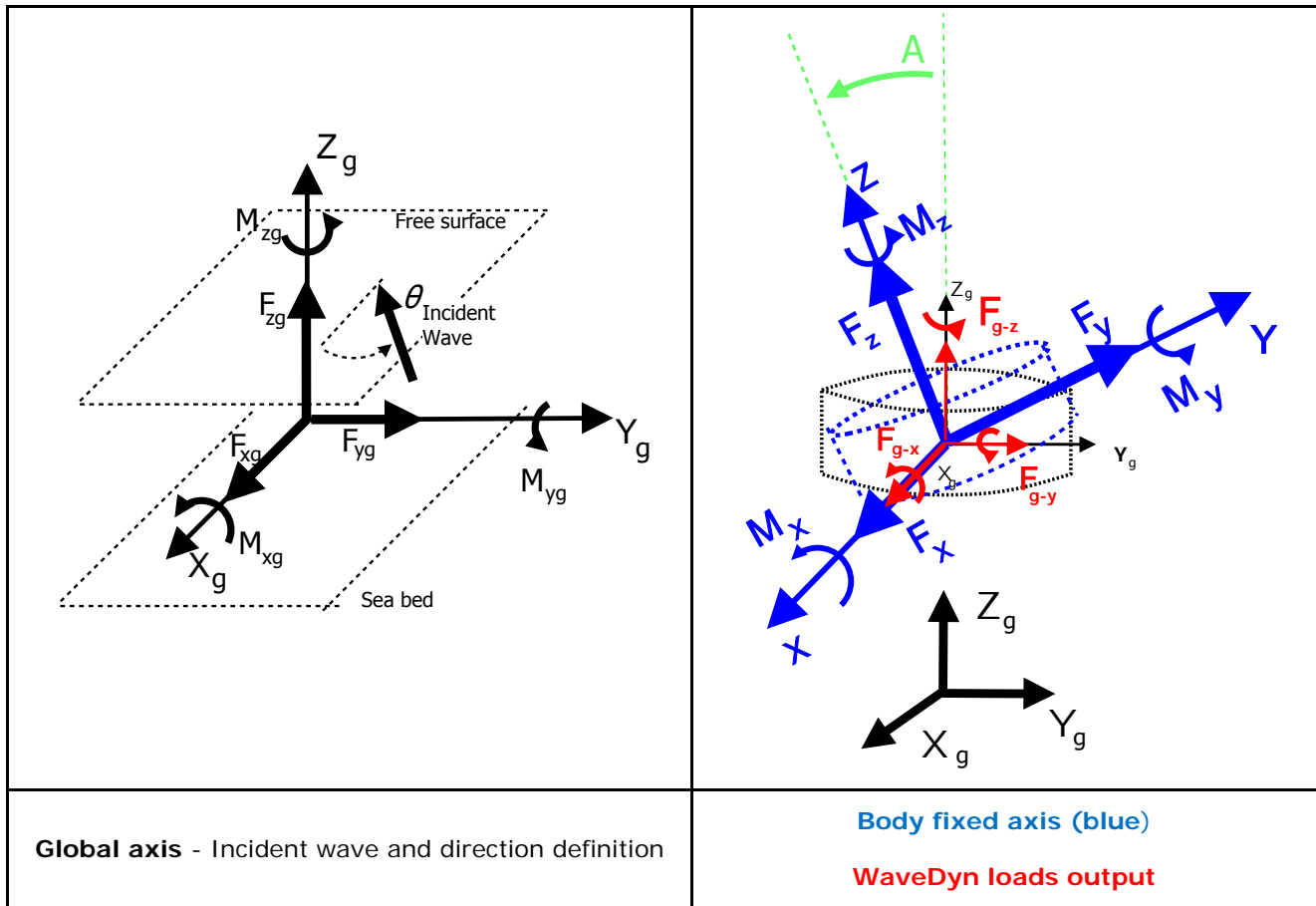
Global axis - Incident wave and direction definition	**Body fixed axis (blue)** **WaveDyn loads output**

The rotation of the loads to body-fixed coordinates is made using a passive rotation matrix. The rotations are made about the coordinate system located at each body's proximal node orientated using the Global coordinates. The rotation around the Z axis is made first, followed by the Y-axis and finally the X-axis. Considering the WaveDyn output force, F_g (red vectors in Figure 7-2), the output forces in a body fixed coordinate system F are found using:

$$\begin{bmatrix} F_x \\ F_y \\ F_z \end{bmatrix} = \begin{bmatrix} \cos C \cos B & \sin C \cos B & -\sin B \\ -\sin C \cos A + \cos C \sin B \sin A & \cos C \cos A + \sin C \sin B \sin A & \cos B \sin A \\ \sin C \sin A + \cos C \sin B \cos A & -\cos C \sin A + \sin C \sin B \cos A & \cos A \cos B \end{bmatrix} \begin{bmatrix} F_{gx} \\ F_{gy} \\ F_{gz} \end{bmatrix}. \tag{3}$$

7.2.1 Reported loads

For the structural analysis, a few nodes of the WaveDyn Centipod model were selected to carry out the loads post-processing described above. The nodes used in the post-processing and a brief description of the loads involved are presented in Table 7-1.

Table 7-1: Post-processed loads locations.

Body	Description of the Loads
Pod 1 Pod 2 Pod 3 Pod 4 Pod 5	Forces in body fixed coordinate system located at the centre of mass of the pod structures. The output loads at these locations include: - Hydrodynamic loads on the pods - Gravity loads - Inertia loads
Pod attachment, 3	Forces acting on the Pod 3 (in body fixed coordinate system) at the attachment location on the back bone.
Mooring lines 1,2,3 and 4	The tension on the mooring lines (F_{Line}) can be calculated as the magnitude of the resultant force of the three components of the mooring force, F_{moor}: $$F_{Line} = \sqrt{F^2_{moor\,gx} + F^2_{moor\,gy} + F^2_{moor\,gz}}$$

For the pods the axial force is defined as being the F_z force on the body fixed coordinate system. The shear force is defined as the magnitude of the resultant of the x and y components.

$$F_{axial} = \boldsymbol{F_z} \qquad (4)$$

$$F_{shear} = F_{xy} = \sqrt{\boldsymbol{F_x^2} + \boldsymbol{F_y^2}} \qquad (5)$$

$$M_{bending} = M_{xy} = \sqrt{\boldsymbol{M_x^2} + \boldsymbol{M_y^2}} \qquad (6)$$

7.3 Global results

The variation of several parameters with the sea state can be of importance in order to understand machine behaviour trends. Below the variation of some elements of the model observed during the simulations is presented, specifically:

- Maximum and minimum *PTO* displacement of the central pod (Pod 3) in Table 7-2 and Table 7-3.

- Maximum and minimum axial forces registered for Pod 3 in Table 7-4 and Table 7-5.

- Resultant shear force and bending moment acting on Pod 3 in Table 7-6 and Table 7-7.

- Mooring line tension for:

    o line 1 (attachment point: (30,-7,-2) in Table 7-8

    o line 2 (attachment point (-30,-7,-2) in Table 7-9

    o line 3 (attachment point (30,7,-2) in Table 7-10

    o line 4 (attachment point (-30,7,-2) in Table 7-11

- Maximum 'backbone' yaw motion in able 7-12.

The PTO displacement for Pod 3 is seen to be highly dependent on Hs and to a lesser extent on Tp. A maximum PTO extension of 8.9m is observed for an Hs=4.75m and Tp=16.7s. No sea states with Hs > 5m were run as specified by DA. No physical end stops of any kind were included in the current model. In future models a system to reduce the displacement of the PTO is advised for use in larger sea states. It should be mentioned as a reminder once again that the applicability of the linear wave theory behind WaveDyn's hydrodynamic load calculation is limited for larger sea states, where waves become steeper and nonlinearities in wave kinematics and the occurrence of breaking increase and where assumptions of a constant wetted profile may be less valid. The results for these sea states should be used with caution and subject to validation using experimental data. Linear theory tends to result in an over prediction of motions in larger sea states. The lack of inclusion of end stops can also lead to inclusion of non-realistic physical motions.

The loading on the mooring lines is very similar for the 4 mooring lines in most of the sea states. The maximum mooring line loads observed are approximately 4.5MN for the sea state with Tp=19.7s and Hs=4.75m. The differences in the maximum tension values for the 4 lines is caused by the motions on the platform that lead to asymmetries in the system, and consequently on the loading. During the simulation it was found that the tension on some of the mooring lines was reaching 0 N in some of the studied sea states (see for example, Figure 7-3). This warrants further investigation to ensure acceptable dynamic behaviour and prevent snap loading in the mooring lines.

This asymmetric behaviour of the WEC can be also observed in the yaw motion of the 'backbone'. The yaw motions are significant in a range of the most common sea states. The cause for this asymmetry may be the small numerical instabilities resulting from the hydrodynamic data. These instabilities lead to small yaw displacements and consequent misalignment of the WEC with the unidirectional incident waves, increasing the asymmetric behaviour due to the excitation forces and possibly leading to some motions in the cross-wave degrees of freedom. The radiation damping (n.b. for low frequencies this is very small) and the viscous damping added to the backbone are unable to damp out the amplitude of these initial yaw displacements.

This indicates that the mooring arrangement and model dynamics should be investigated further, ideally with experimental data for validation.

The impact of these large yaw displacements and the power performance should also be studied further. However, as a first check the total power extracted and the yaw of the backbone for the sea state Hs = 4.75m and Tp = 8.7s were compared in Figure 7-4. The large motion in yaw don't seem to have a direct large on the power performance of the device, but further studies on this should be carried out.

Again it should be noted that these maximum results were obtained for a relatively short simulation lengths (200xTp). This is acceptable for power absorption estimations as specified by [8]. However, when considering extreme values analysis a larger simulation time is necessary. For more comprehensive structural analysis, it is recommended to increase the length of simulation. This can be achieved by increasing the number of seeds for each sea state.

Table 7-2: Maximum PTO displacement [m] for Pod 3 (center pod).

		Peak Period, Tp [s]															
		3.7	4.7	5.7	6.7	7.7	8.7	9.7	10.7	11.7	12.7	13.7	14.7	15.7	16.7	17.7	18.7	19.7
Hs, m	0.25				0.4	0.5			0.8	0.7	0.9	1.2	1.0	1.2		1.4		
	0.75	0.5	0.7	0.8	0.8	1.1	1.2	1.6	1.9	1.9	1.9	2.0	2.1	2.2	2.4	2.6		2.5
	1.25	0.7	1.3	1.2	1.5	1.7	1.9	2.2	2.5	2.4	2.8	2.6	3.1	2.8	3.3	3.2		2.9
	1.75	1.0	1.4	1.7	1.9	2.2	2.4	3.3	3.1	3.3	3.2	3.3	3.3	3.6	3.5	3.6		3.5
	2.25		2.0	2.3	2.1	2.6	3.6	4.2	3.8	3.6	3.5	3.7	3.9	4.1	4.5	5.1		3.8
	2.75			2.1	2.8	3.1	3.3	4.2	4.2	4.2	4.4	4.4	5.0	4.3	5.1	4.6		4.6
	3.25			3.2	2.7	3.5	4.8	4.4	4.8	5.6	5.3	5.3	5.1	5.1	5.3	5.8		5.6
	3.75				3.4	3.5	4.4	5.4	5.1	4.7	5.0	4.8	5.7	5.6	5.6	5.7		6.9
	4.25					3.8	4.7	5.9	7.2	5.6	5.7	6.1	5.8	6.4	6.3	6.7		6.1
	4.75						6.6	5.9	6.5	6.8	5.8	5.9	6.5	8.5	8.9	7.1		8.7

Table 7-3: Minimum PTO displacement [m] for Pod 3 (center pod).

		Peak Period, Tp [s]															
		3.7	4.7	5.7	6.7	7.7	8.7	9.7	10.7	11.7	12.7	13.7	14.7	15.7	16.7	17.7	18.7	19.7
Hs [m]	0.25				-0.1	-0.1			-0.2	-0.3	-0.3	-0.5	-0.5	-0.5		-0.8		
	0.75	-0.4	-0.5	-0.4	-0.5	-0.6	-1.0	-0.9	-1.4	-1.0	-1.6	-1.8	-1.7	-1.8	-1.9	-1.8		-1.7
	1.25	-0.5	-1.1	-1.0	-1.0	-1.2	-1.4	-1.8	-1.6	-1.9	-2.1	-2.0	-2.0	-2.1	-2.0	-1.9		-1.9
	1.75	-1.0	-1.2	-1.3	-1.3	-1.4	-1.7	-2.0	-2.4	-2.0	-2.2	-2.1	-2.6	-2.0	-2.4	-2.3		-2.4
	2.25		-1.6	-1.8	-1.6	-1.7	-2.3	-2.2	-2.2	-2.4	-2.5	-2.3	-2.7	-2.4	-2.6	-2.6		-2.9
	2.75			-1.8	-1.9	-2.0	-2.6	-2.5	-2.5	-2.6	-2.9	-3.2	-2.8	-2.6	-2.9	-2.9		-3.0
	3.25			-2.5	-2.4	-2.4	-2.8	-2.6	-2.4	-3.1	-2.9	-2.9	-3.2	-3.3	-3.4	-3.5		-3.2
	3.75				-2.6	-2.7	-3.0	-2.7	-3.1	-3.1	-3.3	-3.3	-3.8	-3.3	-4.0	-3.1		-3.5
	4.25					-2.8	-3.8	-3.2	-3.2	-3.4	-3.5	-3.7	-3.2	-3.6	-3.6	-4.1		-4.6
	4.75						-3.7	-3.4	-3.6	-3.8	-4.2	-3.7	-4.0	-3.7	-3.8	-3.9		-3.8

Table 7-4: Maximum axial force [kN] for Pod 3 for all sea states investigated.

Hs [m]	Peak Period, Tp [s]																
	3.7	4.7	5.7	6.7	7.7	8.7	9.7	10.7	11.7	12.7	13.7	14.7	15.7	16.7	17.7	18.7	19.7
0.25				230	280			401	399	487	662	570	668		775		
0.75	246	358	440	447	551	600	859	972	1025	1026	1031	1034	1028	1036	1021		1019
1.25	336	631	585	750	863	876	1080	1123	1065	1067	1069	1062	1051	1053	1050		1050
1.75	515	712	817	952	1108	1100	1115	1098	1114	1091	1075	1072	1059	1081	1050		1053
2.25		1005	976	1001	1160	1203	1137	1167	1131	1113	1103	1106	1078	1084	1074		1058
2.75			1033	1186	1234	1215	1206	1164	1157	1133	1112	1123	1107	1099	1093		1082
3.25			1115	1237	1337	1308	1234	1198	1186	1160	1129	1137	1103	1103	1090		1081
3.75				1262	1258	1273	1306	1253	1221	1190	1162	1175	1137	1118	1109		1093
4.25					1353	1375	1313	1277	1207	1218	1192	1161	1159	1168	1151		1126
4.75						1367	1323	1326	1324	1298	1206	1170	1176	1156	1175		1129

Table 7-5: Minimum axial force [kN] for Pod 3 for all sea states investigated.

Hs [m]	Peak Period, Tp [s]																
	3.7	4.7	5.7	6.7	7.7	8.7	9.7	10.7	11.7	12.7	13.7	14.7	15.7	16.7	17.7	18.7	19.7
0.25				-209	-224			-289	-358	-437	-652	-533	-675		-604		
0.75	-191	-257	-324	-471	-570	-678	-721	-789	-719	-985	-1014	-1010	-1019	-1034	-1036		-1021
1.25	-275	-479	-526	-707	-775	-931	-943	-1019	-1018	-1076	-1070	-1055	-1060	-1061	-1043		-1031
1.75	-445	-635	-781	-939	-893	-1056	-1091	-1089	-1047	-1093	-1101	-1092	-1040	-1059	-1054		-1051
2.25		-834	-889	-1046	-1051	-1106	-1078	-1084	-1096	-1088	-1073	-1120	-1075	-1075	-1067		-1058
2.75			-1074	-1147	-1165	-1168	-1185	-1172	-1144	-1128	-1125	-1117	-1120	-1115	-1112		-1090
3.25			-1113	-1235	-1166	-1170	-1138	-1143	-1176	-1157	-1114	-1142	-1115	-1137	-1098		-1098
3.75				-1306	-1222	-1251	-1247	-1176	-1196	-1179	-1163	-1122	-1146	-1145	-1101		-1088
4.25					-1258	-1270	-1237	-1212	-1197	-1181	-1196	-1177	-1131	-1123	-1138		-1152
4.75						-1321	-1278	-1299	-1257	-1208	-1207	-1161	-1213	-1200	-1149		-1125

Table 7-6: Maximum shear force, F_{xy}, [kN] for Pod 3 for all sea states investigated.

Hs [m]	Peak Period, Tp [s]																
	3.7	4.7	5.7	6.7	7.7	8.7	9.7	10.7	11.7	12.7	13.7	14.7	15.7	16.7	17.7	18.7	19.7
0.25				11	8			5	5	5	5	5	6		7		
0.75	56	48	33	30	29	21	26	35	27	28	30	32	31	32	37		30
1.25	80	87	62	48	43	33	50	52	65	44	47	49	55	64	62		48
1.75	119	102	83	65	65	61	93	99	101	83	74	80	71	92	84		74
2.25		124	118	92	88	107	136	112	106	124	107	90	95	111	112		123
2.75			136	129	105	104	127	153	140	112	126	109	121	107	123		129
3.25			163	135	135	137	167	149	128	185	158	182	141	118	120		143
3.75				164	125	174	184	160	184	168	193	156	199	141	181		160
4.25					149	169	202	228	224	216	173	185	160	162	163		186
4.75						209	190	240	232	196	180	228	205	252	181		290

Table 7-7: Maximum bending moment, M_{xy}, [kN.m] for Pod 3 for all sea states investigated.

Hs [m]	Peak Period, Tp [s]																
	3.7	4.7	5.7	6.7	7.7	8.7	9.7	10.7	11.7	12.7	13.7	14.7	15.7	16.7	17.7	18.7	19.7
0.25				72	56			45	33	34	28	26	24		21		
0.75	238	228	212	179	197	170	154	114	108	110	90	82	83	64	64		55
1.25	320	431	328	310	316	311	241	223	171	177	147	119	119	112	105		114
1.75	482	518	512	411	395	377	341	306	244	251	232	182	146	173	154		115
2.25		672	663	613	473	415	463	395	296	286	323	226	189	209	185		152
2.75			774	722	596	555	472	432	474	335	337	323	252	260	225		174
3.25			985	890	793	617	650	590	458	485	423	328	304	306	250		239
3.75				1089	875	915	753	655	527	514	444	396	362	301	291		244
4.25					992	900	744	654	658	658	510	445	530	368	328		307
4.75						1116	1111	856	860	583	583	507	416	427	398		344

Table 7-8 Maximum tension [MN] for mooring line 1.

Hs [m]	Peak Period, Tp [s]																
	3.7	4.7	5.7	6.7	7.7	8.7	9.7	10.7	11.7	12.7	13.7	14.7	15.7	16.7	17.7	18.7	19.7
0.25				1.8	1.8			1.9	2.0	2.1	2.3	2.2	2.3		2.4		
0.75	1.8	1.8	2.0	2.0	2.1	2.3	2.4	2.6	2.4	2.8	2.9	2.9	3.0	3.0	3.0		3.0
1.25	1.9	2.0	2.1	2.3	2.4	2.6	2.9	2.9	3.0	3.0	3.1	3.0	3.1	3.1	3.1		3.1
1.75	1.9	2.0	2.2	2.5	2.6	2.7	2.9	3.0	3.0	3.2	3.2	3.1	3.2	3.1	3.3		3.2
2.25		2.2	2.5	2.6	2.8	3.0	3.0	3.1	3.2	3.3	3.3	3.3	3.3	3.3	3.3		3.2
2.75			2.5	2.8	2.9	3.1	3.2	3.4	3.2	3.3	3.2	3.3	3.4	3.3	3.5		3.5
3.25			2.6	2.8	2.9	3.1	3.5	3.2	3.2	3.5	3.2	3.3	3.4	3.4	3.4		3.5
3.75				3.0	3.0	3.1	3.4	3.4	3.3	3.4	3.5	3.4	3.7	3.7	3.7		3.5
4.25					3.1	3.2	3.5	3.4	3.7	3.6	3.4	3.4	3.5	3.6	3.7		3.6
4.75						3.2	3.2	3.5	3.4	3.6	3.7	3.6	3.9	4.2	3.5		4.5

Table 7-9 Maximum tension [MN] for mooring line 2.

Hs [m]	Peak Period, Tp [s]																
	3.7	4.7	5.7	6.7	7.7	8.7	9.7	10.7	11.7	12.7	13.7	14.7	15.7	16.7	17.7	18.7	19.7
0.25				1.7	1.7			1.8	1.9	1.9	2.0	2.0	2.0		2.3		
0.75	1.8	1.8	1.9	1.9	2.0	2.3	2.3	2.6	2.3	2.7	2.9	2.8	3.0	3.0	3.0		3.0
1.25	1.9	2.0	2.0	2.2	2.3	2.5	2.8	2.6	2.9	3.0	3.1	3.0	3.1	3.1	3.1		3.1
1.75	1.9	2.0	2.2	2.4	2.5	2.6	2.8	3.0	3.0	3.2	3.2	3.1	3.1	3.1	3.3	3.2	3.2
2.25		2.2	2.4	2.5	2.7	3.0	3.0	3.3	3.2	3.2	3.3	3.3	3.3	3.3	3.2		3.2
2.75			2.4	2.6	2.8	3.0	3.1	3.1	3.2	3.4	3.3	3.3	3.3	3.3	3.5		3.5
3.25			2.5	2.8	2.9	3.1	3.1	3.2	3.3	3.3	3.2	3.3	3.4	3.4	3.4		3.5
3.75				2.9	3.0	3.1	3.3	3.2	3.4	3.4	3.5	3.7	3.3	3.7	3.7		3.5
4.25					3.1	3.1	3.2	3.5	3.4	3.4	3.4	3.5	3.5	3.7	3.5		3.6
4.75						3.3	3.3	3.5	3.6	3.7	3.5	3.6	3.9	4.3	3.5		4.5

Table 7-10 Maximum tension [MN] for mooring line 3.

		Peak Period, Tp [s]															
		3.7	4.7	5.7	6.7	7.7	8.7	9.7	10.7	11.7	12.7	13.7	14.7	15.7	16.7	17.7	18.7	19.7
Hs [m]	0.25				1.9	1.9			2.0	2.0	2.0	2.3	2.2	2.3		2.4		
	0.75	1.9	2.0	2.0	2.1	2.2	2.4	2.4	2.6	2.5	2.8	2.9	2.8	2.9	3.0	3.0		2.9
	1.25	2.1	2.3	2.3	2.4	2.5	2.7	2.8	2.7	2.9	3.1	3.0	3.0	3.1	3.0	3.0		3.0
	1.75	2.2	2.4	2.5	2.6	2.6	2.8	2.9	3.0	3.1	3.1	3.1	3.1	3.1	3.1	3.1	3.2	3.1
	2.25		2.6	2.7	2.8	2.8	3.0	3.0	3.2	3.1	3.3	3.2	3.2	3.2	3.2	3.2		3.2
	2.75			2.8	2.8	3.0	3.1	3.1	3.1	3.2	3.3	3.3	3.2	3.3	3.2	3.3		3.2
	3.25			2.9	3.0	3.1	3.0	3.2	3.3	3.3	3.3	3.2	3.3	3.3	3.3	3.4		3.3
	3.75				3.1	3.1	3.1	3.4	3.3	3.3	3.3	3.4	3.2	3.3	3.2	3.2		3.3
	4.25					3.2	3.3	3.2	3.3	3.5	3.2	3.3	3.6	3.4	3.4	3.3		3.9
	4.75						3.3	3.4	3.3	3.7	3.6	3.4	3.7	3.7	3.6	3.4		4.2

Table 7-11 Maximum tension [MN] for mooring line 4.

		Peak Period, Tp [s]															
		3.7	4.7	5.7	6.7	7.7	8.7	9.7	10.7	11.7	12.7	13.7	14.7	15.7	16.7	17.7	18.7	19.7
Hs [m]	0.25				1.7	1.8			1.8	1.9	1.9	2.0	2.0	2.0		2.2		
	0.75	1.9	2.0	1.9	2.0	2.1	2.3	2.3	2.6	2.4	2.7	2.9	2.8	2.9	3.0	3.0		2.9
	1.25	2.0	2.2	2.2	2.3	2.4	2.6	2.8	2.7	2.9	3.0	2.9	3.0	3.0	3.0	3.0		3.1
	1.75	2.2	2.4	2.4	2.5	2.5	2.7	3.0	3.0	3.0	3.1	3.1	3.1	3.1	3.0	3.2	3.2	3.2
	2.25		2.6	2.6	2.7	2.7	3.0	3.0	3.1	3.1	3.3	3.2	3.2	3.2	3.3	3.1		3.2
	2.75			2.7	2.7	2.9	3.1	3.2	3.3	3.1	3.3	3.3	3.2	3.2	3.2	3.3		3.3
	3.25			2.8	2.9	3.0	3.0	3.5	3.2	3.3	3.3	3.3	3.3	3.3	3.4	3.5		3.3
	3.75				3.2	3.2	3.2	3.4	3.3	3.4	3.4	3.3	3.3	3.4	3.2	3.2		3.5
	4.25					3.1	3.3	3.4	3.3	3.5	3.2	3.4	3.8	3.6	3.3	3.4		4.1
	4.75						3.4	3.3	3.4	3.4	3.5	3.4	3.5	3.7	4.0	3.5		4.7

Table 7-12: Maximum 'backbone' yaw displacement [degrees].

		Peak Period, Tp [s]															
		3.7	4.7	5.7	6.7	7.7	8.7	9.7	10.7	11.7	12.7	13.7	14.7	15.7	16.7	17.7	18.7	19.7
Hs [m]	0.25				0.0	0.0			0.0	0.1	0.1	0.7	0.6	0.9		0.9		
	0.75	0.0	0.0	0.0	0.0	0.0	0.3	3.5	9.7	3.0	3.7	2.0	3.2	6.3	2.9	2.3		2.9
	1.25	0.0	0.0	0.0	0.2	0.2	1.8	11.8	11.3	15.0	4.9	3.1	1.9	2.6	1.8	2.0		4.2
	1.75	0.0	0.0	0.0	0.1	6.5	10.0	21.5	21.6	26.1	20.0	18.9	4.8	1.8	4.3	4.9		8.7
	2.25		0.0	0.1	0.1	10.8	16.5	26.7	26.3	27.5	19.8	14.9	5.1	5.2	1.2	2.6		5.4
	2.75			0.2	4.2	12.1	17.2	26.1	28.6	31.7	18.8	11.8	8.4	23.0	4.6	15.2		1.6
	3.25			0.1	0.9	13.8	22.6	31.8	35.1	24.6	30.5	18.1	26.3	7.4	6.6	4.7		15.5
	3.75				6.3	14.0	23.2	39.8	35.2	22.2	32.3	36.4	8.2	25.8	4.6	13.2		10.2
	4.25					12.0	22.5	36.2	35.3	39.3	27.7	26.4	17.0	29.4	19.9	18.7		8.5
	4.75						31.3	32.8	29.8	40.0	29.1	34.0	25.8	12.0	32.5	4.7		6.8

Figure 7-3 Mooring line 1 tension for Hs = 4.75m Tp = 8.7s.
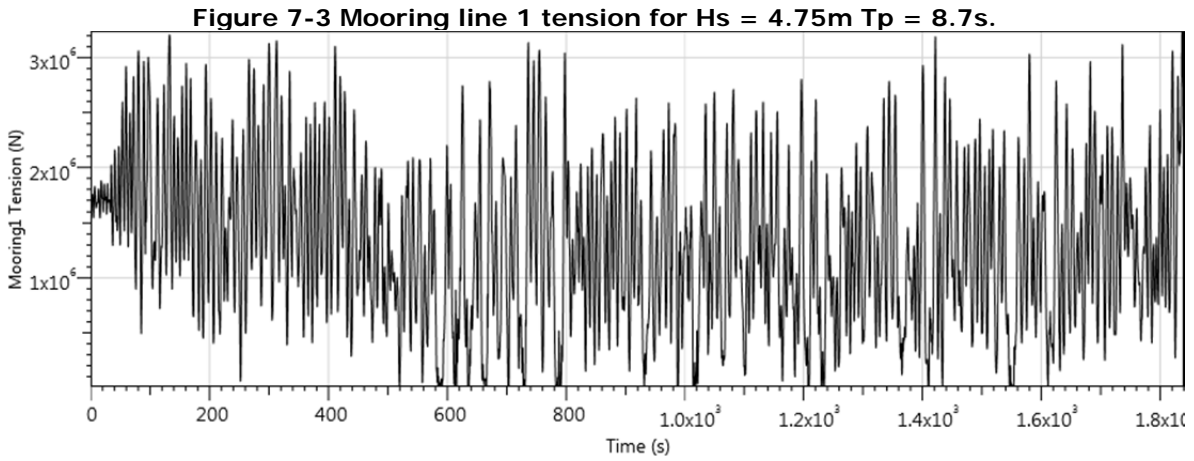
Figure 7-4 Backbone yaw (red line –degrees) and total power extracted (black line MW) for Hs = 4.75m Tp = 8.7s.
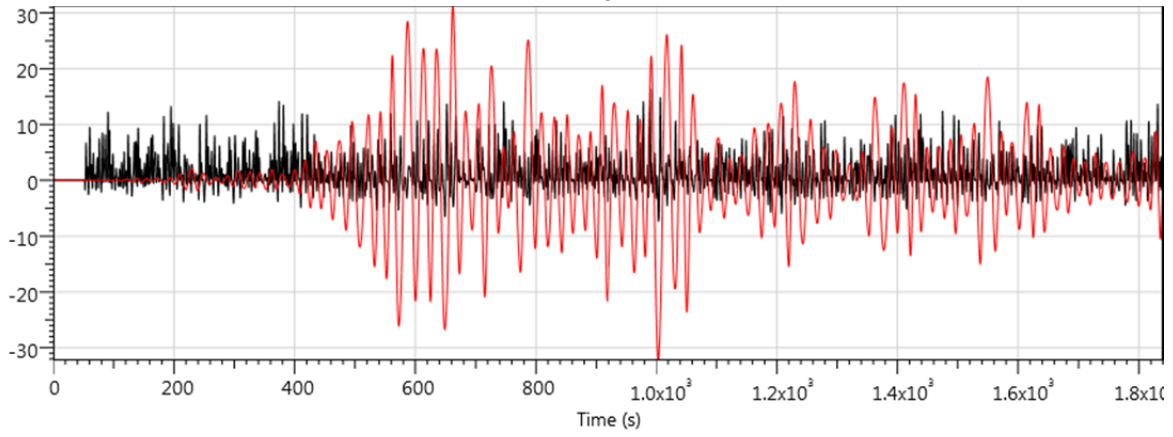
7.4 Non-exceedance probability

7.4.1 Methodology

The maximum loads observed on a WEC in a particular simulated sea state are dependent on the length of the simulation of the sea state. In reality the concept of a 'maximum' load in a particular sea state is slightly misleading. Loading is a stochastic process, with the loads experienced being dependent on both the waves incident on the WEC and the motion history of the WEC. It is more accurate to think of a load level being associated with a non-exceedance probability, dependent on the sea state.

A ranking technique is used to estimate the exceedance probability for each relevant load. The ranking technique involves finding the local peaks for a given signal and then sorting them based on their magnitude (ascending order).

The exceedance probably for each of the loads can be found by

$$p(F < F_n) = 1 - \frac{n}{N + 1}, \tag{7}$$

where n is the ranking of a given relative peak F_n and N is the total number of peaks for a given time series.

For a better understanding of the loads, the distribution of the local minima and maxima were calculated separately. An example of this analysis is given in Figure 7-5. The time series of the axial force (F_z) in the POD 3 for a sea state Hs = 1.75m and 7.7s is illustrated with the probability of exceedance for the minima and maxima.

Figure 7-5: Axial force F_z on Pod 3 for for Hs = 1.75 and Tp = 7.7s (Top – Local maxima (red circles) - Local minima (green circles)). Bottom row: Probability of exceedance for the minima (left) and for the maxima (right).
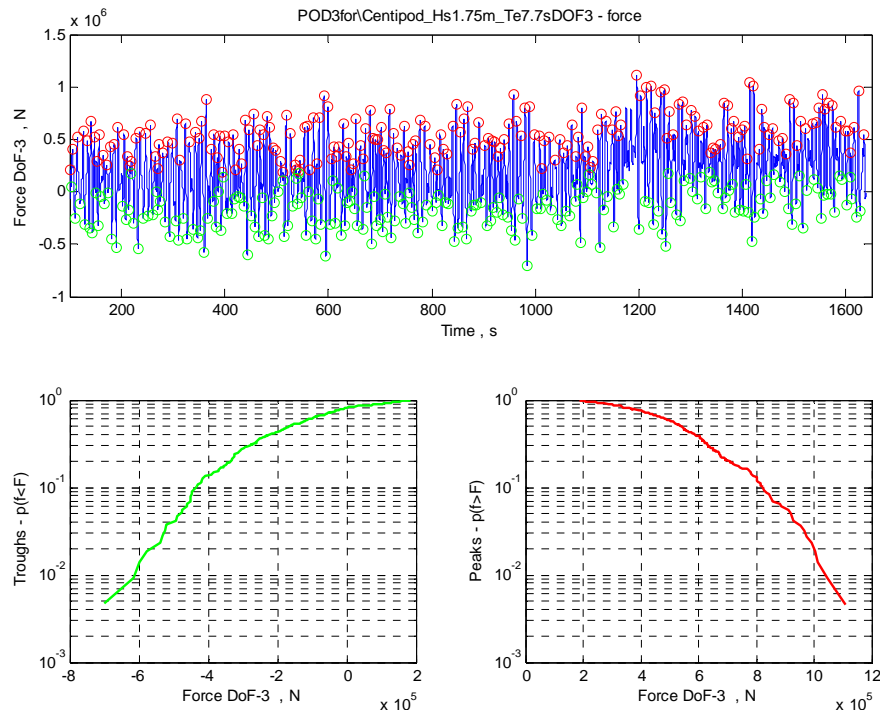
7.4.2   Results

The figures below illustrate the probability of non-exceedance for the axial and shear loads on the center Pod 3. For illustrative proposes, in this report results for three different sea states are used: Hs=3.75m with Tp=8.7s and Tp=14.7s, and the larger sea state Hs=4.75m and Tp=8.7s (see Figure 7-6 to Figure 7-9). The probability of non-exceedance was also calculated for the remaining sea states. A database *.mat* file is to be provided to DA for all the bodies described in Table 7-1 containing the complete results presented in this section.

Figure 7-6 shows the increase of the maximum axial loads on the middle pod are function of the sea state - not only the extreme loads, but also the distribution of the relative peaks over the time series considered. The maximum values registered for the axial forces is approx. 1400kN for the sea state Hs=3.75m and Tp=8.7s. The wave period has an impact on the distribution of the relative peak loads. The larger Tp values result in larger maximum loads.

As expected, the torsion moment (around the axial axis of the pod) is 2 orders of magnitude smaller than the bending moment. A variation of the yaw moment with the sea states is clearly observed. This moment was expected to be small due to the symmetry of the model and the circular geometry of the pods. However, small motions of the platform can lead to asymmetric loading on the center float as mentioned above.

Figure 7-6:   Probability of exceedance for axial force F_z on Pod 3 for 3 sea states
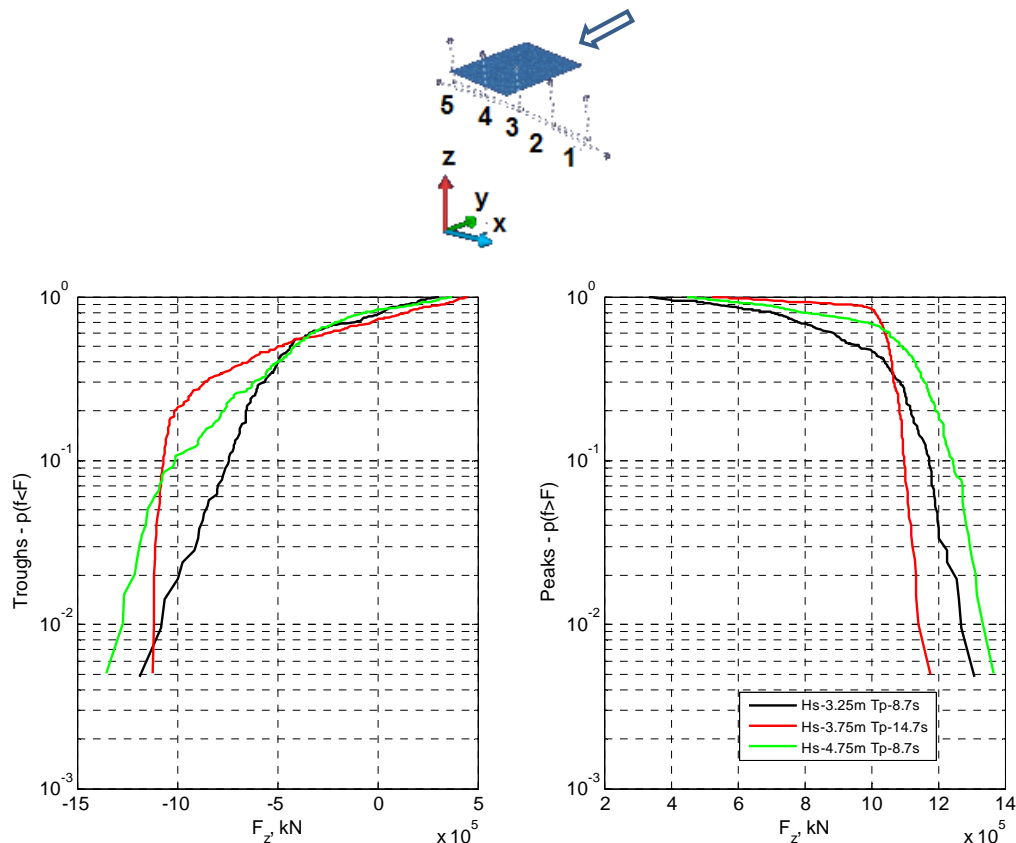
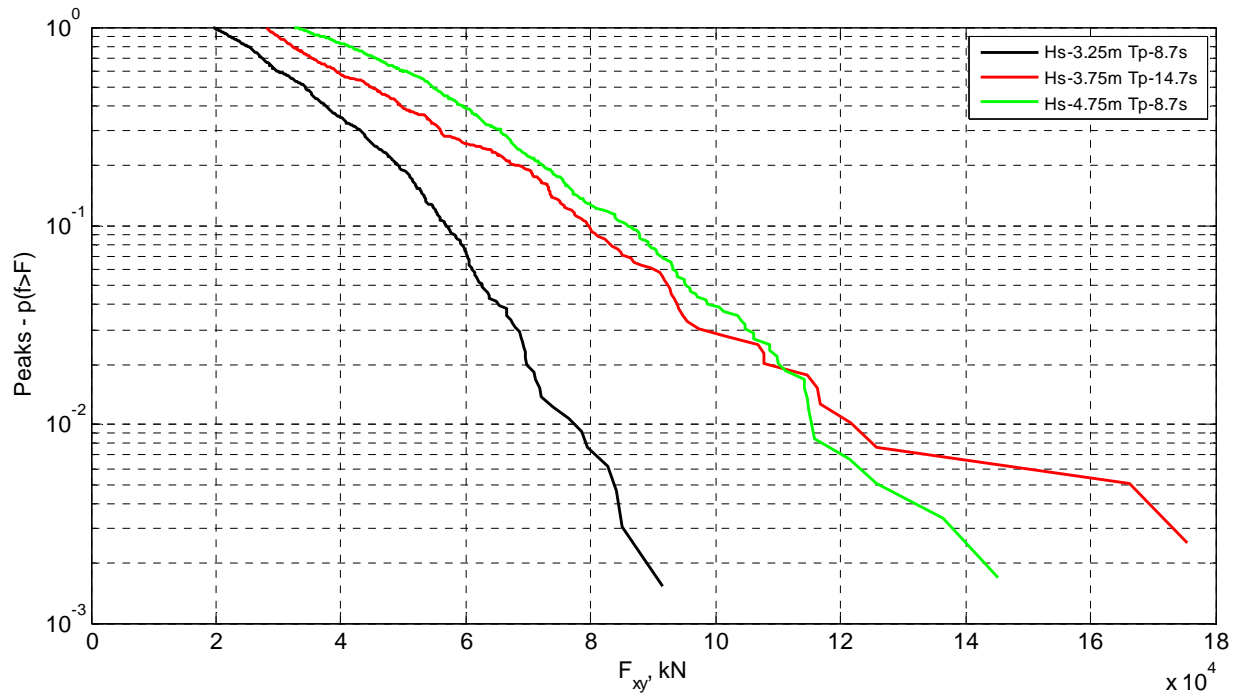**Figure 7-7:** Probability of exceedance for shear force F_{xy} on Pod 3 for 3 sea states

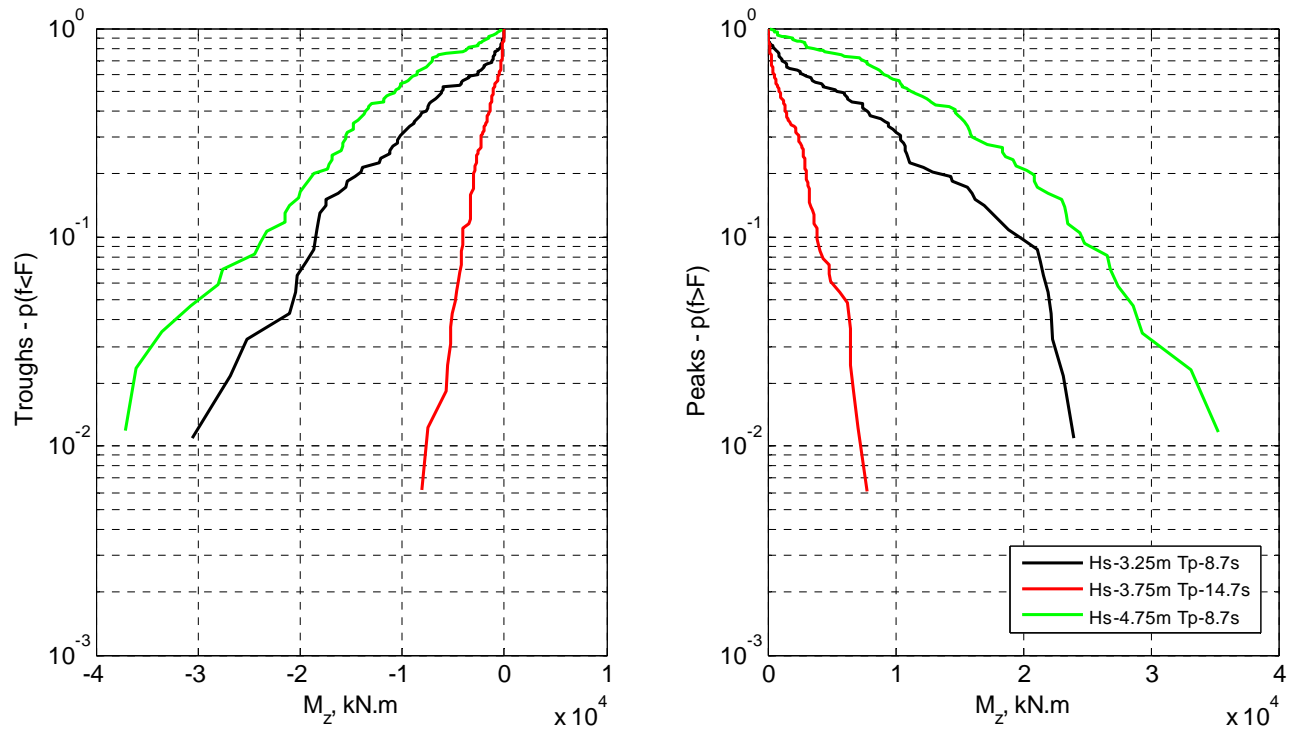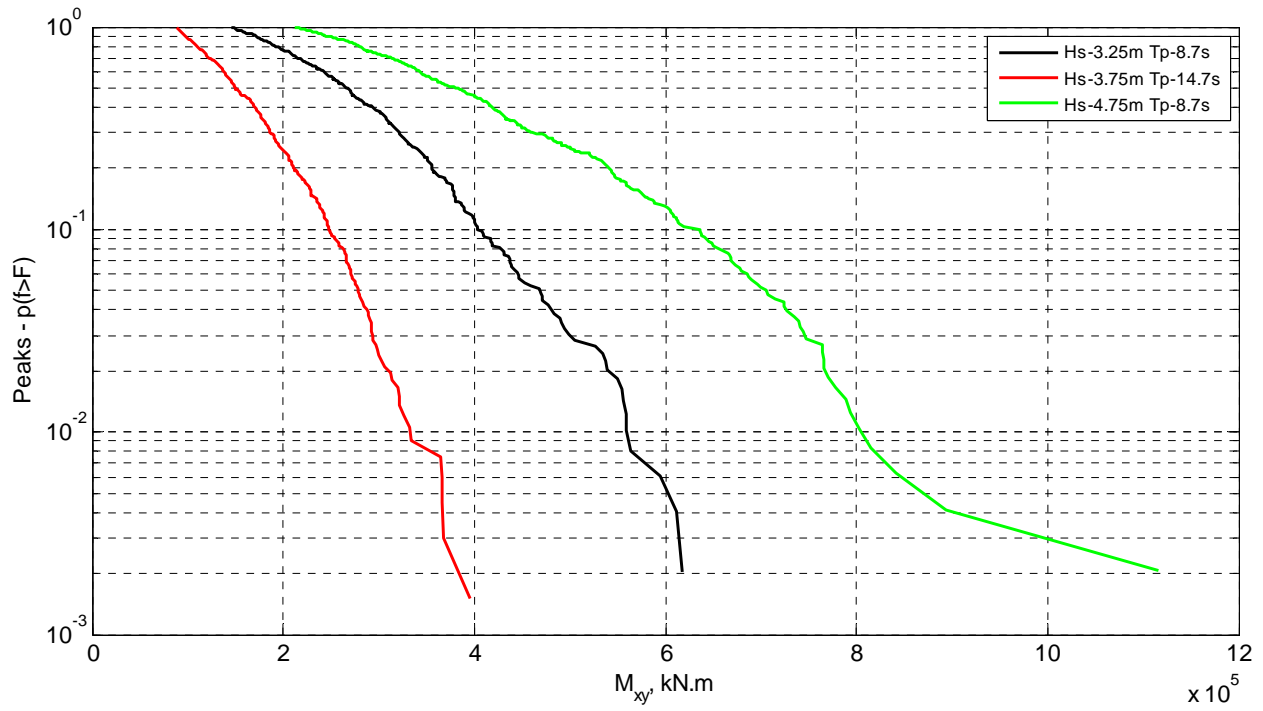**Figure 7-8:** Probability of exceedance for torsional moment M_z on Pod 3 for 3 sea states

Figure 7-9:   Probability of exceedance for bending moment M_{xy} on Pod 3 for 3 sea states

The mooring line tension distributions are illustrated in Figure 7-10 for 3 selected sea states. All mooring lines present a similar load distribution. The variation of the mooring line tension with the sea states appears similar as for the pod forces described on the paragraph above.

Figure 7-10: Non-exceedance probability for the tension on the mooring lines 1-4.
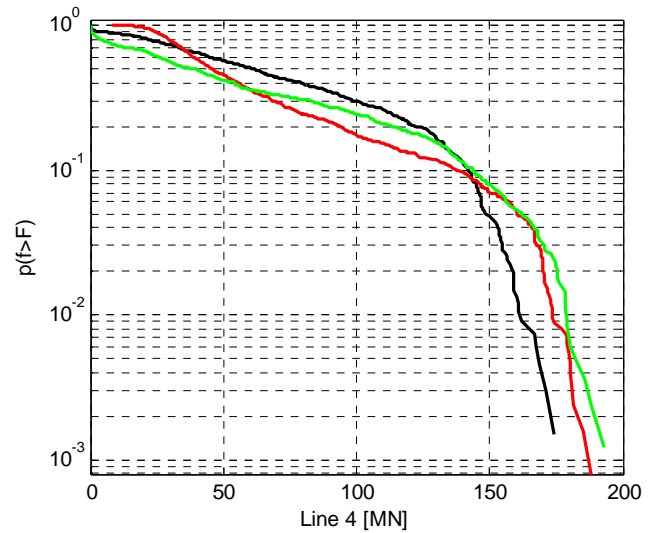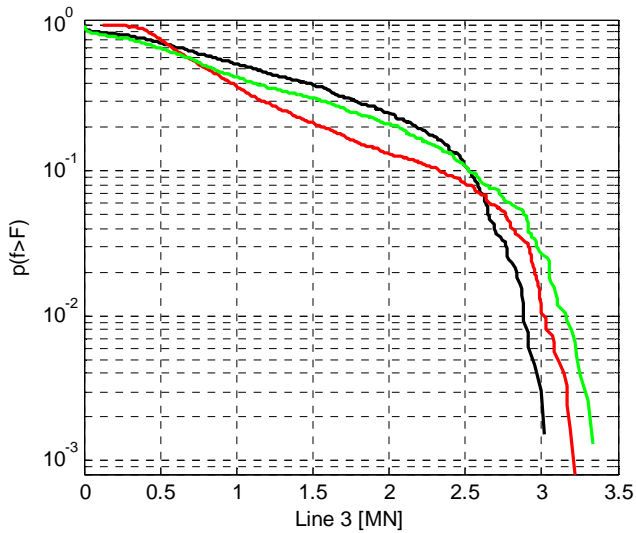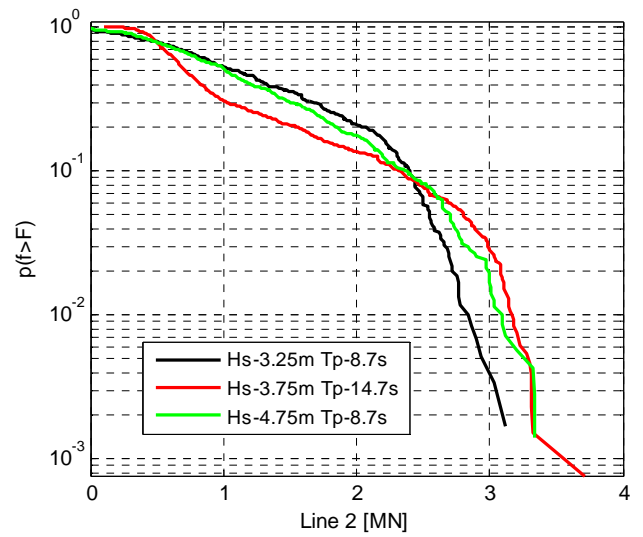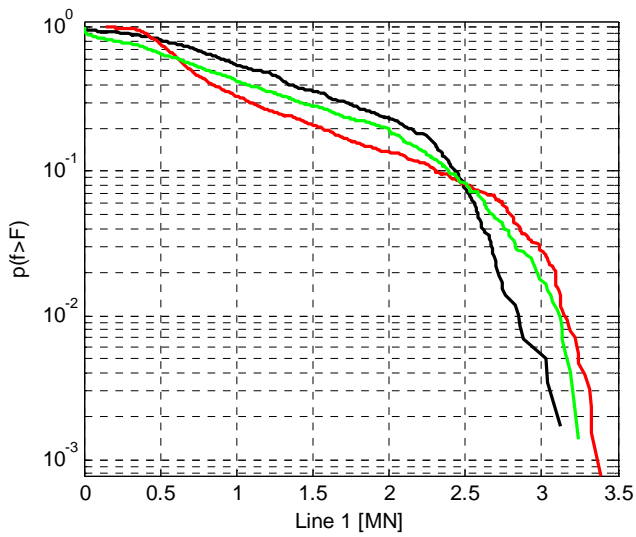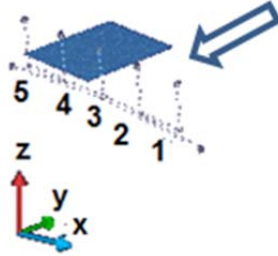
8 CONCLUSIONS

8.1 Summary of Key Findings

DNV GL have carried out an assessment of the Centipod CPX3 WEC with MPC using WaveDyn and derived a power matrix detailing the device performance in a variety of sea states, assuming linear waves and linear hydrodynamic forces.

The maximum capture width of the device is 0.46. This was estimated for a sea state with Hs=0.25m and Tp=13.7s. Due to the low Hs this corresponds to a low mean power absorbed (12.3kW). The maximum mean power extracted was approximately 1.39MW for Hs=4.75m and Tp=8.7s. Using the scatter table provided by DA the total annual energy yield is 3.78GWh. This power matrix can serve as a baseline for the current floating, tension-leg moored Centipod design with a relatively unconstrained PTO incorporating MPC.

The minimum and maximum loads observed in the simulations for various locations and components are presented in scatter tables for all the sea states considered. Besides these tables, curves showing probability of non-exceedance are also presented, providing a good means for comparing the loading of different WEC configurations in the future.

When looking at maximum loads on the center Pod 3, the axial load ranged from 1.37MN (Hs=4.75m and Tp=8.7s) to -1.32MN (Hs=4.75m and Tp=8.7s). The maximum shear force was 290kN (Hs = 4.75m and Tp = 19.7s) and the maximum bending moment was 1.1MNm (Hs=4.74m and Tp=8.7s).

The maximum mooring line tension was estimated to be 4.7MN. This was obtained for the sea state Hs=4.75m and Tp=19.7m.

8.2 Potential Next Steps

Future work could involve:

- The inclusion of end-stops on the machine may also be considered to stop the PTO extension. This is likely to be a design driver, so its inclusion in the early stages of design is advised.
- The use of a partially nonlinear hydrostatics and/or hydrodynamics formulation so that the impact of the instantaneous wetted surface of the bodies in the overall WEC response may be evaluated.
- Improve the representation of viscous drag effects on the 'backbone'. It is advised that this point and the preceding point on nonlinear hydrostatics/hydrodynamics are carried out together with an experimental validation exercise - particularly for the larger sea states where linear wave theory may not be applicable.
- Initial structural assessment of the WEC components - particularly, the connection between the PTO and the floats. A more detailed structural model for the loads on the pods using the hydrodynamic distributed loads can also be performed.
- The inclusion and analysis of any other potential design changes to the overall WEC arrangement.
- The relatively large backbone yaw motion should be investigated further.
- Iterate by reviewing and updating the mooring line sizing and characteristics (e.g. stiffness) based on the new set of dynamic mooring loads.
- Experimental data should be collected for numerical model validation exercises.

9 REFERENCES

[1]   WaveDyn 1.1 User Manual , DNV GL, 2014

[2]   Dehlsen Associates LLC, Dropobox, "TransfertoDNVGL-MPC.rar". 2015-07-23 10:05:25. 6791kb, downloaded 24/07/2015.

[3]   McCall, A., Dehlsen Associates LLC, email: "RE: MPC + WaveDyn Model Status", sent on 24/07/2017

[4]   Dehlsen Associates LLC, "Advanced controls for the Multi-pod Centipod WEC device", DE-FOA-0000848

[5]   Dehlsen Associates LLC, Dropbox, downloaded 04/03/2014

[6]   DNV GL, "Centipod CPX3", 702480-USSD-R-01-A, 06/06/2014

[7]   McCall A., Dehlsen Associates LLC, email: "RE: reminder", sent on 11/21/2014

[8]   LaBonte A., "Standardized cost and Performance Reporting for Marine and Hydrokinetic Technologies", Proceedings of the 1st Marine Energy Technology Symposium, April 2013

[9]   McCall, A., Dehlsen Associates LLC, email: "Sea state and methodology for WaveDyn power matrix", sent on 01/05/2014

[10]   K. Ewans, "Observation of the Directional Spectrum of Fectch Limited Waves," *J. Phys. Oceanography,* pp. 495-512, 1998.

APPENDIX A NOMENCLATURE

APPENDIX A.1 Acronyms

BCS	Body-fixed coordinate system
CoM	Center of mass
DOF	Degree-of-freedom
PTO	Power take-off
WEC	Wave energy converter

APPENDIX A.2 Definitions and equations

A	Wave amplitude (regular waves)
f	Wave frequency (regular waves)
g	Modulus of the acceleration due to gravity
H_s	Significant Wave height
l	Characteristic length
ρ	Water density
EA	Axial stiffness properties of mooring line
L	Initial relaxed length of mooring line
K_{line}	Applied stiffness for each mooring line
$S(f)$	Variance density spectrum
T	Wave period (regular waves)
T_e	Energy Period
T_p	Peak Period
$\overline{E}_{abs}$	Annual averaged absorbed energy by the WEC
$\overline{P}_w$	Incident wave power
$\overline{P}_{abs}$	Average mechanically absorbed power
N	Total number of relative peaks in a sample
n	Ranking position
F_{xy}	Shear force
M_{xy}	Bending moment
p	Probability

SUBSCRIPTS

g	Global coordinate system
$moor$	Mooring lines force

APPENDIX B   DATA DESCRIPTION

This section describes the data that DNV GL will provide Ecomerit as result of the post-processing.

A Matlab data structure for each load output location is presented with:

- Statistical properties of the load signal in all the relevant degrees of freedom.
    - o   Min, Max, Mean, Standard deviation, RMS values
    - o   2 vectors with the probability of non-exceedance curve:
        - ▪   VAR.coord : values of the load , f
        - ▪   VAR.prob : Probability of non-exceedance.

ABOUT DNV GL

Driven by our purpose of safeguarding life, property and the environment, DNV GL enables organizations to advance the safety and sustainability of their business. We provide classification and technical assurance along with software and independent expert advisory services to the maritime, oil and gas, and energy industries. We also provide certification services to customers across a wide range of industries. Operating in more than 100 countries, our 16,000 professionals are dedicated to helping our customers make the world safer, smarter and greener.